

Musical Acoustics

15. Musical Acoustics

Colin Gough

This chapter provides an introduction to the physical and psycho-acoustic principles underlying the production and perception of the sounds of musical instruments. The first section introduces generic aspects of musical acoustics and the perception of musical sounds, followed by separate sections on string, wind and percussion instruments.

In all sections, we start by considering the vibrations of simple systems – like stretched strings, simple air columns, stretched membranes, thin plates and shells. We show that, for almost all musical instruments, the usual text-book description of such systems is strongly perturbed by material properties, geometrical factors and acoustical coupling between the drive mechanism, vibrating system and radiated sound.

For stringed, woodwind and brass instruments, we discuss excitation by the bow, reed and vibrating lips, which all involve strongly non-linear processes, even though the vibrations of the excited system usually remains well within the linear regime. However, the amplitudes of vibration of very strongly excited strings, air columns, thin plates and membranes can sometimes exceed the linear approximation limit, resulting in a number of interesting non-linear phenomena, often of significant musical importance.

Musical acoustics therefore provides an excellent introduction to the physics of both linear and non-linear acoustical systems, in a context of rather general interest to professional acousticians, teachers and students, at both school and college levels.

The subject continues its long tradition in advancing the frontiers of experimental, computational and theoretical acoustics, in an area of wide general appeal and contemporary relevance.

By discussing the theoretical models and experimental methods used to investigate the acoustics of many musical instruments, we have

aimed to provide a useful background for professional acousticians, students and their teachers, for whom musical acoustics provides an exceedingly rich area for original research projects at all educational levels.

Because the subject is ultimately about the sounds produced by musical instruments, a large number of audio illustrations have been provided, which can be accessed on the [Springer EXTRAS](#) server. The extensive list of references is intended as a useful starting point for entry to the current research literature, but makes no attempt to provide a comprehensive list of all important research.

This chapter highlights the acoustics of musical instruments. Other related topics, such as the human voice, the perception and psychology of sound, architectural acoustics, sound recording and reproduction, and many experimental, computational and analytic techniques are described in more detail elsewhere in this volume.

15.1	Vibrational Modes of Instruments	569
15.1.1	Normal Modes	569
15.1.2	Radiation from Instruments	571
15.1.3	The Anatomy of Musical Sounds	575
15.1.4	Perception and Psychoacoustics	586
15.2	Stringed Instruments	588
15.2.1	String Vibrations	589
15.2.2	Nonlinear String Vibrations	597
15.2.3	The Bowed String	600
15.2.4	Bridge and Soundpost	604
15.2.5	String–Bridge–Body Coupling	609
15.2.6	Body Modes	615
15.2.7	Measurements	628
15.2.8	Radiation and Sound Quality	632
15.3	Wind Instruments	635
15.3.1	Resonances in Cylindrical Tubes	636
15.3.2	Non-Cylindrical Tubes	640
15.3.3	Reed Excitation	653
15.3.4	Brass–Mouthpiece Excitation	662

15.3.5 Air-Jet Excitation	667	15.4.2 Bars.....	682
15.3.6 Woodwind and Brass Instruments..	671	15.4.3 Plates	687
15.4 Percussion Instruments	675	15.4.4 Shells	692
15.4.1 Membranes	676	References	696

Musical acoustics is one of the oldest of all the experimental Sciences (see *Levenson* [15.1] for an informative account of the interactions between Music and Science over the ages). The observation of the relationship between the notes produced by the exact fraction divisions of a stretched string and consonant musical intervals like the octave (2 : 1), perfect fifth (3 : 2) and fourth (4 : 3), resulted in the first physical law to be expressed in mathematical terms. It also led to the idea of a divinely created cosmos based on exact fractions, filled with the *music of the spheres* (see, for example, Kepler's account of the ellipticity of the planetary orbits described as notes on a musical scale, in *Harmonies of the World* (1618) [15.2]). Ultimately, such observations led to Newton's discovery of celestial dynamics and the laws of gravity leading to the modern view of the universe subject to physical laws rather than numerical relationships.

In the nineteenth century, musical acoustics continued to occupy a central scientific role. This culminated in Lord Rayleigh's monumental two volumes on the *Theory of Sound* [15.3], which still provide the foundations for almost every branch of modern acoustics. The 19th century advances in understanding waves in acoustics also laid the mathematical framework for quantum wave mechanics in the early part of the 20th century. More recently, the physics of vibrating strings can be said to have come full circle, with the suggestion that string-like vibrations of the quantum field equations account for the mass of the elementary particles (*Hawkins* [15.4]).

Musical acoustics still remains a challenging and exciting field of research and continues to advance mainstream acoustics in many ways. Examples include nonlinear physics and the use of laser holography and both modal and finite-element analysis to investigate complicated vibrating systems. Such developments are described in this chapter and in more detail in other chapters of this Handbook and in the *Physics of Musical Instruments* by *Fletcher* and *Rossing* [15.5], which will often be cited, as an authoritative text and source of additional references for most topics discussed. The *Science of Sound* by *Rossing* et al. [15.6] covers an even wider range of topics at a somewhat less mathematical

level. An informative overview of the history, technology and performance of western musical instruments has recently been published by *Campbell, Greated* and *Myers* [15.7].

The first section of this chapter deals with the generic properties of the vibrations and sounds of musical instruments. A brief description is first given of the properties of both simple and coupled resonators, typifying the vibrational modes of stringed, wind and percussion instruments, where the sound is generated by vibrating strings, air columns, plates, membranes and shells. The radiation of sound by such structures is then described in terms of multipole sources. This is followed by a brief description of the envelopes, waveforms and spectra of the sounds that characterize the sound of individual instruments. The section ends with a consideration of the way the listener perceives such sounds.

The section on stringed instruments first considers the general properties of string vibrations and their excitation by plucking, bowing and striking. Large amplitude vibrations are shown to provide a particular interesting illustration of nonlinearity of much wider applicability than to musical acoustics alone. The coupling of the vibrating string via the bridge to the acoustically radiating surfaces of the instrument is then discussed in some detail, followed by a more detailed discussion of excitation of a string via the bowed slip-stick mechanism. The vibrational modes of the main shell of the instrument and the importance of the bridge and soundpost in determining the efficiency of energy transfer to the radiating surfaces of the instrument are then discussed. The section ends with a description of some of the experiment and computational techniques used to describe the vibrational modes, followed by a brief description of the radiated sound and the subjective assessment of the quality of stringed instruments.

The section on woodwind and brass instruments starts with a consideration of oscillating air columns and sound radiation from cylindrical and conical tubes and the more complicated shapes used for woodwind and brass instruments. This is followed by sections on the highly nonlinear processes involved in the excitation of such vibrations by reed and lip vibrations and air-jets.

The section concludes with a brief description of the acoustical properties of various wind instruments.

The final section on percussion instruments describes the acoustical properties of a range of instruments based on the vibrations of stretched membranes, bars, plates and shells. Typical waveform envelopes

and time-dependent spectra are used to illustrate the relationship between the vibrational modes of such instruments and the radiated sound. Non-linearity at large amplitude excitation is again shown to be important and accounts for the characteristic sounds of certain instruments like gongs and cymbals.

15.1 Vibrational Modes of Instruments

15.1.1 Normal Modes

All musical instruments produce sound via the excitation of a vibrating structure. Woodwind, brass and percussion instruments radiate sound directly. However, stringed instruments radiate sound indirectly, because the vibrating string itself radiates an insignificant amount of energy. Energy from the vibrating string therefore has to be transferred to the much larger area, acoustically efficient, radiating surfaces of the body of the instrument. The resultant modes of vibration are complex and involve the interactions and vibrations of all the component parts, such as the strings, bridge, front and back plates, soundpost, neck, and even the air inside the volume of the violin body.

Any vibrating structure, however complicated, will have a number of what are called normal modes of vibration (Chap. 22). The important influence of damping on the nature of the normal modes will be described in the section on stringed instruments. The normal modes satisfy exactly the same equations of motion as a simple damped mass–spring resonator. The displacement ξ_n of a given excited mode measured at any chosen point p on the structure is given by

$$m_n \left(\frac{\partial^2 \xi_n}{\partial t^2} + \frac{\omega_n}{Q_n} \frac{\partial \xi_n}{\partial t} + \omega_n^2 \xi_n \right) = F(t), \quad (15.1)$$

where the effective mass m_n at the point p is defined in terms of the kinetic energy of the excited mode, $\frac{1}{2} m_n (\partial \xi_n / \partial t)_p^2$, $\omega_n = 2\pi f_n$ is the eigenfrequency (the angular frequency) of free vibration of the excited mode in the absence of damping and Q_n is the quality factor describing its damping. Initially, we consider a local driving force $F(t)$ at the point p , though it could be applied at any chosen point on the structure or distributed over the whole surface.

The effective mass of a one-dimensional string, solid bar or air column, at the point of maximum displacement, is half the mass of the vibrating system, the factor half resulting from averaging the kinetic energy over the

sinusoidal spatial displacement. Likewise, the effective mass of a two-dimensional vibrating object at maximum displacement, like a violin plate or drum skin, is of order 1/4 its mass. The effective mass is very large close to nodal positions, where the displacement is small, and is small at antinodes, where the displacement is large.

Typical driving forces are those acting on the bridge of a bowed or plucked string instrument and the pressure fluctuations at the input end of the air column of a blown woodwind or brass instrument. Such forces are generated by highly nonlinear excitation mechanisms. In contrast, the vibrations of the vibrating structure are generally linear with displacements proportional to the driving force. However, there are important exceptions for almost all types of instruments, when nonlinearity becomes significant at sufficiently strong excitation, as discussed later.

In any continuously bowed or blown musical instruments, feedback from the vibrating system results in a periodic driving force, which will not in general be sinusoidal. Nevertheless, by the Fourier theorem, any periodic force can always be represented as a superposition of sinusoidally varying, harmonic, partials with frequencies that are integer multiple of the periodic repetition frequency. We can therefore consider the induced vibrations of any musical instruments in terms of the induced response of its vibrational modes to a harmonic series of sinusoidal driving forces.

Resonance and Admittance

In the harmonic approach, the applied forces and induced motions are assumed to vary sinusoidally as $e^{i\omega t}$. We will generally use this complex notation for notational and algebraic simplicity, where $\text{Re}(e^{i\omega t}) = \cos \omega t$ and $\text{Im}(e^{i\omega t}) = \sin \omega t$. The resonant response, with displacement $\xi_n e^{i\omega t}$ and velocity $i\omega \xi_n e^{i\omega t}$ at the driving point p , for an applied sinusoidal force $F e^{i\omega t}$, is then given by

$$\frac{\partial \xi_n}{\partial t} = i\omega \xi_n = \frac{F}{m_n} \frac{i\omega}{(\omega_n^2 - \omega^2 + i\omega\omega_n/Q_n)}. \quad (15.2)$$

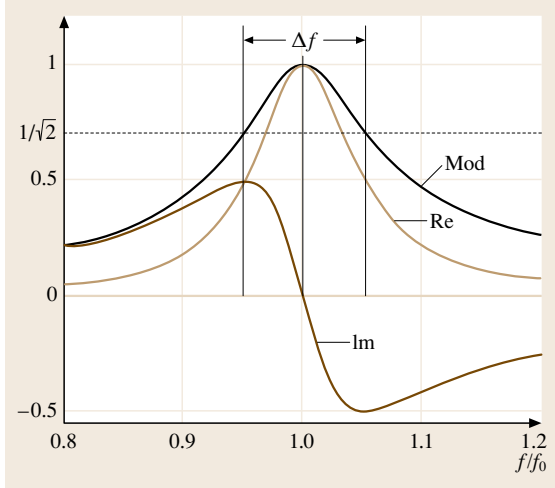


Fig. 15.1 Normalised real (Re) and imaginary (Im) components and the modulus (Mod) of the induced velocity of a simple harmonic resonator driven by a constant amplitude sinusoidal force for a Q -factor of 10

The ratio of induced velocity to driving force is known as the local admittance at the driving point p , and is plotted in normalised form in Fig. 15.1 for a Q -value of 10. The admittance has both real and imaginary components. The real part describes the component of the induced velocity in phase with the driving force, while the imaginary part describes the component in phase quadrature (with phase leading that of the force by 90° degrees).

Well below resonance the induced displacement is in phase with the driving force, while at resonance the phase lags behind the driving force by 90° , and well above resonance lags by 180° . The velocity $v(t)$ leads the displacement by 90° degree and is thus in phase with the driving force at resonance, which corresponds to the maximum rate of energy transfer $i\omega F\xi_n$ to the excited mode. The 180° change in the phase of the response, as the excitation frequency passes from well below to well above resonance, is especially important in interpreting the multiple resonances of any musical instrument.

Provided the damping of an excited mode is not too strong (i. e. Q_n is significantly larger than unity), the peak in the modulus or real part of the admittance occurs at $\omega_n(1 - 1/8Q^2)$, which is very close to the natural resonant frequency ω_n . The width of the resonance is $\Delta f = f_n/Q$, where Δf is defined as the difference in frequency between the points on the resonance curve when the modulus of the induced displacement has fallen to $1/\sqrt{2}$ of its maximum value

(i. e. the stored energy is half that at resonance). The displacement at resonance is $Q \times$ the static displacement.

Multi-Mode Systems

For any musical instrument having a number of vibrational modes, the admittance at the driving point p can be written as

$$A_{pp} = \sum_n \frac{1}{m_n} \frac{i\omega}{\omega_n^2 - \omega^2 + i\omega\omega_n/Q_n}, \quad (15.3)$$

with admittances A_{pp} of individual modes adding in series, equivalent to impedances in parallel. The vibrational response of a multi-resonant mode musical instrument can therefore be characterised by fitting the measured admittance to such a function giving the effective mass at the point of excitation, resonant frequency and Q -value for each of the excited modes. Using such a procedure, *Bissinger* [15.8] typically identifies up to around 40 vibrational modes for the violin below 4 kHz. However, at high frequencies, the width of individual resonances exceeds the spacing between them, making it increasingly difficult to identify individual modes.

It is important to recognise that damping is only important in a relatively narrow frequency range $\approx f_n/Q$ around the individual resonance peaks. Outside such regions, the reactive component associated with each vibrational mode continues to contribute significantly to the overall response. For example, well below resonance, each mode acts as a spring with effective spring constant $m_n(\omega_n^2 - \omega^2)$, while well above resonance it acts as a mass with effective mass $m_n(1 - \omega_n^2/\omega^2)$. The static displacement (at $\omega = 0$) is given by $\xi = F/K_o = \sum_n 1/(m_n\omega_n^2)$. Note that this involves contributions from all the vibrational modes of the structure, which is an important global property describing the low-frequency response of a multi-resonant structure such as the violin or guitar. If displacements are measured at a point p for an applied force at q , a *nonlocal admittance* can be expressed as

$$A_{pq} = \sum_n \frac{1}{m_{n,p}} \frac{i\omega}{(\omega_n^2 - \omega^2 + i\omega\omega_n/Q_n)} \frac{\xi_{n,p}\xi_{n,q}}{\xi_{n,p}^2}, \quad (15.4)$$

where $\xi_{n,p}$ and $\xi_{n,q}$ are the simultaneous displacements of the n th mode at the points p and q , with identical stored modal energy $1/2m_{n,p}\omega^2\xi_{n,p}^2 = 1/2m_{n,q}\omega^2\xi_{n,q}^2$.

Equation (15.4) illustrates the principle of reciprocity in acoustics, which states that the motion at a point p induced by a force at q is identical to the mo-

tion at q induced by the same force at p . Equation (15.4) also shows that, by applying a force at a particular position and measuring the induced motion (amplitude and phase) at a large number of different points $p(x, y, z)$ on the structure, it is possible to map out the amplitude of the modal vibrations $\xi_n(x, y, z)$ over the whole of any excited structure. Alternatively, the measurement point can be fixed and the excitation point moved across the structure. This is the basis of the powerful technique of modal analysis, which has been widely used to investigate the vibrational modes of many stringed and percussion instruments, as described by *Rossing* in Chap. 28 of this Handbook.

It also follows from (15.4) that a particular mode of vibration will never be excited if the driving force is located at a node of its vibrational state. This has important consequences for the spectrum of sound produced by bowed, plucked and struck stringed instruments and all percussion instruments.

Time-Domain Measurements

The vibrational characteristics of an instrument can also be investigated in the time domain. For example, by striking a stringed instrument with a light hammer or exciting the vibrational modes of a woodwind or brass instrument with a short puff of air, the frequencies of free vibration of the vibrational modes and their damping can be determined from their time-dependent decay. Provided the damping is not too strong ($Q \gg 1$), the modes will decay with time as

$$\xi_n(t) = \xi_0 e^{-t/\tau_n} e^{i\omega_n t}, \quad (15.5)$$

where $\tau_n = 2Q_n/\omega_n = Q_n/\pi f_n$. The frequency f_n of a given mode can be determined from its inverse period and Q_n from $\pi \times$ the number of periods for the amplitude to fall by the factor exponential e . The Q -value of strongly excited modes of a musical instrument can be estimated from $\tau_{60\text{dB}} = 13.6\tau$, the Sabine decay time (Chap. 10 *Concert Hall Acoustics*). This is the perceptually significant time taken for the sound pressure to fall by a factor of 10^3 – from a very loud level to just being detectable. Hence, $Q_n = \pi f_n \tau_{60}/13.6 \approx 0.23 f_n \tau_{60}$. For example, the sound of a strongly plucked cello open A-string (220 Hz) can be heard for at least ≈ 2 s, corresponding to a Q -value of ≈ 100 or more.

Damping results in a loss of stored energy given by

$$\frac{dE_n}{dt} = -\frac{\omega_n}{Q_n} E_n = -2\frac{E_n}{\tau_n}. \quad (15.6)$$

Hence, the power P required to maintain a constant amplitude at resonance is $\frac{\omega_n}{Q_n} E_n$, where E_n is the

energy stored. This tends to be the way that Q is defined and measured by physicists, whereas in acoustic spectroscopy it is more usual to define and measure Q -values from either the width of resonances in spectroscopic measurements or from decay times after transient excitation. As illustrated above, all such definitions are equivalent.

15.1.2 Radiation from Instruments

Although a large number of vibrational modes of a musical instrument may be excited simultaneously, they will not be equally important in radiating sound, which has important consequences for the quality of the sound. This section therefore provides a brief introduction to the radiation of sound from the vibrational modes of musical instruments.

Sound Waves in Air

In free space, the longitudinal displacement $\xi(x, t) = \xi_0 e^{i(\omega t - kx)}$ of plane sound waves satisfies the wave equation

$$\frac{\partial^2 \xi}{\partial x^2} = \frac{1}{c_0^2} \frac{\partial^2 \xi}{\partial t^2}. \quad (15.7)$$

The dispersionless (independent of frequency) velocity of sound $c_0 = \sqrt{\gamma P_0/\rho}$, where $\gamma (\approx 1.4)$ is the ratio of specific heats at constant pressure and volume, $P_0 (\approx 10^5 \text{ Pa or N/m}^2)$ is the ambient pressure and $\rho (\approx 1 \text{ kg/m}^3)$ is the density (the brackets give the values for air at ambient pressure and temperature). The ratio of acoustic pressure $p = -\gamma P_0 \partial \xi / \partial x$ to the particle velocity $v = \partial \xi / \partial t$ is referred to as the specific impedance, $z_0 = p/v = \rho c_0$.

The appearance of γ in the expression for the velocity of sound reflects the adiabatic nature of acoustic waves. This arises because acoustic wavelengths are far too long to allow any significant equalisation of the longitudinal temperature fluctuations arising from the compressions and rarefactions of a sound wave. In free space longitudinal heat flow between the fluctuating regions is only important at very high ultrasonic frequencies (MHz), where it leads to significant attenuation. The major source of attenuation of freely propagating acoustic sound waves arises from the water vapour present. However, both viscous and transverse thermal losses to the side walls of woodwind and brass instruments can result in significant attenuation, as described later.

The above expressions neglect first-order, nonlinear, corrections to the compressibility, proportional to

$\partial\xi/\partial x$, and other inertial correction terms in the nonlinear Navier–Stokes equation. This approximation breaks down at the very high intensities in the bores of the trumpet and trombone when played very loudly [15.9], which results in shockwave propagation, with a transition from a relatively smooth to a very brassy sound (*son cuivré* in French). For the present, such corrections will be neglected.

The speed of sound in air depends on the temperature θ (degrees centigrade) and, to a lesser extent, on the humidity. For 50% humidity,

$$c_0(\theta) = 332 (1 + \theta/273)^{1/2} \approx 332(1 + 1.710^{-3}\theta), \quad (15.8)$$

giving a value of 343 m/s at 20 °C. Note that the air inside a woodwind or brass instrument, once the instrument is *warmed up*, will always be warm and humid, which will affect the playing pitch.

Pressure and Intensity

The intensity I of sound radiated by a musical instrument is given by the flow of acoustic energy ($1/2\rho v^2$ per unit volume) crossing unit area per unit time,

$$I = \frac{1}{2}\rho c_0 v_{\max}^2 = \frac{1}{2}z_0 v_{\max}^2 = \frac{1}{2z_0} p_{\max}^2. \quad (15.9)$$

Sound pressure levels (SPL) are measured in dB relative to a reference sound pressure p_0 of 2×10^{-5} Pa or N/m², so that $\text{SPL}(\text{dB}) = 20 \log_{10}(p/p_0)$. The reference pressure is approximately equal to the lowest level of sound that can be heard at around 1–3 kHz in a noise-free environment. Relative changes in sound pressure levels are given by $20 \log_{10}(p_1/p_2)$ dB. A sound pressure of 2×10^{-5} Pa is very close to an intensity of $I_0 = 10^{-12}$ W/m², which is used to define the almost identical intensity level, $\text{IL}(\text{dB}) = 10 \log_{10}(I/I_0)$. The difference between the factor 10 and 20 arises because sound intensity is proportional to the square of the sound pressure.

Spherical Waves

In free space, sound from a localised source will propagate as a spherical wave satisfying the three-dimensional wave equation (*Fletcher and Rossing* [15.5, Sect. 6.2]), with pressure

$$p(r) = A \frac{e^{i(\omega t - kr)}}{r} \quad (15.10)$$

and particle velocity

$$v(r) = \frac{A}{z_0} \left(1 + \frac{1}{ikr} \right) \frac{e^{i(\omega t - kr)}}{r}. \quad (15.11)$$

Near and Far Fields

Note that, unlike plane-wave solutions, the velocity and pressure differ in phase by an amount that depends on the distance from the source and the wavelength. Close to the source, in the *near field* ($kr \ll 1$), the pressure and induced velocity are in phase quadrature. Such terms therefore involve no work being done (proportional to $\int p v dt$) and hence no radiation of sound. The near-field term describes the motion of the air that is forced to vibrate backwards and forwards with the vibrating surface of the source, which simply adds inertial mass to the vibrating mode. This term is responsible for the *end correction* ($\Delta L \approx a$, where a is the pipe radius), which extends the effective length of an open-ended vibrating air column. The additional inertial mass also lowers the vibrational frequency of the relatively light vibrating membranes of a stretched drum skin.

In contrast, in the *far field* ($kr \gg 1$), the pressure is in phase with the velocity, so that work is done on the surrounding gas. This accounts for the fact that sound radiation varies in intensity as $1/r^2$.

The transition from the near- to far-field regions occurs when $r \approx \lambda/2\pi$, where λ is the acoustic wavelength of the radiated sound. At 340 Hz, this corresponds to a distance of only ≈ 15 cm. The difference in the frequency dependencies of the near- and far-field sound means that a violinist or piccolo player, with their ears relatively close to the instrument, experiences a rather different sound from that heard by the listener in the far field. However, for most musical instruments, the distance between the source of radiated sound and the player's head is already at least $\lambda/2$, so that even the player is in the *far field* ($kr > 1$), at least for the high-frequency partials of a musical tone.

Directionality and Multipole Sources

At very low frequencies, the acoustic wavelength λ is often considerably larger than the physical size of the radiating source (e.g. the open ends of woodwind and brass instrument bores and the body of most stringed instruments), which can then be considered as a point source radiating isotropically into space. However, as soon as the wavelength becomes comparable with the size of the radiating source, the radiated sound will acquire directional properties determined by the geometry of the instrument and the vibrational characteristics of the excited modes. The directional properties can then be described by treating the instrument as a superposition of monopole, dipole, quadrupole and higher-order multipole acoustic sources, with the directional radiating properties shown schematically in Fig. 15.2.

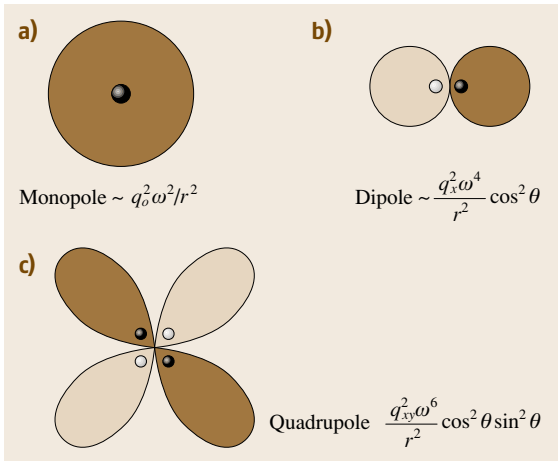


Fig. 15.2a–c Typical radiation patterns and intensities for (a) monopole, (b) dipole and (c) quadrupole sources. The two colours represent monopole sources and sound pressures of opposite signs

A monopole source can be considered as a pulsating sphere of radius a with surface velocity $v e^{i\omega t}$ resulting in a pulsating volume source $4\pi a^2 v e^{i\omega t} = Q e^{i\omega t}$. Equations (15.10) and (15.11) describe the sound field generated by such a source. Equating the velocities on the surface of the sphere to that of the induced air motion gives, at low frequencies such that $ka \ll 1$,

$$p(r, t) = \frac{i\omega\rho}{4\pi r} Q e^{i(\omega t - kr)}. \quad (15.12)$$

The radiated power P is then given by $\frac{1}{2} p^2 / \rho c_0$ integrated over the surface of a sphere at radius r , so that

$$P(ka \ll 1) = \frac{\omega^2 \rho Q^2}{8\pi c_0}. \quad (15.13)$$

In the high-frequency limit ($ka \gg 1$), when the acoustic wavelength is much less than the size of the sphere,

$$P(ka \gg 1) = \frac{\rho c_0}{8\pi a^2} Q^2 = 4\pi a^2 \frac{1}{2} z_0 v^2. \quad (15.14)$$

Equation (15.12) is a special case of the general result that, at sufficiently high frequencies such that the size of the radiating object $\gg \lambda$, the radiated sound is simply $\frac{1}{2} z_0 v^2$ per unit area, though the sound at a distance also has to take into account the phase differences from different parts of the vibrating surface. Note that

$$\frac{P(ka \ll 1)}{P(ka \gg 1)} = (ka)^2. \quad (15.15)$$

The radiated sound intensity from a monopole source therefore initially increases with the square of the fre-

quency but becomes independent of frequency above the crossover frequency when $ka > 1$. Hence members of the violin family and guitar families are rather poor acoustic radiators for the fundamental component of notes played on their lowest strings, as are wind and brass instruments, which radiate sound from the relatively small open ends and side holes. However, it is only because of such low radiation efficiencies, that strong resonances can be excited in the air columns of brass and woodwind instruments.

A dipole source can be formed by displacing two oppositely signed monopoles $\pm Q$ a short distance along the x -, y - or z -directions. For a dipole aligned along the x -axis of strength $q_x = Q \Delta x$. The sound pressure is simply the difference in pressure from monopoles of opposite sign a distance Δx apart, so that in the far field ($kr \gg 1$)

$$p(\theta)_{\text{dipole}} = p(\theta)_{\text{monopole}} \times (ik \Delta x) \cos \theta. \quad (15.16)$$

A polar plot of the sound pressure from a dipole is illustrated schematically in Fig. 15.2, with intensity and radiated power now proportional to ω^4 and q_x^2 . In general, any radiating three-dimensional object will involve three dipole components (p_x , p_y and p_z), with radiation lobes along the three directions.

A quadrupole source is generated by two oppositely signed dipole sources displaced a small distance along the x -, y -, or z -directions (e.g. of the general form $q_{xy} = Q \Delta x \Delta y$). The pressure is now given by the differential of the dipole radiation in the newly displaced direction, so that, for example, the pressure from a quadrupole source q_{xy} in the xy -plane is given by

$$p_{\text{dipole}} = p_{\text{monopole}} \times (-k^2 \Delta x \Delta y) \cos \theta \sin \theta, \quad (15.17)$$

as illustrated in Fig. 15.2. Note that each time the order of the multipole source increases, the radiated pressure depends on one higher power of frequency, while the intensity increases by two powers of the frequency. The radiated power from multipole sources therefore decreases dramatically at low frequencies relative to that of a monopole source. At low frequencies, radiation from most musical instruments is dominated by monopole components.

In general, six quadrupole sources (q_{xx}, \dots, q_{yz}) would be required to describe radiation from a three-dimensional source. However, because the acoustic power radiated by a quadrupole source at low frequencies is proportional to ω^6 , one need often only consider the monopole and three dipole components to describe

the low-frequency radiation pattern of instruments like the violin and guitar family, as described in a recent study of the low-frequency radiativity of a number of quality guitars by Hill et al. [15.10]. However, at high frequencies, when λ is comparable with or less than the size of an instrument, the above simplifications break down. The directionality of the radiated sound then has to be computed from the known velocities over the whole surface, taking into account phase differences and baffling effects from the body of the instrument.

Radiation from Surfaces

Many musical instruments produce sound from the vibrations of two-dimensional surfaces – like the plates of a violin or the stretched membrane of a drum. Imagine first a standing wave set up in the two-dimensional xy -plane with displacements in the z -direction varying as $\sin(k_x x) e^{i\omega t}$. We look for propagating sound waves solutions radiating from the surface of the form $\sin(k_x x) e^{i(\omega t - k_z z)}$, which must satisfy the wave equation and hence the relationship,

$$k_z^2 = \frac{\omega^2}{c_0^2} - k_x^2 = \omega^2 \left(\frac{1}{c_0^2} - \frac{1}{c_m^2} \right), \quad (15.18)$$

where c_m is the phase velocity of transverse waves on the membrane or plate in the xy -plane. Sound will therefore only propagate away from the surface ($k_z^2 > 0$)

when $c_m > c_0$. If the sound velocity is greater than the phase velocity in the plate or membrane, energy will flow from regions of positive to negative vertical displacements and vice versa, with an exponentially decaying sound field, varying as $e^{-z/\delta}$ where $\delta = |k_z|^{-1}$.

Typical dispersionless wave velocities for the stretched drum heads of timpani are around 100 m/s (Fletcher and Rossing [15.5, Sect. 18.1.2]), so that they are not very efficient radiators of sound. This is particularly relevant for asymmetrical modes, when sound energy can flow from the regions of positive to negative displacement and vice versa. However, for even modes, the cancellation between adjacent regions moving out of phase with each other can never be complete, so that such modes will radiate more effectively.

A particularly interesting case occurs for stringed instruments, where the phase velocity of the transverse vibrations of the thin front and back plates increases with frequency as $\omega^{1/2}$ (Sect. 15.2.6). Hence, below a critical crossover or coincidence frequency, when the phase velocity in the plates is less than the speed of sound in air, standing waves on the vibrating plates are relatively inefficient radiators of sound, while above the crossover frequency the plates radiate sound rather efficiently. Cremer [15.11] estimates the critical frequency for a 4 mm-thick cello plate as 2.8 kHz; for a 2.5 mm violin plate the equivalent frequency would be ≈ 2 kHz.

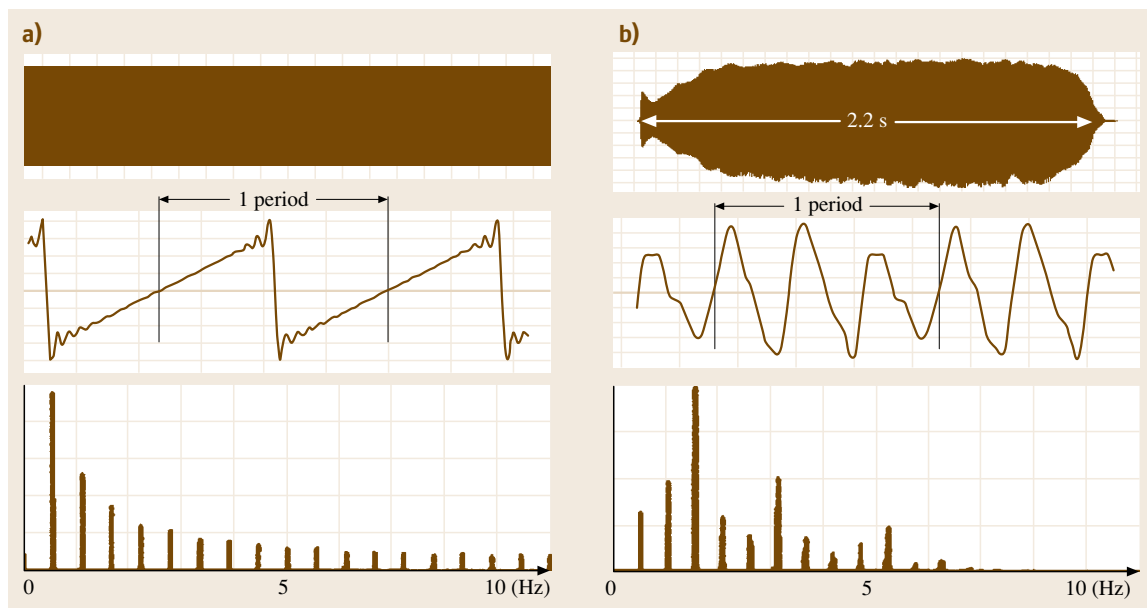


Fig. 15.3a,b Comparison of the envelope, repetitive waveform and spectrum of (a) a synthesised sawtooth and (b) a note played on an oboe

Radiation from Wind Instruments

The holes at the ends or in the side walls of wind instruments can be considered as piston-like radiation sources. At high frequencies, such that $ka \gg 1$, where a is their radius, the holes will be very efficient radiators radiating acoustic energy $\approx 1/2z_0v^2$ per unit hole area. However, over most of the playing range $ka \ll 1$, so that the radiation efficiency drops off as $(ka)^2$, just like the spherical monopole source. Most of the sound impinging on the end of the instrument is therefore reflected, so that strong acoustic resonances can be excited, as discussed in the later section on woodwind and brass instruments.

15.1.3 The Anatomy of Musical Sounds

The singing voice, bowed string, and blown wind instruments produce continuous sounds with repetitive waveforms giving musical notes with a well-defined sense of musical pitch. In contrast, many percussion instruments produce sounds with nonrepetitive waveforms composed of a large number of unrelated frequencies with no definite sense of pitch, such as the side drum, cymbal or rattle. There are also other stringed instruments and percussion instruments, such as the guitar, piano, harp, xylophone, bells and gongs, which produce relatively long sounds, where the slowly decaying vibrations produce a definite sense of pitch.

In all such cases, the complexity of the waveforms of real musical instruments distinguishes their sound from the highly predictable sounds of simple electronic synthesisers. This is why the sounds of computer-generated synthesised instruments lack realism and are musically unsatisfying. In this section, we introduce the way that sound waveforms are analysed and described.

Sinusoidal Waves

The most important, but musically least interesting, waveform is the pure sinusoid. This can be expressed in several alternative forms,

$$a \cos(2\pi ft + \phi) = a \cos(\omega t + \phi) = \operatorname{Re}(a e^{i\omega t}), \quad (15.19)$$

where a is in general complex to account for phase, f is the frequency measured in Hz and equal to the inverse of the period T , $\omega = 2\pi f$ is the angular frequency measured in radians per second, t is time, and ϕ is the phase, which depends on the origin taken for time.

Any sound, however complex, can be described in terms of a superposition of sinusoidal waveforms with a spectrum of frequencies. Figure 15.3 contrasts the envelopes, waveforms and spectra of a synthesised

sawtooth waveform and the much more complex and musically interesting waveform of a note played on the oboe (I3) EXTRAS provides an audio comparison). Note the much more complex fluctuating envelope and less predictable amplitudes of the frequency components in the spectrum of the oboe.

As we will show later, in defining the sound and quality of any musical instrument, the shape and fluctuations in amplitude of the overall envelope are just as important as the waveform and spectrum.

Range of Hearing and Musical Instruments

A young adult can usually hear musical sounds from around 20 Hz to 16 kHz, with the high-frequency response decreasing somewhat with age (typically down to between 10–12 kHz for 60-year olds). Audio I3) EXTRAS provides a sequence of 1 s-long sine waves starting from 25 Hz to 12.8 kHz, doubling in frequency each time. Doubling the frequency of a sinusoidal wave is equivalent in musical terms of increasing the pitch of the note by an octave. Audio I3) EXTRAS is a similar sequence of pure sine waves from 8 kHz to 18 kHz in 2 kHz steps. Any loss of sound at the low frequencies in I3) EXTRAS will almost certainly be due to the limitations of the reproduction system used, which is particularly poor below ≈ 200 Hz on most PC laptops and notebooks, while the decrease in intensity at high frequencies in I3) EXTRAS simply reflects the loss of high-frequency sensitivity of the ear (see Fig. 15.16 and Chap. 13 for more details on the amplitude and frequency response of the human ear).

The above sounds should be compared with the much smaller range of notes on a concert grand piano, typically from the lowest note A0 at 27.5 Hz to the highest note C9 at 4.18 kHz, as illustrated in Fig. 15.4. The nomenclature for musical notes is based on octave sequences of C-major scales with, for example, the note C1 followed by the white keys D1, E1, F1, G1, A1, B1, C2, D2, Alternatively, the octave is indicated by a subscript (e.g. A₄ is concert A). Where the white notes are a tone apart, a black key is inserted to play the semitone between the adjacent white keys. This is indicated by the symbol # from the note below or b from the note above. Figure 15.4 also illustrates the playing range of many of the instruments to be considered in this chapter.

Frequency and Pitch

It is important to distinguish between the terms frequency and pitch. The frequency of a waveform is strictly only defined in terms of a continuous sinusoidal waveform. In contrast, the waveforms of real musical

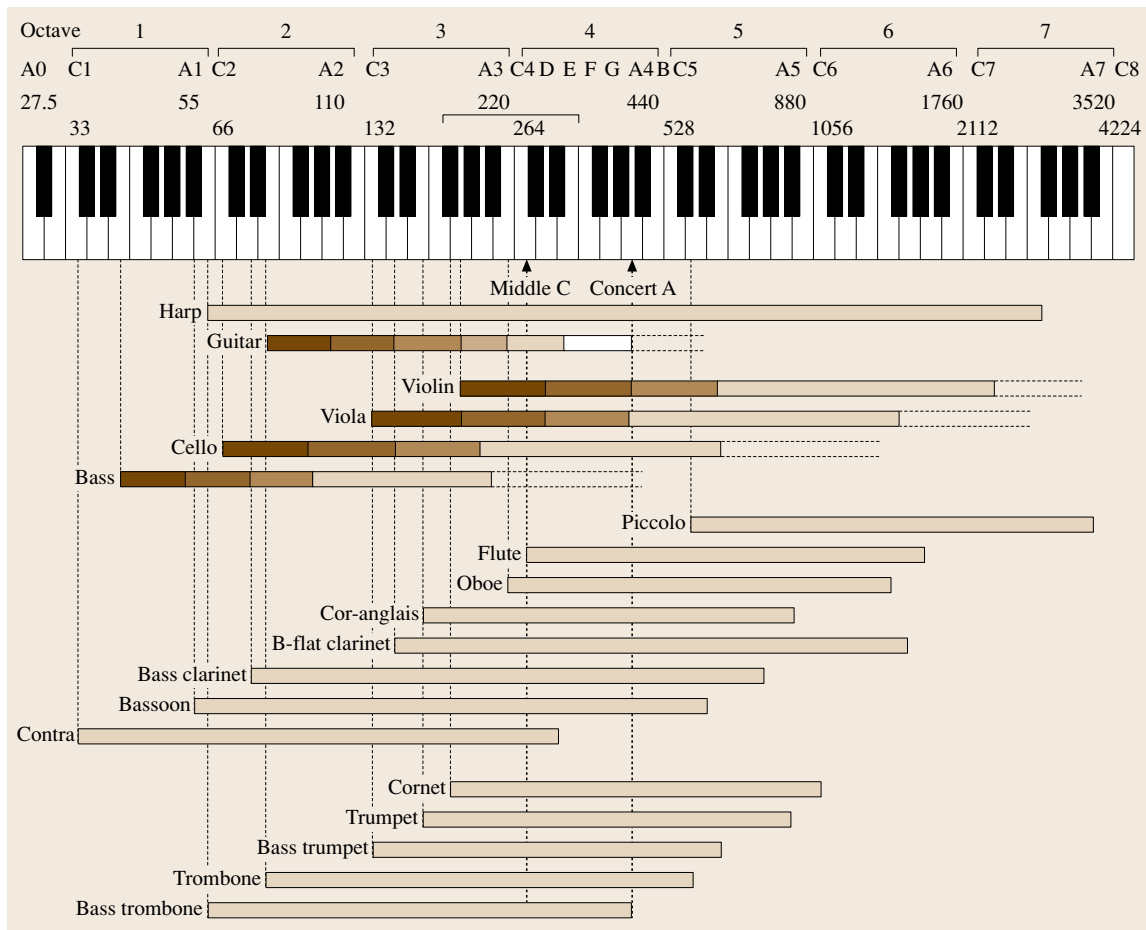


Fig. 15.4 Notation used for notes of the musical scale and the playing range of classical western musical instruments. Subdivisions for stringed instruments represent the tuning of the open strings

instruments are in general complex, as illustrated by the oboe waveform in Fig. 15.3. However, despite such complexity, the repetition frequency and period T can still be defined provided the waveform does not vary too rapidly with time. The periodicity of a note (measured in Hz) can then be defined as the inverse of T . This is generally the note that the player reads from the written music. However, as described later, a repetitive waveform does not necessarily include a sinusoidal component at the repetition frequency, an effect referred to as the *missing fundamental*. Furthermore, depending on the strength of the various sinusoidal components present, there can often be an ambiguity in the pitch of a note perceived by the listener. The subjective pitch, when matched against a pure sinusoidal wave, can often be an octave below or above the repetition frequency.

The subjective pitch, as its name implies, can differ from person to person and within the musical context of the note being played.

Musical Intervals and Tuning

In western music the octave interval is divided into six tones (a whole-tone scale) and 12 semitones (the chromatic scale). Today, an equal temperament, logarithmic scale is used to tune a piano, with a fractional increase in frequency of $2^{1/12} = 1.059$ ($\approx 6\%$) between any two notes a semitone apart. The fractional increase between the frequencies of a given musical interval (a given number of semitones) is then always the same, whatever the starting note. Twelve successive semitones played in sequence therefore raises the frequency by an octave ($(2^{1/12})^{12} = 2$). Any music played on the piano key-

board can therefore be transposed up or down by a given number of semitones, changing the pitch but leaving the relationship between the musical intervals unchanged. Such a scale was advocated as early as 1581, in a treatise by the lutenist Vincenzo Galileo (the father of Galileo Galilei). Although it is sometimes claimed that Bach exploited such a tuning in his 48 Preludes and Fugues, which uses all possible major and minor keys of the diatonic scale, historical research now suggests that Bach used a form of mean-tone tuning, which preserved some of the characteristic qualities of music written in particular keys [15.1].

To provide a greater discrimination in the measurements of frequency, the semitone is divided into 100 further logarithmic increments called cents. The octave is therefore equivalent to 1200 cents and a quarter-tone to ≈ 50 cents, with the exact relationship between frequencies given by

$$\text{interval} = \frac{1200}{\ln 2} \ln(f_2/f_1) \text{ cents} \quad (15.20)$$

corresponding to $\approx 1.73 \times 10^3 (\Delta f/f)$ cents for small fractional changes $\Delta f/f$.

Early musical scales were based on various variants of the natural harmonic series of frequencies, $f_n = n f_1$, where n is an integer (e.g. 200, 400, 600, ... 1600 Hz), illustrated by the audio [🔊 EXTRAS](#). These notes correspond to the *harmonics* produced when lightly touching a bowed string at integral subdivisions of its length (1/2, 1/3, 1/4, etc.) [🔊 EXTRAS](#). These simple divisions give successive musical intervals of the octave, perfect fifth, perfect fourth, major third and minor third, with frequency ratios 2/1, 3/2, 4/3, 5/4 and 6/5, respectively. The seventh member of the harmonic sequence has no counterpart in traditional western classical music, although it is sometimes used by modern composers for special effect [15.12].

Just temperament corresponds to musical scales based on these integer fraction intervals. The Pythagorean scale is based on the particularly consonant intervals of the octave (2/1) and perfect fifth (3/2), which can be used to generate individual intervals of the form $3^p/2^q$ or $2^p/3^q$, where p and q are positive integers. Although the Pythagorean and just-tempered scales coincide for the octave, perfect fifth and fourth, there are musically significant differences in the tuning for all other defined intervals, and all intervals other than the octave differ slightly from those of the equally tempered scale. A comparison between the musical intervals of just and equal temperament tuning is shown in Table 15.1, with the fractional mistuning indicated

Table 15.1 Principal intervals and differences between just- and equal-temperament intervals

Interval	Just	Equal	$\Delta f/f$ Just-equal cents
Octave	2/1	2.00	0
Perfect fifth	3/2	$2^{7/12} = 1.498$	+2
Perfect fourth	4/3	$2^{5/12} = 1.334$	-2
Major third	5/4	$2^{4/12} = 1.260$	-13
Minor third	6/5	$2^{3/12} = 1.189$	+15
Tone	9/8	$2^{2/12} = 1.122$	-4
Semitone	16/15	$2^{1/12} = 1.066$	+1

in cents. Because of the differences in tunings of the musical intervals, music transposed from one key to another will generally sound badly out of tune (particularly for commonly used intervals like the major and minor third) – unlike those played on a modern equal-tempered keyboard. Prior to the now almost universal practice of tuning keyboard instruments to a equal-tempered scale, many tuning schemes were devised which partially overcame the problems of tuning when playing in a succession of different keys (see *Fletcher* and *Rossing* [15.5, Sect. 17.6] and *Barbour* [15.13] for further discussion). Singers, stringed and wind instrument players can adjust the pitch of the notes they produce to optimise the tuning with other performers and for musical effect.

Figure 15.5 and audio [🔊 EXTRAS](#) illustrate the difference in the sounds of a major triad formed from the just intervals (1, 5/4, 3/2) and the equivalent equal-tempered scale intervals (1 : 1.260 : 1.498). The rational Pythagorean intervals give a repetitive waveform of constant amplitude, while the less-consonant, inharmonic, equal-tempered intervals have a nonrepetitive




Fig. 15.5 Wave envelope of a major triad chord based on the just tuning scale followed by the same chord on the equal-tempered scale, with pronounced beats in the amplitude arising from the departures from harmonicity in the frequencies of the major third and perfect fifth

waveform with an easily discernable periodic beat in amplitude resulting from the departures in harmonicity of its component frequencies, as illustrated in Fig. 15.5. Interestingly, the pitch of the equally tempered intervals also sounds slightly higher, though both share the same fundamental.

A sequence of upward fifths (frequency ratio $3/2$) and downward octaves (ratio $1/2$) can be used to fill in all the semitones of an octave scale on the piano keyboard. However, the resulting octave formed from a succession of 12 upward fifths and six downward octaves gives a frequency ratio of $(3/2)^{12}/2^6 = 2.027$, which is significantly *sharper* (higher in frequency) than a true octave. In practice, a skilled piano tuner listens to the beats produced when playing the above intervals and tunes the upward fifth slightly flat, so that the sequence returns to the exact octave. However, there are striking psychoacoustic effects, in addition to physical shifts in the frequencies of upper partials arising from the finite rigidity of the strings, which result in pianos being tuned on a slightly stretched tuning scale with the octaves purposely tuned sharp at higher frequencies and flat at lower frequencies (Fletcher and Rossing [15.5, Sect. 12.8]).

Repetitive Waveforms

Before considering the more complex waveforms of musical instruments, we consider the simple square, triangular, sawtooth and triangular repetitive waveforms (audio  EXTRAS) and the corresponding Fourier spectra illustrated in Fig. 15.6.

Fourier Theorem

Fourier showed that any repetitive waveform, $f(t + nT) = f(t)$, can be described as a linear combination of sinusoidal components with frequencies that are exact multiples of the inverse repetition period T or physical pitch of the wave. This is formally expressed by the Fourier theorem,

$$f(t) = \sum_{n=-\infty}^{\infty} c_n e^{in\omega_1 t}, \quad (15.21)$$

where $\omega_1 = 2\pi/T$ and

$$c_n = \frac{1}{T} \int_0^T f(t) e^{-in\omega_1 t} dt, \quad (15.22)$$

where n takes on all positive and negative integer values. The Fourier coefficients c_n can be evaluated by performing the integral over any single period of the waveform. In general, the Fourier coefficients will have

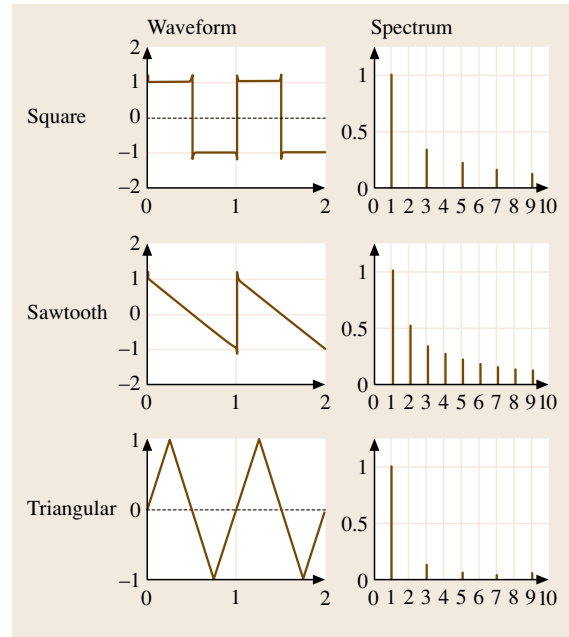


Fig. 15.6 Typical repetitive waveforms (synthesised from the first 100 components of a Fourier series) and the amplitudes of the first few partials normalised to the amplitude of the fundamental

both real and imaginary components describing both the amplitude and phase.

For simple waveforms, such as the square, sawtooth and triangular waveforms, the origin of time can be chosen to make the waveforms symmetric or antisymmetric in time. The Fourier expansion can then be expressed in terms of the even cosine or odd sine functions,

$$f(t) = \sum_{n=0}^{\infty} \left\{ \begin{array}{l} a_n \sin(n\omega_1 t) \\ \text{or} \\ b_n \cos(n\omega_1 t) \end{array} \right\}, \quad (15.23)$$

with corresponding coefficients given by

$$\begin{pmatrix} a_n \\ b_n \end{pmatrix} = \frac{2}{T} \int_0^T f(t) \begin{pmatrix} \sin(n\omega_1 t) \\ \cos(n\omega_1 t) \end{pmatrix} dt, \quad (15.24)$$

where n is now restricted to positive integer values. The factor 2 is replaced by unity for the zero frequency average component b_0 .

The first few terms of the square, sawtooth and triangular waveforms are listed in Table 15.2. The origin of time has been selected to make the waves odd-functions of time, as illustrated in Fig. 15.6, with the Fourier series only including sine terms. The Fourier compo-

nents at integral multiples of the fundamental repetition frequency are referred to as partials, harmonics, or overtones. The n th partial has a frequency $f_n = n f_1$. This differs from the terminology used by musicians, who refer to f_2 as the first harmonic or overtone. Interestingly, a waveform depends critically on the sign (phase) of the individual Fourier components. In contrast, the ear is largely insensitive to the phase of the individual partials, with little change in the perceived sound when the sign or phase of a component partial is changed, though the waveforms will be very different.

For an arbitrarily chosen origin of time, the Fourier expansion will include both sine and cosine terms. The energy or intensity is proportional to the resultant amplitudes squared, $a_n^2 + b_n^2$, which is independent of the origin of time. The phase ϕ_n is given by $\tan^{-1}(b_n/a_n)$. The spectrum of a waveform is often plotted in terms of the modulus of the amplitude as a function of frequency, without reference to phase, as in Fig. 15.6. However, measurements of both amplitude and phase are important in any detailed comparison with theoretical models and in analytic measurements, such as modal analysis.

The square and sawtooth waveforms are closely related to the waveforms excited on bowed and plucked

Table 15.2 Fourier expansions of the square, sawtooth and triangular waveforms

Square	$\frac{4}{\pi} \left(\sin \omega_1 t + \frac{1}{3} \sin 3\omega_1 t + \frac{1}{5} \sin 5\omega_1 t \dots \right)$
Sawtooth	$\frac{2}{\pi} \left(\sin \omega_1 t - \frac{1}{2} \sin 2\omega_1 t + \frac{1}{3} \sin 3\omega_1 t - \frac{1}{4} \sin 4\omega_1 t \dots \right)$
Triangular	$\frac{2}{\pi} \left(\sin \omega_1 t - \frac{1}{3^2} \sin 3\omega_1 t + \frac{1}{5^2} \sin 5\omega_1 t \dots \right)$

strings and loudly played notes on wind and brass instruments. The discontinuities in waveform generate a very rich harmonic spectrum with Fourier components or partials that decrease relatively slowly (as $1/n$) with increasing n . The strong higher partials give a much harsher and more penetrating sound than simple sinusoids, which is why the oboe, which has a sound that is very rich in higher partials, is used to sound concert A when an orchestra tunes up. In contrast, the partials of the triangular wave, with discontinuities in slope instead of amplitude, decrease more rapidly as $1/n^2$, with a resultant sound little different from that of a simple sinusoidal wave.

Note the large difference between the sound of a sawtooth waveform, which is closely related to the

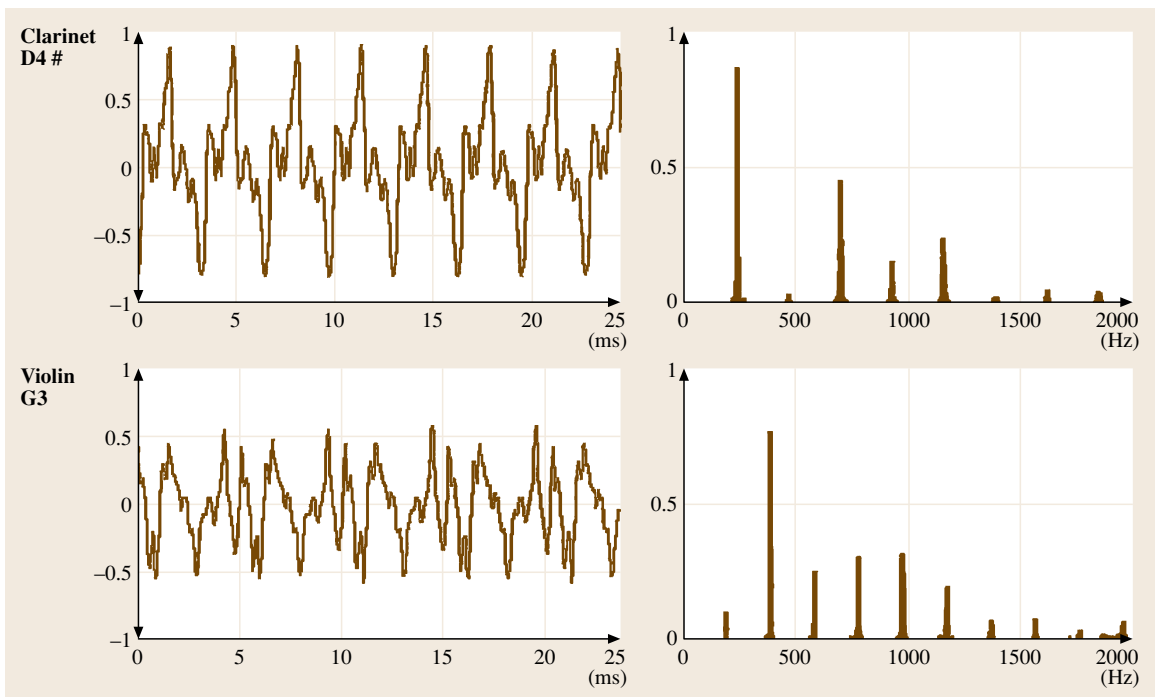



Fig. 15.7 Short-period samples of clarinet (D#4) and bowed violin (G3) tones and the corresponding Fourier spectra. The vertical scales are linear

sound of an oboe in having a complete set of harmonic components, and the *hollow* sound of the square waveform, which is more like the sound of the lowest notes on a clarinet, with rather weak even-integer harmonics or overtones on its lowest notes (Fig. 15.7).

Musical Waveforms and Spectra

The waveforms produced by musical instruments are generally far more complicated than the above simple examples, as already illustrated for an oboe note in Fig. 15.3. Waveforms and associated spectra of the clarinet note D#4 (309 Hz) and the violin bowed open-G-string G3 (195 Hz) are illustrated in Fig. 15.7. These are simply representative waveforms. Unlike the impression given in some elementary textbooks, there is no such thing as a defining violin or clarinet waveform or spectrum. Both the waveforms and the spectra change significantly from one note to the next – and even within a note when played with vibrato, particularly on stringed instruments. Despite the complexity of the waveforms, any repetitive waveform can be described as a linear superposition of sine waves, with frequencies that are integer multiples of the fundamental, as illustrated by the spectra.

Plotting the amplitudes of the Fourier coefficients on a linear scale often highlights the physical processes involved in the production of the sound. For example, the relatively small amplitudes of the second harmonic or partial in the sound of the clarinet reflects the absence of even- n modes of a cylindrical tube closed at one end, which approximates to that of the clarinet. Similarly, the small amplitude of the first partial in the sound of a violin reflects the absence of efficient radiating modes at low frequencies. However, because of the very wide dynamic range of hearing (a factor of $\approx 10^{10}$ – 10^{12} in intensity), it is often more appropriate to plot the Fourier coefficients in decibels on a logarithmic scale. Figure 15.8 shows the spectrum for clarinet and violin notes re-plotted on a dB scale, which illustrates the strength of all the partials over a very wide dynamical range. For bowed instruments such as the cello, well over 40 harmonic partials can be identified below 8 kHz. The sound of an instrument will be determined by all such components and not simply by the fundamental, which may make a relatively small contribution to the perceived sound. This is illustrated for a scale played on the violin with each note first played as recorded and then with the fundamental component removed by a digital filter (audio  EXTRAS). The lowest notes of the scale, for which the fundamental component is already very weak, are little affected by the removal of the fundamental com-

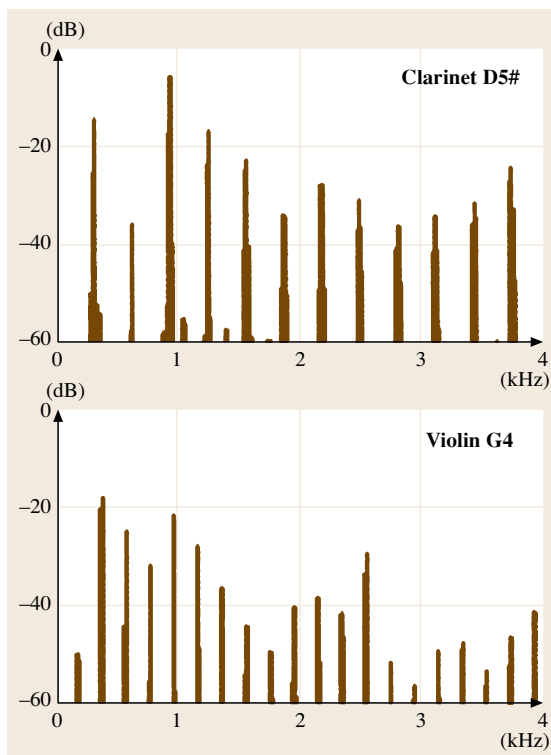


Fig. 15.8 Typical spectra for a clarinet and violin note plotted on a dB scale illustrating the large number of harmonics or overtones excited by bowed and blown instruments

ponent; however, the sound gets progressively *thinner* in the second half of the scale for notes for which the fundamental partial makes an increasingly significant contribution to the *richness* or *warmth* of the sound.

Transient and Non-Repetitive Tones

No musical note lasts for ever, so that musical sounds are all, to some extent, transient. Moreover, the sound of many percussion instruments is composed of many strongly inharmonic partials, with no regime in which the waveforms can be considered even quasi-repetitive. Nevertheless, one can still use the Fourier theorem to extract the spectrum of such a note, by considering each transient signal as one of a sequence of such transients repeated, say, every second, minute or even year. The spectrum of such a repeated waveform will therefore involve frequency components at integer multiples of the inverse repetition period, which we can make as long as we choose. In the limit of infinitely long repetition times, the Fourier series of a nonrepeating waveform can therefore be replaced by a continuous spectral dis-

tribution over all possible frequencies, known as the Fourier transform $F(\omega)$,

$$f(t) = \int_{-\infty}^{\infty} F(\omega) e^{i\omega t} dt, \quad (15.25)$$

where

$$F(\omega) = \frac{1}{2\pi} \int_{-\infty}^{\infty} f(t) e^{-i\omega t} dt. \quad (15.26)$$

The Fourier transform spectra of important nonrepetitive waveforms are shown in Fig. 15.9. In all cases,

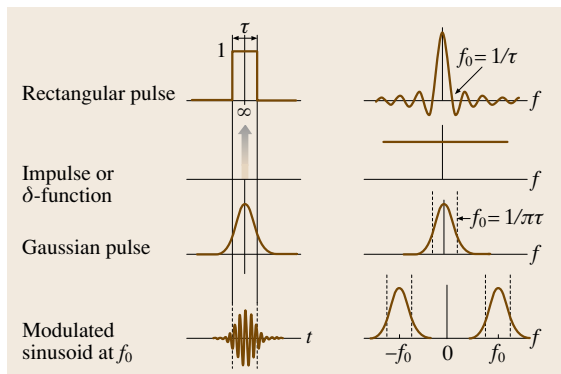


Fig. 15.9 Fourier transforms of transient waveforms

the width Δf of the Fourier spectrum is inversely proportional to the length τ of the input waveform, with $\Delta f \tau \approx 1$. For a rectangular pulse, the spectrum extends over a rather wide frequency range with the first zero when $f\tau = 1$, but with many ripples of decreasing amplitude extending to higher frequencies. For an impulse of negligible width (the delta-function), the spectrum is flat out to very high frequencies. The spectrum of a Gaussian waveform varying as $\exp[-(t/\tau)^2]$ is also a Gaussian proportional to $\exp[-(\pi f\tau)^2]$, with a width $\Delta f = 1/\pi\tau$. Similarly, the spectrum of a sinusoidal waveform with a Gaussian envelope of width τ is broadened by $\Delta f = 1/\pi\tau$.

Any waveform that involves variations on a time scale τ will have Fourier components extending out to frequencies $\approx 1/\tau$. To reproduce such waveforms faithfully, the bandwidth of any recording or reproduction system must therefore extend to frequencies of at least $1/\tau$. Examples of nonrepetitive waveforms and their associated spectra are illustrated in Fig. 15.10 for an orchestral rattle, a cymbal crash and timpani.

The ratchet sound consists of a sequence of short *clicks* illustrated by the selected short-section waveform. The spectrum is very broad with no individual frequencies particularly dominant. The crash of a cymbal generates a very large number of very closely spaced resonances, which appear as a fairly random set of

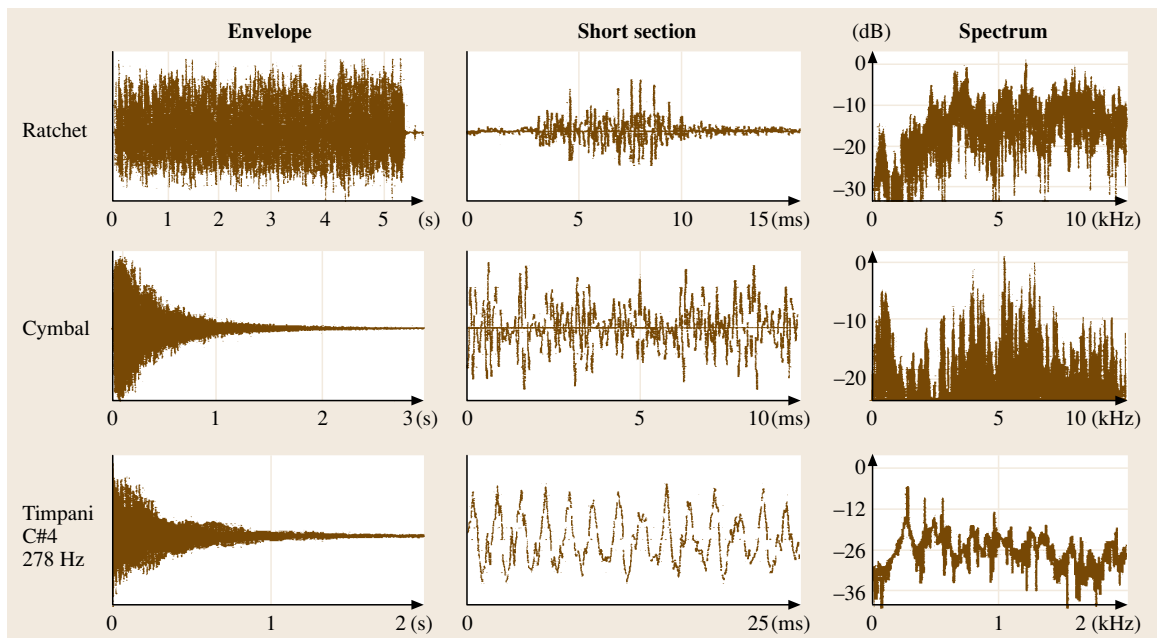


Fig. 15.10 Envelope, typical short-period waveform and spectrum for the sounds of a ratchet, cymbal and timpani

peaks giving an overall broadband spectrum. The timpani spectrum shows a small number of large peaks corresponding to the prominent modes of vibration of the drum head, superimposed on a very wide-band spectrum largely associated with the initial transients involving sound from all parts of drum.

Digital Recording

Nowadays almost all sound is recorded digitally using an analogue-to-digital converter (ADC). This converts the continuously varying analogue input signal into a stream of numbers, which can be recorded digitally on a computer or compact disc. Audio signals are typically recorded at a sampling rate of 44.1 kHz with 16-bit resolution corresponding to 1 part in 2^{16} . This allows signals to be recorded in 65 536 equally divided levels between the maximum positive and negative input signals (i. e. between ± 32.8 k levels).

For the highest-quality digital recordings, even faster recording rates with higher-bit resolution are used (typically 24-bit sampling at 96 kHz). This allows for over-sampling of the recorded signal, so that signals can be averaged, any errors detected and eliminated, and filtered more easily. As already noted, the dynamic range of human hearing can be as large as 100 dB. To exploit such a large range and to capture the details of both loud and soft sounds from a large orchestra accurately requires the recording system to have a large dynamic range. Table 15.3 shows the dynamic range in terms of the number of bits used to record the sound. Audio [EXTRAS](#) illustrates the greatly enhanced signal-to-noise ratio and hence increased dynamic range when sound is recorded at 16-bit rather than 8-bit resolution.

Aliasing

When sound is recorded digitally, ambiguities can arise when any of the input frequencies is larger than half the sampling rate f_D . This is known as the Nyquist limit $f_{\text{Nyquist}} = f_D/2$. For example, if a 2 kHz sine wave were to be sampled at 2 kHz, the digital signal would be recorded at exactly the same point of the waveform each cycle. The recorded digital signal would then be

indistinguishable from a DC signal. It can easily be shown that sinusoidal inputs at $f_{\text{Nyquist}} + \Delta f$ give the same digital output as at $f_{\text{Nyquist}} - \Delta f$ and that the recorded signal is the same for all frequencies differing in frequency by the digitising frequency, $2f_{\text{Nyquist}}$. Thus for a steadily increasing input frequency the digital output is equivalent to that of a frequency which first increases up to f_{Nyquist} then decreases to zero when $f_{\text{in}} = f_D = 2f_{\text{Nyquist}}$, with the process repeating for higher input frequencies, as illustrated in Fig. 15.11. In any replay system, an analogue output is generated that assumes a smooth curve between the sampled points. Hence, recorded frequencies above the Nyquist limit will be misinterpreted and will produce sounds below f_{Nyquist} with no harmonic relevance to the original input.

This ambiguity is illustrated in audio [EXTRAS](#), in which a sinusoidal input is swept in frequency from 200 Hz to 6 kHz. This is first recorded at 22.05 kHz, when aliasing is not a problem, and then at 6 kHz, when halfway through the increasing frequency signal, at 3 kHz, the replayed sound starts to descend to zero frequency at the end of the sweep, when the input signal has the same frequency as the sampling rate. The single-frequency sweep is then followed by an ascending major triad (with intervals in the ratios 1 : 5/4 : 3/2) recorded at 6 kHz, which illustrating the severe problems of aliasing in terms of musical harmonies, as soon as any of the higher-frequency components in a signal exceed the Nyquist limit, with the frequency of some partials ascending while others are descending.

To avoid such problems, a high-frequency cut-off input filter is generally used, with a cut-off frequency slightly below the Nyquist frequency (see Chap. 14 by Hartmann for further details).

Table 15.3 Dynamic range of an analogue-to-digital converter (ADC)

N-bit ADC	Dynamic range $\pm 2^{n-1}$	Dynamic range (dB)
8 bit	128	42
16 bit	32.8 k	90
24 bit	8.39 M	138

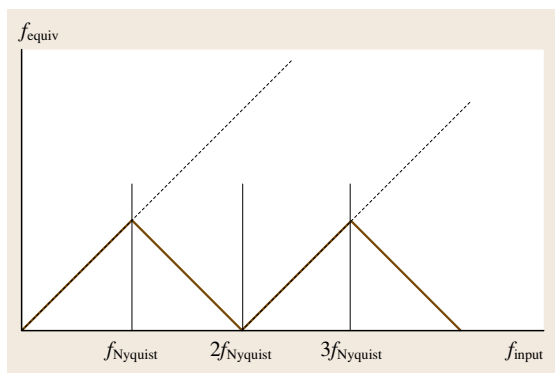


Fig. 15.11 Ambiguity of digital output for a steadily increasing frequency exceeding the Nyquist limit

Table 15.4 Decoded WAVE file information

Data provided	Typical example
Mono (1), stereo (2)	2
Data acquisition rate	2.205×10^4
Resolution in bits	16
Data per second	4.41×10^4
First measurement from left channel	237
Simultaneous measurement from right channel	-1356
Second measurement from left channel	456
Simultaneous measurement from right channel	-1972
Repeated sequence until end of recorded sound	...

Sound File Formats

A sound signal is frequently recorded and stored as an encoded WAVE file of the generic form *.wav, which includes additional information on data acquisition rate, stereo or mono format and bit resolution. The decoded structure of a WAVE file is shown in Table 15.4.

Recording audio signals as WAVE files is very expensive in memory, with 1 hour of stereo music recorded at 22 kHz requiring ≈ 300 MB. Music files on CDs are encoded so that the input is redistributed over time and therefore over the surface of the disc. This enables the original signal to be reproduced even in the presence of dust, scratches and other small imperfections on the disc surface, eliminating the clicks that were a familiar feature of older vinyl records. More sophisticated, adaptive, encoding schemes can be used to significantly reduce the amount of memory used, such as the now widely used mp3 format. An algorithm is used, based on physical principles and on the way the ear responds to musical sounds, to continuously analyse and process the incoming data. The input data can then be recorded using a much reduced number of bits, in much the same sort of way that digital pictures are encoded more efficiently in ZIP files and compact image formats. The information used to encode the digital signal is also recorded, so that the processed data can be unscrambled on playback with relatively little loss in perceived quality.

Discrete Fourier Transform

The digital form of the recorded data allows certain computational efficiencies in calculating the Fourier spectrum. Consider a recorded sample of N measurements, corresponding to a sample of length $T_s = N/f_D$. To calculate the spectrum, this data set is

assumed to repeat indefinitely, to form a continuous waveform with a repetition frequency. From the Fourier theorem, the resulting spectrum is composed of Fourier components that are exact multiples of the repetition frequency, so that $f_n = n/T_s$. Hence, a 1 s set of data points will give a discrete Fourier spectrum with frequencies at 1, 2, ... n... Hz. In practice, the number of Fourier components is limited to $N/2$, because each component has both an amplitude and a phase, which requires at least two independent measurements to be made per Fourier component.

Windowing Functions

Using the sampled waveform to form a continuously repeating waveform will, in general, introduce a repeating discontinuity Δ at the beginning and end of each repeated data set, since the start and end values will not usually be the same. Any such discontinuity will generate spurious contributions to the spectrum, with additional Fourier coefficients with amplitudes proportional to Δ/n . To circumvent this problem, a *windowing function* is used. This applies a smooth envelope to the data set, which reduces the values at the start and end to zero, thus eliminating the discontinuities. However, as described above, the application of such an envelope will give an extra width $\Delta f \approx 1/T_s$ to the spectral features.

A typical windowing function is the Hanning function $\sin^2(2\pi t/T_s)$. A number of other windowing functions are illustrated in Fig. 15.12, each of which has advantages for specific applications [15.14]. The Hanning windowing is widely used for general-purpose measurements, while the Hamming function is used to separate closely spaced sine waves. In general there is a trade-off between the accuracy that can be achieved in

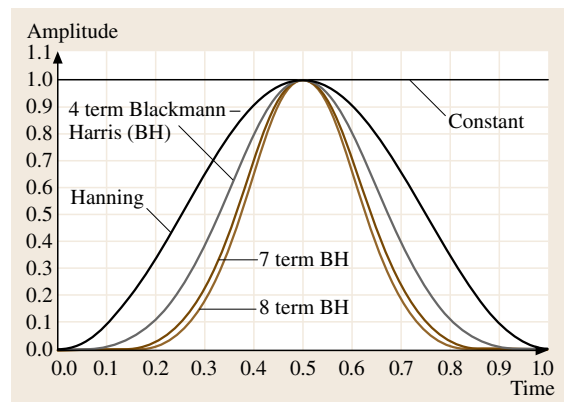


Fig. 15.12 Representative windowing functions (after [15.14])

determining the frequency of individual spectral components and the width of the low-amplitude side lobes generated by application of a windowing function. Various forms of the Blackman–Harris windowing function can be used to optimise the fast Fourier transform (FFT) for specific measurements. Windowing need not be used for the accurate measurements of widely separated sinusoidal waves with similar amplitudes, though one should be aware of the existence of the rather wide side lobes generated unless the sampling period is an exact integer multiple of the period of the waveform being measured.

Fast Fourier Transform (FFT)

To determining the amplitude and phase of the $N/2$ Fourier components from N input measurements requires the inversion of an $N \times N$ matrix, requiring a computation time proportional to N^2 . However, if N is an integral power of 2 (e.g. $2^8 = 256$, $2^{16} = 65\,536$), the FFT computing algorithm can be used to reduce the computing time by many orders of magnitude (by

a factor $\approx N/\log N$). The speed of modern computers is such that FFT spectra of the sound of musical instruments can be calculated and displayed with delays of only a few milliseconds, though any such delay will always be limited by the length and hence frequency resolution of the data set being analysed.

A typical implementation of the FFT method for spectral analysis is shown schematically in Fig. 15.13. An input anti-aliasing filter is first used to remove frequency components above the Nyquist limit $f_D/2$; an ADC then converts the incoming signal to a digital output to give a data set of $N = 2^n$ measurements over a time $T = N/f_D$. A windowing function removes problems from discontinuities at the start and end of the recorded set of data, and the computer evaluates the FFT giving the amplitudes and phases of the Fourier components at $N/2$ discrete frequencies spaced $1/T = f_D/N$ Hz apart.

A sequence of FFTs from data taken over successive short periods of time can be used to illustrate the decay of individual partials in transient and decaying waveforms, such as those of a plucked string, a piano note or struck bell, as illustrated for the sound of a plucked violin A-string in Fig. 15.14.

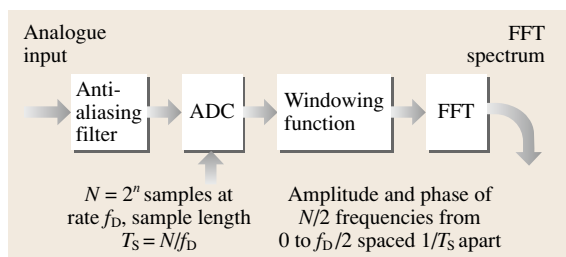


Fig. 15.13 A typical digital sampling and FFT analysis scheme

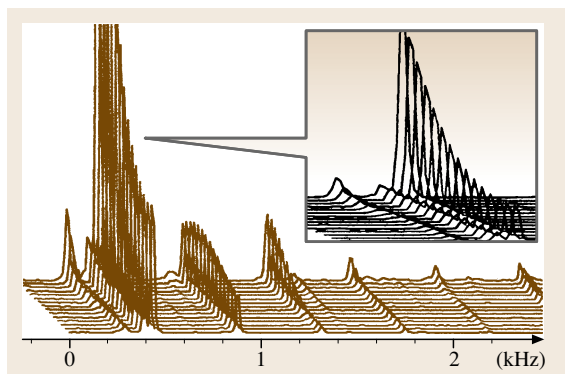


Fig. 15.14 Time sequence of delayed FFTs illustrating the decay of excited modes of a violin, when the A-string is plucked, with an expanded section of the frequency scale for the lowest resonances excited. The time between successive traces is 10 ms

Envelopes of Sound Waveforms

The time dependence or envelope of the amplitude of a sound signal is just as important a factor in the recognition of any musical instrument as the spectrum of the sound produced. In general, the envelope has a starting transient, a period with a quasi-constant amplitude for a continuously bowed or blown instrument, and a period of free decay, when the instrument is no longer being excited. The sound produced by musical instruments is also significantly affected by the acoustic environment in which the instrument is played, but this will be ignored for the moment. Typical initial transients and overall envelopes of single notes played on a violin, clarinet and trumpet are shown in Fig. 15.15.

The starting transient provides an immediate clue to the ear enabling the listener to recognise the instrument being played quickly. However, the characteristic fluctuations in frequency and amplitude within the overall envelope and noise associated with the method of excitation (e.g. bowing and blowing) are just as important in the recognition of specific instruments. This can easily be shown by removing the starting transient from a musical sound altogether, as illustrated in **EXTRAS**. In this example comparisons are made between the sounds of a violin, flute, trombone and oboe played first with the initial 200 ms transient removed and then

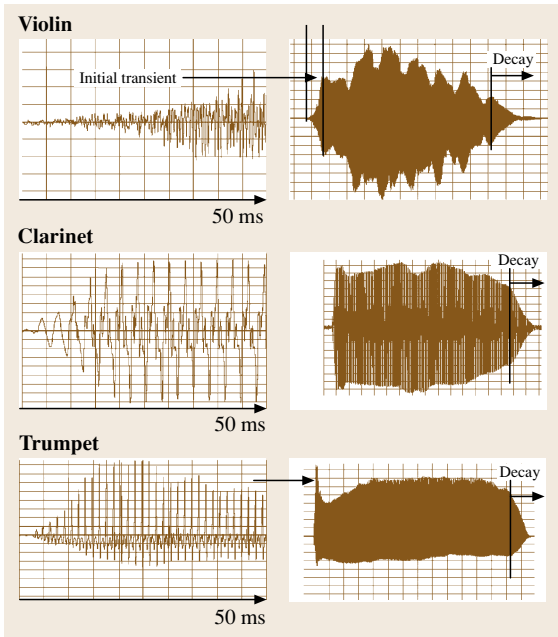


Fig. 15.15 Typical wave envelopes for a violin, clarinet and trumpet with a 50 ms expanded view of the initial starting transient

with the transient reinserted. In each case the instrument can immediately be identified even in the absence of the starting transient. The audio example ends with a constant amplitude sawtooth waveform having an unvarying sound quite unlike the sound of any real musical instrument.

Nevertheless, the starting transient and subsequent decay of sound are extremely important in the identification of the sounds of plucked or hammered strings and all percussion instruments, where the waveform and spectral content changes very rapidly with time after the start of the note. This is illustrated by the dramatic difference in the unrecognisable sound of a piano when played backwards and then replayed in the normal direction (EXTRAS).

Noise

There are several potential sources of fluctuations in the envelope of musical instruments, which help to characterise their characteristic sounds, such as the breathiness induced by the noise of turbulent air passing over the sound hole in a recorder, flute or organ pipe (Verge and Hirschberg [15.15]) and irregularities in the sound of any bowed instrument due to inherent noise in the slip-stick bowing mechanism (McIntyre et al. [15.16]).

Amplitude and Frequency Modulation

Another important source of fluctuations is vibrato, which involves periodic changes in the amplitude, frequency, or spectral content of a note and often all three (Meyer [15.17], Gough [15.18]). Vibrato is produced on a stringed instrument by periodically changing the length of the bowed string by rocking the finger stopping the string backwards and forwards. In singing (Prame [15.19]) and wind instruments (Gilbert et al. [15.20]) vibrato is produced by periodic modulations of the pressure exerted by the lungs or mouth on the exciting reed or air passage.

Amplitude modulation of a sinusoidal frequency component can be expressed as

$$\begin{aligned} y(t) &= (1 + a_m \cos \Omega t) \sin \omega t \\ &= \sin \omega t + \frac{a_m}{2} [\sin(\omega + \Omega)t + \sin(\omega - \Omega)t], \end{aligned} \quad (15.27)$$

where Ω is the modulation frequency and a the modulation parameter. Amplitude modulation introduces two side-bands with amplitude $a_m/2$ at frequencies Ω above and below that of the principal central component. The side-bands have a net resultant that remains in phase with the central component giving a fractional change in amplitude $[1 + a_m \cos \Omega t]$.

Frequency modulation should more strictly be referred to as phase modulation, with the phase varying as

$$\phi(t) = \omega t + a_f \cos \Omega t. \quad (15.28)$$

where a_f is frequency-modulation index. The time-varying frequency can then be defined by the rate of change of phase, such that

$$\frac{d\phi}{dt} = \omega - a_f \Omega \sin \Omega t, \quad (15.29)$$

with a fractional shift in frequency varying as

$$\frac{\Delta\omega(t)}{\omega} = -a_f \frac{\Omega}{\omega} \sin \Omega t. \quad (15.30)$$

For small modulation index, a phase-modulated wave can be written as

$$y(t) = \sin \omega t + \frac{a_f}{2} [\cos(\omega + \Omega)t + \cos(\omega - \Omega)t], \quad (15.31)$$

which again results in equally spaced side-bands about the central frequency with amplitude $a_f/2$, but with a resultant now in phase-quadrature with that of the central frequency giving the above phase modulation.

Because of the multi-resonant frequency response of all musical instruments, changes in driving frequency

also induce significant fluctuations in amplitude. Such fluctuations are particularly important for the strongly peaked multi-resonant instruments of the violin family, as illustrated in Fig. 15.15.

15.1.4 Perception and Psychoacoustics

In this section, we briefly highlight a number of psychoacoustic aspects of particularly importance in any discussion of musical acoustics. See also Chap. 13 on Psychoacoustics by *Brian Moore*.

Sensitivity of Hearing

We have already commented that the brain interprets both frequency and intensity on a logarithmic scale. The recognition of familiar intervals such as the octave, perfect fifth, irrespective of the absolute frequencies, provide an immediate example, as is the use of the dB scale in the measurement of sound levels.

In the 1930s, *Fletcher and Munson* [15.22] undertook a survey of a large population of subjects to investigate how the sensitivity of the ear varies with frequency and intensity (and age). These measurements were later refined by *Robinson and Dadson* [15.21]. Their published values for normal equal-loudness level contours, shown in Fig. 15.16, were adopted by the International Standards Organization, as the original ISO 226 standard for audio sensitivity, with data recently refined to define the new ISO 226:2003 standard.

The plotted curves show population-averaged equal loudness contours for sinusoidal sound waves measured

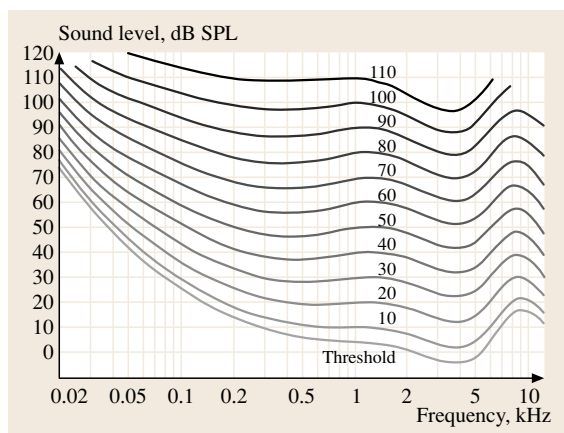


Fig. 15.16 *Robinson–Dadson* curves (after [15.21]) with contours of perceived equal loudness measured in phons on a dB scale

in phons on a dB scale, which equate to sound pressure level (SPL) measurements in dB at 1 kHz. The SPL dB scale is based on a reference root-mean-square pressure of $20 \mu\text{Pa}$ (equivalent to $2 \times 10^{-5} \text{ Nm}^{-2}$), which is very close to an intensity of 10^{-12} Wm^{-2} . The threshold contour is the population-averaged minimum sound pressure that can be just detected under the quietest environmental conditions. Above sound pressures of $\approx 120 \text{ dB}$, the ear experiences pain and potential permanent damage.


The equal subjective sound level contours reflect the dynamics of the ear's detection system. There is a rapid fall-off in sensitivity at low frequencies, where the efficiency of the outer ear drum considered as a piston detector falls off as ω^4 . The fall-off at high frequencies is due to the increasing inertial impedance of the ear drum and bones in the inner ear. However, the fall-off is partially compensated by peaks in sensitivity from the resonances of the outer air channel between the ears and ear-drum. Older people experience a considerable loss in sensitivity at high frequencies, which is strongly correlated with age. Fortunately, the losses are at relatively high frequencies and are generally not too important for the appreciation of music.

The sensitivity of the ear is particularly strong in the frequency range 2–6 kHz, which is important for recognising the consonants in speech. One would therefore expect such frequencies to be equally important in the identification and assessment of sound quality of musical instruments. Below around 200–400 Hz there is an increasingly rapid fall-off in sensitivity, which will differentially affect the subjective loudness of the lower partials of any complex musical sound at these and lower frequencies. At low frequencies the contours of equal amplitude are more closely spaced, so that the effect of increasing the SPL by 20 dB increases the subjective loudness by considerably more. Turning up the volume on any reproduction system changes the perceived quality from a rather thin sound to a more exciting sound with a much stronger bass and a somewhat stronger high-frequency response.


From a musical acoustics viewpoint, it is often sensible to invert the equal contour plot, as the inverted plot essentially acts as a subjective, mid-frequency band filter, de-emphasising the perceived intensities of the lowest and highest-frequency partials in a complex waveform.

Loudness levels will clearly vary with distance from any source. Sounds levels exceed 120 dB close to an aeroplane on take off or close to a loudspeaker in a noisy rock concert, resulting in potential permanent damage

to the ear. Sound levels close to a heavily used motorway are typically around 90 dB, around 70 dB inside a car, about 50 dB in an office, 30 dB inside a quiet house at night, 20 dB in a very quiet recording studio and 0 dB inside an anechoic chamber. At the quietest levels, one begins to hear the beating of the heart and workings of other internal organs, which can be a somewhat disquieting experience. There would clearly be no evolutionary reason to have developed a more sensitive hearing system.

Audio  **EXTRAS** is a short orchestral excerpt played at successively decreasing 6 dB steps (half the amplitude or a quarter the intensity). Musicians indicate the loudness with which music should be played using the dynamic markings *pp*, *p*, *mp*, *mf*, *f* and *ff*, which roughly correspond to a subjective doubling of intensity between each level. Such levels are clearly only relative, since absolute values will vary strongly with the distance of the listener from the source with a 12 dB decrease in intensity on doubling the distance in free space. Although the dynamic range of an individual note on a musical instrument rarely exceeds 20 dB, with only about six distinguishable dynamic levels within this range, the total dynamic range of an instrument is more like 45 dB (*Patterson* [15.23]). However, there is a much larger range of sounds produced by different instruments (e.g. the trombone and violin. The carrying power, penetration and prominence of musical sounds is not simply a matter of absolute intensity, but also depends on the harmonic content and transient structures of the complex tones produced. This helps to explain how a solo violinist can still be heard over the massive sound of a large orchestra.


Subjective Assessment of Pitch


We have already noted that the perceived pitch of a note is determined by the inverse period of a waveform and does not necessarily require the presence of a Fourier component at that frequency. This is illustrated in audio  **EXTRAS**, in which simple sinusoidal tones at 300 Hz and 200 Hz are first played in succession and then played together to produce a repeating waveform sounding an octave lower at 100 Hz, which is then followed by a pure 100 Hz tone of the same amplitude but sounding very much quieter. The final sinusoidal tone at 100 Hz may well not be heard on a typical PC laptop or notebook sound production systems, which radiate little sound below around 200 Hz. The absence of a Fourier component at the pitch of a complex tone is often referred to as the *missing fundamental* phenomenon. It is important in many stringed instruments, which produce

very little sound at the actual frequency of their lowest open strings.

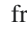
The missing fundamental phenomenon is a psychoacoustic rather than a nonlinear effect produced by a distortion of the waveform in the ear. It reflects the way that the ear processes sounds in the time domain at low frequencies (*Moore* [15.24] and Chap. 13).

The ability of the ear to recognise the pitch at which an instrument is playing, even though the lower partials of the sound of individual instruments may be missing is very important in sound reproduction systems. It enables the listener to recognise the distinctive sounds of all the instruments in an orchestra, even when the recording or reproduction system may have a very poor low-frequency response – as in early gramophones and the loudspeakers used in cheap radios and typical PC laptops and notebooks.

Combining tones to produce a lower tone is exploited on the *quint* combination stop on the organ to produce low-pitched sounds (e.g. a 16 ft pipe and a $16 \times 2/3 = 10.66$ ft pipe sounding a fifth above, when sounded together, reproduce the sound of a 32 ft pipe, as illustrated for the combination of 200 and 300 Hz sine waves in  **EXTRAS** above). Interesting, the effect is nothing like so strong in playing two bowed strings a fifth apart (e.g. open A and open E on a violin), presumably because of the very rich spectrum of higher partials and independent fluctuations of the two sounds. However, such sounds can often be heard when two flutes play well-tuned intervals together. The early 18th century virtuoso violinist Tartini recognised the existence of such mysterious tones, whenever pairs of notes were played together in exact intonation (e.g. integer ratios such as $3/2$ (perfect fifth), $5/4$ (major third), $6/5$ (major third)), and reputedly attributed them to the devil. The effect is small, but is still used by violinists when practising playing such intervals exactly in tune.

In general, complex tones are composed of a number of spectral components which have no particular harmonic relationship to each other. One then has to consider what determines the subjective pitch of the perceived sound. This involves the way the brain processes the signal and the relative emphasis given to the spectral components present, which will depend on their frequencies and intensities. It is important to recognise that the perceived pitch is not necessarily that of the lowest-frequency component present. This is illustrated in  **EXTRAS** in which the fundamental and first octave are fixed in frequency, while an intermediate partial is swept upwards from the lower to the higher note. First the fundamental is sounded by itself and then with


the octave added producing a note at the same pitch but with a different timbre. An intermediate partial is then added and swept upwards in steps from the lower to the upper note, giving the sense of a note of continuously rising pitch, though the fundamental and its octave remain fixed. Although the fundamental and octave remain fixed, the rising partial gives the sense of a note of increasing pitch. In this particularly simple example, it is relatively easy to identify and follow the pitch of each harmonic component separately. However, for a musical instrument like a gong or bell, with no preconceived knowledge of the likely pitch of the individual partials, this is far more difficult. The perceived pitch of the strike note of a bell and many other percussion instruments, with an inharmonic combination of excited modes, depends in a rather complex way on the relative weighting of the partials present and the musical context.

In assessing the subjective pitch of a note there can often be an ambiguity of an octave in the apparent pitch. This is illustrated by the famous example of the apparent, ever-rising pitch of a note generated by a continuously rising comb of logarithmically spaced frequencies passing through a fixed hearing band of frequencies,  EXTRAS [15.25], which appears to be increasing in pitch at all times though clearly repeating itself. This illustrates the *circularity* of pitch perception and is the audio equivalent of the visual illusion of continuously rising steps which return to the same point in space in an Escher drawing.

Precedence Effect

Another important time-domain phenomenon in the perception of musical sounds is the Haas precedence effect, which enables a listener to locate the source of

a distant sound from the small difference in time that sound arriving at an angle to the head takes to reach the two ears. The brain gives precedence to the sound arriving first, even though later sounds from other directions may be significantly stronger. Any sound arriving within the first 20–40 ms (depending somewhat on frequency and intensity) of the first sound to arrive simply adds to the perceived intensity of the first sound. This is very important in musical performance, with reflections from close reflecting surfaces adding strongly to the intensity and definition of the music.

The precedence effect is illustrated in  EXTRAS. This is a stereo recording of identical clicks recorded on the left and right channels with a delay of 20 ms between them, which is then reversed. Although the clicks are too close together for the ear to distinguish them separately, when replayed through a pair of stereo loudspeakers (not earphones), the sound will appear to come from the speaker providing the earlier click.

The precedence effect is one of the ways in which one can locate the origin of a particular sound within an orchestra or the sound of a particular voice in a crowded room. Once located, the brain is able to focus on the subsequent source even against a highly confusing background of other sources. It is likely that fluctuations within the characteristic sound of an individual person or musical instrument enable the brain to focus continuously on a particular source. In musical acoustics one must always recognise the formidable power of the brain's auditory processing capabilities, which is far beyond what can be achieved using present-day computers. Consequently, even very small effects on a physical measurement scale can have a very significant effect on the listener's subjective response to the sound of a particular instrument.

15.2 Stringed Instruments

In this section we describe the production of sound by the great variety of musical instruments based on the plucking, bowing and striking of stretched strings. This will include an introduction to the different modes of string vibrations excited by the player, the transfer of energy from the vibrating string to the acoustically radiating structural vibrations of the body of the instrument via the bridge, and the modification of such sound by the environment in which the instrument is played. Although the production of sound is based on the vibrations of relatively simple structures, such as strings and plates, it is the interactions between these, extending the

physics well beyond introductory text-book treatments, which results in the characteristic sounds of individual stringed instrument, as summarised in this section.

The Physics of Musical Instruments by Fletcher and Rossing [15.5, Chaps. 9–11] provides an authoritative account of the acoustics of a wide range of string instruments, and a comprehensive set of references to the research literature prior to 1998. The four volumes of research papers on violin acoustics, collated and edited by Hutchins [15.26, 27] and Hutchins and Benade [15.28], also includes excellent introductions to almost every aspect of the acoustics of instruments of the violin family,

much of which is just as relevant to other stringed instruments. Carleen Hutchins has been an inspirational figure in the field of violin acoustics. The Catgut Acoustical Society, which she cofounded, published a journal and an earlier newsletter [15.29] containing many important papers on violin research of interest to both professional acousticians and violin makers. Her inspiration has encouraged a world-wide school of violin makers, who use scientific measurements and plate tuning in particular as an aide to making high-quality instruments. The comprehensive monograph on the *Physics of the Violin* by Cremer [15.30] provides an invaluable theoretical and experimental survey of research on instruments of the violin family, with particular emphasis on the bowed string, the action of the bridge, the vibrations of the body and the radiation of sound.

The production of sound by any stringed instrument is based on the same acoustic principles. The player excites the vibrations of a stretched string by bowing, plucking or striking. Energy from the vibrating string is then transferred via the supporting bridge to the acoustically radiating structural vibrations of the instrument. The radiated sound is then conditioned by the performing environment.

There are many different types of stringed instruments formally classified as chordophones. Harp-like lyres appear in Sumerian art from around 2800 BC. However, more primitive instruments, like a plucked string stretched over a bent stick and resonated across the mouth, probably date back to soon after the emergence of man the hunter [15.31, 32].

Stokes [15.33] was the first to recognise that the vibrating string was essentially a linear dipole, which radiated a negligible amount of sound at low frequencies (see also Rayleigh [15.3, Vol. 2, Sect. 341]). To produce sound, the vibrating string has to excite the vibrations of a much larger area radiating surface. For bowed and plucked instruments, such as members of violin, lute and guitar families, almost all the sound is radiated by the shell of the instrument, with the acoustic output at low frequencies usually boosted by the Helmholtz resonance of the air inside the instrument vibrating in and out of the f- or rose-holes cut into the front plate. On larger instruments, such as the piano and harp, the sound is radiated by a large soundboard.

For any continuously bowed (or blown) instrument, the sound is conditioned by a complex feedback loop involving the instrument, player and surrounding acoustic, illustrated schematically for the violin in Fig. 15.17. The expert string player controls the intonation and quality of the sound produced using slight adjustments

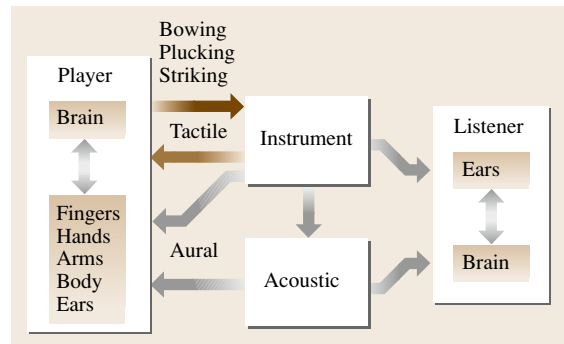


Fig. 15.17 A schematic representation of the complex feedback and sound radiation systems involved in the generation of sound by a bowed string instrument

of the position of the left-hand fingers stopping the string, and the pressure, velocity and position of the bow on the string, in response to the sound heard from both the instrument and the surrounding acoustic. In addition, there is direct tactile feedback through the fingers of both the left hand controlling the pitch of the note and the right hand controlling the bow. A similar overall feedback system is also involved in playing woodwind or brass instrument. The perception of the sound by both player and listener is also strongly influenced by the performing acoustic and the way the brain processes the sound received by the sensory organs in the ears, as illustrated schematically in Fig. 15.17. All such factors are involved in determining the perceived quality of the sound produced by a musical instrument. However, for simplicity and physical insight into the various mechanisms involved, it is convenient to consider the acoustics of musical instruments in terms of their component parts, like the vibrating string, the supporting bridge and shell of the instrument. Nevertheless, it is important not to lose sight of the fact that the sound produced by any instrument will involve the interactions of all such subsystems and, even more importantly, the skill of the player in exciting and controlling the vibrations ultimately responsible for the sound produced.

15.2.1 String Vibrations

The transverse vibrations $\xi(x, t)$ of a perfectly flexible stretched string, of mass μ per unit length and tension T , satisfy the one-dimensional wave equation (d'Alembert, 1747)

$$\frac{\partial^2 \xi}{\partial x^2} = \frac{1}{c_T^2} \frac{\partial^2 \xi}{\partial t^2}, \quad (15.32)$$

where the velocity of transverse waves $c_T = \sqrt{T/\mu}$. The tension $T = ES\Delta L/L$, where E is Young's modulus, S is the cross-sectional area of the string and $\Delta L/L$ is the fractional stretching of the string over its length L . For the relatively small transverse displacements of bowed and plucked strings on musical instruments, changes in tension can be ignored. However, at larger amplitudes, a number of interesting nonlinear effects can be observed, which will be described in Sect. 15.2.2.

A string can also support longitudinal and torsional modes, with velocities $c_L = \sqrt{E/\rho}$ and $c_\theta = \sqrt{E/\rho(1+\nu)}$, where ρ is the density and ν is the Poisson ratio (≈ 0.35 for most materials). The Poisson ratio ν is the ratio of transverse to longitudinal strain when the material is stretched along a given direction. For strings on musical instruments, the longitudinal and torsional wave velocities are typically an order of magnitude larger than the transverse velocity, with $c_L/c_T \approx \sqrt{L/\Delta L}$.

Although both longitudinal and torsional waves play important roles in the detailed physics of the bowed, plucked and struck string, the musically important modes of string vibration are the transverse modes – apart from unwanted squeaks from longitudinal modes, which are often excited by the beginner on the violin. Unless otherwise stated, we only consider transverse waves and drop the defining subscript, unless a distinction needs to be made.

Waves on an ideal string are dispersionless (independent of frequency), so that any wave initially excited on the string will travel along the string without change in amplitude or shape. D'Alembert obtained a general solution of the wave equation of the form

$$f(x, t) = f_1(x + ct) + f_2(x - ct), \quad (15.33)$$

corresponding to two waves of unchanging shape travelling with wave velocity c in opposite directions along the string.

If the string is supported rigidly at its ends, the propagated waves are reflected with a change in sign giving zero displacement at the nodal end-points. Each propagating wave will continue to be reflected with change of sign on reflection at each end. For a string of length L , the string displacement will therefore return to its initial state in multiples of the transit time $2L/c$. The same is also true for the velocity and acceleration waveforms, since, if f satisfies the wave equation, then so must all its temporal and spatial derivatives, $\partial^n f/\partial x^n$ and $\partial^n f/\partial t^n$. It follows that the repetition frequency of any freely propagating wave on a given length of a stretched string will always be the same, however

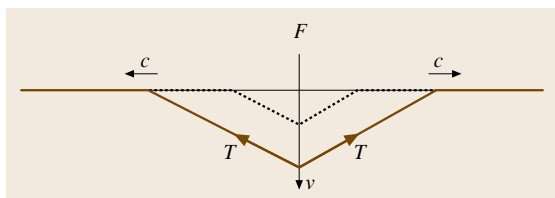


Fig. 15.18 Transverse motion of string induced by a localised force, with the *dotted lines* indicating the displacement at an earlier time

the string is excited (e.g. sinusoidally or by plucking, bowing or striking).

Excitation of Vibrations

First consider a string subject to a localised force F applied suddenly at a point along its length. This causes the string to move with velocity v at the point of contact exciting transverse waves travelling outwards in both directions with velocity c , as illustrated schematically in Fig. 15.18.

In a short time δt , the transverse waves travel a distance $c\delta t$ along the string while the string at the point of contact is displaced by a transverse distance $v\delta t$. For $v \ll c$, one can make the usual small-angle approximations, so that equating the applied force to the transverse force from the deformed string, we obtain

$$v = \left(\frac{c}{2T}\right) F = \frac{1}{2R_0} F, \quad (15.34)$$

where $R_0 = \mu c$ is the characteristic impedance (force/induced velocity) of the string, which for an ideal string ignoring intrinsic losses is purely resistive. The factor of two in the above equation arises because the force acts on the two semi-infinite lengths of string in parallel. In practice, any discontinuity in slope will be rounded by the finite flexibility of real strings, as discussed later.

Force on End-Supports

The characteristic resistance R_0 of the string is an important parameter, because it determines the transfer of energy from the vibrating string to the acoustically radiating modes of the instrument via the supporting bridge at the end of the string. The transverse force exerted by the string on an end-support at the origin can be written as $F_B = T(\partial\xi/\partial x)_0$. This induces a transverse velocity at the point of string support given by

$$v_B = \frac{1}{Z_B} F_B = A_B F_B, \quad (15.35)$$

where Z_B and A_B are the frequency-dependent characteristic impedance and admittance at the end-support. In

general, the induced velocity at the point of string support on the supporting bridge will differ in phase from that of the driving force, so that $Z(\omega)$ and $A(\omega)$ will be complex quantities.

The bridge on a musical instrument is never a perfect node otherwise no energy could be transferred to the radiating surfaces of the instrument. Waves on the string are reflected at the bridge with a frequency-dependent reflection coefficient r and a fractional loss of energy ε given by

$$r = \frac{R_0 - Z_B}{R_0 + Z_B} \quad \text{and} \quad \varepsilon = \frac{2R_0 (Z_B + Z_B^*)}{|R_0 + Z_B|^2}, \quad (15.36)$$

where Z_B^* is the complex conjugate of the complex impedance at the terminating bridge.

For strings on musical instruments, $R_0 \ll |Z_B|$, so that to a first approximation we can consider the bridge as a node. If this were not so, the vibrational frequencies of strings would be strongly perturbed from their harmonic values. Nevertheless, first-order corrections are important, as they determine the energy transfer from the strings to the body of the instrument and hence the intensity of the radiated sound. The coupling via the bridge also affects the string vibrations themselves, with the resistive losses at the bridge causing damping and the reactive component of the admittance perturbing their vibrational frequencies, as described in Sect. 15.2.3. Such perturbations can sometimes be so large that it is no longer possible to sustain a stable bowed note, resulting in what is known as a *wolf-note* (for an illustration of a bad wolf-note on the cello listen to [15.2.3 EXTRAS](#)).

Before considering the interaction of real strings with the supporting structure, we first consider the simplest cases of sinusoidal and simple Helmholtz modes of vibration on an ideal string with perfectly rigid end-supports.

Sine-Wave Modes

An ideally flexible string stretched between rigid end-supports a distance L apart can support standing waves, or eigenmodes, with transverse string displacements given by

$$\xi_n(x, t) = a_n \sin\left(\frac{n\pi x}{L}\right) \cos(\omega_n t + \phi_n), \quad (15.37)$$

where $\omega_n = 2\pi f_n$ and a_n is the amplitude of the n th mode with frequency $f_n = nc/2L$ and phase ϕ_n . Such modes can be considered as the sum of two sine waves of the d'Alembert form (15.33) travelling in opposite directions. For an ideal string, these solutions form a complete orthogonal set of *eigenmodes* with

a *harmonic set of eigenfrequencies*, which are integer multiples of the fundamental frequency $c/2L$.

The resonant response of individual modes of a metal or metal-covered string can be investigated, for example, with a photosensitive device to detect the transverse string motion induced by a sinusoidal current passing through the string placed in a magnetic field to give a transverse Lorentz force (Gough [15.34]).

Because the wave equation is linear, any waveform, however excited, can be described as a Fourier sum of harmonic modes, such that

$$\xi_n(x, t) = \sum_{n=1}^{\infty} \sin\left(\frac{n\pi x}{L}\right) \times [A_n \cos(\omega_n t) + B_n \sin(\omega_n t)], \quad (15.38)$$

where the Fourier coefficients A_n and B_n are determined by the initial transverse displacement and velocity along the length of the string, so that

$$A_n = \frac{2}{L} \int_0^L \xi(x, 0) \sin\left(\frac{n\pi x}{L}\right) dx, \quad (15.39)$$

and

$$B_n = \frac{2}{L\omega_n} \int_0^L \frac{d\xi(x, 0)}{dt} \sin\left(\frac{n\pi x}{L}\right) dx. \quad (15.40)$$

The transverse force on the end-support at $x = L$ is given by

$$\begin{aligned} F_{\text{end}} &= -T \left(\frac{\partial \xi}{\partial x} \right)_L \\ &= -T \sum_n \left(\frac{n\pi}{L} \right) (-1)^n \\ &\quad \times [A_n \cos(\omega_n t) + B_n \sin(\omega_n t)]. \end{aligned} \quad (15.41)$$

Helmholtz Modes

Although many physicists and most musicians intuitively associate waves on strings with the sinusoidal waves of textbook physics, in practice, the vibrations of a bowed, plucked or struck string are very different. Nevertheless, because such waves are repetitive, it follows from the Fourier theorem that all such solutions can be described as a sum of sinusoidal wave components. However, the motions of plucked, bowed and struck strings are much more easily described by what are known as Helmholtz solutions to the wave equation [15.35]. These are illustrated for the plucked and bowed string in Fig. 15.19a,b.

The Helmholtz solutions are made up of straight-line sections of string. There is no net force acting on

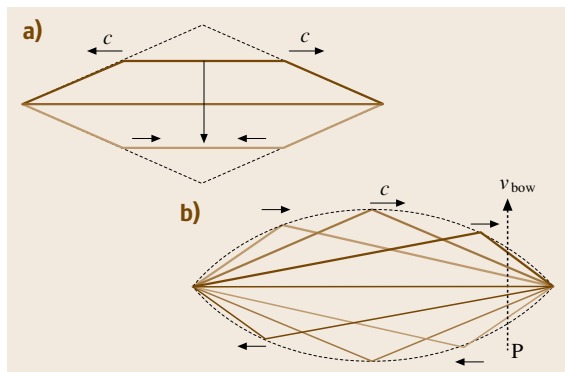


Fig. 15.19a,b Helmholtz waveforms for (a) a centrally plucked and (b) a bowed string. The horizontal arrows indicate the directions that the kinks are travelling in and the vertical arrows the directions of the moving string sections. The different colours represent string displacements at different times. *P* indicates a typical bowing position along the string

any small segment within any such section, because the transverse tension forces acting on its ends are equal and opposite. By Newton's laws, any such segment must therefore be either at rest or moving with constant velocity. Only where there is a *kink* or discontinuity in the slope between adjacent straight-line sections (equivalent to a δ function in the spatial double derivative) can there be any acceleration. From our earlier discussion, any such kink must travel backwards and forwards along the string at the transverse string velocity c , reversing its sign on reflection at the ends. As the kink moves past a specific position along the string, the difference in the transverse components of the tension on either side of the kink results in a localised impulse, which changes the local velocity of the string from one moving or stationary straight-line section to the next. In general, there can be any number of Helmholtz kinks travelling along the string in either direction, each kink marking the boundary between straight-line sections either at rest or moving with constant velocity. Similar solutions also exist for torsional and longitudinal waves.

We now consider the Helmholtz wave solutions for the plucked, bowed and hammered string in a little more detail.

Plucked String

Consider an ideal string initially at rest with an initial transverse displacement a at its mid-point, as illustrated in Fig. 15.19a. On release, kinks will propagate away from the central point in both directions with velocity c ,

but points on the string beyond the kinks will remain at rest. When the kink arrives at a particular point along the string, the associated impulse will accelerate the string from rest to the uniform velocity of the central section of the string. After a time t , the solution therefore comprises a straight central section of the string of width $2ct$ moving downward with constant velocity c ($2a/L$), with the outer regions remaining at rest until a kink arrives. After a time $L/2c$, the kinks separating the straight-line sections reach the ends and are reflected with change of sign. After half a single period L/c , the initial displacement will therefore be reversed and will return to the original displacement after one full period $2L/c$. In the absence of damping, the process would repeat indefinitely.

Now consider the transverse force acting on the end-support responsible for exciting sound through the induced motion of the supporting bridge and vibrational modes of the instrument. The initial transverse force on the bridge is $2Ta/L$, where we assume $a \ll L$. This force is unchanged until the first kink arrives. On reflection, the direction of the force is reversed and is reversed again when the second kink returns after reflection from the other end of the string. The two circulating kinks therefore cause a reversal in sign of the force on the end-supports every half-cycle, resulting in a square-wave waveform, as illustrated in Fig. 15.20. The spectrum of a square wave has Fourier components at odd multiples n of the fundamental frequency with amplitudes proportional to $1/n$, Fig. 15.20b.

Note that plucking a string at the mid-point excites only the odd- n modes. This is a consequence of the initial force being applied at a node of all the even- n modes. If a string is plucked at a fractional position $1/m$ along its length, any partial that is an integer multiples of m will be missing. This is illustrated in Fig. 15.21, showing the spectra of the force on the supporting bridge for a string plucked at points $1/4$ and $1/7$ -th along

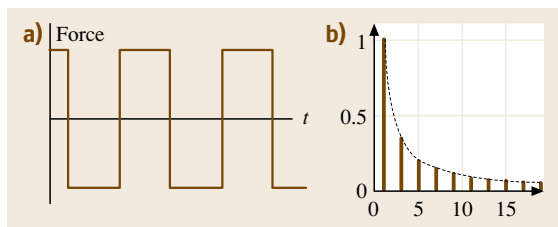


Fig. 15.20 (a) Square-wave time dependence of transverse force acting on the bridge from a string plucked at its centre and (b) the corresponding amplitudes of the odd Fourier components n varying as $1/n$ (dotted curve)

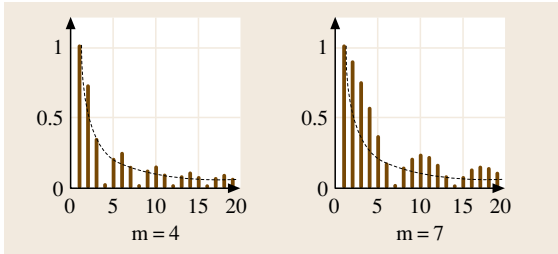


Fig. 15.21 Normalised Fourier amplitudes for the force on the bridge for a string plucked $1/4$ and $1/7$ of the string length from the bridge. The *dashed curves* show the $1/n$ envelope of the partials of a sawtooth waveform

its length. By selecting the plucking position along the string, the guitar or lute player can change the harmonic content of the sound produced. When plucked near the bridge, the sound of the plucked guitar string is rather bright, with nearly all the prominent partials almost equally strongly excited (audio [I3](#) **EXTRAS**).

In practice, the finite width of the plucking point, the finite rigidity of the string and the loss of energy at the bridge perturb the Helmholtz wave, removing the unphysical discontinuities of the idealised model. This results in a more rapid decrease in the intensities of the higher partials excited.

Bowed String

The motion of the bowed string can be described rather accurately by a simple Helmholtz wave with a single kink circulating backwards and forwards along the string. The kink now separates two straight sections moving with constant angular velocity about the nodal end-points, as illustrated in Fig. 15.19b. This is again a solution that satisfies Newton's laws of motion, with the only acceleration occurring as the kink arrives at a particular point along the string. Such a wave is just as valid a solution to the wave equation as a sine wave and once excited would continue indefinitely, if there were no damping or energy losses on reflection at the bow or supported ends.

The energy required to excite and maintain such a wave is provided by frictional forces between the moving bow hair and the string, involving what is known as the *slip-stick* excitation mechanism. For a typical bowing position, marked by the line at P in Fig. 15.19b, the friction between the bow and string forces the string to remain in contact with the bow hair moving with constant bow velocity. This is referred to as the *sticking regime* and occurs all the time the kink is travelling to the left of the bowing position. How-

ever, when the kink is between the bow and supporting bridge, the string moves in the opposite direction to the bow. This is the *slipping regime*. Such motion is possible because the sliding friction between the bow and string can be much smaller than the sticking friction, when the bow and string are in contact. In this highly idealised model, the frictional force is assumed to be infinite in the sticking regime and zero in the slipping regime.

A more detailed discussion of the slip-stick bowing mechanism will be given later (Sect. 15.2.3), taking into account more-realistic models for the frictional forces between the bow and string and the transfer of energy from the string to the vibrational modes of the structure via the bridge. However, the idealised Helmholtz motion provides a surprisingly good description of the vibrations of real strings, as confirmed in early measurements by *Raman* [15.36] and many more-recent publications to be cited later.

The amplitude of the Helmholtz bowed waveform is determined by the velocity of the bow v_{bow} and its distance L_B from the bridge. The transverse displacement of the kink maps out a parabolic path as it traverses the string (Fig. 15.19b). At the mid-point, the string displacement executes a triangular-wave motion with time, moving with velocity $\pm 2ca/L$ in alternate half-periods, where the maximum displacement $a = (L^2/4L_B)(v_B/c)$, for $a \ll L$. At the bowing position, the transverse string velocity alternates between v_{bow} in the sticking regime and $-v_{\text{bow}}(L - L_B)/L_B$ in the slipping regime, as illustrated in Fig. 15.22.

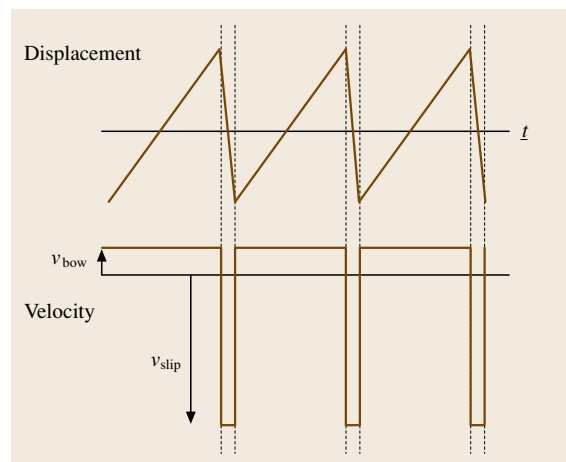


Fig. 15.22 Displacement and velocity of string at the bowing point. The mark-to-space ratio in the velocity is the same as the division of the string by the bow

To increase the sound, the player can therefore either use a faster bow speed or play with the bow nearer the bridge. *Schelling* [15.37] has shown that more-realistic frictional models limit the playing range, as discussed later (Fig. 15.31).

The transverse force on the bridge produced by an idealised Helmholtz bowed wave has a sawtooth-waveform time dependence, as shown in Fig. 15.23. Each time the kink is reflected at the bridge, the transverse force acting on the bridge reverses in sign. It then increases monotonically with time until the process repeats again. The sense of the sawtooth motion reverses with bow direction. The spectrum of the force acting on the bridge includes both even and odd partials, with amplitudes varying as $1/n$.

The spectrum of the sound produced by the lowest plucked and bowed notes on stringed instruments can typically involve 40 or more significant harmonic partials, as illustrated in Fig. 15.24 by the spectrum of the

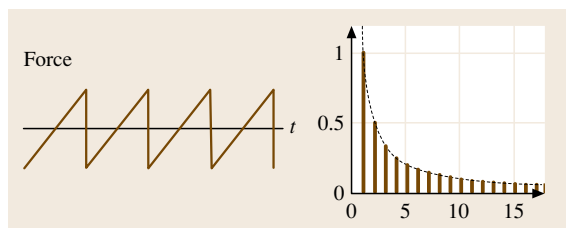


Fig. 15.23 Sawtooth time-dependence of force on the end supports from Helmholtz bowed waveform and corresponding amplitudes of the normalised Fourier spectrum with partials varying as $1/n$

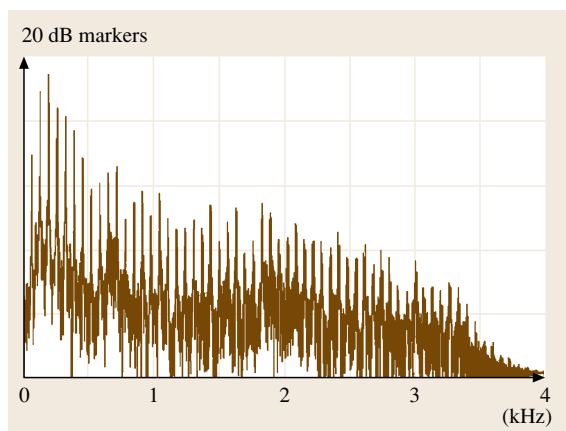



Fig. 15.24 The spectrum of the intensity of the lowest bowed note on a cello, illustrating the very large number of partials contributing to the sound of the instrument

sound produced by a bowed cello open C-string (C2 at ~ 64 Hz, audio  EXTRAS). The FFT spectrum is plotted on a dB scale to illustrate the large range of amplitudes of the partials (Fourier components) excited. The amplitudes of the individual partials depend not only on the force at the bridge exerted by the plucked or bowed strings, but also on the frequency dependent response and radiative properties of the supporting structure, as discussed later.

Struck String

Many musical instruments are played by striking the string with a hammer. The hammer can be quite light and hard, as used for playing the dulcimer, Japanese koto and many other related Asian instruments, or relatively heavy and soft, like the felted hammers on a piano. Some time after the initial impact, the striking hammer bounces away from the string, leaving the string in a free state of vibration. There are a few instruments, such as the clavichord (*Thwaites* and *Fletcher* [15.38]), where the string is struck with a metal bar (the tangent), which remains in contact with the string, defining its vibrating length and hence the note produced.

Consider first a point mass m moving with velocity v striking an ideal stretched string of infinite extent. In any small increment of time, the moving mass will generate a wave moving outwards from the point of impact. This will result in a decelerating force on the mass equal to $2Tv/c = mcv$, as illustrated in Fig. 15.18. The displacement of the mass will then be described by the following equation of motion

$$m \frac{d^2 \xi_m}{dt^2} = -\frac{2T}{c_T} \frac{d\xi_m}{dt}. \quad (15.42)$$

The transverse velocity of the impacting mass therefore decays exponentially with time as

$$\frac{d\xi_m}{dt} = v_m \exp(-t/\tau), \quad (15.43)$$

with $\tau = mc/2T$. This is identical to the dynamics of a trapeze artist dropping onto a stretched wire, with

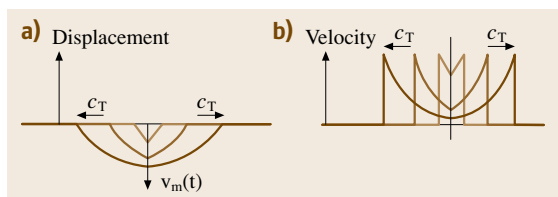


Fig. 15.25a,b Time sequences of (a) string displacement and (b) string velocity for a mass striking a string

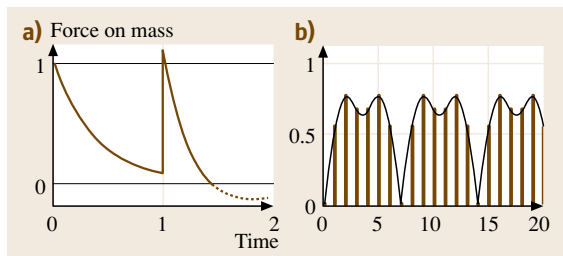


Fig. 15.26 (a) Time dependence of the upward force acting on a light hammer impacting a string in arbitrary units of time, and (b) amplitudes of Fourier coefficients of force acting on end supports for a hammer after hitting the string $1/7$ of the length from an end-support. The *continuous line* shows the continuous spectrum for a string of semi-infinite length

waves of displacement and velocity travelling outwards in both directions away from the point of impact, as illustrated in Fig. 15.25.

In general, the string will be struck at a distance a from one of its end-supports. Hence, in a time $(a/2L)T_0$, a reflected wave will return to the mass and exert an additional force, which will tend to throw the mass back off the string. However, because the mass cannot change its velocity instantaneously, any returning wave will be partially reflected, so that the mass acts as a source of secondary reflected waves travelling outwards in both directions. The total force acting on the hammer is then given by any residual force from the first impact plus the subsequent forces created by the succession of reflections from the end-supports. This problem was first correctly solved by Hall, in the first of four seminal papers on the string–piano hammer interaction [15.39–42].

Hall showed that the first reflected wave exerts an additional decelerating force $g(t') \approx (1 - t'/\tau)e^{-t'/\tau}$ on the mass, where t' is the time after arrival of the first reflection. This is illustrated in Fig. 15.26 for a relatively light mass impacting the string at a position $1/7$ -th of the string length from an end. Provided the mass is sufficiently small, the force from the initial impact will have decayed significantly by the time the first reflection returns, so that the force acting on the mass will become negative (the dotted section in Fig. 15.26a), and the mass will detach itself from the string. The string will then move away from the mass and will vibrate freely, provided the hammer is prevented from falling back onto the string. An elaborate mechanism is used on the piano to prevent this from happening (see Rossing, Fletcher [15.5, Sect. 12.2]), while the zither or dul-

cimer player quickly lifts the hammer well away from the string after the initial impact using much the same striking action as a percussionist playing a drum, where the same considerations apply.

The heavier the mass, the longer it will remain in contact with the string. Hall showed that it may then take several reflections from both ends of the string and sometimes several periods of attachment and detachment before the mass is finally thrown away from the string. A sufficiently heavy mass will never bounce back off the string.

In general, the waveforms excited on the string will therefore be rather complicated functions of the properties of the string, hammer and striking position. However, for a very light mass (\ll mass of the string), which is thrown off the string by the first reflected wave, the Fourier coefficients of the induced velocity waveform, and hence the force on the end-supports, are given by $v_n \approx (1 + e^{-1+in\pi\alpha}) \sin(n\pi\alpha)$, where $\alpha = a/L$, illustrated in Fig. 15.26b for an impact $1/7$ -th of the way along the string. Note that the seventh harmonic is missing, as again expected from general arguments, since no work can be transferred to a particular mode of string vibration for a force applied at a nodal position.

In practice, the spectrum is affected by the finite size of the hammer, multiple reflections occurring before the hammer is thrown from the string, and the elastic and often hysteretic properties of the hammer material [15.39].

Striking Tangent

On the clavichord (Fletcher, Rossing [15.5, Sect. 11.6]), a string is struck by a rising end-support, or tangent, which remains in contact with the string, exciting transverse vibrations of the string on both sides of the tangent. If we assume a simplified model in which the rising tangent moves with constant velocity until its final displacement a is reached, there is again a simple Helmholtz wave solution. In practice, the length of string on one side of the tangent is damped, so that free vibrations are only excited on one side of the striking point. We therefore need only consider the length of string between the tangent and the end connected to the soundboard. The discontinuities $\pm v$ in the tangent velocity, occurring on initial impact and on reaching its final displacement after a time Δt , generate propagating kinks and discontinuities of velocity of opposite sign separated in time by Δt . The striking therefore excites waves with kinks, velocities and displacements along the string shown in Fig. 15.27a. The solutions are again Helmholtz waves, but now with two kinks of op-

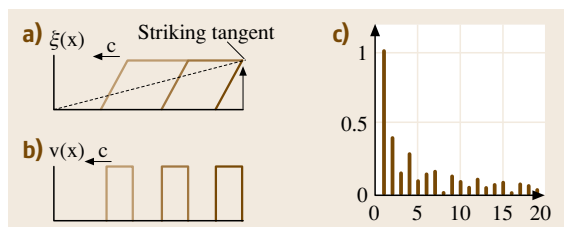


Fig. 15.27a–c Waveforms for a tangent hitting and sticking to string: (a) displacement and (b) velocity profiles along the string, at a succession of times (different colours) after the tangent hits the string, and (c) the spectrum of the resultant force on the end-supports for $\beta = 3/8$ (see text)

posite signs travelling around the string in the same direction.

The Fourier coefficients of the velocity waveform shown in Fig. 15.27b can be written as

$$c_n \approx \frac{1}{n} \frac{a}{L'} \left(1 - e^{in2\pi\beta}\right), \quad (15.44)$$

where $\beta = \Delta t/T_1$ is the fraction of the period $T_1 = L'/2c$ of the freely vibrating length of string during which the striking tangent moves from its initial to final position. Figure 15.27 also includes the spectrum of the force acting on the end-supports for $\beta = 3/8$.

Very similar modes to the above will be excited during the time a heavy hammer is initially in contact with the string on instruments like the dulcimer, zither and piano. Such modes therefore contribute to the initial transient sounds of such instruments. Another related example is the use of *col legno* on stringed instruments, when the strings are struck by the wooden part of the bow. By hitting the string at specific positions along the string, pitched initial transients can be produced, creating special sound effects, *nageln*, sometimes used in avant-garde contemporary music, audio [3] EXTRAS). The above simplistic model for striking a clavichord string will, in practice, be modified by the way the player depresses the key, which is directly coupled to the rising tangent, both during and after the initial impact. The player can therefore influence the initial transient and the after-sound, including the use of a small amount of vibrato on the after-note, resulting in a particularly responsive and intimate but quiet instrument, which was particularly popular in the baroque period.

Real Strings

We now consider a number of departures from the above idealised models for real strings including:

1. The finite size of the plucking or striking point
2. The finite flexibility of the string
3. Nonlinear effects.

In a subsequent section, we consider the even larger perturbations resulting from coupling to the acoustically radiating modes of the body of the instrument via the bridge.

Finite Spatial Variation

Idealised models for the string, with infinitely sharp kinks produced by plucking, bowing or striking, involve waveforms with discontinuities in amplitude and slope and an infinite number of Fourier components are clearly unphysical. In practice, physics and geometrical limitations, like the finite size of the player's finger or plectrum, will always limit the maximum curvature of the string at the point of excitation. The kinks will therefore no longer be δ -functions (infinitely narrow) but will have a finite size. For illustration, travelling kinks can be modelled as Gaussian waveforms, $\xi_{\pm}(x, t) \approx \exp[-(x \pm ct)^2/2(\Delta x)^2]$, which approximate to δ -functions when $\Delta x \rightarrow 0$, where Δx characterises the width of the kink. The Fourier transform of such a function has a Gaussian distribution of Fourier coefficients varying as $c(k) \approx \exp[-(k/\Delta k)^2/2]$, where $\Delta k \Delta x = 1$. This is analogous to the uncertainty principle in position and momentum in quantum wave mechanics. For long bending lengths, the amplitudes of the higher-frequency Fourier components will be strongly attenuated.

The sound of a guitar string played with a sharp plectrum is therefore much brighter, with many more contributing higher partials, than when played with the fleshy part of a finger, which limits the bending radius to a few mm. This is illustrated by the sound of an acoustic guitar plucked first with a plectrum and then with the thumb, both at a distance of ≈ 10 cm from the bridge (audio [3] EXTRAS).

Finite Rigidity

Even for an infinitely narrow plectrum, the bending at the plucking point will be limited by the finite flexibility of the string. The wave equation is then modified by an additional fourth-order bending stiffness term (Morse and Ingard [15.43, (5.1.25)]),

$$\rho S \frac{\partial^2 \xi}{\partial t^2} = T \frac{\partial^2 \xi}{\partial x^2} - ES \kappa^2 \frac{\partial^4 \xi}{\partial x^4}, \quad (15.45)$$

where E is Young's Modulus, S is the cross-sectional area of the string (assumed homogeneous) and κ its ra-

dus of gyration. For a uniform circular wire of radius a , $S\kappa^2 = \pi a^4/4$. Using dimensional arguments, any changes in slope of the string will take place over a characteristic length $\delta \approx (ES\kappa^2/T)^{1/2} = (a^2L/2\Delta L)^{1/2}$, where ΔL is the extension of the string required to bring it to tension. This provides an intrinsic limit to the sharpness with which the string is bent and hence to the wavelength and frequency of the highest partials contributing significantly to the sound of a plucked, bowed or struck string.

The additional stiffness energy required to bend the string will also affect wave propagation on the string and the frequencies of the excited modes. Assuming sinusoidal wave solutions varying as $e^{i(\omega t \pm kx)}$, the modified wave equation (15.45) gives modes with resonant frequencies

$$\omega_n^2 = c^2 k_n^2 \left(1 + \delta^2 k_n^2\right). \quad (15.46)$$

Waves on a real string are therefore no longer dispersionless, but travel with a phase and group velocity that depends on their frequency and wavelength. Any Helmholtz kink travelling around a real string will therefore decrease in amplitude and will broaden with time. To maintain the Helmholtz slip-stick bowed waveform, with a well-defined single kink circulating around the string, the bow has to transfer energy to the string to compensate for such broadening each time the kink moves past the bow (Cremer [15.30, Chapt. 7] and Sect. 15.2.2).

If a rigidly supported string is free to flex at its ends (known as a hinged boundary condition), solutions of the form $\sin(n\pi x/L) \sin(\omega t)$. However, the mode frequencies remain are no longer harmonic;


$$\frac{\omega_n^*}{\omega_n} = \left(1 + Bn^2\right)^{1/2} \approx 1 + \frac{1}{2} Bn^2, \quad (15.47)$$

with $B = (\pi/L)^2 \delta^2$, where the expansion assumes $Bn^2 \ll 1$.

When a string is clamped (e.g. by a circular collet), it is forced to remain straight at its ends. Fletcher [15.44] showed that this raises all the modal frequencies by an additional factor $\approx [1 + 2/\pi B^{1/2} + (2/\pi)^2 B]$. For a real string supported on a bridge, connected to another length of tensioned string behind the bridge, the boundary conditions will be intermediate between hinged and clamped.

Kent [15.45] has demonstrated that finite-flexibility corrections raise the frequency of the fourth partial of the relatively short C5 (an octave above middle-C) string on an upright piano by 18 cents relative to the fundamental. The inharmonicity would be even larger

for the very short, almost bar-like, strings at the very top of the piano. However, the higher partials of the highest notes on a piano rapidly exceed the limits of hearing, so that the resulting inharmonicity becomes somewhat less of a problem. The inharmonicity of the harmonics of a plucked or struck string results in dissonances and beats between partials, providing an *edge* to the sound, which helps the sound of an instrument to penetrate more easily. This is particularly true for instruments like the harpsichord and the guitar when strung with metal strings.

Finite-rigidity effects are particularly pronounced for solid metal strings with a high Young's modulus. To circumvent this problem, modern strings for musical instruments are usually composite structures using a strong but relatively thin and flexible inner core, which is over-wound with one or more flexible layers of thin metal tape or wire to achieve the required mass (*Pickering* [15.46, 47]). The difference in sound of an acoustic guitar strung with metal strings and the same instrument strung with more flexible gut or over-wound strings is illustrated in  **EXTRAS**.

15.2.2 Nonlinear String Vibrations

Large-amplitude transverse string vibrations can result in significant stretching of the string giving a time-varying component in the tension proportional to the square of the periodically varying string displacement. This leads to a number of nonlinear effects of considerable scientific interest, though rarely of musical importance.

Morse and Ingard [15.43] and (Fletcher and Rossing [15.5, Chap. 5]) provide theoretical introductions to the physics of nonlinear resonant systems and to nonlinear string vibrations in particular. Vallette [15.48] has recently reviewed the nonlinear physics of both driven and freely vibrating strings.

The Nonlinear Wave Equation

Transverse displacements of a string result in a fractional increase of its length L by an amount $1/L_0 \int_0^L 1/2(\partial\xi/\partial x)^2 dx$ and hence to a similar fractional increase in tension and related frequency of excited modes. For a spatially varying sinusoidal wave, the induced strain and hence tension will vary with both position and time along the string. Any spatially localised changes in the tension will propagate along the string with the speed of longitudinal waves. As this is typically an order of magnitude larger than for transverse waves, $c_L/c_T \approx \sqrt{L/\Delta L}$, where ΔL is the amount that

the string is stretched to bring it to tension, such perturbations will propagate backwards and forwards along the string many times during a single cycle of the transverse waves. Hence, as pointed out by *Morse and Ingard* [15.43], to a rather good approximation, transverse wave propagation is determined by the spatially averaged perturbation of the tension.

Consider a stretched string vibrating with large amplitude in its fundamental mode with transverse displacement $u = a \sin(\pi x/L) \cos \omega t$. The spatially averaged increase in tension is given by

$$\begin{aligned} & \left(1 + \frac{\pi^2}{4} \frac{a^2}{L\Delta L} \cos^2 \omega t \right) \\ & = [1 + \beta(1 - \cos 2\omega t)a^2], \end{aligned} \quad (15.48)$$

where $\beta = \frac{\pi^2}{8} \frac{1}{L\Delta L}$. Inserting this change in tension into the equation of motion for transverse string vibrations coplanar with a localised external driving force $f(t)$, we can write

$$\begin{aligned} & \frac{\partial^2 u}{\partial t^2} + \frac{\omega_1}{Q} \frac{\partial u}{\partial t} + \omega_1^2 [1 + \beta(1 - \cos 2\omega t)a^2] u \\ & = \frac{2}{m} f(t). \end{aligned} \quad (15.49)$$

Mode Conversion

Nonlinearity results in an increase in the static tension by the factor $(1 + \beta a^2)$ and hence an increase in frequency of all the string modes. In addition, the term varying as $\cos 2\omega t$, at double the frequency of the principal mode excited, will interact with any other modes present to excite additional with frequencies $f_n \pm 2f_1$. Of special note is the effect of this term on the principal mode of vibration itself, exciting a new mode at three times the fundamental frequency $3f_1$ and an additional parametric term (acting on itself) from the $f_1 - 2f_1 = -f_1$ contribution. The parametric term causes an additional increase in frequency of the principal mode excited, so that in total

$$\omega_{1*}^2 = \omega_1^2 \left(1 + \frac{3}{2} \beta a^2 \right), \quad (15.50)$$

where ω_1 is the small-amplitude resonant frequency.

Nonlinear effects depend on the square of the amplitude of the strongly excited mode and inversely on the amount by which the string has been stretched to bring it to tension. To investigate nonlinear effects, it is therefore advantageous to use weakly stretched strings at low initial tension. Conversely, because the tension of strings on musical instruments tends to be rather high, nonlinear effects are not in general important within a musical context.

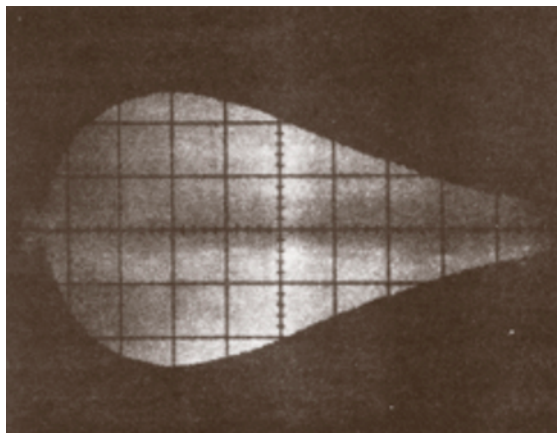


Fig. 15.28 Nonlinear excitation of the third partial of a stretched string plucked 1/3 of the way along its length; the graticule divisions are 50 ms apart (after *Legge and Fletcher* [15.49])

Figure 15.28 shows measurements by *Legge and Fletcher* [15.49], which illustrate the nonlinear excitation and subsequent decay of the third partial of a guitar string plucked one third of the way along its length, so that the third partial was initially absent.

In general, bowed, plucked and struck waveforms have many Fourier components, each of which will contribute a term proportional to a_n^2 to the nonlinear increase in tension. However, in most cases, the fundamental will be the most strongly excited mode and will therefore dominate the nonlinearity.

The inharmonicity and changes in frequency associated with nonlinearity at large amplitudes can give a strongly plucked string an initial rather *twangy* sound. Nonlinear effects can also raise the frequency of a very strongly bowed open C-string of a cello by almost a semitone. However, under normal playing conditions, nonlinearity is rarely musically significant, at least in comparison with other more important perturbations of string vibrations, such as their interaction with the acoustically important structural resonances of an instrument, to be considered later.

Nonlinear Resonances

The nonlinear increase in frequency of modes with increasing amplitude leads to string resonances, which become increasingly skewed towards higher frequencies at large amplitudes, as illustrated in Fig. 15.29. For sufficiently large amplitudes and small damping, the resonance curves develop an overhang. On sweeping through resonance from the low-frequency side, the am-

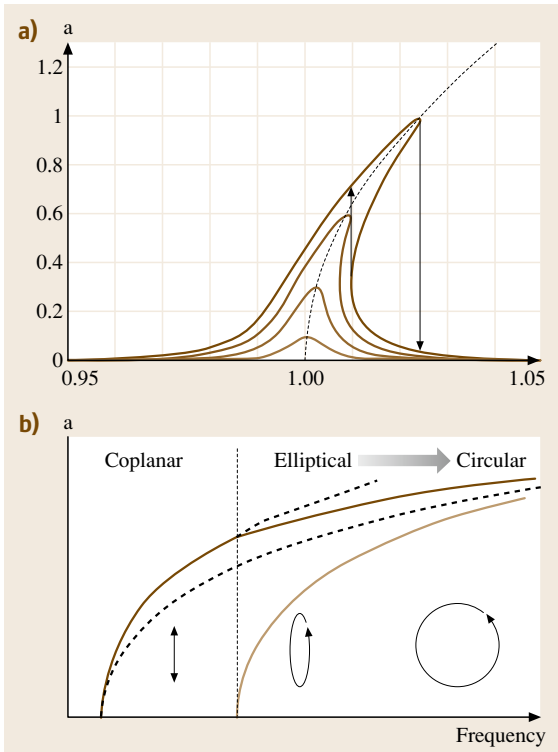


Fig. 15.29 (a) The effect of nonlinearity on the resonance curves of a stretched string with a Q of 100, for increasing drive excitation plotted against normalised resonant frequency. The *dashed curve* represents the nonlinear amplitude of the frequency for free decay. Note the hysteretic transitions at large amplitude; (b) the transition at large amplitudes from linearly polarised vibrations coplanar with the driving force to elliptical and finally circular orbital motion of the string at very large amplitudes. The two *continuous curves* represent the induced amplitudes in the directions parallel and perpendicular to the driving force

plitude rises causing the resonance frequency to shift to higher frequencies, as indicated by the dashed line in Fig. 15.29a. Damping eventually leads to a sudden collapse, with the amplitude dropping to a much lower high-frequency value, illustrated by the downward arrow. On decreasing the frequency, the response initially remains on the low-amplitude curve before making a sudden hysteretic transition back to the large amplitude, strongly nonlinear, regime.

This behaviour is characteristic of any nonlinear oscillator with a restoring force that increases in strength on increasing amplitude. For a spring constant that softens with increases displacement, as we will discuss later

in relation to Chinese gongs, the resonance curves are skewed in the opposite direction.

Orbital Motion

Nonlinearity results in another surprising effect on the driven resonant response. At sufficiently large amplitudes of vibration, a sinusoidally driven string suddenly develops motion in a direction orthogonal to and in phase-quadrature with the driving force, illustrated schematically in Fig. 15.29b. The transverse displacements then execute elliptical orbits about the central axis approaching circular motion at very large amplitudes (*Miles* [15.50]). In this limit, the string is under constant increased tension, producing an amplitude-dependent inward force balancing the centrifugal force of the orbiting string, resulting in an amplitude-dependent orbital frequency $\omega_{1*}^2 = \omega_1^2(1 + 2\beta a^2)$. For circular motion, the extension of the string and hence the increase in tension and resonant frequency are determined by the orbital radius of the whirling string, so there is now no variation in tension with time. The sense of clockwise or anticlockwise rotation is determined by chance or in practice by slight geometrical or material anisotropies of the string or supporting structure.

Such transitions have been investigated by *Hanson* and coworkers [15.51, 52] using a brass harpsichord string stretched to playing tension. The transition from linear to elliptically polarised motion was observed in addition to chaotic behaviour at very large amplitude. However, their measurements were complicated by the very long time constants predicted to reach equilibrium behaviour close to the transitional region and to rather strong and not well-understood splitting of the degeneracy of the transverse modes, even at low amplitudes when nonlinearity is unimportant.

A related effect occurs when a string is plucked so that it is given some orbital motion, as is invariably the case when plucking a string on a stringed instrument such as the guitar. Nonlinearity introduces coupling between motions in orthogonal transverse directions, causing the orbits to precess (*Elliot* [15.53], *Gough* [15.54], *Villagier* [15.48]), as illustrated by computational simulations and measurements in Fig. 15.30. The precessional frequency Ω is given by $\frac{\Omega}{\omega} = \frac{ab}{L\Delta L}$, where a and b are the major and minor semi-axes of the orbital motion and ΔL is the amount by which the string is stretched to bring it to tension [15.54].

Such precession can lead to the rattling of the string against the fingerboard on a strongly plucked instrument, as the major axis of the orbiting string precesses

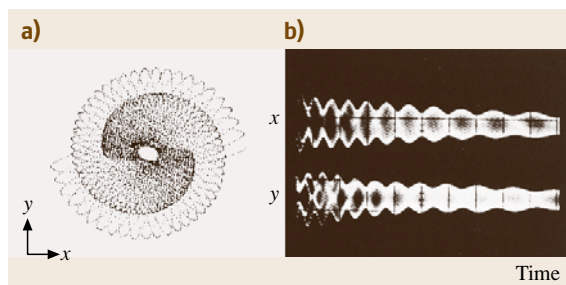


Fig. 15.30 (a) The computed precession of the damped elliptical orbits of a strongly plucked string, and (b) measurements of the orthogonal transverse components of such motion for a string plucked close to its mid-point (after [15.54])

towards the fingerboard. The nonlinear origin of such effects can easily be distinguished from other linear effects causing degeneracy of the string modes and hence beats in the measured waveform, by the very strong dependence of the precession rate on amplitude, as illustrated in Fig. 15.30b.

15.2.3 The Bowed String

Realistic Models

Although the main features of the bowed string can be described by a simple Helmholtz wave, it is important to consider how such waves are excited and maintained by the frictional forces between the bow and string. The simple Helmholtz solution is clearly incomplete for a number of reasons including:

1. The unphysical nature of infinitely sharp kinks.
2. The insensitivity of the Helmholtz bowed waveform to the position and pressure of the bow on the string. In particular, the simple Helmholtz waveform involves partials with amplitudes proportional to $1/n$, whereas such partials must be absent if the string is bowed at any integer multiple of the fraction $1/n$ along its length, since energy cannot be transferred from the bow to the string at a nodal position of a partial.
3. The neglect of frictional forces in the slipping regime.
4. The neglect of losses and reaction from mechanical coupling to structural modes at the supporting bridge.
5. The excitation of the string via its surface, which must involve the excitation of additional torsional modes.

Understanding the detailed mechanics of the strongly nonlinear coupling between the bow and string has been a very active area of research over the last few decades, with major advances in our understanding made possible by the advent of the computer and the ability to simulate the problem using fast computational methods. *Cremer* [15.30, Sects. 3–8], provides a detailed account of many of the important ideas and techniques used to investigate the dynamics of the bowed string. In addition, *Hutchins and Benade* [15.28, Vol. 1], includes a useful introduction to both historical and recent research prefacing 20 reprinted research papers on the bowed string. *Woodhouse and Galluzzo* [15.55] have recently reviewed present understanding of the bowed string.

Pressure, Speed and Position Dependence

In the early part of the 20th century, *Raman* [15.36], later to be awarded the Nobel prize for his research on opto-acoustic spectroscopy, confirmed and extended many of Helmholtz's earlier measurements and theoretical models of the bowed string. Raman used an automated bowing machine to investigate systematically the effect of bow speed, position and pressure on bowed string waveforms. He also considered the attenuation of waves on the string and dissipation at the bridge. From both measurements and theoretical models, he showed that a minimum downward force was required to maintain the Helmholtz bowed waveforms on the string, which was proportional to bow speed and the square of bow distance from the bridge. He also measured and was able to explain the wolf-note phenomenon, which occurs when the pitch of a bowed note coincides with an over-strongly coupled mechanical resonance of the supporting structure. At such a coincidence, it is almost impossible for the player to maintain a steady bowed note, which tends to *stutter* and jump in a quasi-periodic way to the note an octave above, illustrated previously for a cello with a bad wolf note, audio [13](#) **EXTRAS**.

Saunders [15.56], well known for his work in atomic spectroscopy (Russel–Saunders spin-orbit coupling) was a keen violinist and a cofounder of the Catgut Acoustical Society. He showed that, for any given distance of the bow from the bridge, there was both a minimum and a maximum bow pressure required for the Helmholtz kink to trigger a clean transition from the sticking to slipping regimes and vice versa. Subsequently, *Schelling* [15.57] derived explicit formulae for these pressures in terms of the downward bow force F as a function of bow speed v_B , assuming a simple model for friction between bow hair and string in the slipping

region of $\mu_d F$ and a maximum sticking force of $\mu_s F$,

$$F_{\min} = \frac{R_0^2 v_B}{2R\beta^2(\mu_s - \mu_d)} \quad \text{and}$$

$$F_{\max} = \frac{2R_0 v_B}{\beta(\mu_s - \mu_d)} = 4\beta \frac{R}{R_0} F_{\min}, \quad (15.51)$$

where R_0 is the characteristic impedance of the string terminated by a purely resistive load R at the bridge, and β is the fractional bowing point along the string. If the downwards force is larger than F_{\max} the string remains stuck to the string instead of springing free into the slipping regime, while for downward forces less than F_{\min} an additional slip occurs leading to a double-slipping motion.

Figure 15.31 is taken from the article by Schelling on the bowed string in the Scientific American special issue on the *Physics of Musical Instruments* [15.58]. It shows how the sound produced by a bowed cello string changes with bow position and downward bow pressure for a typical bow speed of 20 cm/s. Note the logarithmic scales on both axes. In practice, a string can be bowed over a quite a large range of distances from the bridge, bow speeds and pressures with relatively little change in the frequency dependence of the spectrum and quality of the sound of an instrument, apart from regions very close and very distant from the bridge. Nevertheless, the ability to adjust the bow pressure, speed and distance from the bridge, to produce a good-quality steady tone, is one of the major factors that distinguish an experienced performer from the beginner.

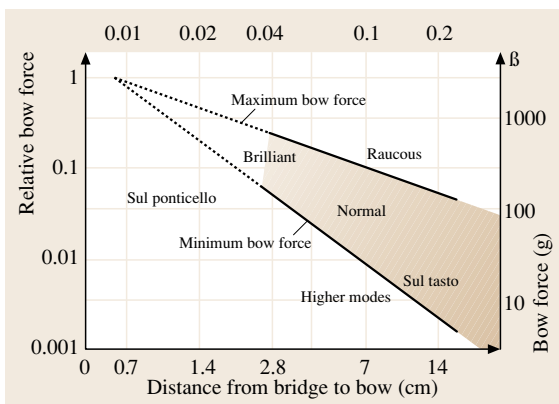


Fig. 15.31 The playing range for a bowed string as a function of bow force and distance from bridge, with the bottom and right-hand axis giving values for a cello open A-string with a constant bow velocity of 20 cm s^{-1} (after Schelling [15.57])

Slip–Stick Friction

An important advance was the use of a more realistic frictional force, dependent on the relative velocity between bow and string, shown schematically for three downward bow pressures in Fig. 15.32. Such a dependence was subsequently observed by Schumacher [15.59] in measurements of steady-state sliding friction between a string and a uniformly moving bow. The frictional force is proportional to the downward bow pressure.

Friedlander [15.60] showed that a simple graphical construction could be used to compute the instantaneous velocity v at the bowing point from the velocity $v_p(t)$ at the bowing point induced by the previous action of the bow. The new velocity is given by the intersection of a straight line with slope $2R_0$ drawn through v_p with the friction curve, where R_0 is the characteristic string impedance. This follows because the localised force between the bow and string generate secondary waves with velocity $F/2Z_0$ at the bowing point as previously described (15.34). In the slipping region well away from capture, there will be just a single point of intersection, so the problem is well defined. However, close to capture, as illustrated by the intersections marked by the black dots with the upper frictional curve, the straight line can intersect in three points (two in the slipping regime and one in the sticking regime) as first noted by Friedlander.

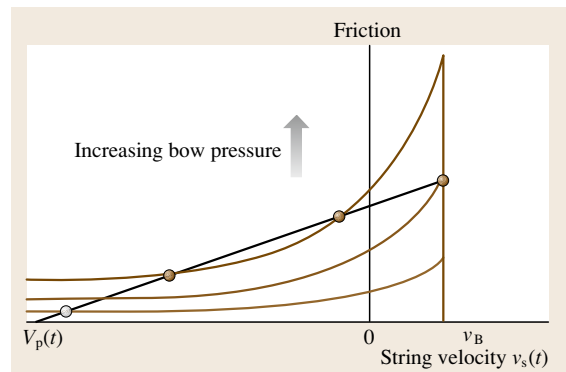


Fig. 15.32 Schematic representation of the dependence of the frictional force between bow and string on their relative velocity and downward pressure of the bow on the string. The straight line with slope $2R_0$ passes through the velocity v_p of the string determined by its past history and the intersection with the friction curves determines its current velocity. The open circle represents the single intersection in the slipping regime at low bow pressures, while the closed circles illustrate three intersections at higher pressures

Computational Models

This model has been used in a number of detailed computational investigations of both the transient and steady-state dynamics of the bowed string, notably by the Cambridge group lead by *McIntyre* and *Woodhouse* [15.61–63], their close collaborator *Schumacher* [15.59, 64] from Carnegie-Mellon, and *Guettler* [15.65], who is also a leading international double-bass virtuoso. Readers are directed to the original publications for details of the various computational schemes used, which are also discussed in some detail by *Cremer* [15.30, Sect. 8.2].

Whenever a string is bowed at an integer interval along its length, the secondary waves excited by the frictional forces between bow and string can give rise to coherent reflections between the bow and bridge, giving rise to pronounced *Schelling ripples* on the Helmholtz waveform and hence significant changes in the spectrum of the radiated sound. However, because the bowing force tends to be distributed across the ≈ 1 cm width of the bow hairs, such effects tend to be smeared out and are not generally of significant musical importance. *McIntyre* et al. [15.63] have also shown that uncertainties in the sticking point from the finite-width strand of bow hairs leads to a certain amount of jitter or aperiodicity in the pitch of the bowed string amounting of a few cents, which is again of little musical significance, though the noise generated may be significant in contributing to the characteristic sound of bowed string instruments.

It is instructive to consider the kind of computational methods developed by *Woodhouse* and his collaborators to investigate both the initial transient and the steady-state dynamics of the bowed string. This is illustrated schematically in Fig. 15.33, where u and u' represent the velocity under the bow from waves travelling

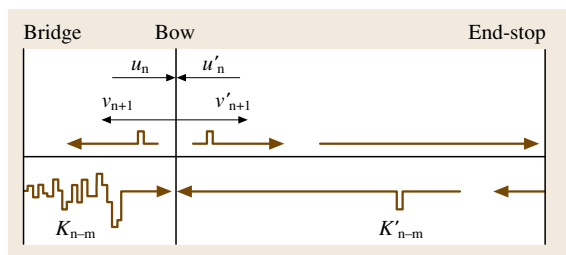


Fig. 15.33 Schematic representation of the model used by *McIntyre* and *Woodhouse* to compute bowed string dynamics. The velocities u and v represent incoming and outgoing waves from the two ends, with reflections of impulse functions from the bridge and end-stop represented in their digitised form

towards the bow from the bridge and from the stopped end of the string respectively, and v and v' are the velocities at the bowing point of the waves travelling away from the bow. In the absence of any bowing force $v = u'$ and $v' = u$. However, in the presence of a frictional force between the bow and string, the outgoing waves will acquire an additional velocity $f/2R_0$, where the frictional force is determined by the velocity from the incoming waves $u + u'$ excited by previous events. The outgoing wave travelling towards the stopped end or nut of the string will simply be reflected, while the outgoing wave reaching the bridge will not only be reflected, but will also excite continuing vibrations at the bridge from the excitation of the coupled structural modes.

Such problems can be solved using a Green's function approach *Cremer* [15.30, Sect. 8.4], in which the outgoing waves can be considered in terms of the response to forces represented as a succession of short impulses. The problem is then reduced to understanding the response of the system for the reflection of a sequence of short impulses or δ functions. At the end-stop, an impulse will simply be reflected with reversed sign, but reduced amplitude in the case of a soft finger stopping the string. The incoming wave u' generated by the reflected impulse will therefore be an impulse function delayed in time by the transit time from the bow to the end-stop and back. Similarly, the impulse returning from the bridge will be an impulse delayed by the transit time between bow and bridge and back followed by a wave generated by the induced motions of the bridge on reflection. The time-delayed impulse responses from reflections at the bridge and end-stop can be described by the functions $K(t)$ and $K'(t)$. The incoming waves ($u(t), u'(t)$) can then be described by the convolution of $K(t)$ and $K'(t)$ with the outgoing waves ($v(t), v'(t)$) considered as a succession of impulse functions at all previous times t' , such that

$$u(t) = \int_0^t v(t')K(t-t')dt' \quad \text{and}$$

$$u'(t) = \int_0^t v'(t')K'(t-t')dt'. \quad (15.52)$$

To compute the resulting dynamics of string motion digitally, one simply computes the above velocities at a succession of short time intervals, with the outgoing waves determined from the incoming waves plus the secondary waves induced by the resulting frictional force, such that

$$v'_{n+1} = u_n + f_n/2R_0 \quad \text{and}$$

$$v_{n+1} = u'_n + f_n/2R_0 \quad (15.53)$$

and

$$u_{n+1} = \sum_{m=1}^n v_m K_{n-m} \quad \text{and} \\ u'_{n+1} = \sum_{m=1}^n v'_m K'_{n-m}, \quad (15.54)$$

where K_j and K'_j are now the digital equivalents of the time-delayed impulse responses, illustrated schematically in Fig. 15.33. The frictional force f_n entering (15.53) is evaluated from the pressure- and velocity-dependent frictional force using the Friedlander construction with the computed string velocity under the bow given by $u_n + u'_n$.

Pressure Broadening and Flattening

As an example, Fig. 15.34 illustrates the computed velocity of the string under the bow as a function of increasing bow pressure (McIntyre et al. [15.61]). In contrast to the rectangular waveform predicted by the simple Raman model, the waveform is considerably rounded, especially at low bow pressures. This results in a less strident, less intense sound, with the higher partials strongly attenuated. At higher pressures, but at

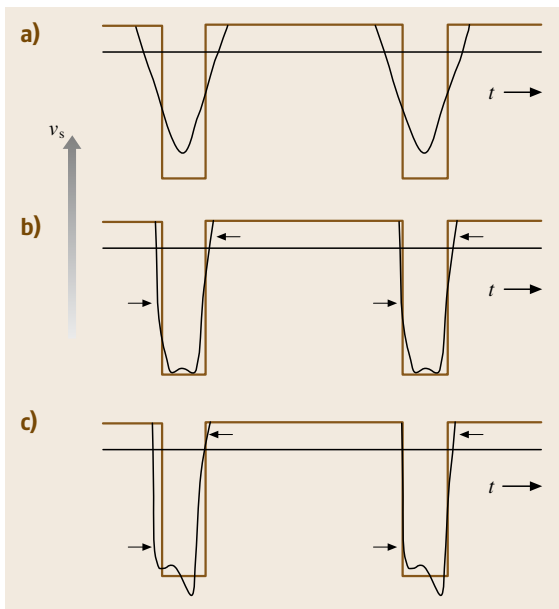


Fig. 15.34a–c Computed velocity of string at bowing point for increasing bow pressures in the ratios 0.4 : 3 : 5 (after McIntyre and Woodhouse [15.61]) illustrating both the broadened waveform and pitch dependence on bow pressure compared with the idealised rectangular Helmholtz bowed waveform

the same position and with the same bow velocity, the rounding is less pronounced, so that higher partials become increasingly important. The increased intensity of the higher partials leads to an increased perceived intensity with bow pressure, in contrast to the Raman model, in which the waveform and hence intensity remains independent of bow pressure. This is referred to as the *pressure effect*. At even higher pressures, the ambiguity in intersections noted by Friedlander leads to a pronounced increase in the capture period and hence the pitch of the bowed note, known as the *flattening effect*. These features are discussed in considerable detail along with his own important research and that of his collaborators on such effects by Cremer [15.30, Chaps. 7 and 8].

Initial Transients

Computational models can also describe the initial transients of the bowed string before the steady-state Helmholtz wave is established. Figure 15.35 compares the computed and measured initial transients of the string velocity under the bow for a string played with a sharp attack (a martelé stroke) (McIntyre and Woodhouse [15.61]). These computations also include the additional excitation of torsional waves, which are excited because the bowing force acts on the outer diameter of the wire, exerting a couple in addition to a transverse force. The excitation and loss of energy to the torsional waves appears to encourage the rapid stabilisation of the bowed Helmholtz waveform.

For low-pitched stringed instruments such as the double bass, it is very important that the Raman bowed waveform is established very quickly, otherwise there will be a significant delay in establishing the required pitch. Remarkably, Guettler [15.65] has shown that, by

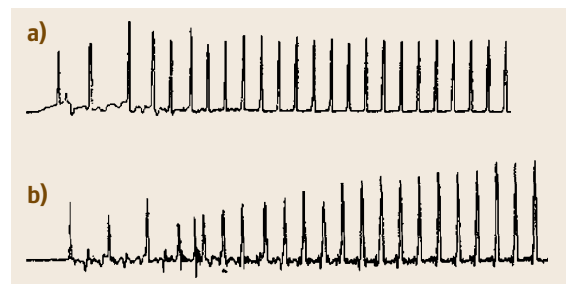


Fig. 15.35 (a) Computed transient string velocity at the bowing point for a strongly bowed string including coupling to both transverse and torsional modes and **(b)** the measured string velocity for a strongly played martelé bow stroke (after McIntyre and Woodhouse [15.61])

simultaneously controlling both bow speed and downward pressure, the player can establish a regular Raman waveform in a single period. The speed with which a steady-state bowed note can be established can be represented on a *Guettler diagram*, where the number of slips before a steady-state Helmholtz motion is established can be illustrated as a two-dimensional histogram as a function of bowing force and acceleration of the bow speed from zero.

To investigate such effects experimentally, *Galluzzo* and *Woodhouse* [15.55, 67] have recently developed a dynamically controlled bowing machine with active feedback, providing programmable control of both downward bow pressure and bow speed. This enables reliable and reproducible results to be made over a very wide range of possible playing parameters, extending *Guettler's* original measurements.

Viscoelastic Friction

Recent measurements have shown that the frictional model assumed in these investigations is oversimplistic. The force between the bow hairs and the string is maintained by a thin layer of rosin which coats them both. Rosin is a rather soft, sticky substance, with a glass-to-liquid transition not far above room temperature, resulting in viscoelastic properties, which are very sensitive to temperature (*Smith, Woodhouse* [15.66]). As the bow slides past the bow hair, the frictional forces will heat the rosin and hence reduce its viscoelasticity frictional properties. During the sticking regime, with no work being done at the bow–string interface,

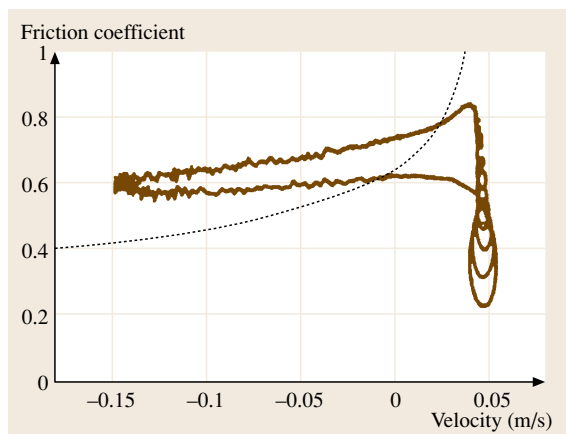


Fig. 15.36 Measured hysteretic frictional force between string and a glass bow coated with rosin, with the *dashed line* indicating previously assumed velocity dependence (after *Smith and Woodhouse* [15.66])

the rosin will cool down and the friction will increase. The frictional forces are therefore hysteretic and will be strongly dependent on past history within a given period of string vibration. *Woodhouse* et al. [15.68] and *Smith* [15.69] have investigated this hysteretic behaviour in some detail using rosin-coated glass rods. The hysteretic properties shown in Fig. 15.36 were deduced from measurements at the two supported ends of the string. *Woodhouse* [15.70] subsequently extended his computational models to incorporate the hysteretic frictional properties. Somewhat surprisingly, this more realistic model made little qualitative difference to the predicted behaviour. Such measurements contribute to our understanding of the physical processes underlying viscoelastic properties of various coatings and lubricants and have become an important tool in the field of tribology (studies of friction).

15.2.4 Bridge and Soundpost

We now consider the role of the bridge and soundpost in providing the coupling between the vibrating strings and the vibrational modes of the body of instruments of the violin family. We also consider the influence of such coupling on the modes of string vibration, which involves a discussion of the very important influence of damping on the normal modes of any coupled system.

Bridges

Many plucked and struck stringed instruments, such as the piano or guitar, use a rather low solid bridge to support the strings and transfer energy directly from the transverse string vibrations perpendicular to the supporting soundboard or front-plate of the instrument. The bridge needs only to be sufficiently high to prevent the strings from vibrating against the fingerboard or shell of the instrument. This is also true for the Chinese two-string violin, the *erhu*, which is held and played so that the bow excites string vibrations perpendicular rather than parallel to the stretched snake-skin membrane supporting the bridge and strings. The strings of a harp are attached to an angled sounding board, so that transverse string vibrations in the plane of the strings couple directly to the perpendicular vibrations of the supporting soundboard *Fletcher and Rossing* [15.5, Sect. 11.2].

For such instruments, the bridge and other string terminations play a relatively insignificant acoustic role, apart from adding a small inertial mass and additional stiffness to the soundboard or top plate, which only slightly perturbs the frequencies of the structural modes of vibration.

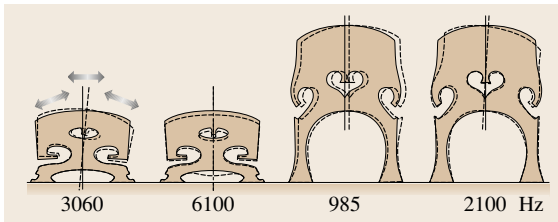


Fig. 15.37 The lowest in-plane resonant modes and frequencies of violin and cello bridges (after *Reinicke* [15.71]). The *arrows* represent the vibrational directions of the bowed outer and middle strings


In contrast, the rather high bridges on instruments of the violin and viol families have a profound influence on the acoustical properties, particularly at frequencies comparable with and above any mechanical resonances of such structures. Figure 15.37 illustrates the shape of modern violin (and viola) and cello bridges and indicates their principal vibrational modes, as measured by *Reinicke* and *Cremer* [15.71, 72] using laser interference holography. Bridges are cut from maple and taper in thickness from the two feet to the top surface supporting the four strings, which are set in small v-shaped locating grooves.

Reinicke [15.71, 72] showed that the lowest violin bridge resonance at typically around 3 kHz involves a rotational motion of the top half of the bridge about its waist. The rotational motion induced by the vibrating strings supported on the top of the bridge results in a couple acting on the top plate via the two feet. The next most important in-plane resonance is at ≈ 6 kHz and involves the top of the bridge bouncing up and down on its feet, resulting in forces via the legs perpendicular to the supporting surface. The cello bridge has rather longer legs, resulting in two low-frequency twisting modes with resonances at around 1 and 2 kHz, both of which exert a couple on the top plate. Longitudinal forces from the vibrating strings can also induce bridge motion perpendicular to its plane (at double the frequency of the vibrating strings), but such motion is generally rather small and will be ignored for the purposes of this chapter.

Any transverse string force at the top of the bridge, from bowing, plucking or striking the string, will be transferred to the supporting body via the two feet. This will induce a linear motion of the centre of mass of the instrument, rotation about its centre of mass and the excitation of both flexural and longitudinal waves in the plates of the instrument. Because bowing involves a static force which reverses with bow direction,

a bowed instrument has to be held fairly firmly by the player, which introduces an extra channel for energy loss through the supporting chin and fingers. The induced linear and rotational motions of an instrument are relatively unimportant at audio frequencies as they involve the whole mass M of the instrument with admittances varying $\approx 1/iM\omega$.

If a tall bridge is placed centrally on a symmetric shell structure, like the body of an early renaissance viol, the plucked or bowed motion of the strings parallel to the supporting top plate would excite only asymmetrical modes of the supporting structure, whereas perpendicular string vibrations would excite only symmetrical modes. For instruments of the violin family, an offset soundpost is wedged between the front and back plates, which destroys the symmetry. The coupled modes will then involve a linear combination of symmetrical and asymmetric body modes, as discussed later (Sect. 15.2.6).

The arching of the top of the bridge allows each of the supported four strings to be bowed separately or together (double stopping), with the bow direction making an angle of around $\pm 15\text{--}20^\circ$ relative to the top plate for the outer two strings and almost parallel for the middle two strings. Bowing on the outer two strings therefore involves significant perpendicular in addition to parallel forces, but only slightly different sounds from a single type of string when supported in different positions on the bridge. Audio  **EXTRAS** compares the sound of a bowed covered-gut D-string mounted in the normal position and in the G-, A- and E-string positions on the same violin. On a guitar almost all the sound is produced by the vertical motion of the plucked string rather than by parallel vibrations, which primarily excite nonradiating longitudinal modes of the top plate.

Simplified Bridge Model

Cremer [15.30, Chap. 9] gives a detailed historical and scientific introduction to research on violin and cello bridges and their coupling to the body of the instrument. Relatively complicated mechanical models are described composed of several masses and springs to account for the various possible vibrational modes of the bridge. However, the principal resonances of the violin bridge shown in Fig. 15.37 can be modelled very simply by a two-degree-of-freedom mechanical model, with effective masses representing the linear and rotational energy of the top of the bridge coupled to the supporting surface through the two supporting feet via a rotational or vertical spring, illustrated schematically in Fig. 15.38. The relatively light mass and added rigid-

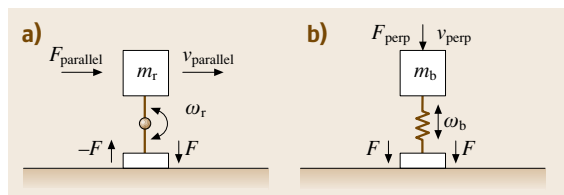


Fig. 15.38a,b Simplified mechanical models for the lowest (a) rotational and (b) bouncing motions of the bridge supported by its two feet on a rigid surface

ity of the lower half of the bridge will only slightly perturb the resonant frequencies of the more massive supporting plates and can therefore be ignored as a first approximation. The effective masses and strength of the coupling springs can be chosen to reproduce the vibrational characteristics of the first two vibrational modes of the violin (or cello) bridge, which dominate the acoustical properties of the instrument.

At low frequencies, well below any resonant frequency, the bridge will vibrate as a rigid body, adding a small amount of additional mass, moment of inertia and rigidity to the top plate, which will again only slightly perturb the vibrational frequencies of the supporting shell structure. The additional relative height of the cello bridge compared with that of the violin bridge enables a rather larger couple to be exerted by the bowed string on the more massive top plate. There is a delicate balance between increasing the coupling to enhance the intensity at low frequencies without making it so strong that troublesome wolf-note problems arise, as referred to earlier.

Bridge-Hill (BH) Feature

Reinicke [15.71, 72] and Cremer [15.30] highlighted the importance of the bridge resonance on both the sound of the violin and on admittance measurements, which are traditionally made by exciting the violin at the top of the bridge using an external force parallel to the top supporting plate. In recent years, this problem has attracted renewed interest, in an attempt to describe the rather broad peak and associated phase changes superimposed on the multi-resonant response of the instrument, which Jansson refers to as the *Bridge-Hill* (BH) feature [15.74, 75].

Figure 15.39 shows recent measurements by Woodhouse [15.73] of the modulus of the admittance at the bridge for a particular instrument using a series of bridges with different masses but the same resonant frequency at ≈ 2 kHz. A strong but rather wide overall BH peak is observed in the vicinity of the bridge resonance.

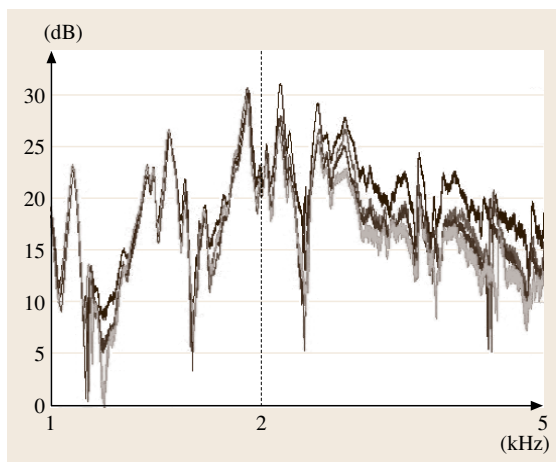


Fig. 15.39 The admittance at the top of the bridge on a single violin, plotted on the same but arbitrary dB scale, for a number of violin bridges having the same height and resonant frequency (≈ 2 kHz) but different masses. The upper curve corresponds to the lightest bridge that could be fabricated from a standard bridge blank and the lowest curve by the heaviest. Subtracting 45 dB from the results would give the approximate admittance in units of $\text{ms}^{-1}\text{N}^{-1}$ (data kindly provided by Woodhouse [15.73])

Note the marked decrease in admittance with increasing bridge mass above the bridge resonance. There is also an associated overall 90° change in the phase of the admittance on passing through the peak.

Evidence for the BH feature can also be seen in Dünwald's [15.76] superimposed measurements of the sound output of a large number of high-quality Italian, modern master and factory violins as a function of sinusoidal input force at top of the bridge, shown in Fig. 15.40. A surprising aspect of these measurements is the apparent lack of any such feature for modern master violins, possibly because of a wider variation in bridge resonances and effective masses of bridge and plate resonances in the chosen instruments. From measurements of the radiated sound of over 700 violins, Dünwald proposed that the presence of a number of strong acoustic resonances in the broad frequency band from 1.5 to 4 kHz was one of the distinguishing features of a really fine instrument. The influence of the bridge in accounting for such a peak and the reduced response at higher frequencies is clearly important.

Woodhouse [15.77] has recently revisited the problem of the coupling between bridge and body of the instrument and the origin of the BH peak. A simple theoretical model shows that the peak depends on

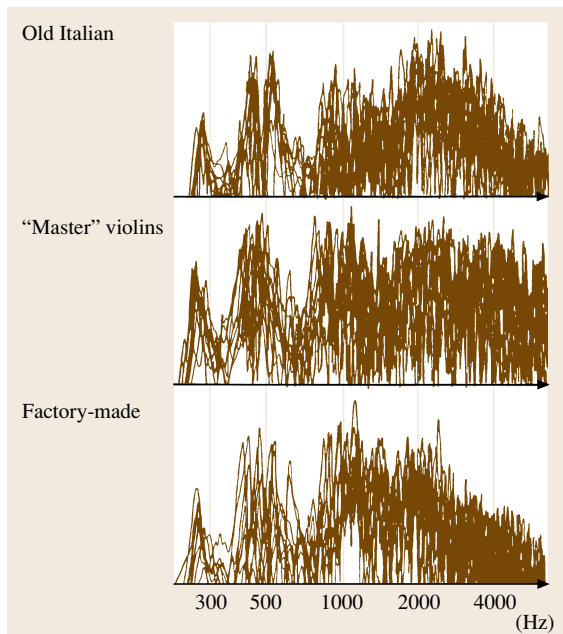


Fig. 15.40 Overlays of the sound output of 10 typical old Italian, modern master instruments, and 10 factory instruments for a constant sinusoidal force at the top of the bridge (after *Dünnwald* [15.76])

many factors, such as the effective masses, Q -values and resonant frequencies of the major vibrational modes of the bridge and the multi-resonant properties of the instrument. To demonstrate the overall effect of the bridge without having to consider the detailed vibrational response of a particular instrument, Woodhouse first considered coupling to a simplified model for the vibrational modes of the coupled instrument. This assumed a set of coupled vibrational modes each having the same effective mass M and Q -value, with a constant spacing of resonances $\omega_0 = 2\pi \Delta f$. Different values for these parameters would need to be used to model the independent rotational or bouncing modes, though Woodhouse concentrates on the influence of the lowest frequency *rocking* bridge mode. The merit of such a model is that the multi-resonant response of such a system varies monotonically with frequency. The features introduced by the resonant properties of the bridge can then be easily identified and the input admittance expressed relative to the admittance A_V for a completely rigid bridge of the same mass, where

$$A_V(\omega) = \frac{1}{M} \sum_n \frac{i\omega}{(n\omega_0)^2 - \omega^2 + i\omega n\omega_0/Q}. \quad (15.55)$$

The corresponding input admittance for the one-degree-of-freedom model bridge is then given by

$$A_{BB}(\omega) = \frac{A_V + i\omega/m\omega_B^2}{1 - (\omega/\omega_B)^2 + i\omega m A_V}, \quad (15.56)$$

where m is the effective mass of the bridge and ω_B its resonant frequency and internal damping of the bridge has been neglected.

We can also define a nonlocal admittance or mobility A_{VB} to describe the induced body motion per unit force at the foot of the bridge given by

$$A_{VB}(\omega) = \frac{A_V}{1 - (\omega/\omega_B)^2 + i\omega m A_V}. \quad (15.57)$$

The simulations in Fig. 15.41 illustrate the major effect of the bridge resonance on both the input response and induced body motion and hence radiated sound at, around and above the resonant frequency of the bridge (3 kHz in the above example). For a real instrument, the spacing and Q -values of the individual modes will be very irregular and highly instrument dependent; nevertheless, the effect of the bridge resonance on the overall response will be very similar. In particular, the bridge resonance gives a broad peak in input admittance followed by a 6 dB/octave decrease in the admittance above resonance, where the response is largely dominated by the bridge dynamics rather than that of the instrument itself, with $A_{BB} \approx 1/im\omega$. Note that the height and width of the peak is largely determined by energy lost to the coupled structural vibrations (including, in practice, additional energy lost to all the supported strings) rather than from internal bridge losses, which have been neglected in this example.

The bridge resonance introduces a somewhat smaller peak in the induced body mobility and hence radiated sound. Well above the bridge resonance, the induced body velocity is given by $A_{VB}(\omega_B/\omega)^2$, with an intensity decreasing by 12 dB/octave. Unlike the input bridge admittance, the induced body motion and output sound retains the characteristic resonances of the instrument, though attenuated.

The predicted difference in admittance at the top of the bridge A_{BB} and top of the instrument A_V is illustrated in Fig. 15.42, in measurements by *Moral* and *Jansson* [15.78] reproduced by *Cremer* ([15.30], Fig. 15.9). Whereas the average admittance of the violin varies relatively little with frequency, the admittance at the bridge shows a pronounced BH peak with a relatively featureless and approximately $1/f$ (the added solid line) variation above the peak, as anticipated from the above model.

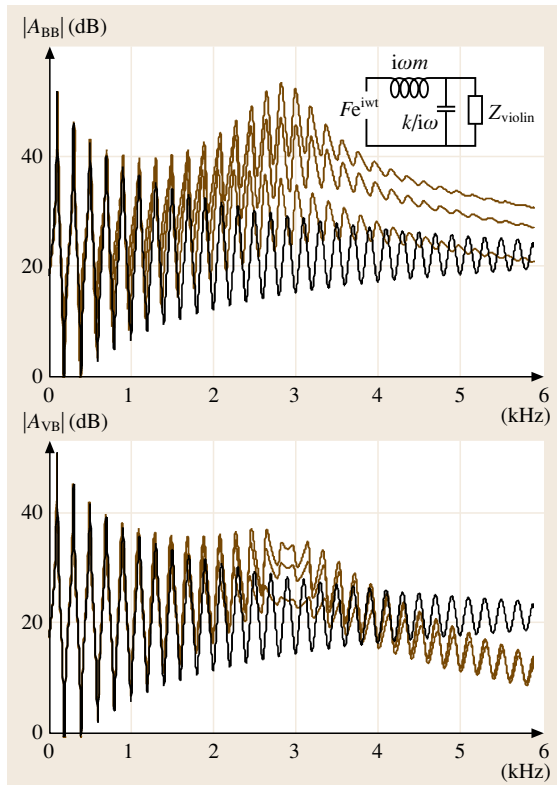


Fig. 15.41a,b Response curves for a one-degree-of-freedom bridge coupled to an artificial set of regularly spaced (200 Hz), constant effective mass (100 g) and constant Q (50) structural resonances. Panel (a) illustrates the effect of bridge mass on the admittance A_{BB} measured at the point of excitation at the top of the bridge, while (b) illustrates the corresponding induced body mobility A_{VB} . The coloured response curves are for lossless bridges with effective masses 1, 1.5 and 3 g (highest to lowest response), having the same resonant frequency at 3 kHz (after Woodhouse [15.77]) The black curves show the violin body response A_V that would be measured using a massless rigid bridge

Woodhouse [15.77] has extended this idealised model to describe the coupling of the bridge to a more realistic, but still simplified, model for the vibrational modes of the violin with a soundpost. This changes the detailed response, but not the overall qualitative features. Because the response of a violin depends rather randomly at higher frequencies on the positions and Q -values of the structural modes, Woodhouse uses a logarithmic scale to average the peaks and troughs at the maxima and minima of the admittance (approx-

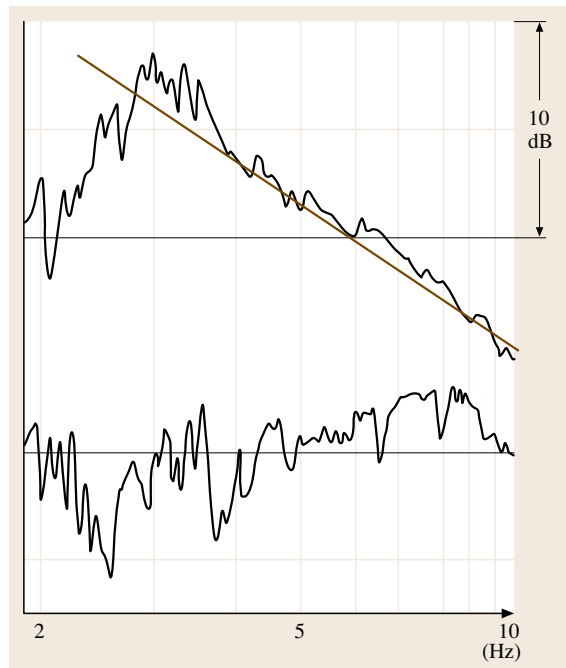


Fig. 15.42 Admittances of a violin measured at the top of the bridge (top trace) and at the left foot of the bridge (lower trace) illustrating a strong BH peak when measured at the top of the bridge but a relatively monotonic dependence of the body of the instrument (after Cremer [15.30, Fig. 12.9]). The added solid line represents the $1/f$ reduction in the predicted BH response above the bridge resonance

imately proportional to Q and $1/Q$), to give a *skeleton curve* describing the global variation of the violin's complex admittance (more details are given in the later Sect. 15.2.3 on shell modes). This enables Woodhouse to illustrate the influence of various bridge parameters on the acoustical properties of the instrument, suggesting ways in which violin makers could vary bridge properties to optimise the sound quality of an instrument, though that will always be a matter of personal taste rather than being scientifically defined.

The important role of the bridge in controlling the sound of the violin or cello has often been overlooked, even by many skilled violin makers. Indeed one of the reasons why Cremonese violins generally produce such highly valued sounds is the experience and skill involved in adjusting the mass, size and fitting of the bridge (and the position of the soundpost) to optimize the sound quality, investigated experimentally by Hacklinger [15.79].

Added Mass and Muting

A familiar demonstration of the importance of the mass of the bridge on the sound of an instrument is to place a light mass or mute on the top of the bridge. This dramatically softens the tone of the instrument by decreasing the resonant frequency of the bridge and hence amplitude of the higher-frequency components in the spectrum of sound. The added mass Δm lowers the resonant frequency ω_B by a factor $[m/(m + \Delta m)]^{1/2}$. Figure 15.43 illustrates changes in resonant frequency measured by Reinicke for a bridge mounted on a rigid support for an additional mass of 1.5 g and when wedges are inserted between the *wings* of the bridge to inhibit the rotational motion of the top of the bridge and hence the resonant frequency. Audio [EXTRAS](#) illustrates the changes in sound of a violin before and after first placing a commonly used 1.8 g mute and then a much heavier practice mute on top of the bridge, and after wedges were inserted in the bridge to inhibit the rocking motion.

Soundpost and Bass Bar

In instruments of the violin family, a soundpost is wedged asymmetrically between the top and back plates, as illustrated schematically in Fig. 15.44. Additionally, a bass bar runs longitudinally along much of the length of the bass-side of the front plate. The soundpost and bass bar give added mechanical strength to the instrument, helping it to withstand the rather large downward force from the angled stretched strings pass-

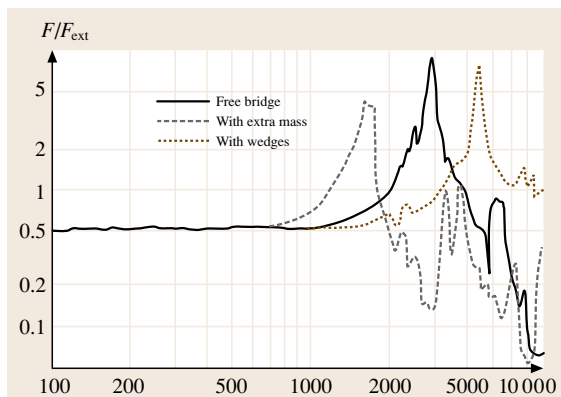


Fig. 15.43 Measurements of bridge resonances from measurements of the ratio of the force exerted by one bridge foot on a rigid surface to the applied force, for an added mass of 1.5 g and for wedges introduced between the *wings* of the bridge to increase its rotational stiffness (after Reinicke data reproduced in Fletcher and Rossing [15.5, Fig. 10.19])

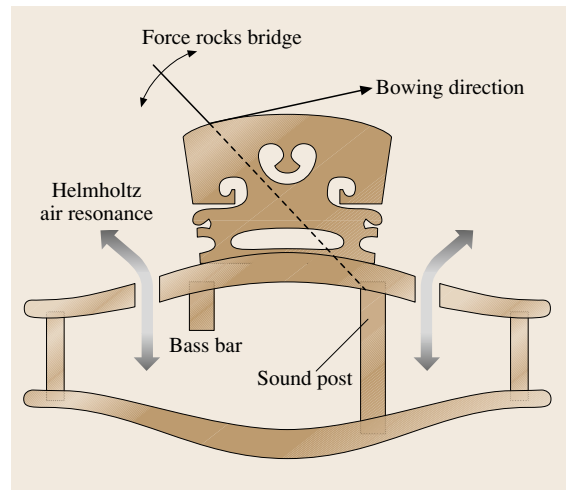


Fig. 15.44 Schematic cross section of the violin illustrating the position of the soundpost, bass-bar and f-hole openings

ing over the bridge, which is typically ≈ 10 kg weight for the violin.

The influence of the soundpost on the quality of sound is so strong that the French refer to it as the *âme* (soul) of the instrument. Its acoustic function is to provide a rather direct coupling of the induced bridge vibrations to both the back and the front plates of the instrument and to provide an additional mechanical constraint, so that the bowed string vibrations excite normal modes, which are linear combinations of the asymmetric and symmetric modes of vibration of the front and back plates of the instrument.

Of modern stringed instruments, only the violin family makes use of a soundpost. However, soundposts were probably used in the medieval fiddle and other early instruments including the viol. The ancient Celtic *crwyth* effectively combined the functions of the bridge and soundpost by using a bridge with feet of unequal length, the first resting on the top plate and the second passing through a hole in the front face to rest on the back plate – a bridge design still used today in the folk-style Greek *rebec* (see Gill [15.80]).

15.2.5 String–Bridge–Body Coupling

We now consider the interaction of the strings with the vibrational modes of the body of the instrument via the bridge. Because we are dealing with the coupling of the vibrational modes of the strings, bridge and body of the instrument, the problem has to be considered in terms

of the normal modes of the coupled system. An important aspect of this problem that is often not widely recognised, but is always important in dealing with musical instruments, is the profound influence of damping on the nature of the coupled modes. This is a generic phenomenon for any system of coupled oscillators. As we will see, the strength of the damping relative to the strength of the coupling determines whether a system can be considered as weakly or strongly coupled.

String–Body Mode Coupling

For simplicity, we only consider the perturbation of string resonances from the induced motion of the bridge and ignore any damping introduced by, for example, a finger stopping the string at its opposite end. In general, as we have already seen, the admittance at the point of string support on the bridge will be a complicated, multi-resonant, function of frequency reflecting the normal modes of vibration of the coupled structure. The normal modes will include the combined motions of all parts of the violin body, including the body, bridge, neck, tailpiece, etc.

Each coupled normal mode will contribute a characteristic admittance, which will be spring-like below its resonant frequency, resistive at resonance and mass-like above resonance. The effect of such terminations on the vibrating string is therefore to shift its effective nodal position, as illustrated in Fig. 15.45a–c, for a spring-like string termination with spring constant K , an effective mass M and a lossy support with resistance R .

For a spring-like termination with spring constant K , the bridge will move in phase with the force acting on it. This will increase the effective length of the vibrating string between nodes by a distance $\Delta_B = T/K$, lowering the frequency of a string mode by a fraction T/KL . For a mass-like termination M , the end-support will move in anti-phase with the forces acting on it, so that the effective string length is shortened. The string frequencies are then increased by the fraction $T/M\omega_n^2 = (1/n\pi)^2 m/M$, where m is the mass of the string. It is less easy to visualise the effect of a resistive support because the induced displacement is in phase-quadrature with the driving force. Mathematically, however, a resistive termination can be considered as an imaginary mass $m^* = R/i\omega$ leading to an imaginary fractional increase in frequency $i\omega_n 1/(n\pi)^2 m/R$. This imaginary frequency is equivalent to an exponential decay $e^{-t/\tau}$ for all modes with $\tau = \pi^2 R/m\omega_1^2$, where ω_1 is the frequency of the fundamental string mode. This result can also be derived using somewhat more physical arguments, by equating the loss of stored

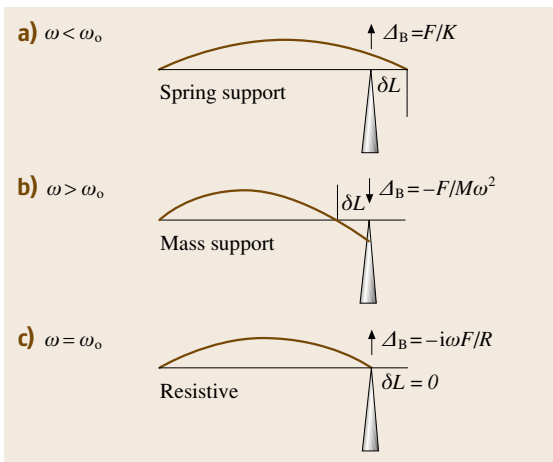


Fig. 15.45a–c Coupling of vibrating string to a weakly coupled normal mode via the bridge for the string resonance (a) below the resonant frequency of the coupled mode, (b) above the resonant frequency, and (c) at resonance

vibrational energy to the energy dissipated at the end-support.

The terminating admittance at the bridge for a single coupled vibrational mode can be written in the form

$$A_n(\omega) = \frac{1}{M_n} \frac{i\omega}{\omega_n^2 - \omega^2 + i\omega\omega_n/Q_n}, \quad (15.58)$$

with the real part of this function determining the decay time of the coupled string resonances and the imaginary part the perturbation in their resonant frequencies. The perturbations are proportional to the ratio of mass of the vibrating string to the effective mass of the coupled resonance at the point of string support on the bridge and vary with frequency with the familiar dispersion and dissipation curves of a simple harmonic oscillator. For a multi-resonant system like the body of any stringed instrument, the string perturbations from each of the coupled structural resonances are additive.

Normal Modes and Damping

Strictly speaking, whenever one considers the coupling between any two or more vibrating systems, one should always consider the normal modes or coupled vibrations rather than treat the systems separately, as we have done above. However, the inclusion of damping has a profound influence on the normal modes of any system of coupled oscillators (Gough [15.81]) and justifies the above *weak-coupling approximation*, provided that the coupling at the bridge is not over-strong. Although we

consider the effect of damping in the specific context of a lightly damped string coupled to a more strongly damped structural resonance, the following discussion is completely general and is applicable to the normal modes of any coupled system of damped resonators.

Consider a string vibrating in its fundamental mode coupled via the bridge to a single damped structural resonance. The string has mass m , an unperturbed resonant frequency of ω_s a Q -value of Q_s and a displacement at its mid-point of v . The coupled structural resonance has an effective mass M at the point of string support, an unperturbed resonant frequency of ω_M a Q -value of Q_M and displacement of u .

The vibrating string exerts a force on the coupled body mode, such that

$$M \left(\frac{\partial^2 v}{\partial t^2} + \frac{\omega}{Q_m} \frac{\partial v}{\partial t} + \omega_M^2 v \right) = T \left(\frac{\pi}{L} \right) u. \quad (15.59)$$

Multiplying this expression through by $\partial v / \partial t$, one recovers the required result that the rate of increase in stored kinetic and potential energy of the coupled mode is simply the work done on it by the vibrating string less the energy lost from damping. Similar energy balance arguments enable us to write down an equivalent expression for the influence of the coupling on the string vibrations,

$$\frac{m}{2} \left(\frac{\partial^2 u}{\partial t^2} + \frac{\omega}{Q_M} \frac{\partial u}{\partial t} + \omega_M^2 u \right) = T \left(\frac{\pi}{L} \right) v, \quad (15.60)$$

where the effective mass of the vibrating string is $m/2$ (i. e. its energy is $1/4 m \omega^2 u^2$). To determine the normal-mode frequencies, we look for solutions varying as $e^{i\omega t}$. Solving the resultant simultaneous equations we obtain

$$\begin{aligned} & \left(\omega_M^2 - \omega^2 (1 - i/Q_M) \right) \left(\omega_m^2 - \omega^2 (1 - i/Q_m) \right) \\ &= \left(T \frac{\pi}{L} \right)^2 \frac{2}{mM} = \alpha^4, \end{aligned} \quad (15.61)$$

where α is a measure of the coupling strength.

Solving to first order in $1/Q$ -values and α^2 we obtain the frequencies of the normal modes Ω_{\pm} of the coupled system,

$$\Omega_{\pm}^2 = \omega_{\pm}^2 \pm \left(\omega_{\pm}^4 + \alpha^4 \right)^{1/2}, \quad (15.62)$$

where

$$\omega_{\pm}^2 = \frac{1}{2} \left[\omega_M^2 \pm \omega_m^2 + i \left(\frac{\omega_M^2}{Q_M} \pm \frac{\omega_m^2}{Q_m} \right) \right]. \quad (15.63)$$

If the damping terms are ignored, we recover the standard perturbation result with a splitting in the

frequencies of the normal modes at the crossover frequency (when the uncoupled resonant frequencies of the two systems coincide) such that $\Omega_{\pm}^2 = \omega_M^2 \pm \alpha^2$.

In the absence of damping, the two normal modes at the crossover frequency are linear combinations of the coupled modes vibrating either in or out of phase with each other, with equal energy in each, so that $v/u = \pm \sqrt{m/2M}$. Well away from the crossover region, the mutual coupling only slightly perturbs the individual coupled modes, which therefore retain their separate identities. However, close to the crossover region, when $|\omega_M - \omega_m| \leq 2\alpha^2 / (\omega_M + \omega_m)$, the coupled modes lose their separate identities, with the normal modes involving a significant admixture of both.

The inclusion of damping significantly changes the above result. If we focus on the crossover region, coupling between the modes will be significant when

$$\alpha^2 \approx \omega_M^2 - \omega_m^2. \quad (15.64)$$

At the crossing point, when the uncoupled resonances coincide, the frequencies of the coupled normal are given by

$$\Omega_{\pm}^2 = \omega_M^2 (1 + i/2Q_+) \pm \left(\alpha^4 - \left(\frac{\omega_M^2}{2Q_-} \right)^2 \right)^{1/2}, \quad (15.65)$$

where

$$\frac{1}{Q_{\pm}} = \frac{1}{Q_M} \pm \frac{1}{Q_m}. \quad (15.66)$$

The sign of the terms under the square root clearly depends on the relative strengths of the coupling and damping terms. When the damping is large and the coupling is weak, such that $(\omega_M^2/2Q_-)^2 > \alpha^4$, one is in the *weak-coupling* regime, with no splitting in frequency of the modes in the crossover region. In contrast, when the coupling is strong and the damping is weak, such that $(\omega_M^2/2Q_-)^2 < \alpha^4$, the normal modes are split, but by a somewhat smaller amount than had there been no damping.

Figure 15.46 illustrates the very different character of the normal modes in the crossover region in the weak- and strong-coupling regimes. The examples shown are for an undamped string interacting with a structural resonance with a Q of 25, evaluated for coupling factors,

$$K = \frac{2Q_M}{\omega_M^2} \alpha = \frac{2Q_M}{n\pi} \sqrt{\frac{2m}{M}}, \quad (15.67)$$

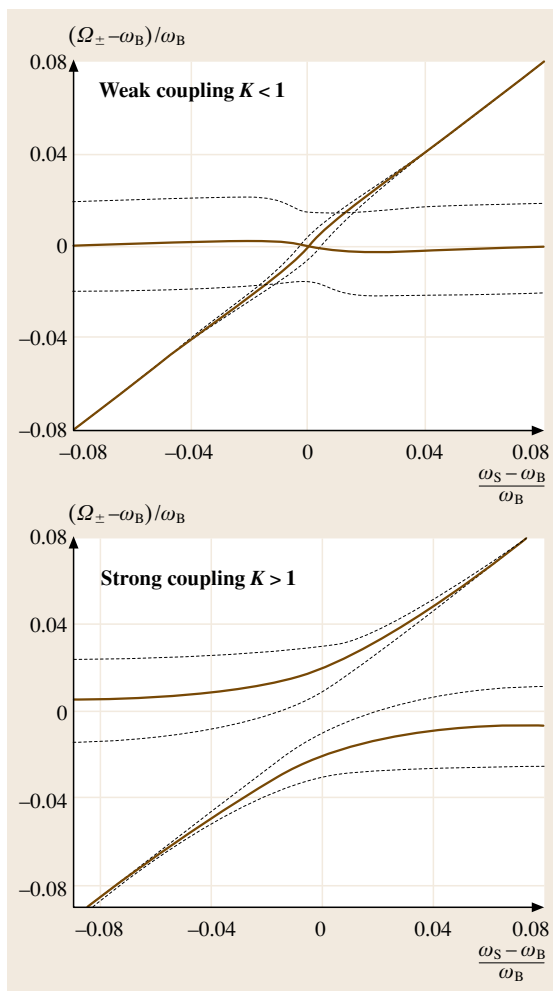


Fig. 15.46 Normal modes of coupled oscillators illustrating the profound effect of damping on the behaviour in the cross-over region illustrated for K -values of 0.75 and $\sqrt{5}$ for an undamped string resonance coupled to a body resonance with a typical $Q = 25$. The *solid line* shows the shifted frequencies of the normal modes as the string frequency is scanned through the body resonance, while the *dashed lines* show the 3 dB points on their damped resonant response (Gough [15.81])

of 0.75 and $\sqrt{5}$, in the weak- and strong-coupling regimes, respectively.

In the weak-coupling limit, the frequency of the vibrating string exhibits the characteristic perturbation described in the previous section, with a shift in frequency proportional to the imaginary component of the terminating admittance and an increased damping pro-

portional to the real part. Note that the coupling also weakly perturbs the frequency and damping of the coupled structural resonance. However, there is no splitting of modes at the crossover point and the normal modes retain their predominantly string-like or body-like character throughout the transition region.

In the strong-coupling limit, $K > 1$, the normal modes are split at the crossover point. The losses are also shared equally between the split modes. As the string frequency is varied across the body resonance, one mode changes smoothly from a normal mode with a predominantly string-like character, to a mixed mode at cross over, and to a body-like mode at higher frequencies, and vice versa for the other normal mode.

Our earlier discussion of the perturbation of string resonances by the terminating admittance is therefore justified in the weak-coupling regime ($K \ll 1$), which is the usual situation for most string resonances on musical instruments. However, if the fundamental mode of a string is over-strongly coupled at the bridge to a rather light, weakly damped body resonance, such that $K > 1$, the normal-mode resonant frequency of the vibrating string, when coincident in frequency with the coupled body mode, will be significantly shifted away from its position as the fundamental member of the harmonic set of partials. It is then impossible to maintain a steady Helmholtz bowed waveform on the string at the pitch of the now perturbed fundamental, which is the origin of the wolf-note problem frequently encountered on otherwise often very fine-stringed instruments, and cellos in particular.

To overcome such problems, it is sometimes possible to reduce K by using a lighter string, but more commonly the effective Q -value is reduced by extracting energy from the coupled system by fitting a resonating mass on one of the strings between the bridge and tailpiece. A lossy material can be placed between the added mass and the string to extract energy from the system, which might otherwise simply move the wolf note to a nearby frequency.

String Resonances

Figure 15.47 illustrates: (a) the frequency dependence of the in-phase and phase-quadrature resonant response of an A-string as its tension increased, so that its frequency passes through a relatively strongly coupled body resonance at ≈ 460 Hz; (b) the splitting in frequency of the normal modes of the second partial of the heavier G-string frequency tuned to coincide with the frequency of the coupled body resonance. Superimposed on these relatively broad resonances is

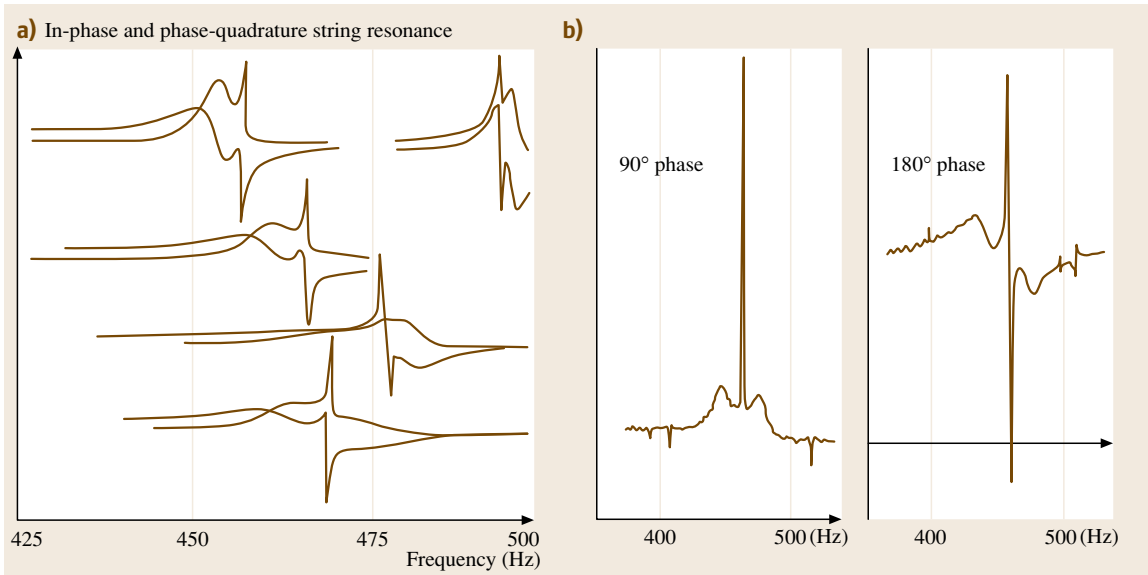


Fig. 15.47a,b Measurements of the in-phase and in-quadrature resonant response of violin strings coupled via the bridge to a strong body resonance (Gough [15.34]). The shift of the broader resonances relative to the unperturbed narrow resonance indicates the extent of the perturbative coupling. **(a)** tuning the A-string resonance through a coupled resonance at ≈ 460 Hz; **(b)** the splitting of the string–body normal modes for the more strongly coupled, second partial, of the heavier G-string

a very sharp resonance arising from transverse string vibrations perpendicular to the strong coupling direction, to be explained in the next section. This very weakly perturbed string resonance provides a marker, which enables us to quantify the shifts and additional damping of string vibrations in the strong coupling direction.

When the frequency of the lighter A-string is tuned below that of the strongly coupled body resonance, the coupling lowers the frequency of the coupled string mode, as anticipated from our earlier discussion. In contrast, when tuned above the coupled resonance the frequency of the coupled string mode is increased, while at coincidence there is a slight indication of split modes somewhat smaller than the widths. The splitting of modes is clearly seen for the second partial of the much heavier G-string (Fig. 15.47b), with symmetrically split broad string/body modes above and below the narrow *uncoupled mode*. Not surprisingly, this violin suffered from a pronounced wolf note when played at 460 Hz in a high position on the G-string, but not on the lighter D- or A-string. Such effects tend to be even more pronounced on cellos due to the very high bridge providing strong coupling between the vibrating strings and body of the instrument.

On plucked string instruments the inharmonicity of the partials of a plucked note induced by coupling at the bridge to prominent structural resonances causes beats in the sound of plucked string, which contribute to the characteristic sound of individual instruments. Woodhouse [15.82,83] has recently made a detailed theoretical, computational and experimental study of such effects for plucked notes on a guitar taking account of the effect of damping on the coupled string–corpus normal modes. This is sometimes not taken into proper account in finite-element software, in which the normal modes of an interacting system are first calculated ignoring damping, with the damping of the modes then added. As is clear from Fig. 15.46, such an approach will always break down whenever the width of resonances associated with damping becomes comparable with the splitting of the normal modes in the absence of damping, as is frequently the case in mechanical and acoustical systems.

Polarisation

We have already commented on the response of a bridge mounted centrally on a symmetrically constructed instrument, with string vibrations perpendicular to the front plate exciting only symmetric modes of the body

of the instrument, while string vibrations parallel to the front plate induce a couple on the front plate exciting only asymmetric modes. The terminating admittance at the bridge end of the string will therefore be a strongly frequency dependent function of the polarisation direction of the transverse string modes. The angular dependence of the terminating admittance lifts the degeneracy of the string modes resulting in two independent orthogonal modes of transverse string vibration, with different perturbed frequencies and damping, polarised along the frequency-dependent principal directions of the admittance tensor. If a string is excited at an arbitrary angle, both modes will be excited, so that in free decay the directional polarisation will precess at the difference frequency. The resultant radiated sound from the excited body resonances will also exhibit beats, which unlike the nonlinear effects considered earlier will not vary with amplitude of string vibration.


In instruments of the violin family, the soundpost removes the symmetry of the instrument, with normal modes involving a mixture of symmetric and asymmetric modes. Measurements like those shown in Fig. 15.47 demonstrate that below ≈ 700 Hz, the effect of the soundpost is to cause the bridge to rock backwards and forwards about the treble foot closest to the soundpost, which acts as a rather rigid fulcrum. This accounts for the very narrow string resonances shown in Fig. 15.47, which correspond to string vibrations polarised parallel to the line between the point of string support and the rigidly constrained right-hand foot, as indicated in Fig. 15.44. In contrast, string vibrations polarised in the orthogonal direction result in a twisting couple acting on the bridge, with the left-hand foot strongly exciting the vibrational modes of the front plate giving the frequency-shifted and broadened string resonances of the strongly coupled string modes.

By varying the polarisation direction of an electromagnetically excited string, one can isolate the two modes and determine their polarisations (*Baker et al.* [15.84]). When such a string is bowed, it will in general be coupled to both orthogonal string modes. The unperturbed string mode may well help stabilise the repetitive Helmholtz bowed waveform.

String–String Coupling

A vibrating string on any multi-stringed instrument is coupled to all the other strings supported on a common supporting bridge. This is particularly important on the piano, where pairs and triplets of strings tuned to the same pitch are used to increase the intensity of the notes

in the upper half of the keyboard. Such coupling is also important on instruments like the harp, where the strings and their partials are coupled via the soundboard. On many ancient bowed and plucked stringed instruments, a set of coupled sympathetic strings were used to enhance the sonority and long-term decay of plucked and bowed notes. Even on modern instruments like the violin and cello, the coupling of the partials of a bowed or plucked string with those of the other freely vibrating open (unstopped) strings enhances the decaying after-sound of a bowed or plucked note. This may be one of the reasons why string players have a preference for playing in the bright key signatures of G, D and A major associated with the open strings, where both direct and sympathetic vibrations can easily be excited.

The musical importance of such coupling on the piano is easily demonstrated by first playing a single note and holding the key down so that the note remains undamped and then holding the sustaining pedal down, so that many other strings can also vibrate in sympathy and especially those with partials coincident with those of the played note. Composers, such as Debussy, exploit the additional sonorities produced by such coupling, as in *La Cathédrale Engloutie*  EXTRAS.

The influence of coupling at the bridge of the normal modes of string vibration on the piano has been discussed by *Weinreich* [15.85] and for sympathetic string in general by the present author [15.81]. Consider first two identically tuned strings terminated by a common bridge with string vibrations perpendicular to the soundboard and relative phases represented by arrows. The normal modes can therefore be described by the combination $\uparrow\uparrow$ and $\downarrow\uparrow$ with the strings vibrating in phase or in anti-phase. When the strings vibrate in anti-phase $\downarrow\uparrow$, they exert no net force on the bridge, which therefore remains a perfect node inducing no perturbation in frequency or additional damping or transfer of energy to the soundboard. In contrast, when the strings vibrate in the same phase $\uparrow\uparrow$, the force on the bridge and resultant amplitude of sound produced will be doubled, as will the perturbation in frequency and damping of the normal modes, and the amplitude of the resultant sound, relative to that of a single string.

Reactive terms in the common bridge admittance tend to split the frequencies of the normal modes in the vicinity of the crossover frequency region, while resistive coupling at the bridge tends to draw the modal frequencies together over an appreciable frequency range. This is illustrated by *Weinreich's* predictions for two strings coupled at the bridge by a complex admittance shown in Fig. 15.48, which shows the veer-

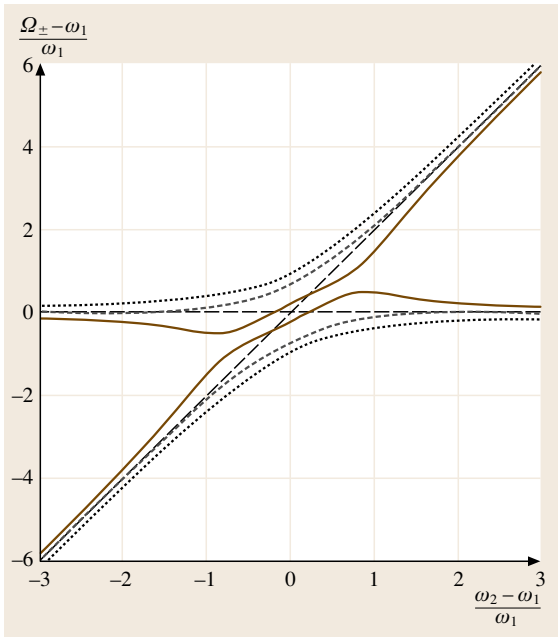


Fig. 15.48 Normal modes of a string doublet coupled at the bridge by a complex impedance. The *dashed* and *dotted* curves illustrate the effect of increasing the reactive component (after Weinreich [15.85])

ing together of the normal modes induced by resistive coupling and the increase in splitting as the reactive component of the coupling is increased.

If the two strings are only slightly mistuned, the amplitudes of the string vibrations involved in the normal modes can still be represented as $\uparrow\uparrow$ and $\downarrow\uparrow$, but the amplitudes of the two string vibrations will no longer be identical. Hence, when the two strings of a doublet are struck with equal amplitude by a hammer, the mode can be represented by a combination of vibrations $\uparrow\uparrow$ with equal amplitude with a small component with opposite amplitudes the $\downarrow\uparrow$ dependent on the mistuning. This leads to a double decay in the sound intensity, with the strongly excited $\uparrow\uparrow$ mode decaying relatively quickly, leaving the smaller amplitude but weakly damped $\downarrow\uparrow$ mode persisting at longer times. Figure 15.49, from Weinreich [15.85], shows the rapid decay of a single C4 string, when all other members of the parent string triplet are damped, followed by the much longer long-term decay of the normal mode excited when one other member of the triplet is also allowed to vibrate freely. More-complicated decay patterns with superimposed slow beats are observed for various degrees of mistuning, from interference with small-amplitude

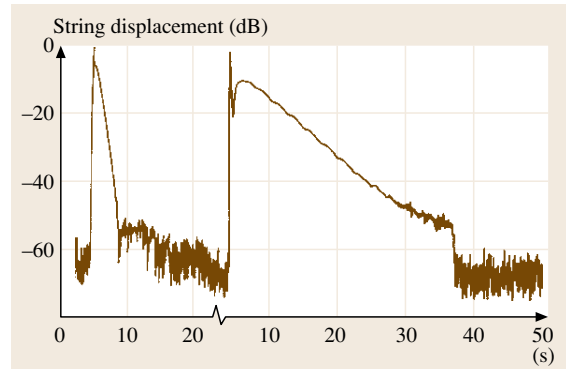


Fig. 15.49 Decay in string vibration of a struck C4 (262 Hz) piano string, first with other members of the string triplet damped and then with one other similarly tuned string allowed to vibrate also (after Weinreich [15.85])

orthogonally polarised string modes excited when the strong-coupling direction is not exactly perpendicular to the soundboard. Weinreich suggests that skilled piano tuners deliberately mistune the individual strings of string doublets and triplets to maximise their long-term ringing sound. Any weakly decaying component of a decaying sound is acoustically important because of the logarithmic response of the ear to sound intensity.

15.2.6 Body Modes

Stringed instruments come in a great variety of shapes and sizes, from strings mounted on simple boxes or on skins stretched over hollow gourds to the more complex renaissance shapes of the viols, guitars and members of the violin family. The vibrational modes of all such instruments, which are ultimately responsible for the radiated sound, involve the collective modes of vibration of all their many component parts. For example, when a violin or guitar is played, all parts of the instrument vibrate – the individual strings, the bridge, the front and back plates and ribs that make up the body of the instrument, the air inside its hollow cavity, the neck, the fingerboard, the tailpiece and, for members of the violin family, the internal soundpost also.

Because of the complexity of the dynamical structures, it would be well nigh impossible to work out the modal shapes and frequencies of even the simplest stringed instruments from first principles. However, as we will show later in this section, with the advent of powerful computers and finite-element analysis software, it is possible to compute the modal vibrations and frequencies of typically the first 20 or more nor-

mal modes for the violin and guitar below around 1 kHz. Such calculations do indeed show a remarkable variety of vibrational modes, with every part of the instrument involved in the vibrations to some extent. Such modes can be observed by direct experiment using Chladni plate vibrations, laser holography and modal analysis techniques, as briefly described in this section.

The frequencies of the vibrational modes can be obtained even more simply from the admittance measured at the position of string support or other selected position on the body of an instrument, when the instrument is excited at the bridge by a sinusoidal electromagnetic force or a simple tap. However, unless a large number of measurements over the whole body of the instrument (normal-mode analysis) are made, such measurements provide very little direct information about the nature of the normal modes and the parts of the violin which contribute most strongly to the excited vibrations.

Although a particular structural mode can be very strongly excited, it may contribute very little to the radiated sound and hence the quality of sound of an instrument. Examples of such resonances on the violin or guitar include the strong resonances of the neck and fingerboard. However, even if such resonances produce very little sound, their coupling to the strings via the body and bridge of the instrument can lead to considerable inharmonicity and damping of the string resonances, as discussed in the previous section. Such effects can have a significant effect on the sound of the plucked string of a guitar and the ease with which a repetitive waveform can be established on the bowed string.

To produce an appreciable volume of sound, the normal modes of instruments like the violin and guitar have to involve a net change in volume of the shell structure forming the main body of the instrument. This then acts as a monopole source radiating sound uniformly in all directions. However, when the acoustic wavelength becomes comparable with the size of the instrument, dipole and higher-order contributions also become important.

For the guitar and instruments of the violin family, there are several low-frequency modes of vibration which involve the flexing, twisting and bending of the whole body of the instrument, contributing very little sound to the lowest notes of the instruments. To boost the sound at low frequencies, use is often made of a Helmholtz resonance involving the resonant vibrations of the air inside the body cavity passing in and out of f-holes or rose-hole cut into the front plate of the instrument. This is similar to the way in which the low-frequency sound of a loudspeaker can be boosted by

mounting it in a bass-reflex cabinet. The use of a resonant air cavity to boost the low-frequency response has been a common feature of almost every stringed instrument from ancient times.

Although finite-element analysis and modal analysis measurement techniques provide a great wealth of detailed information about the vibrational states of an instrument, considerable physical insight and a degree of simplification is necessary to interpret such measurements. This was recognised by *Savart* [15.86] in the early part of the 19th century, when he embarked on a number of ingenious experiments on the physics of the violin in collaboration with the great French violin maker Vuillaume. To understand the essential physics involved in the production of sound by a violin, he replaced the beautiful, ergonomically designed, renaissance shape of the violin body by a simple trapezoidal shell structure fabricated from flat plates with two central straight slits replacing the elegant f-holes cut into the front. As Savart appears to have recognised, the detailed shape is relatively unimportant in defining the essential acoustics involved in the production of sound by a stringed instrument.

We will adopt a similar philosophy in this section and will consider a stringed instrument made up of its many vibrating components – the strings and bridge, which we have already considered, the supporting shell structure, the vibrations of the individual plates of such a structure, the soundpost which couples the front and back plates, the fingerboard, neck and tailpiece, which vibrate like bars, and the air inside the cavity. Although we have already emphasised that it is never possible to consider the vibrations of any individual component of an instrument in isolation, as we have already shown for the string coupled to a structural resonance at the bridge, it is only when the resonant frequencies of the coupled resonators are close together that their mutual interactions are so important that they change the character of the vibrational modes. Otherwise, the mutual interactions between the various subsystems simply provide a first-order correction to modal frequencies without any very significant change in their modal shapes.

Flexural Thin-Plate Modes

To radiate an appreciable intensity of sound, energy has to be transferred via the bridge from the vibrating strings to the much larger surfaces of a soundboard or body of an instrument. The soundboards of the harp and keyboard instruments and the shell structures of stringed instruments like the violin and guitar can formally be considered as thin plates. Transverse or

flexural waves on their surface satisfy the fourth-order thin-plate equation (Morse and Ingard [15.43, Sect. 5.3]), which for an isotropic material can be written as

$$\frac{\partial^2 z}{\partial t^2} + \frac{Eh^2}{12\rho(1-\nu^2)} \left(\frac{\partial^4 z}{\partial x^4} + 2\frac{\partial^2 z}{\partial x^2} \frac{\partial^2 z}{\partial y^2} + \frac{\partial^4 z}{\partial y^4} \right) = 0, \quad (15.68)$$

where z is the displacement perpendicular to the xy -plane, h is the plate thickness, E is the Young's modulus, ν is the Poisson ratio, and ρ the density.

It is instructive first to consider solutions for a narrow quasi-one-dimensional thin plate, like a wooden ruler or the fingerboard on a violin. One-dimensional solutions can be written in the general form

$$z = (a \cos kx + b \sin kx + c \cosh kx + d \sinh kx) e^{i\omega t}, \quad (15.69)$$

where

$$\omega = \left(\frac{E}{12\rho(1-\nu^2)} \right)^{1/2} h k^2. \quad (15.70)$$

The hyperbolic functions correspond to displacements that decay exponentially away from the ends of the bar as $\exp(\pm kx)$. Well away from the ends, the solutions are therefore very similar to transverse waves on a string, except that the frequency now depends on k^2 rather than k with a phase velocity $c = \omega/k$ proportional to $k \approx \omega^{1/2}$. Flexural waves on thin plates are therefore dispersive and unlike waves travelling on strings any disturbance will be attenuated and broadened in shape as it propagates across the surface.

The k values are determined by the boundary conditions at the two ends of the bar, which can involve the displacement, couple $M = -ES\kappa^2 \partial^2 z / \partial x^2$ and shearing force $F = \partial M / \partial x = -ES\kappa^2 \partial^3 z / \partial x^3$ at the ends of the bar, where κ is the radius of gyration of the cross section (Morse and Ingard [15.43, Sect. 5.1]).

For a flexible bar there are three important boundary conditions:

1. Freely hinged, where the free hinge cannot exert a couple on the bar, so that

$$z = 0 \quad \text{and} \quad \frac{\partial^2 z}{\partial x^2} = 0, \quad (15.71)$$

2. Clamped, where the geometrical constraints require

$$z = 0 \quad \text{and} \quad \frac{\partial z}{\partial x} = 0, \quad (15.72)$$

3. Free, where both the couple and the shearing force at the ends are zero, so that

$$\frac{\partial^3 z}{\partial x^3} = \frac{\partial^2 z}{\partial x^2} = 0. \quad (15.73)$$

A bar of length L , freely hinged at both ends, supports simple sinusoidal spatial solutions with m half-wavelengths between the ends and modal frequencies

$$\omega_m = h \sqrt{\frac{E}{12\rho(1-\nu^2)}} \left(\frac{m\pi}{L} \right)^2. \quad (15.74)$$

For long bars with clamped or free ends, the nodes of the sinusoidal component are moved inwards by a quarter of a wavelength and an additional exponentially decaying solution has to be added to satisfy the boundary conditions, so that at the $x = 0$ end of the bar

$$z \approx A \left[\sin(k_m x - \pi/4) \pm \frac{1}{\sqrt{2}} e^{-k_m x} \right], \quad (15.75)$$

where the plus sign corresponds to a clamped end and the minus to a free end, and $k_m = (m + 1/2)\pi/L$. The modal frequencies are given by

$$\omega_m = h \sqrt{\frac{E}{12\rho(1-\nu^2)}} \left(\frac{(m + 1/2)\pi}{L} \right)^2 \quad (15.76)$$

which, for the same m value, are raised slightly above those of a bar with hinged ends. Corrections to these formulae from the leakage of the exponentially decaying function from the other end of the bar are only significant for the $m = 1$ mode and are then still less than 1%.

The solutions close to the end of a bar for hinged, clamped and free boundary conditions are illustrated in Fig. 15.50, with the phase-shifted sinusoidal component for the latter two indicated by the dotted line. The exponential contribution is only significant out to distances $\approx \lambda/2$.

The above formulae can be applied to the bending waves of quasi-one-dimensional bars of any cross section, by replacing the radius of gyration $\kappa = h/\sqrt{12}$ of the thin rectangular bar with $a/2$ for a bar of circular cross section and radius a , and $\sqrt{a^2 + b^2}/2$ for a hollow cylinder with inner and outer radii a and b (Fletcher and Rossing [15.5, Fig. 2.19]).

Another case of practical importance in musical acoustics is a bar clamped at one end and free at the other. This would, for example, describe the bars of a tuning fork or could be used to model the vibrations of the neck or finger board on a stringed instrument. In this

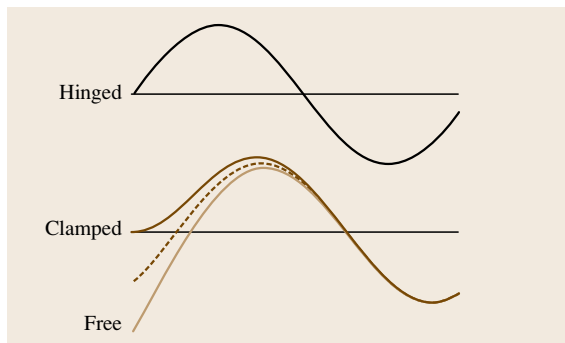


Fig. 15.50 Boundary conditions for flexural waves at the end of a one-dimensional bar. The *dashed line* represents the phase-shifted sinusoidal component, to which the exponentially decaying component has to be added to satisfy the boundary conditions

case, there is an addition $m = 0$ vibrational mode, with exponential decay length comparable with the length of the bar. The modal frequencies are then given (Fletcher and Rossing [15.5, (2.64)]) by

$$\omega_m = \frac{h}{4} \left(\frac{\pi}{L} \right)^2 \sqrt{\frac{E}{12\rho(1-\nu^2)}} \times [1.194^2, 2.988^2, 5^2, \dots, (2m+1)^2]. \quad (15.77)$$

In the above discussion, we have described the modes in terms of the number m of half-wavelengths of the sinusoidal component of the wave solutions within the length of the bar. A different nomenclature is frequently used in the musical acoustics literature, with the mode number classified by the number of nodal lines (or points in one dimension) m in a given direction *not including the boundaries* rather than the number of half-wavelengths m between the boundaries, as in Fig. 15.51.

Twisting or Torsional Modes

In addition to flexural or bending modes, bars can also support twisting (torsional) modes, as illustrated in Fig. 15.51 for the $z = xy$ (1,1) mode.

The frequencies of the twisting modes are determined by the cross section and shear modulus G , equal to $E/2(1+\nu)$ for most materials (Fletcher and Rossing [15.5, Sect. 2.20]). The wave velocity of torsional waves is dispersionless (independent of frequency) with $\omega_n = nc_T k$, where

$$c_T = \frac{\omega}{k} = \sqrt{\frac{GK_T}{\rho I}} = \alpha \sqrt{\frac{E}{2\rho(1+\nu)}}, \quad (15.78)$$

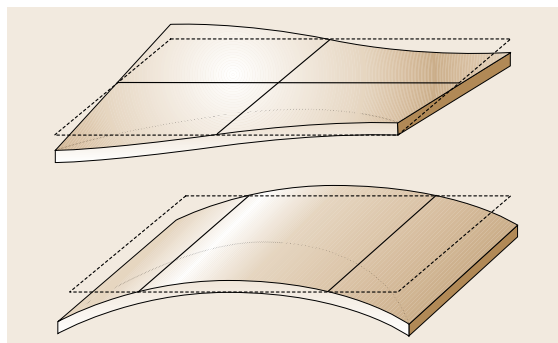


Fig. 15.51 Schematic illustration of the lowest-frequency twisting (1,1) and bending (2,0) modes of a thin bar with free ends

where GK_T is the torsional stiffness given by the couple, $C = GK_T \partial\theta/\partial x$, required to maintain a twist of the bar through an angle θ and $I = \int \rho r^2 dS$ is the moment of inertia per unit length along the bar. For a bar of circular cross section $\alpha = 1$, for square cross section $\alpha = 0.92$, and for a thin plate with width $w > 6h$, $\alpha = (2h/w)$. For a bar that is fixed at both ends, $f_n = nc_T/2L$, while for a bar that is fixed at one end and free at the other, $f_n = (2n+1)c_T/4L$, where n is an integer including zero.

Thin bars also support longitudinal vibrational modes, but since they do not involve any motion perpendicular to the surface they are generally of little acoustic importance, other than possibly for the lowest-frequency soundpost modes for the larger instruments of the violin family.

Two-Dimensional Bending Modes

Solutions of the thin-plate bending wave solutions in two dimensions are generally less straightforward, largely because of the more-complicated boundary conditions, which couple the bending in the x - and y -directions. For a free edge parallel to the y -axis, the boundary conditions are (Rayleigh [15.3, Vol. 1, Sect. 216])

$$\frac{\partial^2 z}{\partial x^2} + \nu \frac{\partial^2 z}{\partial y^2} = 0$$

and

$$\frac{\partial}{\partial x} \left[\frac{\partial^2 z}{\partial x^2} + (2-\nu) \frac{\partial^2 z}{\partial y^2} \right] = 0. \quad (15.79)$$

Thus, when a rectangular plate is bent downwards along its length, it automatically bends upwards along its width and vice versa. This arises because downward bending causes the top surface of the plate to stretch and

the bottom surface to contract along its length. But by Poisson coupling, this causes the top surface to contract and lower surface to stretch in the orthogonal direction, causing the plate to bend in the opposite direction across its width. This is referred to as anticlastic bending. The Poisson ratio ν can be determined from the ratio of the curvatures along the bending and perpendicular directions.

In addition, for orthotropic materials like wood, from which soundboards and the front plates of most stringed instruments are traditionally made, the elastic constants are very different parallel and perpendicular to the grain structure associated with the growth rings. *McIntyre* and *Woodhouse* [15.88] have published a detailed account of the theory and derivation of elastic constants from measurement of plate vibrations in both uniform and orthotropic thin plates, including the influence of damping.

For an isotropic rectangular thin plate, hinged along on all its edges, a simple two-dimensional (2-D) sine-wave solution satisfies both the wave equation (15.68) and the boundary conditions, with m and n half-wavelengths along the x - and y -directions, respectively, giving modal frequencies

$$\omega_{mn} = h \sqrt{\frac{E}{12\rho(1-\nu^2)}} \left[\left(\frac{m\pi}{L_x} \right)^2 + \left(\frac{n\pi}{L_y} \right)^2 \right]. \quad (15.80)$$

By analogy with our discussion of flexural waves in one-dimensional bars, we would expect the modal frequencies of plates with clamped or free edges to be raised, with the nodes of the sinusoidal components of the wave solution moved inwards from the edges by approximately quarter of a wavelength. For the higher-order modes, the modal frequencies would therefore be given to a good approximation by

$$\omega_{mn} = h \sqrt{\frac{E}{12\rho(1-\nu^2)}} \times \left[\left(\frac{(m+1/2)\pi}{L_x} \right)^2 + \left(\frac{(n+1/2)\pi}{L_y} \right)^2 \right]. \quad (15.81)$$

As recognised by *Rayleigh* [15.3, Vol. 1, Sect. 223], it is difficult to evaluate the modal shapes and modal frequencies of plates with free edges. The method used by Rayleigh was to make an intelligent guess of the wave-functions which satisfied the boundary conditions and to determine the frequencies by equating the resulting

potential and kinetic energies. *Leissa* [15.89] has reviewed various refinements of the original calculations. For a plate with free edges, the nodal lines are also no longer necessarily straight, as they were for plates with freely hinged edges.

Chladni Patterns

The modal shapes of vibrating plates can readily be visualised using Chladni patterns. These are obtained by supporting the plate at a node of a chosen mode excited electromagnetically, acoustically or with a rosined bow drawn across an edge. A light powder is sprinkled onto the surface. The plate vibrations cause the powder to bounce up and down and move towards the nodes of the excited mode, allowing the nodal line patterns to be visualised. Figure 15.52 illustrates Chladni patterns measured by *Waller* [15.87] for a rectangular plate with dimensions $L_x/L_y = 1.5$, with the number of nodal lines between the boundary edges determining the nomenclature of the modes. Note the curvature of the nodal lines resulting from the boundary conditions at the free edges.

Figure 15.53 illustrates the nodal line shapes and relative frequencies of the first 10 modes of a square plate with free edges, where $f_{11} = hc_L/L^2 \sqrt{1-\nu/2}$ (after *Fletcher* and *Rossing* [15.5, Fig. 3.13]).

Another important consequence of the anticlastic bending is the splitting in frequencies of combination modes that would otherwise be degenerate. This is illustrated in Fig. 15.54 by the combination $(2, 0) \pm (0, 2)$ normal modes of a square plate with free edges. The $(2, 0) \pm (0, 2)$ modes are referred to as the X - and ring-modes from their characteristic nodal line shapes. The $(2, 0)-(0, 2)$ X -mode exhibits anticlastic bending in the same sense as that induced naturally by the Poisson coupling. It therefore has a lower elastic energy and hence

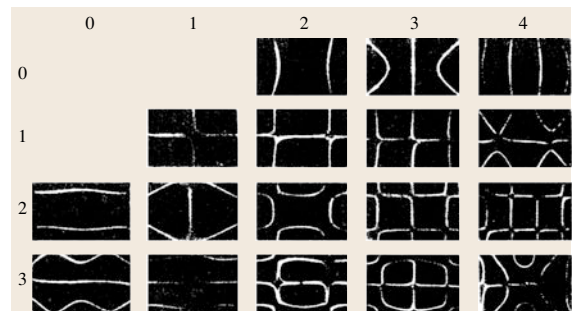


Fig. 15.52 Chladni pattern with white lines indicating the nodal lines of the first few modes of a rectangular plate (after *Waller* [15.87])

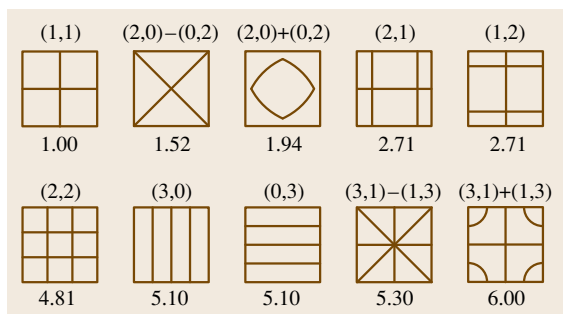


Fig. 15.53 Schematic representation of the lowest 10 vibrational modes of a square plate with free edge

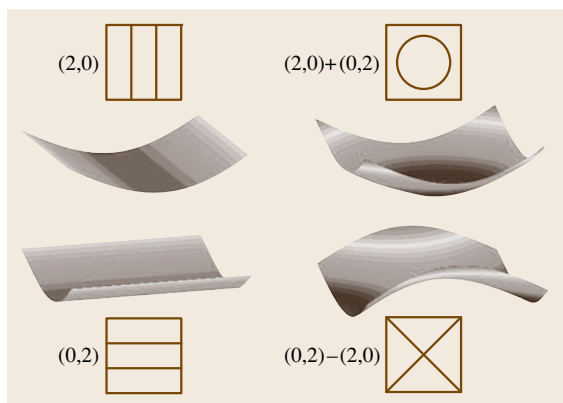


Fig. 15.54 Formation of the ring- and X-modes by the superposition of the (2, 0) and (0, 2) bending modes

lower vibrational frequency than the (0, 2)+(2, 0) ring-mode, with curvatures in the same sense in both the x - and y -directions. The ring- and X-modes will therefore be split in frequency above and below the otherwise degenerate mode, as illustrated in *Fletcher and Rossing* [15.5, Fig. 13.11].

Plate Tuning

The modal shapes and frequencies of the lowest-order (1,1) twisting mode and the X- and ring-modes are widely used for the *scientific tuning* of the front and back plates of violins following plate-tuning guidelines developed by *Hutchins* [15.90, 91]. These are referred to as violin plate modes 1, 2 and 5, as illustrated in Fig. 15.55 by Chladni patterns for a *well-tuned* back plate. The violin maker aims to adjust the thinning of the plates across the area of the plate to achieve these symmetrical nodal line shapes at specified modal frequencies.

The use of such methods undoubtedly results in a high degree of quality control and reproducibility of

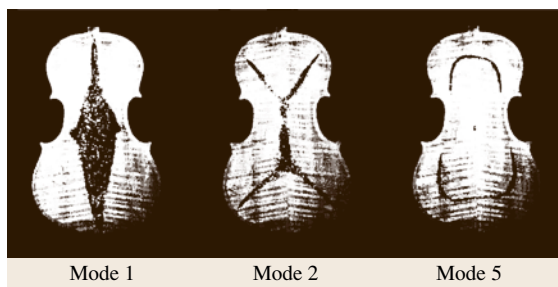


Fig. 15.55 Chladni patterns for the first twisting- (#1), X- (#2) and ring- (#5) modes of a viola back plate (after *Hutchins* [15.90])

the acoustic properties of the individual plates before assembly and, presumably, of the assembled instrument also, especially for the lower-frequency structural resonances. Unfortunately, they do not necessarily result in instruments comparable with the finest Italian instruments, which were made without recourse to such sophisticated scientific methods. Traditional violin makers instinctively assess the elastic properties of the plates by their feel as they are twisted and bent, and also by listening to the sound of the plates as they are tapped or even rubbed around their edges, rather like a bowed plate. From our earlier discussion, it is clear that the mass of the plates is also important in governing the acoustical properties.

Geometrical Shape Dependence

The above examples demonstrate that the lower-frequency vibrational modes of quite complicated shaped plates can often be readily identified with those of simple rectangular plates, though the frequencies of such modes will clearly depend on the exact geometry involved. This is further illustrated in Fig. 15.56 by the modal shapes of a guitar front plate obtained from time-averaged holography measurements by *Richardson and Roberts* [15.92], where the contours indicate lines of constant displacement perpendicular to the surface. For the guitar, the edges of the top plate are rather good nodes, because of the rather heavy supporting ribs and general construction of the instrument. The boundary conditions along the edges of the plate are probably intermediate between hinged and clamped. The modes can be denoted by the number of half-wavelengths along the length and width of the instrument. Note that circular rose-hole opening in the front face, which plays an important role in determining the frequency of the Helmholtz air resonance boosting the low-frequency response of the instrument, tends to concentrate most of

the vibrational activity to the lower half of the front plate.

Mode Spacing

Although the frequencies of the modes of complicated shapes such as the violin, guitar and piano soundboard are rather irregularly spaced, at sufficiently high frequencies, one can use a statistical approach to estimate the spacing of the modal frequencies (Cremer [15.30, Sect. 11.2]). For large m and n values, the modal frequencies of an isotropic rectangular plate are given by

$$\omega_{mn} \approx h \sqrt{\frac{E}{12\rho(1-\nu^2)}} (k_m^2 + k_n^2), \quad (15.82)$$

where $k_m = m\pi/L_x$ and $k_n = n\pi/L_y$. The modes can be represented as points (m, n) on a rectangular grid in k -space, with a grid spacing of π/L_x and π/L_y along the k_x and k_y directions. Each mode therefore occupies an area in k -space of $\pi^2/L_x L_y$. For large m and n , the number of modes ΔN between k and $k + \Delta k$ is therefore on average just the number of modes in the k -space area between k and $k + \Delta k$, so that

$$\Delta N = \frac{\pi}{2} k \Delta k \frac{L_x L_y}{\pi^2} = \frac{\pi}{2} \frac{\Delta \omega}{2\beta} \frac{L_x L_y}{\pi^2}, \quad (15.83)$$

where we have made use of the dispersion relationship $\omega = \beta k^2$.

The density of modes per unit frequency is then constant and independent of frequency,

$$\frac{dN}{df} = \frac{1}{2\beta} L_x L_y = \frac{\sqrt{3(1-\nu^2)}}{c_L h} S \approx 1.5 \frac{S}{c_L h}, \quad (15.84)$$

where S is the area of the plate. The spacing of modes Δf will therefore on average be $\approx c_L h / 1.5 S$, proportional to the plate thickness and inversely proportional to plate area. For large k values, this result becomes independent of the shape of the plate. For an orthotropic plate like the front plate of the violin or guitar, the spacing is determined by the geometric mean $(c_x c_y)^{1/2}$ of the longitudinal velocities parallel and along the grain. For the violin, Cremer [15.30, p. 292] estimates an asymptotic average mode spacing of 73 Hz for the top plate and 108 Hz for the back plate. Above around 1.5 kHz the width of the resonances on violin and guitar plates becomes comparable with their spacing, so that experimentally it becomes increasingly difficult to excite or distinguish individual modes.

On many musical instruments such as the violin and guitar, the presence of the f- and rose-hole open-

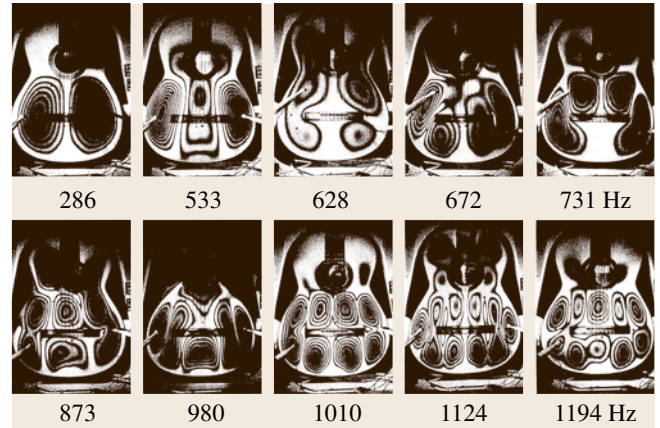


Fig. 15.56 Typical modal shapes for a number of low-frequency modes of a guitar top plate from time-averaged holographic measurements by Richardson and Roberts [15.92]

ings introduce additional free-edge internal boundary conditions, which largely confine the lower-frequency modes to the remaining larger areas of the plate. The effective area determining the density of lower-frequency modes for both instruments will therefore be significantly less than that of the whole plate. Any reduction in plate dimensions, such as the island region on the front plate of the violin between the f-holes, will limit the spatial variation of flexural waves in that direction. Such a region will therefore not contribute significantly to the normal modes of vibration of the plate until $\lambda(\omega)/2$ is less than the limiting dimension.

Anisotropy of Wood

Wood is a highly anisotropic material with different elastic properties perpendicular and parallel to the grain. Furthermore, the wood used for soundboards and plates of stringed instruments are cut from nonuniform circular logs (slab or quarter cut), so that their properties can vary significantly across their area.

McIntyre and Woodhouse [15.88] have described how the anisotropic properties affect the vibrational modes of rectangular thin plates and have shown how the most important elastic constants including their loss factors can be determined from the vibrational frequencies and damping of selected vibrational modes. For a rectangular plate with hinged edges

$$\omega_{mn}^2 = \frac{h^2}{\rho} \left[D_1 k_m^4 + D_3 k_n^4 + (D_2 + D_4) k_m^2 k_n^2 \right], \quad (15.85)$$

where D_1 – D_4 are the four elastic constants required to describe the potential energy of a thin plate with orthotropic symmetry. These are related to the more familiar elastic constants by the following relationships

$$\begin{aligned} D_1 &= E_x/12\mu, \quad D_3 = E_y/12\mu, \quad D_4 = G_{xy}/3, \\ D_2 &= \nu_{xy}E_y/6\mu = \nu_{yx}E_x/6\mu, \end{aligned} \quad (15.86)$$

where $\mu = 1 - \nu_{xy}\nu_{yx}$. G_{xy} gives the in-plane shear energy when a rectangular area on the surface is distorted into a parallelogram. This is the only energy term involved in a pure twisting mode (i.e. $z = xy$). For an isotropic plate, $D_4 = E/6(1 + \nu)$.

For many materials, $(D_2 + D_4) \approx 2\sqrt{D_1D_3}$, so that (15.82) can be rewritten as

$$\begin{aligned} \omega_{mn}^2 &= \frac{h^2}{\rho} \sqrt{D_1D_3} \\ &\times \left[\sqrt[4]{\frac{D_1}{D_3}} \left(\frac{m\pi}{L_x} \right)^2 + \sqrt[4]{\frac{D_3}{D_1}} \left(\frac{n\pi}{L_y} \right)^2 \right]^2. \end{aligned} \quad (15.87)$$

The vibrational frequencies are therefore equivalent to those of a shape of the same area with averaged elastic constant $\sqrt{D_1D_3}$ and length scales L_x multiplied by the factor $\sqrt[4]{D_1/D_3}$ and L_y by its inverse. The relative change in scaled dimensions is therefore $\sqrt[4]{D_1/D_3}$. These scaling factors account for the elongation of the equal contour shapes along the stiffer bending direction in the holographic measurements of mode shapes for the front plate of the guitar (Fig. 15.56), where the higher elastic modulus along the grains is further increased by strengthening bars glued to the underside of the top plate at a shallow angle to the length of the top plate.

Typical values for the elastic constants of spruce and maple traditionally used for modelling the violin are listed in Table 15.5 from Woodhouse [15.77]. The anisotropy of the elastic constants along and perpendicular

Table 15.5 Typical densities and elastic properties of wood used for stringed instrument modelling (after Woodhouse [15.77]). (The values with asterisks are intelligent guesses in the absence of experimental data)

Property	Symbol	Units	Spruce	Maple
Density	ρ	kg/m ³	420	650
	D_1	MPa	1100	860
	D_2	MPa	67	140*
	D_3	MPa	84	170
	D_4	MPa	230	230*
Relative scaling factors	$\sqrt[4]{D_1/D_3}$		1.9	1.4

ular to the grain of a spruce plate cut with the growth rings running perpendicular to the surface would give a relative scaling factor for a violin front plate of almost double the relative width, if one wanted to consider the flexural vibrations in terms of an equivalent isotropic thin plate. The anisotropy is therefore very important in determining the vibrational modes of such instruments.

Plate Arching

The front and back plates of instruments of the violin family have arched profiles, which give the instrument a greatly enhanced structural rigidity to support the downward component of the string tension (≈ 10 kg weight). The arching also significantly increases the frequencies of the lowest flexural plate modes. In the case of lutes, guitars and keyboard instruments with a flat sounding board or front plate, the additional rigidity is achieved by additional cross-struts glued to the back of the sounding board. The bass bar in members of the violin family serves a similar purpose in providing additional strengthening to that of the arching.

The influence of arching on flexural vibration frequencies is easily understood by considering the transverse vibrations of a thin circular disc. For a flat disc, the modal frequencies are determined by the flexural energy associated with the transverse vibrations. The longitudinal strains associated with the transverse vibrations are only second order in displacement and can therefore be neglected. However, if the disc is *belled out* to raise the centre to a height H , the transverse vibrations now involve additional first-order longitudinal strains stretching the disc away from its edges. The energy involved in such stretching, which is resisted by the rigidity of the circumferential regions of the disc, introduces an additional potential energy proportional to H^2 . By equating the kinetic to the increased potential energy, it follows that the frequency of the lowest-order symmetrical mode will be increased by a factor $[1 + \alpha(H/h)^2]^{1/2}$, where $\alpha \approx 1$ has to be determined by detailed calculation. Reissner [15.93] showed that, when the arching is larger than the plate thickness, $H \gg h$, the frequency of the fundamental mode is raised by a factor $\omega/\omega_0 = 0.68H/h$ for a circular disc with clamped edges, and $0.84H/h$ with free edges. For a shallow shell with $H/a < 0.25$, where a is the radius of the disc, the asymptotic frequency can conveniently be expressed as $\omega_n \approx 2(E/\rho)^{1/2}H/a^2$. The arching dependence of the modal frequencies is greatest for the lowest-frequency modes. At high frequencies, the radius of curvature is large compared to the wavelength, so arching is much less important.

The combined effect of the arching and the f- and rose-holes cut into the front face of many stringed instruments is to raise the frequency of the acoustically important lower-frequency modes to well above the asymptotic spacing of modal frequencies predicted by (15.82). For example, the lowest-frequency plate modes of the violin front and back plates are typically in the range 400–500 Hz compared with Cremer's predictions for an asymptotic spacing of modes ≈ 73 Hz for the top plate and 108 Hz for the back plate [15.30, p. 292].

The more highly arched the plates the stiffer they will be and, for a given mass, the higher will be their associated vibrational frequencies. High arching may well contribute to the relatively soft and sweet sounds of the more highly arched early Amati and Stainer violins and the more powerful and brilliant sounds of the flatter later Stradivari and Guarneri models.

Shell Structures

Although it is interesting to investigate the free plates of violins and other instruments before they are assembled into the instrument as a whole, once assembled their vibrational properties will generally be very different, as they are subject to completely different boundary conditions at their supporting edges and by the soundpost constraint for instruments of the violin family. The supporting ribs tie the outer edges of the back and front plates together. The curvature of the outer edge shape gives the 1–2 mm-thick ribs of a violin considerable structural strength and rigidity, in much the same way as the bending of a serpentine brick wall. In many instruments there are extra strips and blocks attached to the ribs and plate edges to strengthen the joint, which still allow a certain amount of angular flexing, as indicated by the schematic normal-mode vibrations illustrated in Fig. 15.57. The supporting ribs add mass loading at the edges of the plates and impose a boundary condition for the flexing plates intermediate between freely hinged and clamped.

For a simple shell structure, Fig. 15.57a represents a low-frequency twisting mode in which the two ends of the instrument twist in opposite directions, just like the simple ($z = xy$) twisting mode of a rectangular plate. Figure 15.57b–d schematically represent normal modes involving flexural modes of the front and back plates. Mode (b) is the important *breathing mode*, which produces a strong monopole source of acoustic radiation at relatively low frequencies. In mode (c), the two plates vibrate in the same direction, resulting in a much weaker dipole radiation source along the vertical axis. The above examples assumed identical top and back

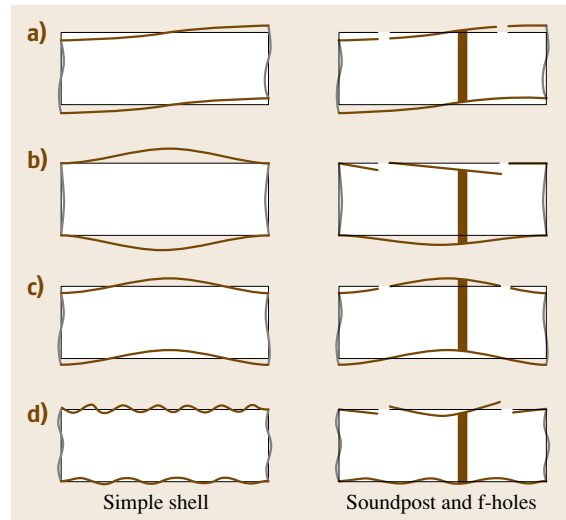


Fig. 15.57a–d Schematic cross-sectional representation of typical shell modes for a simple box and a *violin-type* structure with f-holes and a soundpost

plates, whereas in general they will have different thicknesses arching, and will be constructed from different types of wood with different anisotropic elastic properties: spruce for the front and maple for the back plate of the violin. Hence, for typical high-frequency normal modes (e.g. shown schematically in Fig. 15.57d), the wavelengths of flexural vibrations will be different in the top and back plates.

Note that, at low frequencies, several of the normal modes involve significant motion of the outer edges of the front and back plate, since the centre of mass of the freely supported structure cannot move. Hence, when an instrument is supported by the player, additional mode damping can occur by energy transfer to the chin, shoulder or fingers supporting the instrument at its edges, as indeed observed in modal analysis investigations on hand-held violins by *Marshall* [15.94] and *Bissinger* [15.95].

Skeleton Curves

In this idealised model, the normal modes of the structure at high frequencies will be similar to those of the individual plates. Such modes will only be significantly perturbed when the resonances of the separate plates are close together, apart from a general background interaction from the average weak but cumulative interaction with all other distant modes. *Woodhouse* [15.77] has recently shown that the averaged amplitude and phase of the admittance can be described by *skeleton*

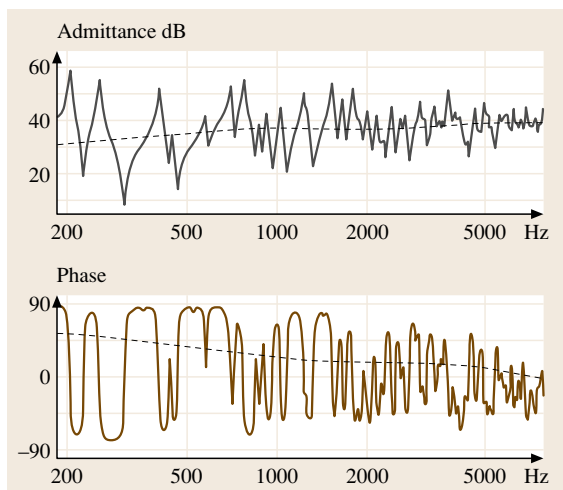


Fig. 15.58 The rotational admittance across the two feet of a bridge on an idealised rectangular violin structure with a soundpost under the treble foot but with no f-holes (after Woodhouse [15.77])

curves, indicated by the dashed lines in Fig. 15.58, on which peaks and troughs of height Q and $1/Q$ and phase changes from individual resonances are superimposed. These curves were evaluated analytically for the rotational admittance across the two feet of a bridge mounted on the front plate of an idealised rectangular box-like violin without f-holes but with a soundpost close to the treble foot of the bridge.

At low frequencies the averaged input impedance across the two feet of the bridge is largely reactive, with a value close to the static *springiness*, which can be identified with the low-frequency limit of the normal-mode admittance $\sum_n i\omega/m_n\omega_n^2$, where the effective mass of each mode will depend on where and how the instrument is excited. However, at high frequencies the admittance becomes largely resistive resulting from internal damping and energy loss to the closely overlapping modes. The use of skeleton curves enables Woodhouse to illustrate the effect of various different bridge designs on the overall frequency response of a violin, without having to consider the exact positions, spacing or damping of the individual resonances of the shell structure. Although the idealised model is clearly over-simplistic, the general trends predicted by such a model will clearly be relevant to any multi-resonant shell model.

Soundpost and f-Holes

The soundpost and f-holes cut into the front plate of the violin and related instruments have a profound ef-

fect on the frequencies and waveforms of the normal modes, illustrated schematically by the right-hand set of examples in Fig. 15.57. The f-holes create an island area on which the bridge sits, which separates the top and lower areas of the front plate. Like the rose-hole on a guitar illustrated in Fig. 15.56, the additional internal free edges introduced by the f-holes tend to localise the vibrations of the front plate to the regions above and below the *island area*. In addition, the soundpost acts as a rather rigid spring locking the vibrations of the top and back plates together at its ends. At low frequencies, the soundpost introduces an approximate node of vibration on both the top and back plates, unless the frequencies of the uncoupled front and back plates modes are close together.

For some low-frequency modes, the soundpost and f-hole have a relatively small effect on the modes of the shell structure, such as the twisting mode (a) and mode (c), when the plates vibrate in the same direction. However, the breathing mode (c) will be strongly affected by the soundpost forcing the front and back plates to move together across its ends.

As indicated earlier, any string motion parallel to the plates will exert a couple on the top of the bridge. In the absence of the soundpost, only asymmetric modes of the top plate could then be excited. However, to satisfy the boundary conditions at the soundpost position, the rocking action now induces a combination of symmetric and antisymmetric plate modes (illustrated schematically in Fig. 15.57b), approximately doubling the number of modes that can contribute to the sound of an instrument including the very important lower-frequency symmetric *breathing modes*. Because of the f-holes, the central island can vibrate in the opposite direction to the wings on the outer edges of the instrument. The mixing of symmetric and antisymmetric modes is strongly dependent on the position of the soundpost relative to the nodes of the coupled waveforms. As a result, the sound of a violin instrument is very sensitive to the exact placing of the soundpost. The difference in the sound of a violin with the soundpost first in place and then removed is illustrated in [13> EXTRAS](#).

To a good approximation, in the audible frequency range, the violin soundpost can be considered as a rigid body, as its first longitudinal resonance is ≈ 100 kHz, though lower-frequency bending modes can also be excited, particularly if the upper and lower faces of the soundpost fail to make a flat contact with the top and back plates (Fang and Rogers [15.96]). At high frequencies, there is relatively little induced motion of the outer edges of top and back plates, so that the

impedance $Z(\omega)$ (force/induced velocity) measured at the soundpost position is simply given by the sum of the impedances at the soundpost position, $Z(\omega)_{\text{top}} + Z(\omega)_{\text{back}}$, of the individual plates with fixed outer edges. If one knows the waveforms of the individual coupled modes, it is relatively straightforward to evaluate the admittance at any other point on the two surfaces, and hence to evaluate the rotational admittance across the two feet of the bridge (*Woodhouse* [15.77]).

We have already described the important role of the bridge dynamics in the coupling between the strings and the vibrational modes of the instrument. For instruments of the violin family, the island region between the f-holes probably plays a rather similar role to the bridge, as it is via the vibrations of this central region that the larger-area radiating surfaces of the front plate are excited. At low frequencies this will be mainly by the lowest-order twisting and flexing modes of the central island region. It therefore seems likely that the dynamics of the central island region also contributes significantly to the BH hill feature and the resulting acoustical properties of the violin in the perceptually important frequency range of $\approx 2\text{--}4\text{ kHz}$, as recognised by *Cremer* and his colleagues [15.11].

Historically, the role of the soundpost and the coupling of plates through enclosed air resonances were first considered analytically using relatively simple mass–spring models with a limited number of degrees of freedom to mimic the first few resonances of the violin, as described in some detail by *Cremer* [15.30, Chap. 10]. Now that we can obtain detailed information about not only the frequencies, but also the shapes of the important structural modes of an instrument from finite-element calculations, holography and modal analysis, there is greater emphasis on analytic methods based on the observed set of coupled modes.

The Complete Instrument

Bowing, plucking or striking a string can excite every conceivable vibration of the supporting structure including, where appropriate, the neck, fingerboard, tailpiece and the partials of all strings both in front of and behind the bridge. Many of the whole-body lower-frequency modes can be visualised by considering all the possible ways in which a piece of soft foam, cut into the shape of the instrument with an attached foam neck and fingerboard, can be flexed and bent about its centre of mass.

Figure 15.59 illustrates the flexing, twisting and changes in volume of the shell of a freely supported violin for two prominent structural resonances com-

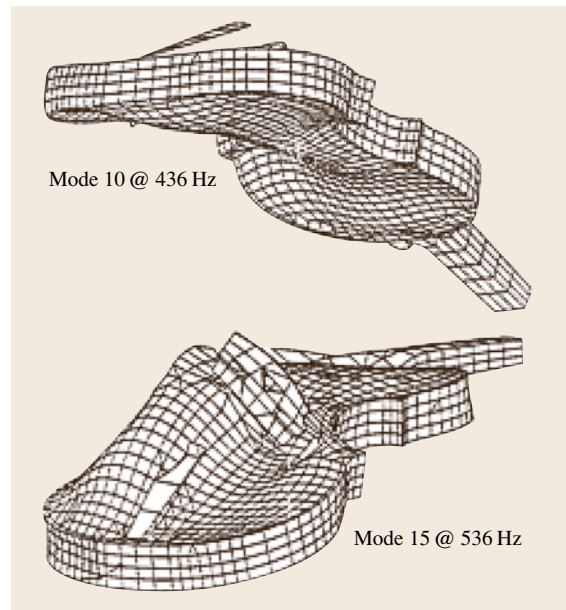


Fig. 15.59 Representative finite element simulations of the structural vibrations of a violin, with greatly exaggerated vibrational amplitudes (after *Knott* [15.97])

puted by *Knott* [15.97] using finite-element analysis. However, not all modes involve a significant change in net volume of the shell, so that many of the lower-frequency modes are relatively inefficient acoustic radiators. Nevertheless, since almost all such modes involve significant bridge motion, they will be strongly excited by the player and will produce prominent resonant features in the input admittance at the point of string support on the bridge. They can therefore significantly perturb the vibrations of the string destroying the harmonicity of the string resonances and resulting playability of particular notes on the instrument, especially for bowed stringed instrument.

Helmholtz Resonance

Almost all hand-held stringed instruments and many larger ones such as the concert harp make use of a Helmholtz air resonance to boost the sound of their lowest notes, which are often well below the frequencies of the lowest strongly excited, acoustically efficient, structural resonances. For example, the lowest acoustically efficient body resonance on the violin is generally around 450 Hz, well above the bottom note G₃ of the instrument at $\approx 196\text{ Hz}$. Similarly, the first strong structural resonance on the classical acoustic guitar is $\approx 200\text{ Hz}$, well above the lowest note of $\approx 82\text{ Hz}$.

To boost the sound in the lower octave, a relatively large circular rose-hole is cut into the front plate of the guitar and two symmetrically facing f-holes are cut into the front plate of instruments of the violin family. The air inside the enclosed volume of the shell of such instruments vibrates in and out through these openings to form a Helmholtz resonator.

The frequency of an ideal Helmholtz cavity resonator of volume V , with a hole of area S in one of its rigid walls is given by

$$\omega_H = \sqrt{\frac{\gamma P}{\rho} \frac{S}{L'V}} = c_0 \sqrt{\frac{S}{L'V}}, \quad (15.88)$$

where L' is the effective length of the open hole. For a circular hole of radius a , *Rayleigh* [15.3, Vol. 2, Sect. 306] showed that $L' = \frac{\pi}{2}a$, while for an ellipse $L' \approx \frac{\pi}{2}(ab)^{1/2}$, provided the eccentricity is not too large. Noting that the effective length depends largely on area, *Cremer* [15.30, Fig. 10.6] modelled the f-hole as an ellipse having the same width and area as the f-hole. The two f-holes act in parallel to give an air resonance for the violin at ≈ 270 Hz, at an interval of just over a fifth above the lowest open string. For the acoustic guitar, the circular rose-hole produces an air resonance around 100 Hz, which, like for the violin, is close to the frequency of the second-lowest open string on the instrument.

Any induced motion of the top and bottom plates that involves a net change in volume results in coupling to the Helmholtz mode. Such coupling will perturb the Helmholtz and body-mode frequencies, in just the same way that string resonances are perturbed by coupling to the body resonances (see *Cremer* [15.30, Sect. 10.3] for a detailed discussion of such coupling). Since the acoustically important coupled modes are at considerably higher frequencies than the Helmholtz resonance, the mutual perturbation is not very large. Because of such coupling, purists often object to describing this resonance as a Helmholtz resonance. Similar objections could apply equally well to string resonances, since they too are perturbed by their coupling to body modes. But, as already discussed, in many situations the normal modes largely retain the character of the individually coupled modes other than when their frequencies are close together and, even then, when the damping of either of the coupled modes is large compared to the splitting in frequencies induced by the coupling in the absence of damping (Fig. 15.46).

Well below the Helmholtz resonance, any change in volume of the shell of the violin or guitar induced

by the vibrating strings will be matched by an identical volume of air flowing out through the rose- or f-holes, with no net volume flow from the instrument as a whole. Since at low frequencies almost all the radiated sound is monopole radiation associated with the net flow of air across the whole surface of an instrument, little sound will be radiated. However, above the air resonance, the response of the air resonance will lag in phase by 180° , so that the flow from body and cavity will now be in phase, resulting in a net volume flow and strong acoustic radiation. The Helmholtz resonance serves the same purpose as mounting a loudspeaker in a bass-reflex cabinet, with the air cavity resonance boosting the intensity close to and above its resonant frequency.

A number of authors have considered the influence of the enclosed air on the lowest acoustically important modes of the violin (*Beldie* [15.98]) and guitar (*Meyer* [15.99], *Christensen* [15.100] and *Rossing* et al. [15.101]) using simple mechanical modes of interacting springs and masses with damping and their equivalent electric circuits. Figure 15.60 shows the me-

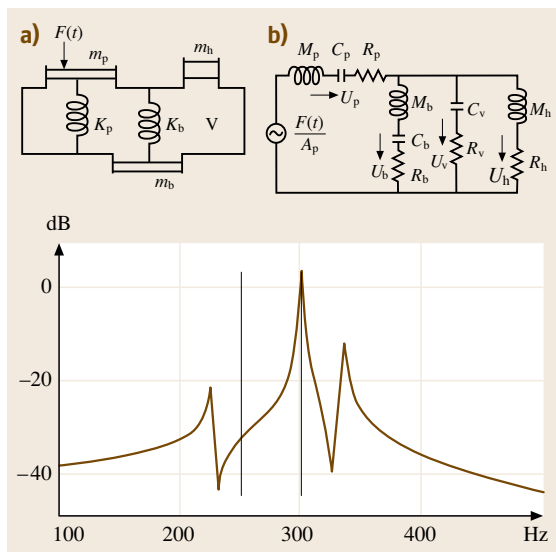


Fig. 15.60a,b The mechanical (a) and equivalent electrical (b) circuit for a three-mass model describing the vibrations of the front and back plates of a stringed instrument coupled via a Helmholtz resonance (after *Fletcher* and *Rossing* [15.5]). The modulus of the admittance at the top plate has been evaluated for identical front and back plates with uncoupled frequencies of 300 Hz, coupled via a Helmholtz air resonator at 250 Hz in the absence of coupling. The frequencies of the uncoupled air and body resonances are indicated by the vertical lines

chanical and equivalent electrical circuits and resulting admittance curve for the top plate for the illustrative three-mass model used by Rossing et al., which accounts for the qualitative features of the first three most important resonances of a guitar body. To emphasise a number of important points, we have calculated the admittance for a cavity with identical front and back plates with uncoupled resonances at 300 Hz, coupled via a cavity Helmholtz resonance at 250 Hz. The closeness in frequencies of the coupled resonators has been chosen to emphasise the influence of the coupling on the modal frequencies.

Without concerning oneself with mathematical detail, one can immediately recognise an unshifted normal mode associated with the uncoupled body resonances at 300 Hz, corresponding to the two plates vibrating in the same phase, with no volume change and hence no coupling to the air resonance. However, the coupling via the Helmholtz resonance splits the degenerate plate modes, to give a normal mode at a raised frequency, with the plates vibrating in opposite directions in a breathing mode. The coupling also decreases the frequency of the Helmholtz cavity resonance. The unperturbed mode may dominate the measured admittance and affect the playability of the instrument via its perturbation of string resonances. But, because there is no associated volume change, it will be an inefficient acoustic radiator. One should note that, because of the changes in phase of the air resonance on passing through resonance, it appears as a dispersive curve superimposed on the low-frequency wings of the stronger higher-frequency body resonances. The frequency of the excited normal mode is not the peak in the admittance curve (i. e. its modulus), as often assumed but is more nearly mid-way between the maximum and minimum, where its phase lags 90° relative to the phase of the higher frequency normal modes. Similarly, the upper body mode results in a dispersive feature in the opposite sense, as its phase changes from almost 180° to 0° relative to the unshifted normal mode. Very similar, but narrower, dispersive features are also observed in admittance-curve measurements from string resonances, unless they are purposely damped.

Cavity Modes

In addition to the Helmholtz air resonance, there will be many other cavity resonances of the air enclosed within the shell of stringed instruments, all of which can in principle radiate sound through the f- or rose-holes. Alternatively, the internal air resonances can radiate sound via the vibrations they induce in the shell of the instru-

ment, as discussed in some detail by *Cremer* [15.30, Sect. 11.4]. Because of the relatively small height of the violin ribs, below around 4 kHz the cavity air modes are effectively two dimensional in character. Simple statistical arguments based on the overall volume of the violin cavity show that there are typically ≈ 28 resonances below this frequency, as observed in measurements by *Jansson* [15.102]. Whether or not such modes play a significant role in determining the tonal quality of an instrument remains a somewhat contentious issue. However, at a given frequency, the wavelengths of the flexural modes of the individual plates and the internal sound modes will not, in general, coincide. The mutual coupling and consequent perturbation of modes will therefore tend to be rather weak. Even if such coupling were to be significant, it is likely to be far smaller than the major changes in modal frequencies and shapes introduced by the f-holes and soundpost.

Finite-Element Analysis

To progress further in our understanding of the complex vibrations of instruments like the violin and guitar, it is necessary to include the coupled motions of every single part of the instrument and to consider the higher-order front and back plate modes, which will be strongly modified by their mutual coupling via the connecting ribs and, for the violin, the soundpost as well.

Such a task can be performed by numerical simulations of the vibrations of the complete structure using finite-element analysis (FEA). This involves modelling any plate or shell structure in terms of a large number of interconnected smaller elements of known shape and elastic properties. This division into smaller segments is known as tessellation. Provided the scale of the tessellation is much smaller than the acoustic wavelengths at the frequencies being considered, the motion of the structure as a whole can be described by the three-dimensional translations and rotations of the tessellated elements. The motion of each element can be related to the forces and couples acting on the adjoining faces of each three-dimensional (3-D) element. The problem is then reduced to the solution of N simultaneous equations proportional to the number of tessellated elements. Deriving the frequencies and mode shapes of the resulting normal modes of the system involves the inversion of a $N \times N$ matrix. Such calculations can be performed very efficiently on modern computer systems, though the computation time, proportional to N^2 , can still be considerable for complex structures, particularly if a fine tessellation is used to evaluate the higher-frequency, shorter-wavelength, modes.

Figure 15.59 has already illustrated the potential complexity of the vibrational modes of a violin. The displacements have been greatly exaggerated for graphical illustration. In practice, the displacements of the plates are typically only a few microns, but can easily be sensed by placing the pad of a finger lightly on the vibrating surfaces. The first example shows a typical low-frequency mode involving the flexing and bending of every part of the violin, but with little change in its volume, so that it will radiate very little sound. The second example illustrates a mode involving a very strong asymmetrical vibration of the front plate, excited by the rocking action of the bridge with the soundpost inhibiting motion on the treble side of the instrument. Such a mode involves an appreciable change in volume of the shell-like structure, which will therefore radiate sound quite strongly.

One of the virtues of FEA is that the effects of changes in design of an instrument, or of the materials used in its construction, can be investigated systematically, without having to physically build a new instrument each time a change is made. For example, Roberts [15.104] has used FEA to investigate the changes in normal-mode frequencies of freely supported violin as a function of thickness and arching, the effects of cutting the f-holes and adding the bass bar, and the affect of the soundpost and mass of the ribs on the normal modes of the assembled body of the instrument, but without the neck and fingerboard. This enables a systematic correlation to be made between the modes and frequencies of the assembled instrument with the modes of the individual plates before assembly. Without the soundpost, the modes of the assembled violin were highly symmetric, with the bass-bar having only a marginal effect on the symmetry and frequency of modes. As expected, adding the soundpost removed the symmetry and changed the frequencies of almost all the modes, demonstrating the critical role of the soundpost and its exact position in determining the acoustic response of the violin.

Similar FEA investigations have been made of several other stringed instruments including the guitar (Richardson and Roberts [15.105]). Of special interest is the recent FEA simulation from first principles of the sound of a plucked guitar string by Derveaux et al. [15.103]. Their model includes interactions of the guitar plates, the plucked strings, the internal cavity air modes and the radiated sound. A DVD illustrating the methodology involved in such calculations [15.106] recently won an international prize, as an outstanding example of science com-

munication. The effects of changing plate thickness, internal air resonances and radiation of sound on both admittance curves and the decay times and sound waveforms of plucked strings were investigated. Figure 15.61 compares the admittance curves at the guitar bridge computed for damped strings for a front-plate thickness of 2.9 mm first in vacuo and then in air. Note the addition of the low-frequency Helmholtz and higher-order cavity resonances in air and the perturbations of the structural resonances by coupling to the air modes.

15.2.7 Measurements

In this section we briefly consider the various methods used to measure the acoustical properties of stringed instruments, a number of which have already been referred to illustrate specific topics in the preceding section.

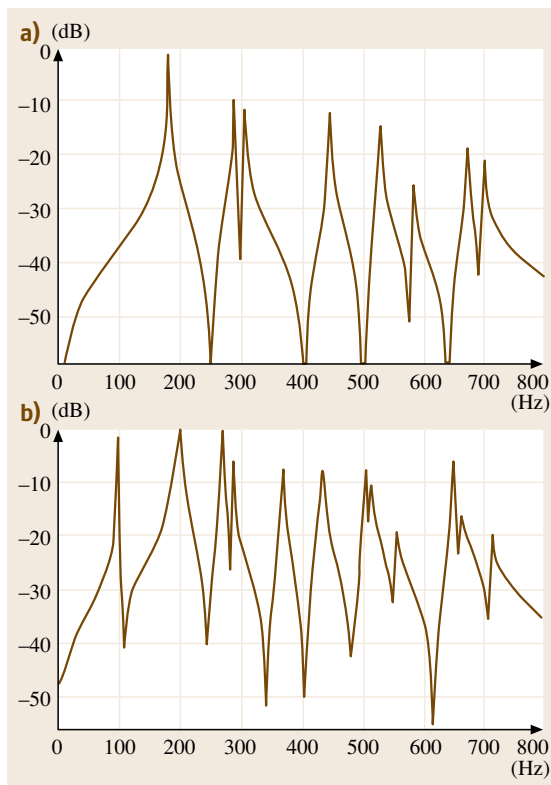


Fig. 15.61a,b FEA computations of admittance at bridge for a guitar with a 2.9 mm-thick front plate (a) in vacuo and (b) coupled to the air-cavity resonances (after Derveaux et al. [15.103])

Admittance

The most common and easiest method used to investigate and characterise the acoustical properties of any stringed instrument is to measure the admittance $A(\omega)$ (velocity/force) at the point of string support on the bridge. *Fletcher* and *Rossing* [15.5] give examples of typical admittance curves for many stringed (and percussion) instruments including the violin, guitar, lute, clavichord and piano soundboard.

As described earlier, the admittance is in reality a complex tensor quantity, with the induced velocity dependent on and not necessarily parallel to the direction of the exciting force. In practice, most published admittance curves for the high-bridge instruments of the violin family show the amplitude and phase of the component of induced bridge velocity in the direction of an applied force parallel to the top plate. In contrast, for low-bridge instruments like the guitar, piano or harpsichord, the induced motion perpendicular to the top plate or soundboard is of primary interest.

The admittance at the bridge can be expressed in terms of the additive response of all the damped normal modes, which includes the mutual interactions of the plates of the instrument and all the component parts including, where appropriate, the neck, tailpiece, fingerboard, and all the strings. The admittance can then be written as

$$A(\omega) = \sum_n \frac{1}{m_n} \frac{i\omega}{\omega_n^2 - \omega^2 + i\omega\omega_n/Q_n}, \quad (15.89)$$

where ω_n and Q_n are the frequency and Q -value of the n th normal mode and m_n is the associated effective mass at the point of measurement. The value of m_n depends on how well the normal mode is excited by a force at the point of measurement on the bridge. If, for example, the bridge on a guitar is at a position close to the nodes of particular normal modes, then the coupling will be weak and the corresponding effective mass will be rather large. Conversely, the low-frequency rocking action of the bridge on a bowed stringed instrument couples strongly into the breathing mode of the violin shell, so that the effective mass will be relatively low. The strength of this coupling plays an important role in determining the sound output from a particular instrument and also affects the playability of the bowed string and the sound of a plucked string.

In practice, by measuring the frequency response of the admittance, including both amplitude and phase, it is possible to decompose the admittance into the sum of the individual modal contributions and hence determine the effective mass, frequency and damping of the con-

tributing normal modes. For the violin there are ≈ 100 identifiable modes below ≈ 4 kHz (*Bissinger* [15.107]), though not all of these are efficient acoustic radiators.

To avoid complications from the numerous sympathetic string resonances that can be excited, which includes all their higher-frequency partials, measurements are often made with all the strings damped by a piece of soft foam or a piece of card threaded between the strings. However, it should always be remembered that the damped strings still contribute significantly to the measured admittance. At low frequencies the strings still exert the same lateral restoring force on the bridge whether damped or not, while at high frequencies the damped strings present a resistive loading with their characteristic string impedances μc in parallel. When undamped, the strings present an additional impedance and transient response, which reflects the resonances of all the partials of the supported strings. This can make a significant difference to the sound of an instrument, notably when the sustaining pedal is depressed on a piano and in the ringing sound of any multi-stringed instrument, when a note is plucked or bowed and especially instruments like the theorbo and viola d'amore with freely vibrating sympathetic strings.

Figure 15.62 illustrates admittance measurements for six different violins by *Beldie* [15.98] reproduced from *Cremer* [15.30, Fig. 10.1]. The arrows indicate the position of the dispersive-shaped Helmholtz air resonance, which is the only predictable feature in such measurements, though its relative amplitude varies significantly from one instrument to the next. Such measurements provide a fingerprint for an individual instrument, highlighting the very large number of almost randomly positioned resonances that can be excited, which must ultimately be responsible for the distinctive sound of an instrument. As described earlier, above ≈ 1500 Hz the admittance often exhibits an underlying BH peak at ≈ 2 kHz followed by a characteristic decrease at higher frequencies, which can be attributed to a resonance of the bridge/central island region [15.75, 77].

Although most instruments have very different acoustic fingerprints, Woodhouse (private communication), in a collaboration with the English violin maker David Rubio, demonstrated that it is possible to construct instruments with almost identical admittance characteristics, provided one uses closely matching wood from the same log, with a nearly perfect match of plate thickness and arching. The German violin maker *Martin Schleske* [15.108] also claims considerable success in producing *tonal copies* with almost

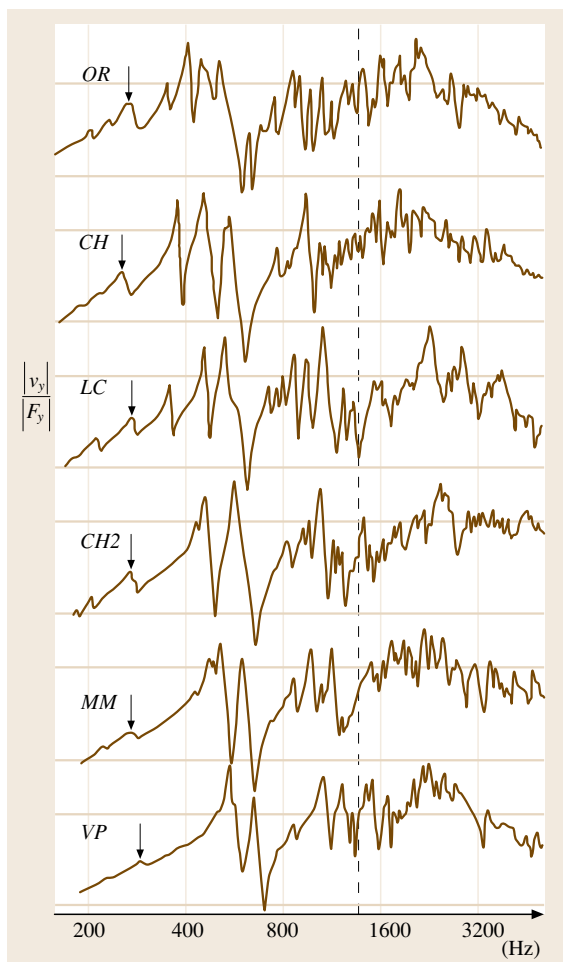


Fig. 15.62 Admittance measurements at bridge for six violins (after Beldie [15.98]). The arrows indicate the position of the Helmholtz air resonance. The horizontal lines are 20 dB markers

identical acoustical properties to those of distinguished Cremonese instruments by grading the thickness and arching of the plates to reproduce both the input admittance and radiated sound.

In contrast, slavishly copying the dimensions of a master violin rarely produces an instrument with anything like the same tonal quality. This is easily understood in terms of the differing elastic and damping properties of the wood used to carve the plates, which remains a problem of great interest, but beyond the scope of this article.

Traditionally, the admittance is usually measured using a swept sinusoidal frequency source, often gener-

ated by a small magnet waxed to the bridge and driven by a sinusoidally varying magnetic field. The admittance can equally well be determined from the transient response $f(t)$ following a very short impulse to the bridge, since it is simply the Fourier transform,

$$A(\omega) = \int_0^{\infty} f(t) e^{i\omega t} dt. \quad (15.90)$$

If signal-to-noise ratio from a single measurement is insufficient, one can use a sequence of impulses or a noise source, which is equivalent to a random succession of short pulses. In addition to many professional systems, relatively inexpensive PC-based versions using sound cards have been developed for researchers and instrument makers, such as the WinMLS system by *Morset* [15.109].

Laser Holography

Admittance measurements at the bridge provide detailed information on the frequencies, damping and effective masses of the normal modes of vibration of an instrument, but provide no information on the nature of the modes excited. Laser holography, which is essentially the modern-day equivalent of Chladni plate measurements, enables one to visualise the vibrational modes of stringed and percussion instruments. In such measurements, photographs or real-time closed-circuit television images of the interference patterns of laser light reflected from a stationary mirror and from the vibrating object are recorded. Using photographic or electronic/software reconstruction of the original image from the recorded holograms, a 3-D image of the vibrating surface is formed with superimposed contours indicating lines of equal vibrational amplitude, as already illustrated for a number of prominent guitar modes in Fig. 15.56.

Recent developments in laser and electronic data-acquisition technology allow one to record such interferograms electronically and to display them in real time on a video monitor (for example, *Saldner et al.* [15.110]). To record the shapes of individual vibrational modes of an instrument excited by a sinusoidal force, care has to be taken to avoid contamination from neighbouring resonances, by judicious placing of the force transducer (e.g. placing it at a node of an unwanted mode). *Cremer* [15.30, Chap. 12] reproduces an interesting set of holograms by *Jansson et al.* [15.111] for the front plate of a violin at various stages of its construction, before and after the f-holes are cut, before and after the bass-bar is added and with a soundpost sup-

ported on a rigid back plate. These highlight the major effect of the f-holes and soundpost on the modal shapes and frequencies, but the relatively small influence of the bass-bar, consistent with the FEA computations by *Roberts* [15.104] referred to earlier. However, the bass bar strengthens the coupling between the island area between the f-holes and the larger radiating surfaces of the top plate and therefore has a strong influence on the intensity of radiated energy.

With modern intense pulsed laser sources, one can also investigate the transient response of instruments using single pulses. For example, *Fletcher* and *Rossing* [15.5, Fig.10.15] reproduce interferograms of the front and back plate of a violin by *Molin* et al. [15.112, 113], which illustrate flexural waves propagating out from the feet of the bridge on the front face and from the end of the soundpost on the back plate at intervals from 100–450 μs after the application of a sharp impulse at the bridge. Holograms can even be recorded while the instrument is being bowed [15.112, 113].

Modal Analysis

Modal analysis measurements have been extensively used to investigate the vibrational modes of the violin, guitar, the piano soundboards and many other stringed and percussion instruments (Chap. 28). Briefly, the method involves applying a known impulse at one point and measuring the response at a large number of other points on the surface of an instrument, which allows one to determine both the modal frequencies and the vibrations at all points on the surface. The Fourier transform of the impulse response is directly related to the nonlocal admittance, which in terms of the normal modes excited can be written as

$$A(r_1, r_2, \omega) = i\omega \sum_n \frac{1}{m_n} \frac{\psi_n(r_1)\psi_n(r_2)}{\omega_n^2 - \omega^2 + i\omega\omega_n/Q_n}, \quad (15.91)$$

where $\psi_n(r_1)\psi_n(r_2)$ is the product of the wavefunctions describing the displacements at the measurement and excitation points normalised to the product at the point of maximum displacement, and m_n is now the effective mass of the normal mode at its point of maximum amplitude of vibration (i. e. $KE_{\text{max}} = 1/2m_n\omega^2\psi_n^2|_{\text{max}}$). An FFT of the recorded transient response will give peaks in the frequency response, which can be decomposed into contributions from all the excited normal modes. By keeping the point of excitation fixed and moving the measurement point, one can record the amplitude and phase of the induced motion for a specific mode and, using the spatial dependence in (15.91), can

map out the nodal waveform. Alternatively, one can keep the measurement point fixed and apply the impulse over the surface of the structure to derive similar information.

One of the first detailed modal analysis investigations of the violin was made by *Marshall* [15.94], who used a fixed measurement point on the top plate of the violin near the bass-side foot of the bridge with a force hammer providing calibrated impulses at a large number of points over the surface of the violin. From the FFT of the resultant transient responses, the amplitudes and phases of the excited normal modes of the violin involving all its component parts including the body shell, neck, fingerboard and tailpiece could be determined. *Marshall* identified and characterised around 30 normal modes below ≈ 1 kHz. Many of the modes involved the relatively low-frequency flexing and twisting of the instrument as a whole. However, because such modes involved little appreciable change in overall volume of the shell of the instrument structure, they resulted in little radiated sound. Nevertheless, it was suggested that such modes might well play an important role for the performer in determining the feel of the instrument and its playability.

In any physical measurement, the instrument has to be supported in some way. Rigid supports introduce additional boundary conditions, which can significantly perturb the normal modes of the instrument. Many measurements are made with the instrument supported by rubber bands, which provide static stability without significant perturbation of the higher-frequency structural modes. However, *Marshall* [15.94] showed that, when an instrument is held and supported by the player under the chin, the damping of many of the normal modes was significantly increased, which will clearly affect the sound of the instrument when played. This observation has also been confirmed in more recent modal analysis measurements by *Bissinger* [15.95] and by direct measurements of the decaying transient sound of a freely and conventionally supported violin by the present author [15.18].

Bissinger [15.107] has made extensive admittance, modal analysis and sound radiation measurements on a large number of instruments. Measurements were made using impulsive excitation at the bridge and a laser Doppler interferometer to record the induced velocities at over 550 points on the surface of the violin. Simultaneous measurements of the overall radiation and directivity were made using 266 microphone positions over a complete sphere. Figure 15.63 shows cross sections illustrating the displacements associated with four

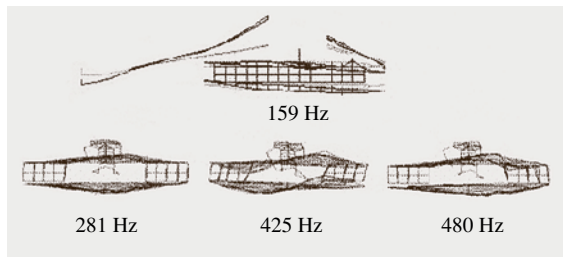






Fig. 15.63 Modal analysis measurements illustrating the displacements associated with four representative low-frequency modes of a violin (data provided by George Bissinger)

low frequency modes. The 159 Hz mode  **EXTRAS** involves major vibrations of the neck, fingerboard, tailpiece and body of the instrument. The second example at 281 Hz  **EXTRAS** illustrates the body displacements associated with the Helmholtz air resonance. The mode at 425 Hz  **EXTRAS** illustrates a mode with asymmetric in-phase vibrations of the front and back plates, with little net volume change and hence little radiated sound, while the mode at 480 Hz  **EXTRAS** is a strong breathing mode.

By combining the modal analysis and radiativity measurements, Bissinger has shown that the radiation efficiency of the plate modes (i. e. the fraction of sound energy radiated by the violin relative to a baffled piston of the same surface area having the same root mean square surface velocity displacement) rises to nearly 100% at a *critical frequency* of $\approx 2\text{--}4$ kHz, when the wavelength of the flexural vibrations of the plates matches that of sound waves in air. Little apparent correlation was observed between the perceived quality of the measured violins and the frequencies and strengths of prominent structural resonances below ≈ 1 kHz or with the internal damping of the front and back plates. This runs contrary to the general view of violin makers that the front and back plates of a fine violin should be made of wood with a very long ringing time when tapped. Interestingly, the American violin maker Joseph Curtin has also observed that individual plates of old Italian violins often appear to be more heavily damped than their modern counterparts [15.114]. This is clearly an area that merits further research.

15.2.8 Radiation and Sound Quality

As already emphasised, at low frequencies, when the acoustic wavelength is smaller than the size of an instrument, the radiated sound is dominated by isotropic

monopole radiation. As the frequency is increased, higher-order dipole and then quadrupole radiation become progressively important, while above the critical frequency, when the acoustic wavelength is shorter than the that of the flexural waves on the shell of an instrument, the radiation patterns become increasingly directional, so that it is no longer appropriate to consider the radiation in terms of a multipole expansions.

Fletcher and Rossing [15.5, Fig. 10.30] reproduce measurements on both the violin and cello by Meyer [15.115], which highlight the increasing directionality of the sound produced with increasing frequency and the rather strong masking effect of the player at high frequencies. More recently, Weinreich and Arnold [15.116, 117] have made detailed theoretical and experimental studies of multipole radiation from the freely suspended violin at low frequencies (typically below 1 kHz). Interestingly, they made use of the principle of acoustic reciprocity, based on the fact that the amplitude of vibration at the top of the bridge produced by incoming sound waves is directly related to the sound radiated by a force applied to the violin at the same point. The violin was radiated by an array of loudspeakers to simulate incoming spherical or dipole sound fields and the induced velocity at the bridge recorded by a very light gramophone pick-up stylus.

Hill et al. [15.118] have used direct measurements to investigate the angular dependence of the sound radiated by a number of high-quality modern acoustic guitars with different cross-strutting, when excited by a sinusoidal force at the bridge. From such measurements, they were able to derive the fraction of sound radiated as the dominant monopole and dipole (with components in three directions) radiation, in addition to effective masses and Q -values, for a number of prominent modes up to ≈ 600 Hz. Significant differences were observed for the three different strutting schemes investigated.

Bissinger [15.119] has made an extensive investigation of radiation from both freely supported and hand-held violins, including measurements above 1 kHz, where the multimodal radiation expansion is no longer appropriate. Bissinger correlates the sound radiated over a large number of points on a sphere surrounding the violin with measurements of the input admittance at the bridge and the induced surface velocities over the whole violin structure. Figure 15.64 shows a typical set of simultaneous measurements up to 1 kHz. Although the low-frequency Helmholtz resonance contributes strongly to the radiated sound, it results in a relatively small feature on the mobility curves for the body of the instrument (or on the measured admit-

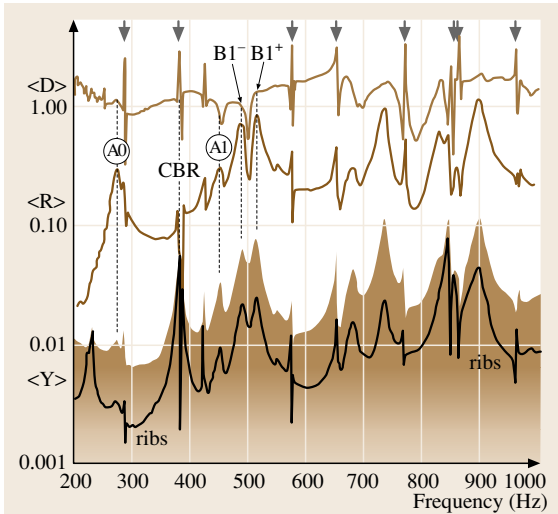


Fig. 15.64 Plots of the root-mean-square (rms) mobility $\langle Y \rangle$ (m/sN) averaged over the surface of the front and back plate (solid shaded region) and ribs (white curve) of the instrument, the radiativity $\langle R \rangle$ (Pa/N) averaged over a sphere, and directivity $\langle D \rangle$, the ratio of forward to backward radiation averaged over hemispheres. The top arrows represent the positions of the open-string resonances and their partials. A0 is the position of the Helmholtz air resonance and A1 the first internal cavity air resonance, CBR is a strong corpus bending mode and B1 and B2 are the two strong structural normal mode resonances of the coupled front and back plates (data kindly supplied by George Bissinger)

tance at the bridge, not shown). Bissinger was unable to find any significant correlation between the frequencies and Q -values of the prominent *signature* modes excited (see, for example, Jansson [15.120]) below ≈ 1 kHz and the perceived quality of the instruments investigated. Above ≈ 1 kHz the modes strongly overlap, so that it becomes more appropriate to compare the frequency averaged global features. The measurements show that the fraction of mode energy radiated increases monotonically from close to zero at low frequencies up to around almost 100% efficient at 4 kHz and above, where almost all the energy is lost by radiation rather than internal damping. The ultimate aim of these detailed modal analysis studies is to correlate the measured acoustical properties with the results obtained from finite-element analysis and to produce sufficient information about the acoustical properties that might allow a more realistic comparison between physical properties and the properties of an instrument judged from their perceived sound quality and playability.

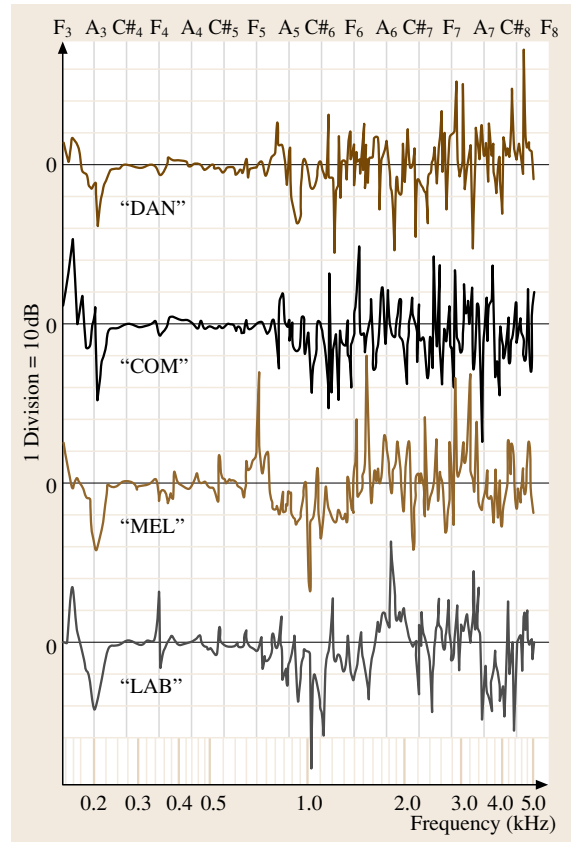


Fig. 15.65 Ratio of sound intensities along neck and perpendicular to front plate for four violins of widely different qualities (after Weinreich [15.121])

Directional Tone Colour

Although the acoustic power radiated averaged over a given frequency range is clearly an important signature of the sound of a particular instrument, the intensity at a particular frequency in the important auditory range above 1 kHz can vary wildly from note to note. This is illustrated in Fig. 15.65 by Weinreich [15.121], which compares the intensities of radiated sound in an anechoic chamber along the direction of the neck and perpendicular to the front plate for four violins of widely differing quality, with 0 dB representing an isotropic response. Above around 1 kHz, the wavelengths of flexural waves on the plates of the instrument become comparable with the wavelength of the radiated sound. This leads to strong diffraction effects in the radiated sound, which fluctuate wildly with direction as different modes are preferentially excited. At a particular point in the listening space, the spectral

content of the bowed violin therefore varies markedly from note to note, as will the sound within a single note played with vibrato resulting in frequency modulation. The spectral content will also vary from position to position around the violin, especially if the player moves whilst playing. Weinreich has emphasised the importance of such effects in producing a greater sense of *presence* and *vibrancy* in the perceived sound from a violin than would be produced by a localised isotropic sound source, such as a small loudspeaker. Weinreich has coined the term *directional tone colour* to describe such effects. He has also designed a loudspeaker system based on the same principles, which gives a greater sense of realism to the sound of the recorded violin than a simple loudspeaker.

In addition to the intrinsic directionality of the violin, the time-delayed echoes from the surrounding walls of a performing space also have a major influence on the complexity of the sound waveforms produced by a violin (or any other instrument) played with vibrato, as first noted by Meyer [15.122]. This arises from the interference between the different frequencies associated with the prompt sound reaching the listener (or microphone) and the sound generated at earlier times reflected from the surrounding surfaces. As discussed by the present author (*Gough* [15.18]), the additional complexity is largely a dynamic effect associated with the time-delayed interference between signals of different frequencies rather than caused by the amplitude modulation of individual partials associated with the multi-resonant response of the violin, first highlighted by Fletcher and Sanders [15.123] and Matthews and Kohut [15.124].

Perceived Quality

No problem in musical acoustics has attracted more attention or interest than the attempts made over the last 150 or so years to explain the apparent superiority of old Cremonese violins, such as those made by Stradivarius and Guarnerius, over their later counterparts, which have often been near exact copies. Many explanations have been proposed – a magic recipe for the varnish, chemical treatment of the wood and finish of the plates prior to varnishing [15.125], the special quality of wood resulting from micro-climate changes [15.126], etc. However, despite the committed advocacy for particular explanations by individuals, there is, as yet, little agreement between researchers, players or dealers on the acoustical attributes that distinguish a fine Italian violin worth \$1M or more from that of a \$100 student instrument.

From a physicist's point of view, given wood of the same quality as that used by the old Italian makers, there is no rational reason why a modern violin should not be just as good from an acoustic point of view as the very best Italian instrument. We have already commented on Martin Schleske's attempts to replicate the sounds of fine Italian instruments, by making *tonal copies* having as near as possible the same acoustical properties [15.108]. In addition, we have also highlighted Dünnewald's attempt to correlate the physical properties of well over 200 violins with their acoustical properties [15.76], including the comparison of selected student, modern and master violins reproduced in Fig. 15.62. Such studies appear to show a correlation between the amount of sound radiation in the acoustically important range around 3–4 kHz. As we have emphasized, this is just the region where the resonant properties of the bridge have a major influence on the spectrum.

It must also be remembered that the changed design of the bridge, the increase in string tension, higher pitch, increased size of the bass-bar, neck and soundpost, and the use of metal-covered rather than gut strings have resulted in a modern instrument sounding very different from the instruments heard by the 17th and early 18th century maker and performer. Even amongst the violins of the most famous Cremonese luthiers, individual instruments have very different distinctive tones and degrees of playability, particular as judged by the player. The gold standard itself is therefore very elusive. What is currently and may always be lacking is reliable measurements on the individual plates and shells of a large number of really fine instruments. We still largely rely on a small number of measurements performed by Savart in the nineteenth century and a few measurements by Saunders in the 1950s on which to base scientific guidelines for modern violin makers.

Performance Acoustic

It should also be recognised that, when a violin (or any other instrument) is played, the performer excites not only the vibrational modes of the instrument but also the multi-resonant normal modes of the performance space. Whereas the sound heard by a violinist is dominated by the sound of the violin, for the listener the acoustics of the performance space can dominate the timbre and quality of the perceived sound. To distinguish between the intrinsic sound qualities of violins, comparisons should presumably best be made in a rather dry acoustic, even though such an acoustic is generally disliked

by the performer (and listener), who appreciates the improvement in sound quality provided by a resonant room acoustic.

One cannot review progress towards our understanding of what makes a good violin without recognising the inspiration and enthusiastic leadership of Carleen Hutchins, the doyenne and founder of the Catgut Society and scientific school of violin making, which has attracted many followers world-wide. By matching the frequencies and shapes of the first few modes of free plates before they are assembled into the completed instrument (Fig. 15.55), the scientific school of violin makers clearly achieve a high degree of quality control, which goes some way towards compensating for the inherent inhomogeneities and variable elastic properties of the wood used to carve the plates. However, in practice, there is probably just as much variability in the sound of such instruments as there is in instruments made by more traditional methods, where makers tap, flex and bend the plates until they feel and sound about right, this being part of the traditional skills handed down from master to apprentice even today. That is certainly the way that the Italian masters must have worked, without the aid of any scientific measurements beyond the feel and the sound of the individual plates as they are flexed and tapped.

15.3 Wind Instruments

In this section we consider the acoustics of wind instruments. These are traditionally divided into the woodwind, played with a vibrating reed or by blowing air across an open hole or against a wedge, and brass instruments, usually made of thin-walled brass tubing and played by buzzing the lips inside a metal mouthpiece attached to the input end of the instrument.

In general, the playing pitch of woodwind instruments is based on the first two modes of the resonating air column, with the pitch changed by varying the effective length by opening and closing holes along its length. In contrast, brass players pitch notes based on a wide range of modes up to and some times beyond the 10th. The effective length of brass instruments can be changed by sliding interpenetrating cylindrical sections of tubing (e.g. the trombone) or by a series of valves, which connect in additional length of tubing (e.g. trumpet and French horn). The pitch of many other instruments, such as the organ, piano-accordion and harmonium, is determined by the resonances of a set of

Scientific Scaling

The other interesting development inspired by Carleen Hutchins and her scientific coworkers Schelling and Saunders has been the development of the modern violin octet [15.127], a set of eight instruments designed according to physical scaling laws based on the premise that the violin is the most successful of all the bowed stringed instruments. The aim is to produce a consort of instruments all having what are considered to be the optimised acoustical properties of the violin. Each member of the family is therefore designed to have the frequencies of the main body and Helmholtz resonances in the same relationship to the open strings as that on the violin, where the Helmholtz air resonance strongly supports the fundamental of notes around the open D-string, while the main structural resonances support notes around the open A-string and the second and generally strongest partial of the lowest notes played on the G-string. Several sets of such instruments have been constructed and admired in performance, though not all musicians would wish to sacrifice the diversity and richness of sounds produced by the different traditional violin, viola, cello and double bass in a string quartet or orchestra. Nevertheless, the scaling methods have led to rather successful intermediate and small-sized instruments.

separate pipes or reeds to excite the full chromatic range of notes, rather like the individual strings on a piano.

A detailed discussion of the physics and acoustical properties underlying the production of sound in all types of wind instruments is given by *Fletcher and Rossing* [15.5], which includes a comprehensive list of references to the most important research literature prior to 1998. As in many fields of acoustics, *Helmholtz* [15.128] and *Rayleigh* [15.3] laid the foundations of our present-day understanding of the acoustics of wind instruments. In the early part of the 20th century, *Bouasse* [15.129] significantly advanced our understanding of the generation of sound by the vibrating reed. More recently, *Campbell and Greated* [15.130] have written an authoritative textbook on musical acoustics with a particular emphasis on musical aspects, including extensive information on wind and brass instruments. Recent reviews by *Nederveen* [15.131] and *Hirschberg et al.* [15.132] provide valuable introductions to recent research on both wind

and brass instruments. Earlier texts by *Backus* [15.133] and *Benade* [15.134], both leading pioneers in research on wind-instrument acoustics, provide illuminating insights into the physics involved and provide many practical details about the instruments themselves. A recent issue of *Acta Acustica* [15.135] includes a number of useful review articles, especially on problems related to the generation of sound by vibrating reeds and air jets and on modern methods used to visualise the associated air motions. For a mathematical treatment of the physics underlying the acoustics of wind instruments, *Morse and Ingard* [15.136] remains the authoritative modern text. Other important review papers will be cited in the appropriate sections, and selected publications will be used to illustrate the text, without attempting to provide a comprehensive list of references.

We first summarise the essential physics of sound propagation in air and simple acoustic structures before considering the more complicated column shapes used for woodwind and brass instruments. An introduction is then given to the excitation of sound by vibrating lips and reeds, and by air jets blown over a sharp edge. The physical and acoustical properties of a number of woodwind and brass instruments will be included to illustrate the above topics.


A brief introduction to freely propagating sound in air was given in Sect. 15.1.3. In this section, we will be primarily concerned with the propagation of sound in the bores of wind and brass instruments, the excitation of standing-wave modes in such bores, the mechanics involved in the excitation of such modes and the resultant radiation of sound.


15.3.1 Resonances in Cylindrical Tubes

Standing waves in cylindrical tubes with closed or open ends provide the simplest introduction to the acoustics of wind instruments. For example, the flute can be considered as a first approximation as a cylindrical tube open at both ends, while the clarinet and trombone are closed at one end by the reed or the player's lips. For a cylindrical pipe open at both ends, wave solutions are of the general form

$$p_n(x, t) = A \sin(k_x x) \sin(\omega_n t), \quad (15.92)$$

with the acoustic pressure zero at both ends. Neglecting end-corrections, open ends are therefore displacement antinodes and pressure nodes. These *boundary conditions* result in eigenmodes with $k_n = n\pi/L$ and $\omega_n = nc_0\pi/L$, where L is the length of the pipe and n is an integer.

Such modes are closely analogous to the transverse standing-wave solutions on a stretched string having n half-wavelengths along the length L and a *harmonic* set of frequencies $f_n = nc_0/L$, which are integral multiples of the *fundamental* (lowest) frequency $f_1 = c_0/2L$. When a cylindrical pipe open at both ends, such as a flute, is blown softly, the pitch is determined by the fundamental mode, but when it is *overblown* the frequency doubles, with the pitch stabilising on the second mode an octave above (audio  **EXTRAS**).

A cylindrical pipe played by a reed or vibrating lips has a pressure antinode and displacement node at the playing end. This results in standing-wave solutions with an odd number of 1/4-wavelengths between the two ends, such that $k_n = n\pi/4L$, where n is now limited to odd integer values. The corresponding modal frequencies, $\omega_n = n\pi/4L$, are therefore in the ratios 1 : 3 : 5 : 7 : etc. The lowest note on the cylindrical bore clarinet, closed at one end by the mouthpiece, is therefore an octave below the lowest note on a flute of the same length. Furthermore, when overblown, the clarinet sounds a note three times higher than the fundamental, musical interval of an octave plus a perfect fifth (audio  **EXTRAS**). The weak intensity of the even- n -value modes in the spectrum accounts for the clarinet's characteristic hollow sound, particularly for the lowest notes on the instrument.

Real Instruments

For real wind and brass instruments, the idealised model of cylindrical tube resonators is strongly perturbed by a number of important factors. These include:

1. The shape of the internal bore of an instrument, which is often noncylindrical including conical and often flared tubes with a flared bell on the radiating end
2. The finite terminating impedance of the reed or mouthpiece used to excite the resonances, no longer providing a perfect displacement node
3. Radiation of sound from the end of the instrument, which is therefore no longer a perfect displacement antinode
4. Viscous and thermal losses to the walls of the instrument
5. Open and shut tone holes in the sides of wind instruments used to vary the pitch of the sounded note
6. Bends and valves along the length of brass instruments, connecting additional lengths of tubing, which allow the player to play all the notes of

a chromatic scale within the playing range of the instrument.

The skill of wind-instrument makers lies in their largely intuitive understanding of the way that changes in bore shape and similar factors affect the resonant modes of an instrument. This allows the design of instruments that retain, as closely as possible, a full set of harmonic resonances across the whole playing range of the instrument. This facilitates the stable production of continuous notes by the player, as the resulting harmonic set of Fourier components or partials coincide with the natural resonances of the instrument. For brass instruments with a flaring end this can often be achieved for all but the lowest natural resonance of the air column.

In discussing the acoustics of wind instruments with variable cross-sectional area S , the flow rate $U = Sv$ is a more useful parameter than the longitudinal particle velocity v . For example, the force acting on an element of air of length Δx along the bore length of an air column is then given by

$$-S \frac{\partial p}{\partial x} \Delta x = \rho S \frac{\partial v}{\partial t} \Delta x = \rho \frac{\partial U}{\partial t} \Delta x. \quad (15.93)$$

For travelling waves, $e^{i(\omega t \pm kx)}$, this results in a ratio between the pressure and flow rate, defined as the tube impedance

$$Z = \frac{p}{U} = \pm \frac{\rho c_0}{S}, \quad (15.94)$$

where the plus and minus signs refer to waves travelling in the positive and negative x -directions, respectively. There is a very close analogy with an electrical transmission line, with pressure and flow rate the analogue of voltage and current, as discussed later. Because the impedance is inversely proportional to area, it can be appreciably higher at the input end of a brass or wind instrument than at its flared output end. The flared bore of a brass instrument or the horn on an old wind-up gramophone can therefore be considered as an acoustic transformer, which improves the match between the high impedance of the vibrating source of sound to the much lower impedance presented by air at the end of the instrument. There is clearly an optimum matching, which enhances the radiated sound without serious degradation of the excited resonant modes.

Acoustic Radiation

In elementary textbook treatments, the pressure at the end of an open pipe is assumed to be zero and the flow rate a maximum, so that $Z_{\text{closed}} = p/U = 0$. However,

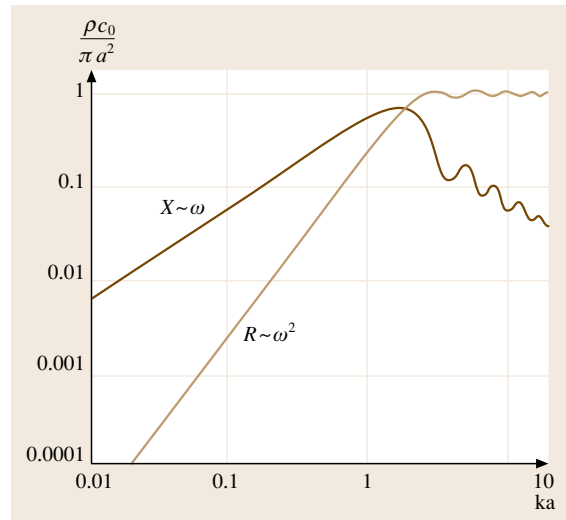


Fig. 15.66 Real and imaginary components of f , the impedance at the un baffled open end of a cylindrical tube of radius a , in units of $\rho c_0/\pi a^2$, as a function of ka (after *Beranek* [15.137])

in practice, the oscillatory motion of the air extends somewhat beyond the open end, providing a pulsating source that radiates sound, as described by *Rayleigh* [15.3, Vol. 1, Sect. 313]. Such effects can be described by a complex terminating load impedance, $Z_L = R + jx$. Figure 15.66 shows the real (*radiation resistance*) R and imaginary (*inertial end-correction*) x components of Z_L as a function of ka , where a is the radius of the open-ended pipe. The impedance is normalised to the tube impedance $\rho c_0/\pi a^2$.

When $ka \ll 1$, the reactive component is proportional to ka and corresponds to an effective increase in

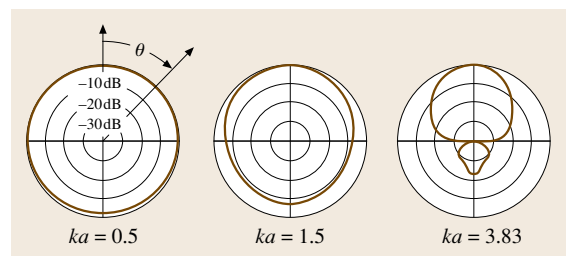


Fig. 15.67 Polar plots of the intensity radiation from the end of a cylindrical pipe of radius a for representative ka values, calculated by *Levine and Schwinger* [15.138]. The radial gradations are in units of 10 dB. The intensities in the forward direction ($\theta = 0$) relative to those of an isotropic source are 1.1, 4.8 and 11.8 dB (*Beranek* [15.137])

the tube length or end-correction of $0.61a$. At low frequencies, the real part of the impedance represents the radiation resistance $R_{\text{rad}} = \rho c/4S(ka)^2$. In this regime, the sound will be radiated isotropically as a monopole source of strength $U e^{i\omega t}$, illustrated in Fig. 15.67 by the polar plots of sound intensity as a function of angle and frequency.

When ka is of the order of and greater than unity, the real part of the impedance approaches that of a plane wave acting across the same area as that of the tube. Almost all the energy incident on the end of the tube is then radiated and little is reflected. For $ka \gg 1$, sound would be radiated from the end of the pipe as a beam of sound waves. The transition from isotropic to highly directional sound radiation is illustrated for a sequence of ka values in Fig. 15.67. The ripples in the impedance in Fig. 15.66 arise from diffraction effects, when the wavelength becomes comparable with the tube diameter.

For all woodwind and brass instruments, there is therefore a crossover frequency $f_c \approx c_0/2\pi a$, below which incident sound waves are reflected at the open end to form standing waves. Above f_c waves generated by the reed or vibrating lips will be radiated from the ends of the instrument strongly with very little reflection. Narrow-bore instruments can have a large number of resonant modes below the cut-off, while instruments with a large output bell, like many brass instruments, have far fewer.

For a narrow-bore cylindrical bore wind instrument with end radius $a \approx 1$ cm, the cut-off frequency ($ka \approx 1$) is ≈ 5.5 kHz. Below this frequency the instrument will support a number of relatively weakly damped resonant modes, which will radiate isotropically from the ends of the instrument or from open holes cut in its sides. In contrast, for brass instruments the detailed shape and size of the flared end-bell determines the cut-off frequency. The large size of the bell leads to an increase in intensity of the higher partials and hence brilliance of tone-color, especially when the bell is pointed directly towards the listener. For French horns, much of the higher-frequency sound is therefore projected backwards relative to the player, unless there is a strongly reflecting surface behind.

For $ka \ll 1$, the open end of a musical instrument acts as an isotropic monopole source with radiated power P given by

$$P = U_{\text{rms}}^2 R_{\text{rad}} = \omega^2 \frac{\rho}{8\pi c} (S\omega\xi)^2. \quad (15.95)$$

For a given vibrational displacement, the radiated power therefore increases with the fourth power of both fre-

quency and radius. This very strong dependence on size explains why brass instruments tend to have rather large bells and why high-fidelity (HI-FI) *woofer* speakers and the horns of public address loudspeakers tend to be rather large. Conversely, it explains why the sound of small loudspeakers, such as those used in PC notebooks, fall off very rapidly below a few hundred Hz.

Acoustic radiation will lower the height and increase the width of resonances in a cylindrical tube. The resulting Q -values can be determined from

$$Q = \omega \frac{\text{stored energy}}{\text{radiated energy}} = \omega \frac{\frac{1}{4}\rho SL\omega^2\xi^2}{\omega^4 (\rho/8\pi c) S^2\xi^2} = 2\pi cL/\omega S. \quad (15.96)$$

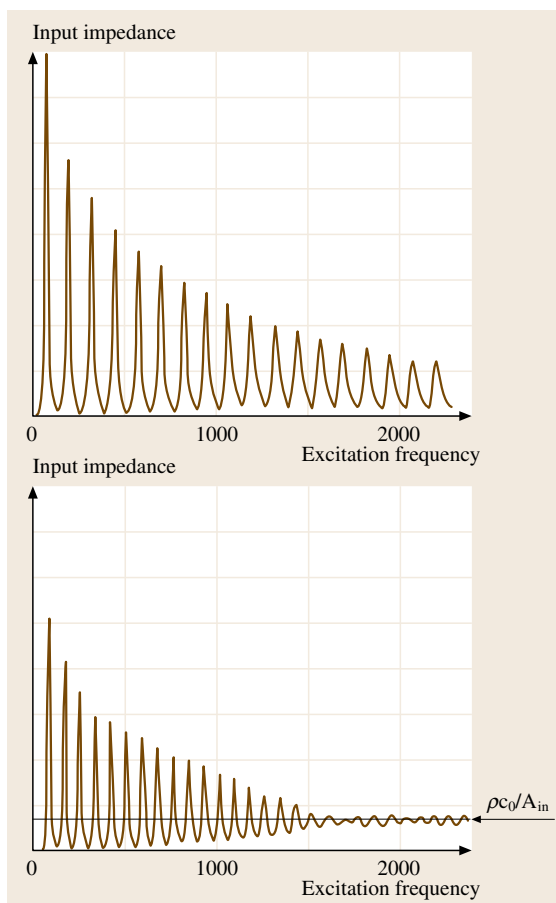


Fig. 15.68 Input impedance of a length of 1 cm diameter trumpet tubing with and without a bell attached to the output end (after *Benade* [15.134])

Narrow-bore instruments will therefore have larger Q -values and narrower resonances than wide-bore instruments such as brass instruments, where the flared end-sections enhance the radiated energy at the expense of increasing the net losses.

The increased damping introduced by radiation from the end of an instrument is illustrated in Fig. 15.68, which compares the resonances of a length of 1 cm-diameter trumpet tubing, first with a normal open end and then with a bell attached (Benade [15.133, Fig. 20.4]). Attaching a bell to such a tube dramatically increases the radiated sound from the higher partials and perceived intensity, but at the expense of a cut-off frequency at around ≈ 1.5 kHz and a significant broadening of the resonances at lower frequencies. Audio **EXTRAS** demonstrates the sound of a mouthpiece-blown length of hose pipe with and without a conical chemical filter funnel attached to its end.

Viscous and Thermal Losses

In addition to radiation losses, there can be significant losses from viscous damping and heat transfer to the walls, as discussed in detail in Fletcher and Rossing [15.5, Sect. 8.2]. Although simple models for waves propagating along tubes assume a constant particle displacement across the whole cross-section, in reality the air on the surface of the walls remains at rest. The particle velocity only attains the assumed plane-wave constant value over a boundary-layer distance of δ_η from the walls. This is determined by the viscosity η , where $\delta_\eta = (\eta/\omega\rho)^{1/2}$, which can be expressed as $\approx 1.6/f^{1/2}$ mm for air at room temperature. At 100 Hz, $\delta_\eta \approx 0.16$ mm, which is relatively small in comparison with typical wind-instrument pipe diameters. Nevertheless, it introduces a significant amount of additional damping of the lower-frequency resonances of wind and brass instruments.

The viscous losses lead to an attenuation of sound waves, which can be described by adding an imaginary component to the k value such that $k' = k - i\alpha$. Waves therefore propagate as $e^{-\alpha x} e^{i(\omega t - kx)}$, with an attenuation coefficient

$$\alpha = \frac{1}{ac_0} \sqrt{\frac{\eta\omega}{2\rho}} = \frac{k\delta_\eta}{a}. \quad (15.97)$$

In addition, heat can flow from the sinusoidally varying adiabatic temperature fluctuations of the vibrating column of air into the walls of the cylinder. At acoustic frequencies, this takes place over the thermal diffusion boundary length $\delta_\theta = (\kappa/\omega\rho C_p)^{1/2}$, where κ is the thermal conductivity and C_p is the heat capacity of the gas

at constant pressure. In practice, $\delta_\theta \approx \delta_\eta$, as anticipated from simple kinetic theory (for air, the values differ by only 20%). Viscous and heating losses are therefore comparable in size giving an effective damping factor for air at room temperature, $\alpha = 2.210^4 k^{1/2}/a \text{ m}^{-1}$ (Fletcher and Rossing [15.5, Sect. 8.2]). The ratio of the real to imaginary components of k determines the damping and effective Q -value of the acoustic resonances from wall losses alone, with $Q_{\text{walls}} = k/2\alpha$.

The combination of radiation and wall losses leads to an effective Q_{total} of the resonant modes given by

$$\frac{1}{Q_{\text{total}}} = \frac{1}{Q_{\text{radiation}}} + \frac{1}{Q_{\text{wall-damping}}}. \quad (15.98)$$

Because of the different frequency dependencies, wall damping tends to be the strongest cause of damping of the lowest-frequency resonances of an instrument. It can also be significant in the narrow-bore tubes and *crooks* used to attach reeds to wind instruments.

Input Impedance

The method used to characterize the acoustical properties of a wind or brass instrument is to measure the input impedance $Z_{\text{in}} = p_{\text{in}}/U_{\text{in}}$ at the mouthpiece or reed end of the instrument. Such measurements are frequently made using the capillary tube method. This involves connecting an oscillating source of pressure fluctuations to the input of the instrument through a narrow-bore tube. This maintains a constant oscillating flow of air into the instrument, which is largely independent of the frequency-dependent induced pressure fluctuations at the input of the instrument. Several examples of such measurements, similar to those for the length of trumpet tubing (Fig. 15.68), for woodwind and brass instruments are shown and discussed by Backus [15.133] and Benade [15.134], who pioneered such measurements, and in Fletcher and Rossing [15.5, Chap. 15]. Alternatively, a piezoelectric driver coupled to the end of the instrument can provide a known source of acoustic volume flow.

The input impedance of a cylindrical tube is a function of both the tube impedance $Z_0 = \rho c_0/S$ and the terminating impedance Z_L at its end. It can be calculated using standard transmission-line theory, which takes into account the amplitude and phases of the reflected waves from the terminating load. The reflection and transmission coefficients R and T for a sound wave impinging on a terminating load Z_L are given by

$$R = \frac{Z_L - Z_0}{Z_L + Z_0} \quad \text{and} \quad T = \frac{2Z_L}{Z_L + Z_0}. \quad (15.99)$$

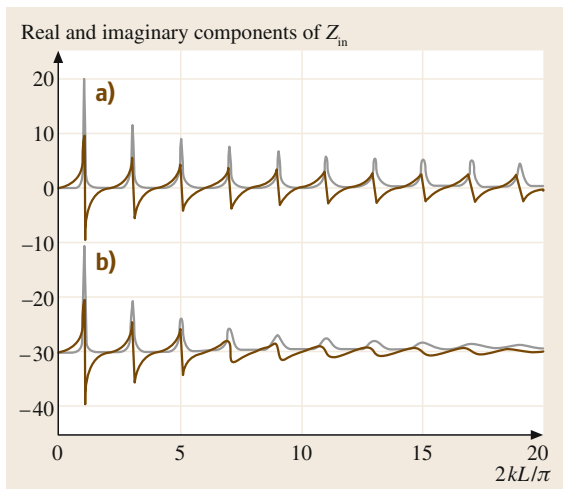


Fig. 15.69a,b Real and imaginary components of the input impedance in units of Z_0 as a function of $2kL/\pi$ for (a) an ideally open-ended, $Z_L = 0$, cylindrical tube with wall losses varying as $k^{1/2}$, and (b) the same components shifted downwards for a pipe with radiation resistance proportional to k^2 also included

For a cylindrical tube of length L , the input impedance is given by

$$Z_{\text{in}} = Z_0 \frac{Z_L \cos kl + iZ_0 \sin kl}{iZ_L \sin kl + Z_0 \cos kl}, \quad (15.100)$$

with complex k values $k - i\alpha$, if wall losses need to be included.

In Fig. 15.69 we have plotted the kL dependence of the real and imaginary components of the input impedance of an open-ended cylindrical pipe. The upper plot includes wall losses alone proportional to $k^{1/2}$ while the lower plot includes losses from the end of the instrument with radiation resistance $\text{Re}(Z_L)$ varying as k^2 . The input impedance is high when $k_n = nc_0/4L$, where n is an odd integer. The input impedance is a minimum when n is even.

It is instructive to consider the magnitude of the input impedances on a logarithmic scale, as shown in Fig. 15.70. When plotted in this way, the resonances and anti-resonances are symmetrically placed about the tube impedance Z_0 . The magnitude of the impedance of the n th resonance is $Q_n Z_0$, where Q_n is the quality factor of the excited mode. In contrast the anti-resonances have values of Z_0/Q . The widths $\Delta\omega/\omega$ of the modes at half or double intensity are given by $1/Q_n$.

For efficient transfer of sound, the input impedance of a wind instrument has to match the impedance of the

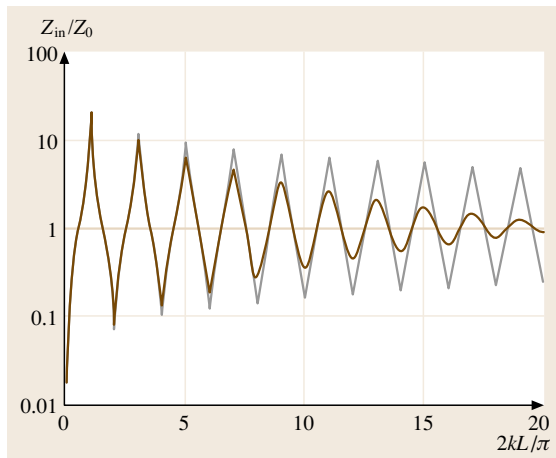


Fig. 15.70 The modulus of the input impedance plotted on a logarithmic scale of cylindrical pipe with wall damping alone and with additional radiative damping as a function of k in units of $\pi/2$

sound generator. For instruments like the flute, recorder and pan pipes, sound is excited by imposed fluctuations in air pressure across an open hole, so that the generator impedance is small. The resonances of such instruments are therefore located at the minima of the anti-resonance impedance dips, corresponding to the evenly spaced resonances, $f_n = nc_0/2L$, of a cylindrical tube with both ends open. In contrast, for all the brass instruments and woodwind instruments played by a reed, the playing end of the tube is closed by a relatively massive generator (the lips or reed). Resonances then occur at the peaks of the input impedance with frequencies $f_n = nc_0/4L$, where n is now an odd integer, corresponding to the resonances of a tube closed at one end. If we had plotted the magnitude of the input admittance, $A(\omega) = 1/Z(\omega)$, instead of the impedance, the positions of the resonances and anti-resonances would have been reversed. The resonant modes of a double-open-ended wind instrument therefore occur at the peaks of the input admittance, whereas the resonant modes of wind or brass instruments played with a reed or mouthpiece are at the peaks of the input impedance. This is a general property of wind instruments, whatever the size or shape of their internal bores.

15.3.2 Non-Cylindrical Tubes

Although there are simple wind instruments with cylindrical bores along their whole length, the vast majority of modern instruments and many ancient and ethno-

logically important instruments have internal bores that flare out towards their ends. One of the principle reasons for such flares is that they act as acoustic transformers, which help to match the high impedance at the mouthpiece to the much lower radiation impedance of the larger-area radiating output end. However, increasing the fraction of sound radiated decreases the amplitude of the reflected waves and hence the height and sharpness of the natural resonances of the air resonances. In addition, the shape of the bore can strongly influence the frequencies of the resonating air column, which destroys the harmonicity of the modes. This makes it more difficult for the player to produce a continuous note that is rich in partials, since any repetitive waveform requires the excitation of a harmonic set of frequencies.

Conical Tube

We first consider sound propagation in a conical tube, approximating to the internal bore of the oboe, saxophone, cornet, renaissance cornett and bugle. If side-wall interactions are neglected, the solutions for wave propagation in a conical tube are identical to those of spherical wave propagating from a central point. Such waves satisfy the wave equation, which may be written in spherical coordinates as

$$\nabla^2(rp) = \frac{1}{c_0^2} \frac{\partial^2(rp)}{\partial t^2}. \quad (15.101)$$

We therefore have standing-wave solutions for rp that are very similar to those of a cylindrical tube, with

$$p = C \frac{\sin kr}{r} e^{i\omega t}. \quad (15.102)$$

Note that the pressure remains finite at the apex of the cone, $r = 0$, where $\sin(kr)/r \rightarrow k$. For a conical tube with a pressure node $p = 0$ at the open end, we therefore have standing wave modes with $k_n L = n\pi$ and $f_n = nc_0/2L$, where n is any integer. The frequencies of the excited modes are therefore identical to the modes of a cylindrical tube of the same length that is open at both ends. The lowest note at $f_1 = c_0/2L$ for a conical tube instrument with a reed at one end (e.g. the oboe and saxophone) is therefore an octave above a reed instrument of the same length with a cylindrical bore (e.g. the clarinet) with a fundamental frequency of $c_0/4L$.

The flow velocity U is determined by the acceleration of the air resulting from the spatial variation of the pressure, so that

$$\rho \frac{\partial U}{\partial t} = \frac{\partial(r^2 p)}{\partial r} = C(\sin kr + kr \cos kr) e^{i\omega t}. \quad (15.103)$$

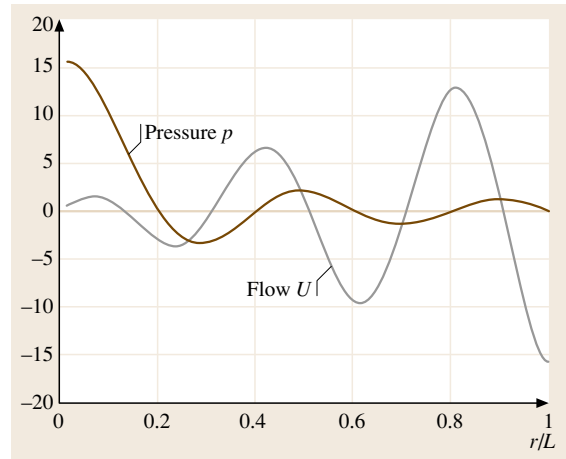


Fig. 15.71 Pressure and flow velocity of the $n = 5$ mode along the length of a conical tube

Figure 15.71 illustrates the pressure and flow velocity for the $n = 5$ mode of a conical tube. Unlike the modes of cylindrical tube, the nodes of U no longer coincide with the peaks in p , which is especially apparent for the first few cycles along the tube. Furthermore, the amplitude fluctuations increase with distance r from the apex ($\approx r$), whilst the fluctuations in pressure decrease $\approx 1/r$. A conical section therefore acts as an acoustic transformer helping to match the high impedance at the input mouthpiece end to the low impedance at the output radiating end.

Attaching a mouthpiece or reed to the end of a conical tube requires truncation of the cone, which will clearly perturb the frequencies of the harmonic modes. However, using a mouthpiece or reed unit having the same internal volume as the volume of the truncated section removed will leave the frequencies of the lowest modes unchanged. Only when the acoustic wavelength becomes comparable with the length of truncated section will the perturbation be large.

Fletcher and Rossing [15.5, Sect. 8.7] consider the physics of the truncated conical tube and give the input impedance derived by Olson [15.139]

$$Z_{\text{in}} = \frac{\rho c_0}{S_1} \frac{iZ_L \left(\frac{\sin(kL - \theta_2)}{\sin \theta_2} \right) + \left(\frac{\rho c_0}{S_2} \right) \sin kL}{Z_L \frac{\sin(kL + \theta_1 - \theta_2)}{\sin \theta_1 \sin \theta_2} + j \left(\frac{\rho c_0}{S_2} \right) \frac{\sin(kL + \theta_1)}{\sin \theta_1}}, \quad (15.104)$$

where x_1 and x_2 are the distances of the two ends from the apex of the truncated conical section. The length $L = x_2 - x_1$, the end areas are S_1 and S_2 , with $\theta_1 = \tan^{-1} kx_1$ and $\theta_2 = \tan^{-1} kx_2$.

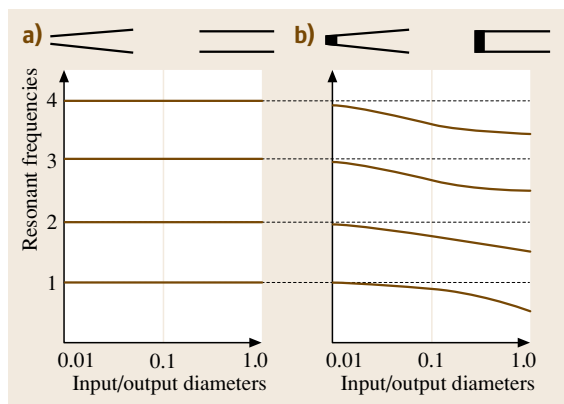


Fig. 15.72a,b The first four resonant frequencies of truncated cones with (a) both ends open, and (b) the input end closed, as a function of the ratio of their input to output diameters (after Ayers et al. [15.140])

For a cone with $Z_L = 0$ at the open end, (15.104) reduces to

$$Z_{\text{in}} = -j \frac{\rho c_0}{S_1} \frac{\sin kL \sin \theta_1}{\sin(kL + \theta_1)}, \quad (15.105)$$

which is zero for $kL = n\pi$. The resonant frequencies of truncated cones with both ends open are therefore independent of cone angle and are the same as the equally spaced harmonic modes of a cylinder of the same length with both ends open, as shown in Fig. 15.72a. In contrast, the resonant frequencies of a truncated cone with one end closed (e.g. by the reed of an oboe or saxophone or mouthpiece of a bugle) are strongly dependent on the cone angle or ratio of input to output diameter, as shown in Fig. 15.72b, adapted from Ayers et al. [15.140]. As the ratio of input to output diameters of a truncated cone increases, the modes change from the evenly spaced harmonics of an open-ended cylinder of the same length, to the odd harmonics of a cylinder closed at one end. In the transitional regime, the frequencies of the modes are no longer harmonically re-

lated. This has a significant effect on the playability of the instrument, as the upper harmonics are no longer coincident with the Fourier components of a continuously sounded note. However, for an instrument such as the oboe, with a rather small truncated cone length, the perturbation of the upper modes is relatively small, as can be seen from Fig. 15.71b.

Cylindrical and nontruncated conical tubes are the only tubes that can produce a harmonically related set of resonant modes, independent of their length. Hence, when a hole is opened in the side walls of such a tube, to reduce the effective length and hence pitch of the note played, to first order, the harmonicity of the modes is retained. This assumes a node at the open hole, which will not be strictly correct, as discussed later in Sect. 15.3.3.




In reality, the bores of wind instruments are rarely exactly cylindrical or conical along their whole length. Moreover, many wind instruments have a small flare at the end to enhance the radiated sound, while others, like the cor anglais and oboe d'amore, have an egg-shaped cavity resonator towards their ends, which contributes to their characteristic timbre or tone colour. Table 15.6 lists representative wind instruments that are at least approximately based on cylindrical and conical bore shapes. The modern organ makes use of almost every conceivable combination of closed- and open-ended cylindrical and conical pipes.

Hybrid Tubes

Although many brass instruments include considerable lengths of cylindrical section, they generally have a fairly long, gently flared, end-section terminated by a very strongly flared output bell to enhance the radiated sound. The shape of such flares can be optimized to preserve the near harmonicity of the resonant modes, as described in the following section.

One can use (15.104) to model the input impedance of a flared tube of any shape, by approximating the shape by a number of short truncated conical sections

Table 15.6 Instruments approximately based on cylindrical and conical air columns

		
$f_n = nc_0/2L$ n even and odd	$f_n = nc_0/4L$ n odd	$f_n = nc_0/2L$ n even and odd
Flute Recorders Shakuhachi Organ flue pipes (e.g. diapason)	Clarinet Crumhorn Pan pipes Organ flue pipes (e.g. bourdon) Organ reed pipes (e.g. clarinet)	Oboe Bassoon Saxophone Cornett Serpent Organ reed pipes (e.g. trumpet)

joined together. Starting from the radiating end, one evaluates the input impedance of each cone in turn and uses it to provide the terminating impedance for the next, until one reached the mouthpiece end.

A weakness of all such models is the assumed plane wavefront across the air column, whereas it must always be perpendicular to the walls and belled outwards in any rapidly flaring region. We will return to this problem later.

Typical brass instruments, like the trumpet and trombone, have bores that are approximately cylindrical for around half their length followed by a gently flared section and end bell, while others have initial conical sections, like the bugle and horn. The affect on the resonant frequencies of the first six modes of adding a truncated conical section to a length of cylindrical tubing is shown as a function their relative lengths in Fig. 15.73, from *Fletcher and Rossing* [15.5, Fig. 8.9]. Note the major deviations from harmonicity of the resonant modes, apart from when the two sections are of nearly equal lengths. These results highlight the complexity involved, when adding flaring sections to brass instruments to increase the radiated sound.

Horn Equation

Physical insight into the influence of bore shape on the modes of typical brass instruments is given by the *horn equation* introduced by *Webster* [15.141], though similar models date back to the time of *Bernoulli* (*Rossing*

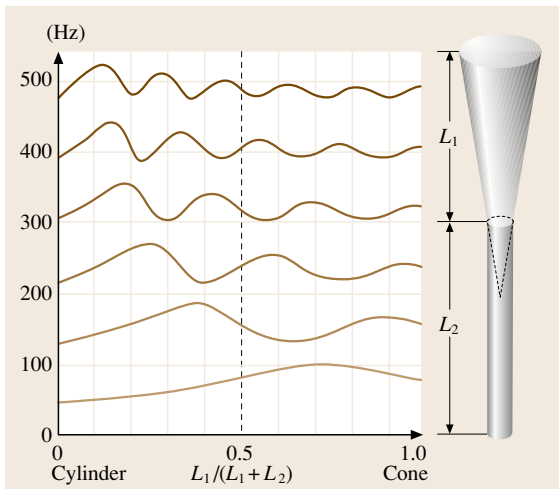


Fig. 15.73 The frequencies of the first six modes of a compound horn formed from different fractional lengths of cylindrical and conical section (after *Fletcher and Rossing* [15.5])

and *Fletcher* [15.5, Sect. 8.6]). In its simplest form, the horn equation can be written as

$$\frac{1}{S} \frac{\partial}{\partial x} \left(S \frac{\partial p}{\partial x} \right) = \frac{1}{c_0^2} \frac{\partial^2 p}{\partial t^2}, \quad (15.106)$$

where $S(x)$ is the cross-sectional area of the horn at a distance x along its length. Provided the flare is not too large, the above plane-wave approximation gives a good approximation to the exact solutions and preserves the essential physics involved.

If we make the substitution $p = \psi S^{1/2}$ and look for solutions varying as $\psi(x)e^{i\omega t}$, the horn equation can be expressed as

$$\frac{\partial^2 \psi}{\partial x^2} + \left[\left(\frac{\omega}{c_0} \right)^2 - \frac{1}{a} \frac{\partial^2 a}{\partial x^2} \right] \psi = 0, \quad (15.107)$$

where the radius $a(x)$ is now a function of position along the length. The above equation is closely related to the Schrödinger wave equation in quantum mechanics, with $1/a \partial^2 a / \partial x^2$ the analogue of potential energy and $-\partial^2 \psi / \partial x^2$ the analogue of kinetic energy $-\hbar^2 / 2m \partial^2 \psi / \partial x^2$, where m is the mass of the particle and \hbar is Planck's constant. One can look for solutions of the form $e^{i(\omega t \pm kx)}$. At any point along the horn at radius x the radius of curvature of the horn walls, $R = (\partial^2 a / \partial x^2)^{-1}$, so that

$$k^2 = \left(\frac{\omega}{c_0} \right)^2 - \frac{1}{aR}. \quad (15.108)$$

If $\omega > \omega_c = c_0 / (aR)^{1/2}$, k is real, so that unattenuated travelling and standing-wave solutions exist. However, when $\omega < \omega_c$, k is imaginary and waves no longer propagate, but are exponentially damped as $e^{-x/\delta} e^{i\omega t}$ with a decay length of $c_0 / (\omega_c^2 - \omega^2)^{1/2}$.

The propagation of sound waves in a horn is therefore directly analogous to the propagation of particle waves in a spatially varying potential. If the curvature is sufficiently large sound waves will be reflected before they reach the end of the instrument. However, just like particle waves in a potential well, sound waves can still tunnel through the potential barrier and radiate into free space at the end of the flared section. For a horn with a rapidly increasing flare, the reflection point occurs when the wavelength $\lambda^2 \approx (2\pi)Ra$. The effective length of an instrument with a flared horn on its end is therefore shorter for low-frequency modes than for the higher-frequency modes. This is illustrated schematically in Fig. 15.77 for resonant modes of a flared Bessel horn, which will be considered in more detail in the next section.

Exponential Horn

We now consider solutions of the horn equation, for a number of special shapes that closely describe sections of the internal bore of typical brass instrument. Cylindrical and conical section horns are special solutions with $(1/a)\partial^2 a/\partial x^2 = 0$, so that ψ satisfies the simple dispersionless wave equation. Figure 15.74 illustrates a number of other horn shapes described by analytic functions.

The radii of exponential and cosh function horns vary exponentially as Ae^{mx} and $A\cosh(mx)$, respectively, so that $(1/a)\partial^2 a/\partial x^2 = m^2$. The cosh mx function provides a smooth connection to a cylindrical tube at the input end. For both shapes, the horn equation can then be written as

$$\frac{\partial^2 \psi}{\partial x^2} + \left[\left(\frac{\omega}{c_0} \right)^2 - m^2 \right] \psi = 0, \quad (15.109)$$

which has travelling solutions for the sound pressure $p = \psi/S^{1/2}$, where

$$p(x) = e^{-mx} e^{i(\omega t - \sqrt{k^2 - m^2}x)}, \quad (15.110)$$

and $k = \omega/c_0$. Above a critical cut-off frequency, $f_c = c_0 m/2$, waves can propagate freely along the air column with a dispersive phase velocity of $c_0/\sqrt{1 - (\omega_c/\omega)^2}$, while below the cut-off frequency the waves are exponentially damped. The cut-off frequency occurs when the free-space wavelength is approximately six times the length for the radius to increase by the exponential factor e .

Figure 15.75 compares the input resistance and reactance of an infinite exponential horn with that of a baffled piston having the same input area (Kinsler et al. [15.142, Fig. 14.19]). The plots are for an exponential horn with $m = 3.7 \text{ m}^{-1}$, which corresponds to a cut-off frequency of $\approx 100 \text{ Hz}$, and a baffled piston having the same radius of 2 cm as the throat of the

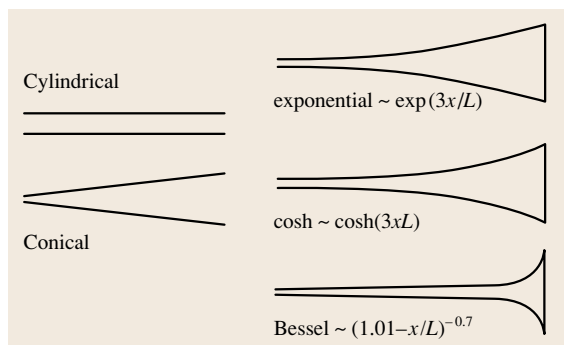


Fig. 15.74 Analytic horn shapes

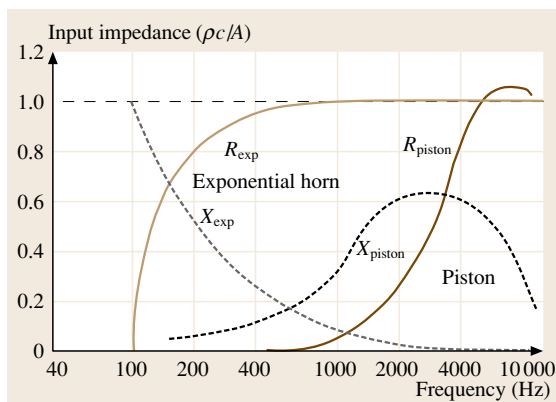


Fig. 15.75 Comparison of input impedance at the input throat of an infinitely long exponential horn and a piston of the same area set into an infinite baffle (after Kinsler et al. [15.142])

exponential horn. Above $\approx 400 \text{ Hz}$, there is very little difference between the impedance of an infinitely long horn and a horn with a finite length of $\approx 1.5 \text{ m}$ or longer, though below this frequency reflections cause additional fluctuations around the plotted values. Below the cut-off frequency, no acoustic energy can be radiated. Above the cut off the input resistance rises rather rapidly towards its limiting 100% radiating value. The exponential horn with a piston source at its throat is therefore a much more efficient radiator of sound than a baffled piston at all frequencies above the cut-off frequency.

The exponential horn illustrates how the flared cross section of brass instruments enhances the radiation of sound, though brass instruments are never based on exponential horns, otherwise no resonant modes could be set up. However, exponential horns were widely used in the early days of the gramophone. In the absence of any electronic amplification, they amplified the sound produced by the input diaphragm excited by the pick-up stylus on the recording cylinder or disc. They are still widely used in powerful public address systems. Such horns can also be used in reverse, as very efficient detectors of sound, with a microphone placed at the apex of the horn.

Bessel Horn

We now consider more realistic horns with a rapidly flaring end bell, which can often be modelled by what are known as Bessel horn shapes, with the radius varying as $1/x^m$ from their open end. Typical flared horn shapes are shown in Fig. 15.76 for various values of m , where the horn functions $A/(x+x_0)^m$ have been nor-

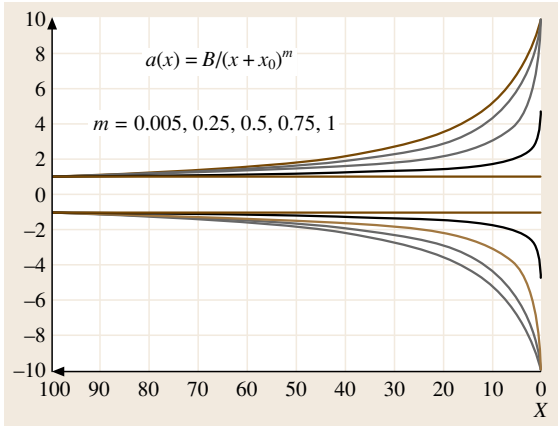


Fig. 15.76 Bessel horns representing the rapid outward flare of the bell on the end of a brass instrument, for a sequence of m values giving a ratio of input to output diameters of 10

malised by suitable choice of A and x_0 , to model horns with input and output values 1 and 10. Increasing the value of m increases the rapidity with which the flare opens out at the end.

Again assuming the plane-wave approximation, the horn equation can be written as

$$\frac{\partial^2 \psi}{\partial x^2} + \left[\left(\frac{\omega}{c_0} \right)^2 - \frac{m(m+1)}{x^2} \right] \psi = 0, \quad (15.111)$$

with solutions

$$\psi(kx) = x^{1/2} J_{m+1/2}(kx) \quad (15.112)$$

and pressure varying from the end as

$$p(kx) = \frac{1}{x^{1/2}} J_{m+1/2}(kx), \quad (15.113)$$

where $J_{m+1/2}(kx)$ is a Bessel function of order $m + 1/2$, giving the name to such horns.

In the plane-wave approximation, the sharpness and height of the barrier to wave propagation arising from the curvature could result in total reflection of the incident waves, so that no sound would be emitted from the end of the instrument. In reality, the curvature of the waveform will smear out any singularity in the horn function over a distance somewhat smaller than the output bell radius. Nevertheless, despite its limitations, the plane-wave model provides an instructive description of the influence of a rapidly flaring bell on a brass instrument. This is illustrated in Fig. 15.77 for

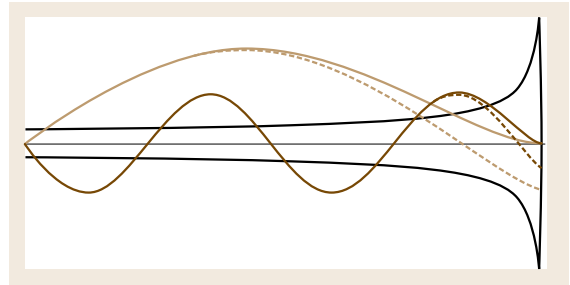


Fig. 15.77 Fundamental and fourth mode of an $m = 1/2$ Bessel horn, illustrating the increase in wavelength and resulting shift inwards of the effective nodal position. The dashed lines illustrate the extrapolated sine-wave solutions from well inside the bore. The plot is of $p(x)/x$

the fundamental and fourth modes of a Bessel horn with $m = 1/2$, with the pressure $p(x)$ varying from the output end as $xJ_1(kx)$.

The most important point to note is the way that the flare pushes the effective node of the incident sine-wave solutions (extended into the flared section as dashed curves) away from the end of the instrument. The effective length is therefore shortened and resonant frequencies increased, the effect being largest for the lower frequency modes. The flare and general outward curvature of the horn cross section therefore destroys the harmonicity of the modal frequencies. This is a completely general result for any horn with a flared end. In practice, the nodal positions will also be affected by the curvature of the wavefront, which will further perturb the modal frequencies, but without changing the above qualitative behaviour.

Benade [15.134, Sect. 20.5] notes that, from the early 17th century, trumpets and trombones have been designed with strongly flaring bell corresponding to m values of 0.5–0.65, while French horns have bells with a less sudden flare with m values of 0.7–0.9.

From Fig. 15.77, it is easy to see how the player can significantly affect the pitch of a note on the French horn, by moving the supporting hand up into the bell of the instrument, which is referred to as hand-stopping. The pitch can be lowered by around a semitone, by placing the downwardly cupped hand and wrist against the top of the flared bell, effectively reducing the flare and increasing the effective length of the instrument. Alternatively, the pitch can be raised by a similar amount when the hand almost completely closes the inner bore. This leads to a major perturbation of the boundary conditions, effectively shortening the air column and reducing the output sound. The increase in frequency can

be explained by the player using an almost unchanged embouchure to excite a higher frequency mode of the shortened tube. Because of the increased reflection of sound by the presence of the hand, the resultant sound although quieter is also much richer in higher partials (Fig. 15.113). Both effects are illustrated in Audio example 13 EXTRAS.

Flared Horns

Use is made of the dependence of modal frequencies on the curvature of horn shapes to design brass instruments with a set of resonances, which closely approximate to a harmonic series with frequencies $f_n = n f_1$. This should be contrasted with the modes of a cylindrical tube closed at one end by the mouthpiece, which would

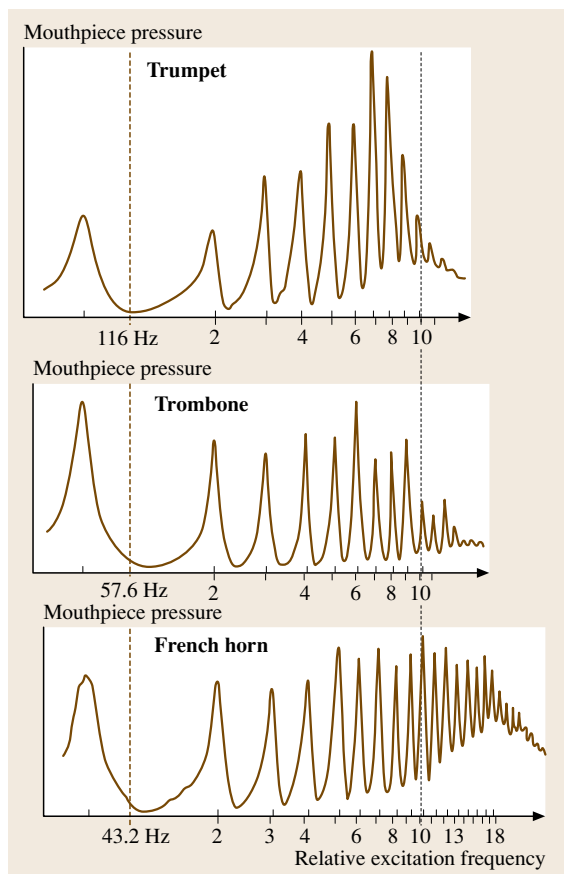


Fig. 15.78 Input impedances of the trumpet, trombone and French horn with the positions of the resonant peaks marked above the axis to show their position relative to a harmonic series based on the second harmonic of the instrument (after Backus [15.133])

only involve the odd- n integer modes with frequencies of $f_n = c/2L$.

Historically, this has been achieved by empirical methods, with makers adjusting the shapes of brass instrument to give as near perfect a set of harmonic resonances as possible, as illustrated in Fig. 15.78 from Backus [15.133, Chap. 12]. A harmonic set of modes enhances the playability of the instrument, as the partials of any continuously blown note then coincide with the natural resonances of the instrument. However, the fundamental mode is always significantly flatter than required and is therefore not normally used in musical performance. Nevertheless, the brass player can still sound a *pedal note* corresponding to the *virtual fundamental* of the higher harmonics by exciting a repetitive waveform involving the higher harmonics, but with only a weak Fourier component at the pitch of the sounded note.

The way that this is achieved is shown schematically in Fig. 15.79 starting from the odd- n resonances of a cylindrical tube closed at one end by the mouthpiece to an appropriately flared horn of the same length. In practice, one can achieve a nearly perfect set of harmonic resonances, midway between the odd-integer modes of a cylindrical tube closed at one end, for all but the fundamental mode, which cannot be shifted upwards by a sufficient amount to form a harmonic fundamental, stopping and of the new set of modes.

Benade [15.134, Sect. 20.5] has given an empirical expression for the frequencies of the partials of Bessel horns closed at the mouthpiece end, which closely de-

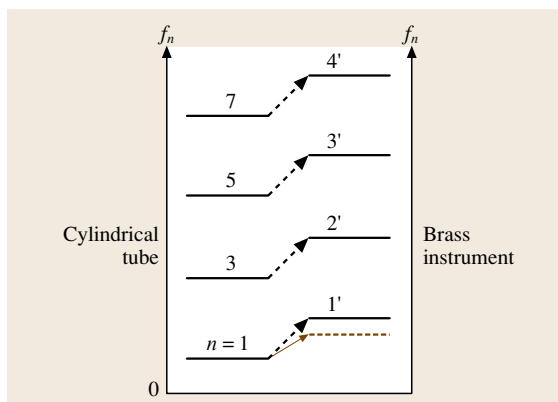


Fig. 15.79 The transformation of the odd- n modes of a cylindrical air column closed at one end to the near harmonic, all integer, n' modes of a flared brass instruments. The lower dashed line indicates schematically what can be achieved in practice for the lowest

scribes these perturbations,

$$\frac{f'_n}{f_n} \approx \left(1 + 0.637 \frac{\sqrt{m(m+1)}}{2n-1} \right), \quad (15.114)$$

where the $(2n-1)$ in the denominator emphasising the preferential raising in frequency of the lower-frequency modes. This gives frequencies for the first six modes of a Bessel function horn with $m=0.7$ are in the ratios 0.94, 2.00, 3.06, 4.12, 5.18 and 6.24, normalised to the $n=2$ mode. These should be compared with the ideal 1, 2, 3, 4, 5, 6 ratios. Apart from the lowest note, which is a semitone flat, the higher modes are less than a semitone sharp compared with their ideal values.

Perturbation Models

Perturbation theory can be used to describe how changes in bore shape perturb the resonant modes of brass and woodwind instruments. *Fletcher and Rossing* [15.5, Sect. 8.10] show that the change of frequency of a resonant mode $\Delta\omega$ resulting from small distributed changes $\Delta S(x)$ in bore area $S(x)$ is given by

$$\frac{\Delta\omega_n}{\omega_n} = -\frac{1}{2} \left(\frac{c_0}{\omega_n} \right) \int_0^L \left[\frac{\partial}{\partial x} \left(\frac{\Delta S(x)}{S(x)} \right) p_n \frac{\partial p_n}{\partial x} dx \right] / \times \int_0^L [S(x)p_n^2 dx]. \quad (15.115)$$

An alternative equivalent derivation uses Rayleigh's harmonic balance argument and equates the peak kinetic energy to the peak potential energy. To first order, the perturbation is assumed to leave the shape of the modal wavefunction unchanged. The kinetic and potential energy stored in a particular resonant mode can be expressed in terms of the local kinetic $\frac{1}{2}\rho\omega_n^2\xi_n^2$ and strain $\frac{1}{2}\gamma P_0(\partial\xi_n/\partial x)^2$ energy densities. For simplicity, we consider the perturbation of the n th resonant mode of a cylindrical air column open at one end, with particle displacement $\xi_n \approx \sin(n\pi x/L) \cos(\omega_n t)$, where n is an odd integer. Equating the peak kinetic and potential energy over the perturbed bore of the cylinder, we can then write

$$\begin{aligned} \omega_n'^2 \int_0^L \rho [S + \Delta S(x)] \sin^2(kx) dx \\ = \gamma P_0 k_n^2 \int_0^L [S + \Delta S(x)] \cos^2(kx) dx, \end{aligned} \quad (15.116)$$

where ω_n' is the perturbed frequency. This can be rewritten as

$$\begin{aligned} \frac{\omega_n'^2}{\omega_n^2} &= \int_0^L [S + \Delta S(x)] \cos^2(kx) dx / \\ &\times \int_0^L [S + \Delta S(x)] \sin^2(kx) dx. \end{aligned} \quad (15.117)$$

Because the perturbations are assumed to be small, we can rearrange (15.117) to give the fractional change in frequency

$$\frac{\Delta\omega_n}{\omega_n} = \frac{1}{L} \int_0^L \frac{\Delta S(x)}{S} (\cos^2 kx - \sin^2 kx) dx. \quad (15.118)$$

Hence, if the tube is increased in area close to a displacement antinode, where the particle flow is large (low pressure), the modal frequency will increase, whereas the frequency will decrease, if constricted close to a nodal position (large pressure) (*Benade* [15.134, Sect. 22.3]). This result can be generalised to a tube of any shape. Hence, by changing the radius over an extended region close to a node or antinode, the frequencies of a particular mode can be either raised or lowered, but at the expense of similar perturbations to other modes. Considerable art and experience is therefore needed to correct for the inharmonicity of several modes simultaneously.

Electric Circuit Analogues

It is often instructive to consider acoustical systems in terms of equivalent electric circuit analogues, where voltage V and electrical current I can represent the acoustic pressure p and flow along a pipe U . For example, a volume of air with flow velocity U in a pipe of area S and length l has a pressure drop $(\rho l/S)\partial U/\partial t$ across its length, which is equivalent to the voltage $L\partial I/\partial t$ across an inductor in an electrical circuit. Likewise, the rate of pressure rise, $\partial p/\partial t = \gamma P_0 U/V$, as gas flows into a volume V , is equivalent to the rate of voltage rise, $\partial V/\partial t = I/C$ across a capacitance $C \equiv V/\gamma P_0$.


As a simple example, we re-derive the Helmholtz resonance frequency, previously considered in relation to the principal air resonance of the air inside a violin or guitar body (Sect. 15.2.4), but equally important, as we will show later, in describing the resonance of air within the mouthpiece of brass instruments.

In its simplest form, the Helmholtz resonator consists of a closed volume V with an attached cylindrical

pipe of length l and area S attached, through which the air vibrates in and out of the volume. All dimensions are assumed small compared to the acoustic wavelength, so that the pressure p in the volume and the flow in the pipe U can be assumed to be spatially uniform. The volume acts as an acoustic capacitance $C = V/\gamma P_0$, which resonates with the acoustic inductance $L = \rho l/S$ of the air in the neck. The resonant frequency is therefore given by

$$\omega_{\text{Helmholtz}} = \frac{1}{\sqrt{LC}} = \sqrt{\frac{S}{\rho l} \frac{\gamma P_0}{V}} = c_0 \sqrt{\frac{S}{lV}}, \quad (15.119)$$

as derived earlier.

Any enclosed air volume with holes in its containing walls acts as a Helmholtz resonator, with an effective *kinetic inductance* of the hole region equivalent to a tube of the same diameter with an effective length of wall thickness plus ≈ 0.61 hole radius (Kinsler et al. [15.142, Sect. 9.2]). This is the familiar end-correction for an open-ended pipe (Kinsler et al. [15.142, Sect. 9.2]). Open holes of different diameters will therefore give resonances corresponding to different musical tones. The ocarina is a very simple musical instrument based on such resonances, in which typically four or five holes with different areas can be opened and closed in combination, to give a full range of notes on a chosen musical scale (audio  EXTRAS). Because the sound is based on the single resonance of a Helmholtz resonator, there are no simply related higher-frequency modes that can be excited. Ocarinas appear in many ancient and ethnic cultures around the world and are often sold as ceramic toys.

Acoustic Transmission Line

There is also a close equivalence between acoustic waves in wind instruments and electrical waves on transmission lines, with an acoustic pipe having an equivalent inductance $L_0 = \rho/S$ and capacitance $C_0 = S/\gamma P_0$ per unit length. For a transmission line the wave velocity is therefore $c_0 = \sqrt{1/L_0 C_0} = \sqrt{\gamma P_0/\rho}$ and characteristic impedance $Z_0 = \sqrt{L_0/C_0} = \rho c_0/S$, as expected. The input impedance of a transmission line as a function of its characteristic impedance and terminating load is given by (15.100).

Valves and Bends

To enable brass instruments to play all the notes of the chromatic scale, short lengths of coiled-up tubing are connected in series with the main bore by a series of

piston- or lever-operated air valves. The constriction of air flow through the air channels within the valve structures and the bends in the tubing, used to reduce the size of the instruments to a convenient size for the player to support, will clearly present discontinuities in the acoustic impedance of the air bore and will lead to reflections. Such reflections will influence the feel of the instrument for the player exciting the instrument via the mouthpiece and will also perturb the frequencies of the resonant modes of the instrument.

If the discontinuities are short in size relative to the acoustic wavelengths involved, the discontinuity can be considered as a discrete (localised) lumped circuit element. Using our electromechanical equivalent, a short, constricted channel through a valve can be represented as an inductance $\rho L_{\text{valve}}/S_{\text{valve}}$ in series with the acoustic transmission line, or an equivalent additional extra length of bore tubing $L_{\text{valve}} S_{\text{tube}}/S_{\text{valve}}$ of cross section S_{tube} . For all frequencies such that $kL_{\text{valve}} \ll 1$, the valve simply increases the length of the acoustic air column slightly and the frequencies of all the lower modes by the same fractional amount. Only at very high frequencies, outside the normal playing range, will the constricted air channel significantly change the modal frequencies.

When a straight length of cylindrical tube of radius a is connected to the same size tubing but bent into a circle of radius R , there will be a small change in the acoustic impedance and velocity of sound waves, which arises because the forces acting on each element induces rotational in addition to linear motion. The presence of bends will lead to reflections and slight perturbations of resonant frequencies, though these effects will again be relatively small. *Nederveen* [15.143] showed that fractional increase in phase velocity and decrease in wave impedance of a rectangular duct is given by the factor $F^{1/2}$, where

$$F = \frac{B^2}{2} \left/ \left[1 - (1 - B^2)^{1/2} \right] \right. \\ = 1 - B^2/4 \quad \text{for } B \ll 1, \quad (15.120)$$

$B = a/R$, a is the half-width of the duct and R its radius. *Keefe* and *Benade* [15.144] subsequently generalised this result to a bent circular tube, with its radius r replacing a .

Finger Holes

In many woodwind instruments, tone holes can be opened or closed to change the effective resonating length of an air column and hence pitch of the sounded

note. The holes can be closed by the pad of the finger or a hinged felt-covered pad operated with levers. To a first approximation, opening a side hole creates a pressure node at that position, shortening the effective length of the instrument and raising the modal frequencies. However, as described in *Fletcher and Rossing* [15.5, Sect. 15.2] and in detail by *Benade* [15.134, Chaps. 21 and 22], the influence of the side holes is in practice strongly dependent on the hole size, position and frequency, as summarised below.

At low frequencies, when the acoustic wavelength is considerably longer than the size and spacing of the tone holes, one can account for the effect of the tone holes by considering their equivalent capacitance when closed and their inductance when open, as illustrated schematically in Fig. 15.80.

Because the walls of wind instruments and particularly woodwind instruments have a significant thickness, the tone holes when shut introduce additional small volumes distributed along the length of the vibrating air column. Each closed hole will introduce an additional volume and equivalent capacitance $C_{c\text{-hole}} = \pi b^2/\gamma P_0$, which will perturb the frequencies of the individual partials upwards or downwards by a small amount that will depend on its position relative to the pressure and displacement nodes and the closed volume of the hole. In severe cases, the perturbations can be as large as a few per cent (one semitone is 6%), which requires compensating changes in bore diameter along the length of the instrument, to retain the harmonicity of the partials. However, this is essentially a problem that depends on geometrical factors involving the air column alone. Once solved, like all acoustic problems involving the shape and detailed design, instruments can be mass-produced with almost identical

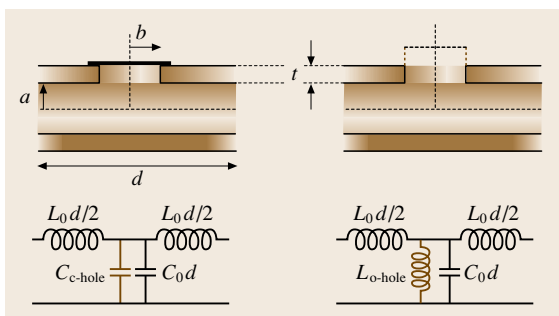


Fig. 15.80 Equivalent circuits for a short length d of cylindrical pipe containing a closed and an open tone hole, shunting the acoustic transmission line with a capacitance and inductance, respectively

acoustic properties, quite unlike the problems that arise for stringed instruments.

The more interesting situation is when the holes are opened, introducing a pressure node at the exit of the tone hole and shortening the effective acoustical length of the instrument. An open hole can be considered as an inductance, $L \approx \rho(t + 0.6b)/\pi b^2$, where the effective length of the hole is increased by the unflanged hole end-correction. Neglecting radiation losses from the hole (*Fletcher and Rossing* [15.5, (15.21, 22)]), the effective impedance Z^* of an open-ended cylindrical pipe of length l and radius a shunted by the inductive impedance of a circular hole of radius b set into the wall of thickness t is given by

$$\begin{aligned} \frac{1}{Z^*} &\approx \frac{\pi b^2}{i\omega\rho(t+0.6b)} + \frac{\pi a^2}{i\rho c_0 \tan kl} \\ &= \frac{\pi a^2}{i\rho c_0 \tan kl'} \end{aligned} \quad (15.121)$$

Thus can be expressed in terms of an impedance of an effectively reduced length l' .

$$\text{For } kl \ll 1, \quad \frac{l'}{l} = \left[1 + \frac{t+0.6b}{l} \left(\frac{a}{b} \right)^2 \right]^{-1}. \quad (15.122)$$

The change in effective length introduced by the open hole depends strongly on its area relative to that of the cylinder, the thickness of the wall and its length from the end. This gives the instrument designer a large amount of flexibility in the positioning of individual holes on an instrument. Figure 15.81 illustrates the dependence of the effective pipe length on the ratio of hole to cylinder radii for two lengths of pipe between the hole and end of the instrument.

Not surprisingly, a very small hole with $b/a \ll 1$ has a relatively small effect on the effective length of an instrument. In contrast, a hole with the same diameter as that of the cylinder shortens the effective added length to about one hole diameter.

In practice, there will often be several holes open beyond the first open tone hole, all of which can affect the pitch of the higher partials.

Consider a regular array of open tone holes spaced a distance d apart. The shunting kinetic inductance of each open hole is in parallel with the capacitance associated with the volume of pipe between the holes. At low frequencies, such that $\omega \ll 1/\sqrt{L_{\text{hole}}C_0d}$, the impedance is dominated by the hole inductance, so that each hole attenuates any incident wave by approxi-

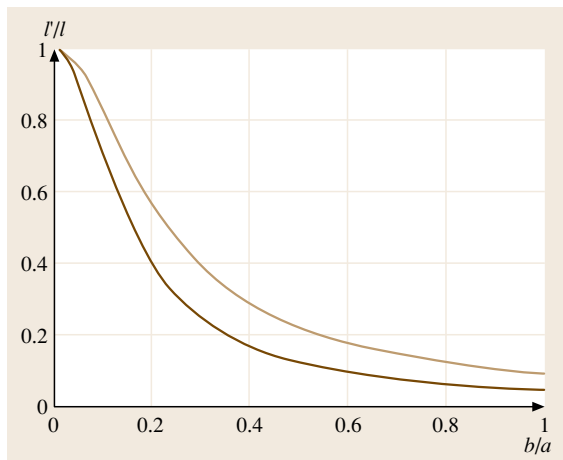


Fig. 15.81 Low-frequency ($kl \ll 1$) fractional reduction of effective length of a cylindrical end-pipe as a function of hole to cylinder radius, for additional lengths of 10 (lower curve) and 20 (upper curve) times the tube radius in length. The side wall thickness is 0.4 times the tube radius

mately the ratio

$$\approx L_{\text{hole}} / (L_{\text{hole}} + L_0 d) = \left[1 + \frac{d}{t + 1.5b} \left(\frac{a}{b} \right)^2 \right]^{-1}, \quad (15.123)$$

where L_0 is the inductance of the pipe per unit length. Incident waves are therefore attenuated with an effective node just beyond the actual hole as discussed above.

However, for frequencies such that $\omega \gg 1/\sqrt{L_{\text{hole}} C_0 d}$, the impedance of the shunting hole inductance is much larger than that of the capacitance of the air column, so that the propagating properties of the incident waves is little affected by the presence of the open hole. There is therefore a *crossover* or *cut-off* frequency

$$\omega \approx 1/\sqrt{L_{\text{hole}} C_0 d} = c_0 \frac{a}{b} \left(\frac{1}{t_{\text{eff}} d} \right)^{1/2}, \quad (15.124)$$

below which the incident waves are reflected to give a pressure node just beyond the first hole of the array and above which waves propagate increasingly freely through the array to the open end of the instrument.

Figure 15.82 (Benade [15.134, Fig. 21.1]) illustrates the effect of an array of open holes on the first few partials of a typical woodwind instrument, highlighting the increase in acoustic length of the instrument (indicated

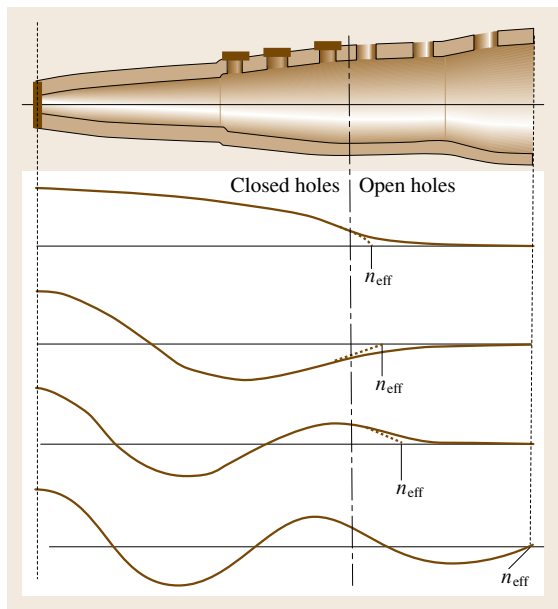


Fig. 15.82 Schematic representation of the influence of open holes on the first four partials of a woodwind instrument, with the effective length indicated by the intercept n_{eff} on the axis of the extrapolated incident wave (after Benade [15.134])

by the intercept of the extrapolated incident waveform) with increasing frequency. The dependence of the effective length of the acoustic air column on frequency is therefore rather similar to the influence of the flare on the partials of a brass instrument.

A consequence of the greater penetration at high frequencies of the acoustic wave through the array of open tone holes is the greater attenuation of such waves by radiation and the consequent reduction in the amplitude of the higher resonant modes in measurements of the input impedance. This is illustrated in Fig. 15.83 for a length of clarinet tubing first without and then with an added section containing an array of equally spaced tone holes (Benade [15.134, Fig. 21.3]).

Benade [15.134, Sect. 21.1] states that

specifying the cut-off frequency for a woodwind instrument is tantamount to describing almost the whole of its musical personality

– assuming the proper tuning and correct alignment of resonances for good oscillation. His measured values of the cut-off frequency for the upper partials of classical and baroque instruments are 1200–2400 Hz for

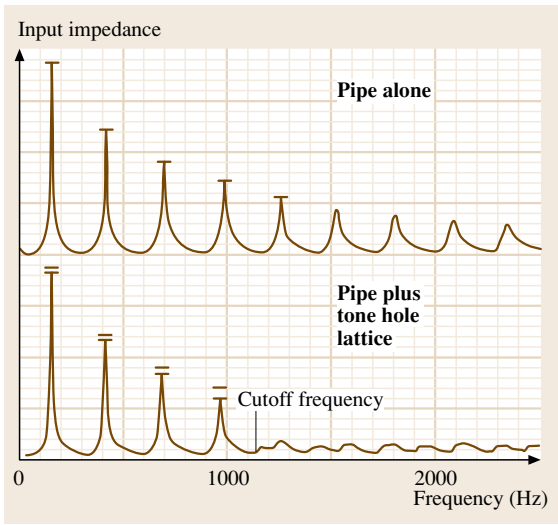


Fig. 15.83 Illustration of the cut-off-frequency effect, when adding an additional length of tubing with an array of open tone holes (after *Benade* [15.134])

oboes, 400–500 Hz for bassoons, and 1500–1800 Hz for clarinets.

Cross-Fingering

The notes of an ascending scale can be played by successively opening tone holes starting from the far end of the instrument. In addition, by overblowing, the player can excite notes in the *second register* based on the second mode. As remarked earlier, instruments like the flute and oboe overblow at the octave, whereas the clarinet overblows at the twelfth (an octave plus a perfect fifth). To sound all the semitones of the western classical scale on the flute or oboe would therefore require 12 tone holes and the clarinet 20 – rather more than the fingers on the two hands! In practice, the player generally uses only three fingers on the left hand and four on the right to open and close the finger holes. The thumb on the left hand is frequently used to open a small *register* hole near the mouthpiece, which aids the excitation of the overblown notes in the higher register.

In practice, *cross-* or *fork-fingering* enables all the notes of the chromatic scale to be played using the seven available fingers and combinations of open and closed tone holes. This is illustrated in Fig. 15.84 for the baroque recorder (*Fletcher and Rossing* [15.5, Fig. 16.21]). The bottom two notes can be sharpened by a semitone by half-covering the lower two holes and the overblown notes an octave above are played with

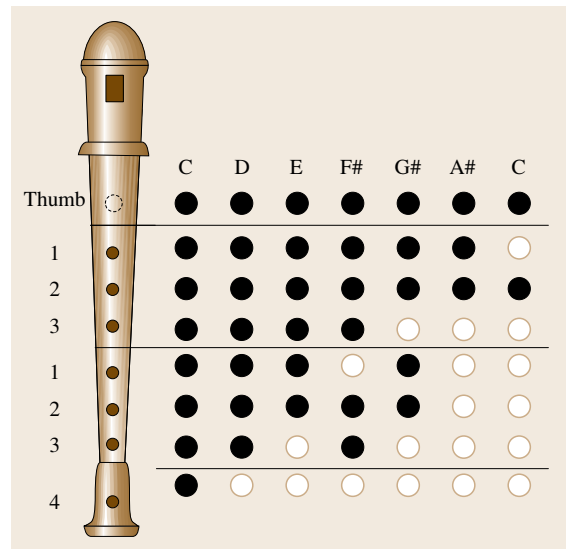


Fig. 15.84 Soprano recorder fingering for the first seven notes of a whole-tone scale (after *Fletcher and Rossing* [15.5])

the thumb hole either fully open or half closed. Cross-fingering makes use of the fact that the standing waves set up in a pipe extend an appreciable distance into an array of open tone holes (Fig. 15.82), so that opening and closing holes beyond the first open hole can have an appreciable influence on the effective length of the resonating air column.

Modern woodwind instruments use a series of interconnected levers operated by individual keys, which facilitates the ease with which the various hole-opening combinations can be made.

Radiated Sound

Although the reactive loading of an open hole determines the effective length of the resonant air column, particularly at low frequencies, it does not follow that all the sound is radiated from the open tone holes. Indeed, since the intensity of the radiated sound depends on $(ka)^2$, very little sound will be radiated by a small hole relative to the much wider opening at the end of an instrument. The loss in intensity of sound passing an open side hole may therefore, in large part, be compensated by the much larger radiating area at end of the instrument. This also explains why the characteristic hollow sound quality of a cor anglais, derived in part from the egg-shaped resonating cavity near its end, is retained, even when the tone holes are opened on the mouthpiece side of the cavity.

In practice, the sound from the end and open tone holes of a woodwind instrument act as independent monopole sources. When the acoustic wavelength becomes comparable with the hole spacing, interesting interference effects in the output sound can occur contributing to strongly directional radiation patterns, as discussed by *Benade* [15.134, Sect. 21.4]. Similarly, reciprocity allows one to make use of such interference effects to produce a highly directional microphone by placing a microphone at the end of a cylindrical tube with an array of open side holes.

Brass Mouthpiece

Brass instruments are played using a mouthpiece insert, against which the lips are pressed and forced to vibrate by the passage of air between them. The mouthpiece not only enables the player to vibrate their lips over a wide range of frequency, but also provides a very important acoustic function in significantly boosting the amplitude of the higher partials, helping to give brass instruments their bright and powerful sounds.

Typical mouthpiece shapes are shown in Fig. 15.85. Mouthpieces can be characterized by the mouthpiece volume and the *popping* frequency characterizing the Helmholtz resonator comprising the mouthpiece volume and backbore. The popping frequency can easily be estimated from the sound produced when the mouthpiece is slapped against the open palm of the hand (audio [EXTRAS](#)).

By adjusting the tension in the lips, the shape of the lips within the mouthpiece (the embouchure), and the flow of air between the lips via the pressure in the mouth, the skilled brass player forces the lip to vibrate at the required frequency of the note to be played. This can easily be demonstrated by making a pitched buzzing sound with the lips compressed against the rim of the mouthpiece cup. The circular rim constrains the lateral motion of the lips making it far easier to produce stable high notes. A brass player can sound all the notes on an instrument by simply blowing into the mouthpiece alone, but the mouthpiece alone produces relatively little volume. The instrument both stabilises the playing

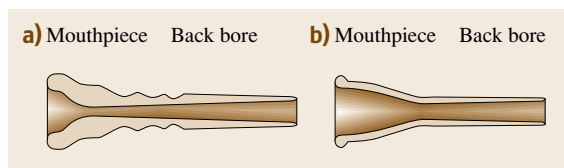


Fig. 15.85a,b Cross sections of (a) trumpet mouthpiece and (b) horn mouthpiece (after *Backus* [15.133])

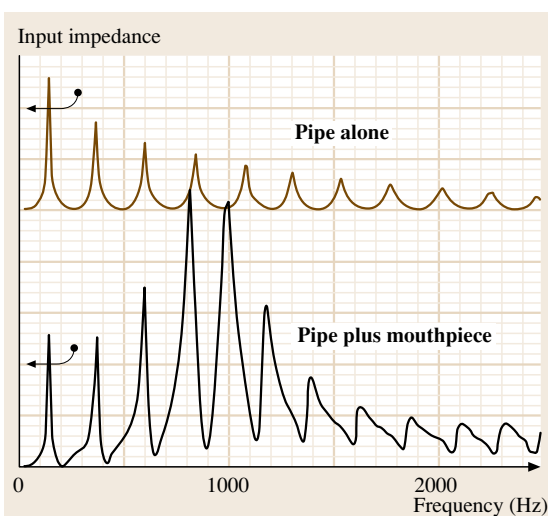


Fig. 15.86 Input impedance of a length of cylindrical trumpet pipe with and without a mouthpiece attached (after *Benade* [15.134])

frequencies and increases the coupling between the vibrating lips and radiated sound.

Figure 15.86 illustrates the enhancement in the input impedance around the popping frequency, when a mouthpiece is attached to the input of a cylindrical pipe, as measured by *Benade* [15.134]. *Benade* showed that the influence of the mouthpiece on the acoustical characteristics of a brass instrument is, to a first approximation, independent of the internal bore shape and can be characterized by just two parameters, the internal volume of the mouthpiece and the popping frequency.

Benade also measured the perturbation of the resonant frequencies of an instrument by the addition of a mouthpiece, as illustrated in Fig. 15.87. At low frequencies, the mouthpiece simply extends the effective input end of a terminated tube by an equivalent length of tubing having the same internal volume as the mouthpiece. In the measurements shown, *Benade* removed lengths of the attached tube to keep the resonant frequencies unchanged on adding the mouthpiece. However, since the fractional changes in frequency are small, the measurements are almost identical to the effective increase in length from the addition of the mouthpiece.

At the mouthpiece *popping* frequency (typically in the range 500 Hz to 1 kHz depending on the mouthpiece and instrument considered), the effective increase in length is $\lambda/4$. This can result in decreases in resonant frequencies by as much as a tone, which could have

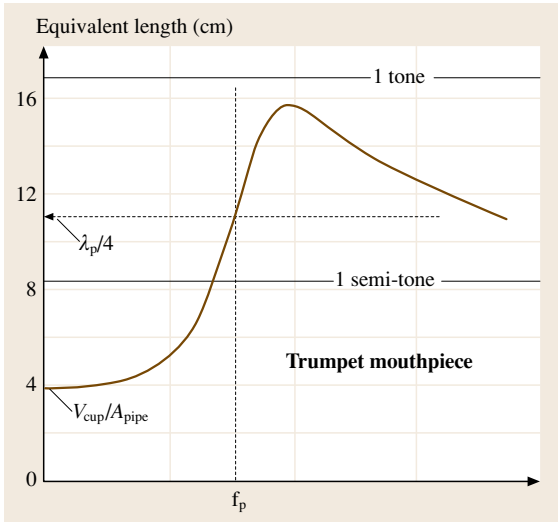


Fig. 15.87 The amount by which a trumpet tube of length 137 cm would have to be lengthened to compensate for the lowering in frequency of the instrument's resonant frequencies when a mouthpiece is attached (after *Benade* [15.134]). The changes in length to give a semitone and a whole-tone change in frequency are indicated by the horizontal lines

a significant influence on the harmonicity, and hence the playability, of an instrument. The effective length continues to increase above the popping frequency before decreasing at higher frequencies. In many brass instruments, such as the trumpet, there is also a longer transitional conical section (*the lead pipe*) between the narrow bore of the mouthpiece and the larger-diameter main tubing. This reduces the influence of the mouthpiece on the tuning of individual resonances and the overall formant structure of resonances.

It is straightforward to write down the input impedance inside the cup of a mouthpiece attached to an instrument using an equivalent electrical circuit. The volume within the cup is represented by a capacitance C in parallel with the inductance L and resistance R of air flowing through the backbore, which is in series with the input impedance of the instrument itself, so that

$$Z_{\text{in}} = \frac{1}{i\omega C} \frac{i\omega L + R + Z_{\text{horn}}}{(1/i\omega C) + i\omega L + R + Z_{\text{horn}}} \quad (15.125)$$

Figure 15.88 shows the calculated input impedance of an 800 Hz Helmholtz mouthpiece resonator, of volume 5 cm^3 with a narrow-backbore neck section resulting in a Q -value of 10, before and after attachment to a cylindrical pipe of length 1.5 m and radius 1 cm,

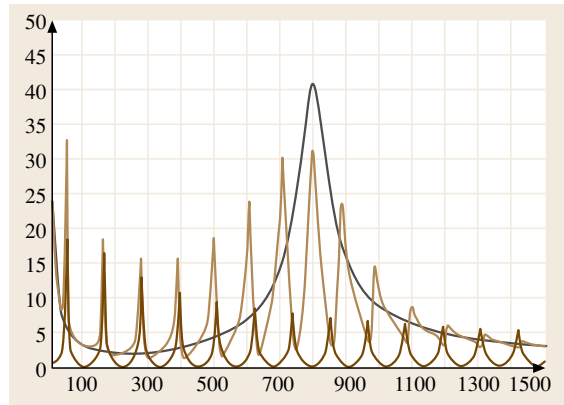


Fig. 15.88 The calculated impedance of an 800 Hz Helmholtz mouthpiece (*dark brown*), an attached pipe (*black*) and the combination of mouthpiece and pipe (*light brown*)

radiating into free space at its open end. The input impedance of the pipe alone is also shown. Note the marked increase in heights and strong frequency shifts of the partials in the neighbourhood of the mouthpiece resonance. As anticipated from our previous treatment of coupled resonators in the section on stringed instruments, the addition of the mouthpiece introduces an additional normal mode resonance in the vicinity of the Helmholtz resonance. In addition, it lowers the frequency of all the resonant modes below the popping frequency and increases the frequency of all the modes above.

Above the mouthpiece resonance, the input impedance is dominated by the inertial input impedance of the mouthpiece. The resonances of the air column are superimposed on this response and exhibit the familiar dispersive features already noted for narrow violin string resonances superimposed on the much broader body resonances. The calculated behaviour is very similar to the measured input admittance of typical brass instrument (Fig. 15.78) as extended to instruments with realistic bore shapes by *Caussé*, *Kergomard* and *Lurton* [15.145].

15.3.3 Reed Excitation

In the next sections, we consider the excitation of sound by: (a) the single and double reeds used for many woodwind instruments and selected organ pipes, (b) the vibrating lips in the mouthpiece of brass instrument, and (c) air jets used for the flute, certain organ stops and many ethnic instruments such as pan pipes.

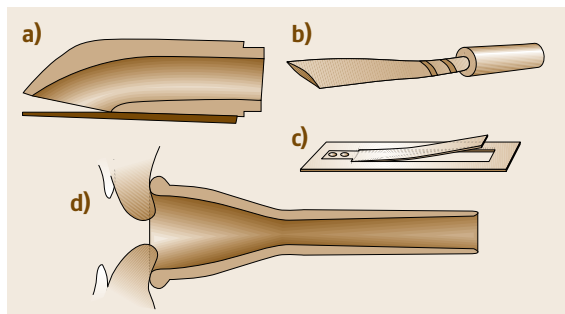


Fig. 15.89a–d Examples of wind and brass instrument reeds: (a) a single reed (clarinet), (b) a double reed (oboe), (c) a cantilever reed (harmonium) and (d) the mouthpiece lip-reed (horn) (after Fletcher and Rossing [15.5])

Reed Types

Figure 15.89 shows a number of reed types used in woodwind and brass instruments (Fletcher and Rossing [15.5, Figs. 13.1, 7]).

Helmholtz [15.128] classified two main types of reed: *inward-striking reeds*, which are forced shut by an overpressure within the mouth, and *outward-striking reeds*, forced open by an overpressure. Modern authors often prefer to call such reeds inward-closing and outward-opening or swinging-door reeds. In addition there are reeds that are pulled shut by the decreased Bernoulli pressure created by the flow of air between them. Such reeds are often referred to as sideways-striking or sliding-door reeds.

A more formal classification (Fletcher and Rossing [15.5, Sect. 13.3]) characterises such reeds by a doublet symbol (σ_1, σ_2), where the values of $\sigma_{1,2} = \pm 1$ describe the action of over- and under-pressures at the input and output ends of the reed. When the valve is forced open by an overpressure at either end, $\sigma_{1,2} = +1$; if forced open by an under-pressure, $\sigma_{1,2} = -1$. The force tending to open the valve can then be written as $(\sigma_1 p_1 S_1 + \sigma_2 p_2 S_2)$, where $S_{1,2}$ and $p_{1,2}$ are the areas and pressures at the reed input and output. The operation of reeds can therefore be classified as $(+, -)$, $(-, +)$, $(-, -)$ or $(+, +)$. Single and double woodwind reeds are inward-striking $(-, +)$ valves, while the vibrating lips in a mouthpiece and the vocal cords involve both outward-swinging $(+, -)$ and sideways-striking $(+, +)$ actions.

Figure 15.90 summarises the steady-state and dynamic flow characteristics of the above reeds for typical operating pressures across the valve, $\Delta p = p_m - p_{ins}$, where p_m and p_{ins} are the input and output pressures in the mouth and instrument input, respectively. For the

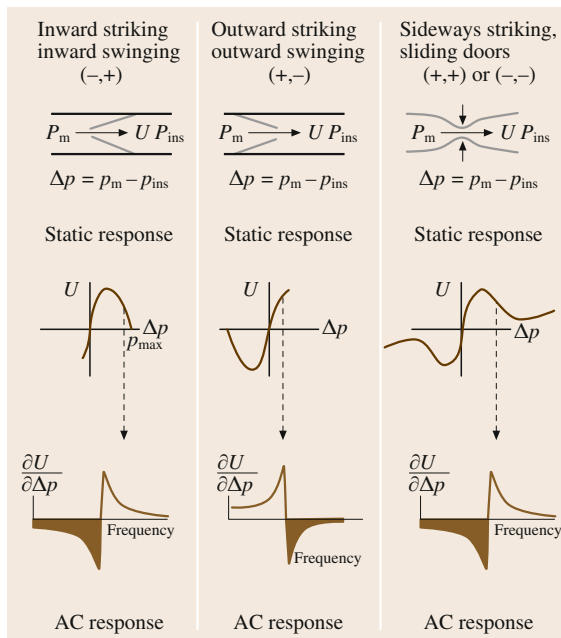


Fig. 15.90 Main classifications of vibrating reeds summarising reed operation, nomenclature and the associated static and *ac* conductance, with the negative resistance frequency regimes indicated by *solid shading*

inward-swinging $(-, +)$ reed, the flow rate initially increases for a small pressure difference across the valve, but then decreases as the difference in pressures tends to close the valve, leading to complete closure above a certain pressure difference p_{max} . Before closure, there is an extended range of pressures where the flow rate decreases for increasing pressure difference across the reed. This is equivalent to an input with a negative resistance to flow. This results in positive feedback exciting resonances of any attached air column, provided the feedback is sufficient to overcome viscous, thermal and radiation losses.

It is less obvious why the outward-swinging $(-, +)$ reed can give positive feedback, because the steady-state flow velocity always increases with increasing pressure across the valve. However, this is only true at low frequencies below the mechanical resonance of the reed. Above its resonant frequency, the reed will move in anti-phase with any sinusoidally varying fluctuations in pressure. This will result in a regime of negative resistance and the resonant excitation of any attached air column, as discussed by Fletcher et al. [15.146].

Sideways-striking $(+, +)$ or $(-, -)$ reeds behave rather like inward-striking reeds, with an extended re-

gion of negative conductance. However, such reeds will never cut off the flow completely, so that for large pressure differences the dynamic conductance again becomes positive, as indicated in Fig. 15.90.

Bernoulli Pressures

Figure 15.91 schematically illustrates the variation of flow velocity and pressure as air flows from the mouth into the reed and attached air column. To solve the detailed dynamic response from first principles for a specific reed geometry would require massive computer modelling facilities. Fortunately, the physics involved is reasonably well understood, so that relatively simple models can be used to reproduce reed characteristics rather well, as illustrated for the clarinet reed in the next section.

The operation of all reed generators is controlled by the spatial variations in Bernoulli pressure exerted by the air flowing across the reed surfaces. Such variations in P arise because, within any region of streamlined flow with velocity v , $P + \frac{1}{2}\rho v^2$ remains constant. Hence the pressure will be lowered on any surface over which the air is flowing. The flow of air is determined by the specific reed assembly geometry and the nonlinear Navier–Stokes equation, which also includes the effects of viscous damping.

After passing through the narrow reed constriction, the air emerges as a jet, which breaks down into turbulent motion on the downstream side of the reed. The turbulence leads to a rapid lateral mixing of the air, so that the flow is no longer streamlined. As a result, the

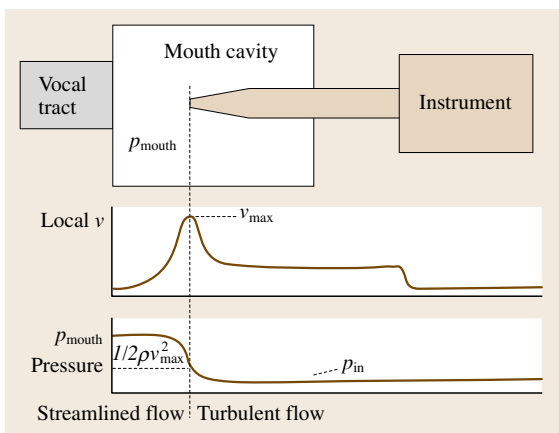


Fig. 15.91 Schematic representation of vocal tract, mouth cavity, reed and instrument, illustrating the variation of local velocity and pressure for air flowing into and along the reed and attached instrument

pressure on the downstream end of the reed opening remains low and fails to recover to the initial pressure inside the mouth. The double reeds used for playing the oboe, bassoon and bagpipe chanter are mounted on a relatively long, narrow tube connected to the wider bore of the instrument. Turbulent flow in this region could contribute significantly to the flow characteristics, though recent measurements by Almeida et al. [15.147] have shown that such effects are less important than initially envisaged, as discussed later.

Single Reed

We first consider the clarinet reed, which is one of the simplest and most extensively studied of all woodwind reeds (Benade [15.134, Sect. 21.2], Fletcher and Rossing [15.5, Chap. 13], and recent investigations by Dalmont and collaborators [15.148, 149]). Figure 15.92 shows a cross section of a clarinet mouthpiece, defining the physical parameters of a highly simplified but surprisingly realistic model.

The lungs are assumed to supply a steady flow of air U , which maintains a steady pressure P_{mouth} within the mouth. Air flows towards the narrow entrance or lip of the reed through which it passes with velocity v . Because the air flowing into the reed is streamlined, the pressure drops by $\frac{1}{2}\rho v^2$ on entering the reed, while the much slower-moving air on the outer surfaces of the reed leaves the pressure on the outer reed surfaces largely unchanged. The air is then assumed to stream through the narrow gap of the reed to form an outward-going jet, which breaks up into vortices and turbulent flow on the far side of the input constriction, with no further change in overall pressure p in the relatively wide channel on the downstream side of the reed entrance.

The resulting pressure difference $\frac{1}{2}\rho v^2$ across the reed forces the reed back towards its closing position on the curved *lay* of the mouthpiece, indicated by the dashed line in Fig. 15.92. The pressure difference Δp is

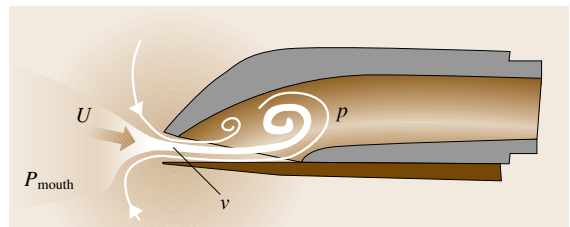


Fig. 15.92 Cross section of air flow through a clarinet mouthpiece and reed assembly, illustrating the streamlined flow into the gap with jet formation and turbulence on exiting the reed entrance

assumed to reduce the area of reed opening from S_0 to $S_0(1 - \Delta p/p_{\max})$, where p_{\max} is the pressure difference required to close the reed. The net flow of air through the reed is therefore given by

$$U(\Delta p) = \alpha(\Delta p)^{1/2}(1 - \Delta p/p_{\max}). \quad (15.126)$$

The player can control these characteristic by varying the position and pressure of the lips on the reed, which is referred to as the *embouchure*. A lower pressure is required to close the reed, if the reed is already partially closed by pressing the lips against the reed to constrict the entrance gap.

The flow rate U as a function of static pressure across a clarinet reed is illustrated by the measurements of *Backus and Nederween* [15.150] redrawn in Fig. 15.93. Apart from a small region near closure, where the exact details of the closing geometry and viscous losses may also be important, the shape of these curves and later measurements by *Dalmont et al.* [15.149, 151], which exhibit a small amount of hysteresis from viscoelastic effects on increasing and decreasing pressure, are in excellent agreement with the above model. The measurements also illustrate how the player is able to control the flow characteristics by changing the pressure of the lips on the reed.

The *reed equation* can be written in the universal form

$$\frac{U\left(\frac{\Delta p}{p_{\max}}\right)}{U_{\max}} = \frac{3^{3/2}}{2} \left(\frac{\Delta p}{p_{\max}}\right)^{1/2} \left(1 - \frac{\Delta p}{p_{\max}}\right), \quad (15.127)$$

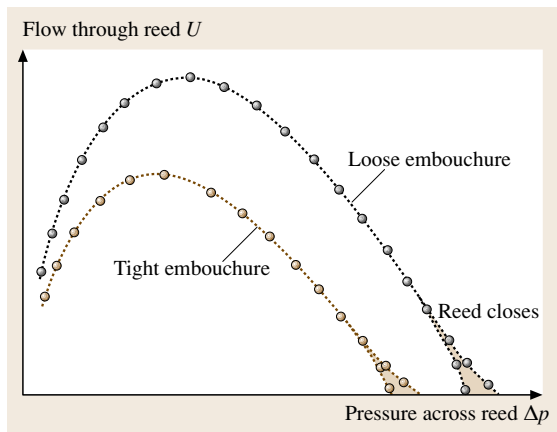


Fig. 15.93 Quasistatic flow through a clarinet single reed as a function of pressure across it illustrating the influence of the player's embouchure on the shape (after *Benade* [15.134])

with just two adjustable parameters: U_{\max} the maximum flow rate and p_{\max} , the static pressure required to force the reed completely shut. The maximum flow occurs when $\Delta p/p_{\max} = 1/3$.

Double Reeds

Instruments like the oboe, bassoon and bagpipe chanters use double reeds, which close against each other with a relatively long and narrow constricted air channel on the downstream side before entering the instrument. The turbulent air motion in the constricted air passage would result in an additional turbulent resistance proportional to the flow velocity squared, which would add to the pressure difference across the reed. This could result in strongly hysteretic re-entrant static velocity flow characteristics as a function of the total pressure across the reed and lead pipe (see, for example, *Wijnands and Hirschberg* [15.152]).

A recent comparison of the flow-pressure characteristics of oboe and bassoon double reeds and a clarinet single reed, Fig. 15.94, by *Almeida* [15.147]) shows no evidence for re-entrant double-reed features. Nevertheless, the measurements are strongly hysteretic, because of changes in the properties of the reeds (elasticity and mass), as they absorb and desorb moisture from the damp air passing through them. In the measurements the static pressure was slowly increased from zero to its maximum value and then back again. Under normal

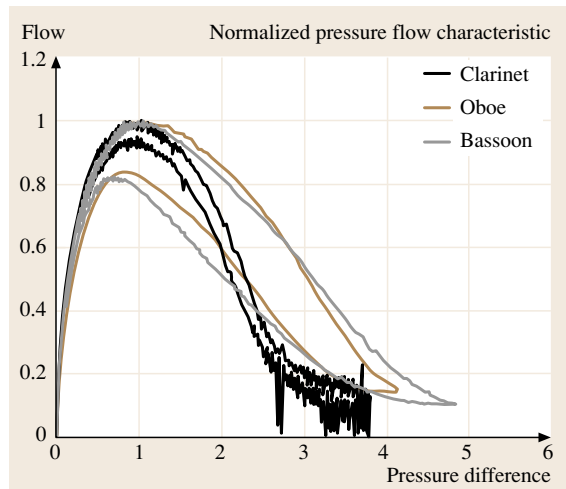


Fig. 15.94 A comparison of the normalised, hysteretic static pressure/flow characteristics of single (clarinet) and double (oboe and bassoon) reeds measured on first increasing and then decreasing the flow rate of moist air through the reeds (after [15.147])

playing conditions, one might expect to play on a non-hysteretic operating characteristic somewhere between the two extremes of the hysteretic static measurements. Thus, although the shape of the flow-pressure curves for the double reeds differs significantly from those of the clarinet single reed, the general form is qualitatively similar, with a region of dynamic negative resistance above the peak flow. The strongly moisture dependent properties of reeds are very familiar to the player, who has to moisten and *play-in* a reed before it is ready for performance.

There therefore appears to be no fundamental difference between the way single and double reeds operate. Indeed, the sound of an oboe is apparently scarcely changed, when played with a miniature clarinet reed mouthpiece instead of a conventional double reed (Campbell and Gilbert, private communication).

Dynamic Characteristics

Fletcher [15.153] extended the quasistatic model by assuming the reed could be described as a simple mass-spring resonator resulting in a dynamic conductance of

$$Y(\omega) = Y(0) \frac{1}{1 - (\omega/\omega_0)^2 + i\omega/\omega_0 Q} \quad (15.128)$$

where $Y(0) = \partial U/\partial(\Delta p)|_{\omega=0}$ is the quasistatic flow conductance and the denominator describes the dynamic resonant response of the reed. The Q -value is determined by viscous and mechanical losses in the reed.

The resistive and reactive components of $Y(\omega)_{\text{reed}}$ given by (15.128) are plotted in Fig. 15.95a,b for an inward-closing reed (–, +), in the negative flow conductance regime above the velocity flow maximum,

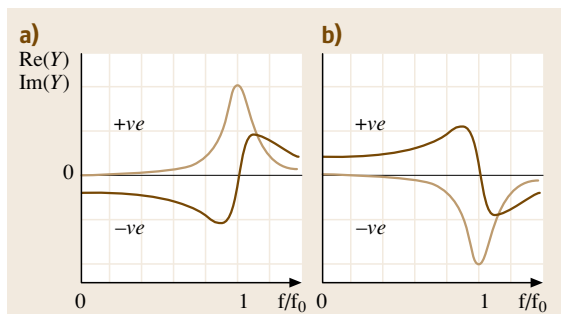


Fig. 15.95a,b Real (dark brown) and imaginary (light brown) components of the reed admittance $Y(\omega)$ for (a) an inward-closing reed in the negative dynamic conductance regime and for (b) an outward-opening reed, as a function of frequency normalised to the resonant frequency of the reed for reeds having Q -values of 5

and for the outward-closing (+, –) reed. As discussed qualitatively above, the negative input dynamic conductance of the inward-striking reed remains negative at all frequencies below its resonant frequency, whereas the conductance of the outward-opening reed only becomes negative above its resonant frequency.

For the oscillations of any attached air column to grow, feedback theory requires that

$$\begin{aligned} \text{Im}(Y_r + Y_p) &= 0 \\ \text{Re}(Y_r + Y_p) &< 0, \end{aligned} \quad (15.129)$$

where Y_p and Y_r are the admittances of the pipe and reed, respectively. The negative dynamic conductance of the reed must therefore be sufficiently small to overcome the losses in the instrument. Furthermore, the reactive components of the reed conductance will perturb the frequencies of the attached air column.

Fletcher and Rossing [15.5, Chap. 13] give an extended discussion of the dynamics of reed generators including polar plots of admittance curves for typical outward and inward-striking reed generators as a function of blowing pressure.

For the inward-striking reeds of the clarinet, oboe and bassoon, the real part of the reed admittance is negative below the resonant frequency of the reed. For the oboe this is typically around 3 kHz, above the pitch of the reed attached to its staple (joining section) alone (EXTRAS). However, when attached to an instrument, the negative conductance will excite the lower-frequency natural resonances of the attached tube (EXTRAS). In this regime, the reactive load presented by the reed is relatively small and positive and equivalent to a capacitive or spring loading at the input end of the attached pipe. This results in a slight increase in the effective length of the pipe and a slight lowering of the frequencies of the resonating air column.

Free reeds, like the vibrating brass cantilevers used in the mouth organ, harmonium and certain organ reed pipes (Fig. 15.89c), are rather weakly damped inward-closing (–, +) reeds (Fletcher and Rossing [15.5, Sect. 13.4]). The reed is initially open. High pressure on one side or suction on the other (as in the harmonium or American organ) forces the reed back into the aperture, controlling the air flow. Like the clarinet reed, above a certain applied pressure the reed will close and restrict the flow resulting in a negative conductance regime. If the reed is forced right through the aperture, it becomes an outward-opening (+, –) reed with a positive conductance. Because of its low damping, the blown-closed reed tends to vibrate at a frequency rather close to its

resonant frequency. In practice, as soon as a threshold pressure is reached that is significantly below the maximum in the static characteristics, a harmonium reed starts to vibrate with a rather large sinusoidal amplitude (typically ≈ 4 mm) resulting in highly non-sinusoidal flow of air through the aperture (Koopman et al. [15.154]). For such high- Q -value mechanical resonators, the vibrational frequency is strongly controlled by the resonant frequency of the reed itself, so that a separate reed is needed for each note, as in the piano accordion, harmonium, mouth organ and reed organ pipes. The reeds in a mouth organ are arranged in pairs in line with the flow of air. They are individually excited by overpressure and suction.

In contrast, the dynamic conductance of an outward-opening reed (+, -) is only negative above its resonant frequency. The conductance then decreases rather rapidly with increasing frequency, so that there may only be a relatively narrow range of frequencies above resonance over which oscillations can occur. The vibrating lips provide a possible example of such a reed, with an increase in steady-state pressure always increasing the static flow through them. Above their resonant frequency, the dynamic conductance becomes negative and could excite oscillations in an attached pipe. In such a regime, the reactive component of the reed admittance is negative. This corresponds to an inductive or inertial load, which will shorten the effective length of the air column and increase its resonant frequencies. The influence of the reed on the resonant frequencies of an attached instrument therefore provides a valuable clue to the way in which a valve is operating, as we will discuss later in relation to the vibrations of the lips in a brass-instrument mouthpiece.

Small-Amplitude Oscillations

We now consider the stability of the oscillations excited by the negative dynamic conductance of the reed. In particular, it is interesting to consider whether the oscillations, once initiated, are stabilised or grow quickly in amplitude into a highly nonlinear regime. Surprisingly, this depends on the bore shape of the attached air column, as discussed by Dalmont et al. [15.155]. Several authors have investigated such problems, including Backus [15.156] using simple theoretical models and measurements, Fletcher [15.157] using analytic models, Schumacher [15.158, 159] in the time rather than the frequency domain, and Gilbert et al. [15.155, 160] using a harmonic balance approach, which we will briefly outline in the following section. Recent overviews of the nonlinear dynamics of both wind and brass instru-

ments have been published by Campbell [15.161] and by Dalmont et al. [15.155].

We first consider the excitation of small-amplitude oscillations based on the reed equation, which is replotted in Fig. 15.96 as a universal curve together with the negative dynamic admittance or conductance, $-\partial U/\partial p$ above the flow-rate maximum.

The onset of self-oscillations occurs when the sum of the real and the imaginary parts of the admittance of the reed and attached instrument are both zero (15.129). If losses in the reed and the attached instrument were negligible, resonances of the air column would be excited as soon as the mouthpiece pressure exceeded $\frac{1}{3}p_{\max}$. However, when losses are included, the negative conductance of the reed has to be sufficiently large to overcome the losses in the instrument. The onset then occurs at a higher pressure, as illustrated schematically in Fig. 15.96.

The onset of oscillations depends not only on the mouthpiece pressure but also on the properties of the reed, such as the initial air gap and its flexibility, which will depend on its thickness and elastic properties. The elastic properties also change on the take up of moisture during playing. It is not surprising that wind players take great care in selecting their reeds. Furthermore, notes are generally tongued. This involves pressing the

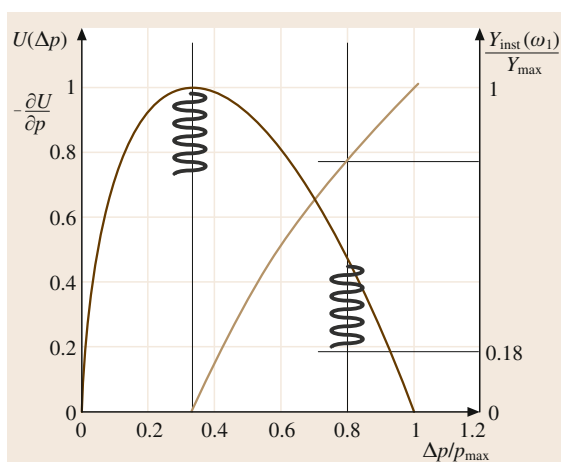


Fig. 15.96 Plot of normalised flow rate and differential negative conductance of an inward-striking reed valve as a function of pressure across the reed normalised to the pressure required for closure. The intersection of the negative conductance curve with the real part of the input admittance $Y_{\text{inst}}(\omega)$ of the instrument determines the pressure in the mouthpiece for the onset of oscillations, illustrated schematically for $Y_{\text{inst}}(\omega) \approx 0.78Y_{\text{max}}$

tongue against the lip of the reed to stop air passing through it, so that the pressure builds up to a level well above that required to just excite the note. When the tongue is removed, the note sounds almost immediately giving a much more precise definition to the start of a note.

The transition to the oscillatory state can be considered using the method of small variations and harmonic balance (Gilbert et al. [15.160]). For a given mouth pressure defining the overall flow rate, oscillations of the flow rate u can be written as a Taylor expansion of the accompanying small pressure fluctuations p at the output of the reed, such that

$$u = Ap + Bp^2 + Cp^3 + \dots \quad (15.130)$$

From the reed equation plotted in Fig. 15.96, the coefficient A is positive for mouthpiece pressures above $p_{\max}/3$, while B and C are positive and negative respectively. We look for a periodic solution with Fourier components that are integer multiples of the fundamental frequency ω , so that

$$p(t) = \sum p_n e^{in\omega t}, \quad (15.131)$$

with a corresponding oscillatory flow $u(t)$ superimposed on the static flow U ,

$$u(t) = \sum u_n e^{in\omega t}. \quad (15.132)$$

At the input to the instrument, the oscillatory flow can be expressed in terms of the Fourier components of the input pressure and admittance, so that

$$u(t) = \sum p_n Y(n\omega) e^{in\omega t}. \quad (15.133)$$

Using the method of harmonic balance, we equate the coefficients of the Fourier components in (15.130) with those in (15.133) having substituted (15.131) for the pressure. The first three Fourier components are then given by

$$\begin{aligned} p_1 &= \pm \left(\frac{Y_1 - A}{2B^2 / (Y_2 - A) + 3C} \right), \\ p_2 &= \left(\frac{B}{Y_2 - A} \right) p_1^2, \\ p_3 &= \left(\frac{C}{Y_3 - A} \right)^{1/2} p_1^3. \end{aligned} \quad (15.134)$$

For a cylindrical-bore instrument like the clarinet at low frequencies, only the odd- n partials will be strongly excited, so that Y_2 is very large. The amplitude of the fundamental component is then given by $\pm[(Y_1 - A)/C]^{1/2}$, with a vanishingly small second harmonic p_2 . The amplitude p_1 of small oscillations is then

stabilised by the cubic coefficient C . Stable, small-amplitude oscillations can therefore be excited as soon as the negative conductance of the reed exceeds the combined admittance of the instrument and any additional losses in the reed itself.

Because the transition is continuous, p_1 rises smoothly from zero, taking either positive or negative values (simply solutions with opposite phases). The transition is therefore referred to as a *direct bifurcation*. The player can vary the pressure in the mouthpiece and the pressure of the lips on the reed to vary the coefficients A and C and hence can control the amplitude of the excited sound continuously from a very quiet to a loud sound, as often exploited by the skilled clarinet player.

In contrast, for a conical-bore instrument, the amplitude of the fundamental,

$$p_1 = \pm \left(\frac{(Y_1 - A)(Y_2 - A)}{2B^2 + 3C(Y_2 - A)} \right)^{1/2}, \quad (15.135)$$

involves the admittance of both the fundamental and second partial. On smoothly increasing A by increasing the pressure on the reed, Grand et al. [15.162] showed that there can again be a direct smooth bifurcation to small-amplitude oscillations, if $2B^2 > -3C(Y_2 - Y_1)$. However, if this condition is not met, there will be an indirect transition, with a sudden jump to a finite-amplitude oscillating state. This gives rise to the hysteresis in the amplitude as the mouth pressure is first increased and then decreased. This means that the player may have to exert a larger pressure to sound the note initially, but can then relax the pressure to produce a rather quieter sound. It may also explain why it is more difficult to initiate a very quiet note on the saxophone with a conical bore than it is on the clarinet with a cylindrical bore.

For a direct bifurcation transition, the small nonlinearities in the dynamic conductance will result in a spectrum of partials with amplitudes varying as p_1^n , where p_1 is the amplitude of the fundamental component excited. The spectral content or *timbre* of wind and brass instruments, as discussed later, therefore changes with increasing amplitude. This is illustrated by measurements of the amplitude dependence of the partials of a trumpet, clarinet and oboe by Benade [15.134, Fig. 21.6c], which are reproduced for the trumpet in Fig. 15.104. For the largely cylindrical-bore trumpet and clarinet, nonlinearity results in partials varying as p_1^n over quite a large range of amplitudes. However, for the oboe, with its conical bore, the relative increase in strength of the partials is rather more complicated

(Benade [15.134, Sect. 21.3]). Eventually, the small-amplitude approximation will always break down, with a transition to a strongly nonlinear regime. Benade associates this transition with a change in timbre and responsiveness of the instrument for the player.

Large-Amplitude Oscillations

For a *lossless* cylindrical-bore instrument with only odd integer partials, the large-amplitude solutions are particularly simple. The flow of air from the lungs and pressure in the mouth is assumed to remain constant resulting in an average flow rate through the instrument. The pressure at the exit of the reed then switches periodically from a high-pressure to a low-pressure state, with equal amplitudes above and below the mean mouth pressure, spending equal times in each. The net acoustic energy fed into the resonating air column per cycle is therefore zero, $U \int p(t) dt = 0$, as required for a lossless system.

Such a solution can easily be understood in terms of the excess-pressure wave propagating to the open end of the instrument, where it is reflected with change of sign. On return to the reed it reverses the pressure difference across the reed, which switches to the reduced pressure state. The subsequent reflection of the reduced pressure wave then switches the reed back to its original high-pressure state and the process repeats indefinitely, with a periodic time of $4L/c_0$, as expected.

The dependence of the square-wave pressure fluctuations on the applied pressure can be obtained by the simple graphical construction illustrated in Fig. 15.97. The locus of the static pressure required to excite square-wave pressure fluctuations above and below the mouth pressure is shown by the solid line drawn from $p_{\text{mouth}} = 1/3$ to $1/2 p_{\text{max}}$, which bisects the high and low pressures for a given flow rate. If losses are taken into account, the horizontal lines are replaced by load lines with a downward slope given by the real part of the instrument's input admittance (Fletcher and Rossing [15.5], Fig. 15.9). At large amplitudes, the solutions can then involve periods during which the reed is completely closed. The transition from small-amplitude to large-amplitude solutions is clearly of musical importance, as it changes the sound of an instrument, and remains an active area of research [15.155].

Analogy with Bowed String

In recent years, an interesting analogy has been noted between the large-amplitude pressure fluctuations of a vibrating air column in a cylindrical or truncated conical tube and simple Helmholtz waves excited on

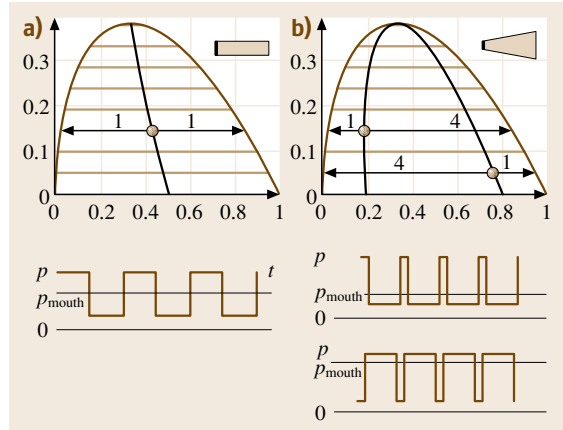


Fig. 15.97a,b Large-amplitude Helmholtz pressure fluctuation of (a) a cylinder and (b) a truncated cone with length to apex of $1/4$ of its length, illustrating the dependence of fluctuation amplitudes as a function of mouthpiece pressure. For the cylinder, the mouthpiece pressure is single valued for a given flow rate, but for the truncated cone there are two possible solutions referred to as the standard and inverted Helmholtz solutions

a bowed string (Dalmont and Kergomard [15.163]). For example, the square-wave pressure fluctuations at the output of the reed attached to a cylindrical tube are analogous to the velocity of the bowed Helmholtz transverse waves of a string bowed at its centre, illustrated schematically in Fig. 15.98. Helmholtz waves

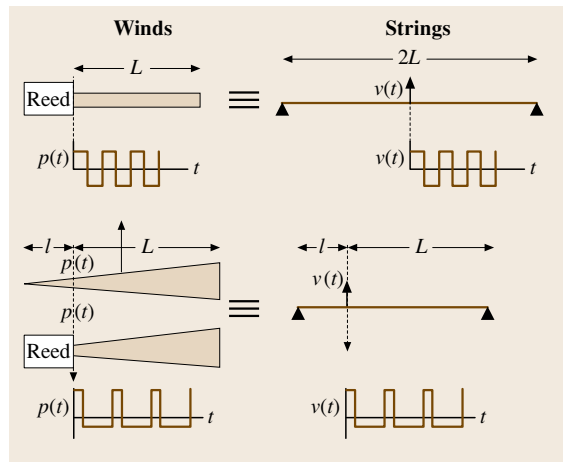


Fig. 15.98 Analogy between large-amplitude pressure waves in the bores of wind instruments and the transverse velocity of Helmholtz waves on a bowed stretched string, where the reed position is equivalent to the bowing position

could equally well be excited on a bowed string by a transducer with a square-wave velocity output placed halfway along the length of the string, in just the same way that the reed with a square-wave pressure output excites Helmholtz sound pressure waves into a cylinder, which acts like half the string length.

The analogy is particularly useful in discussing the large-amplitude pressure fluctuations in conical-bore instruments such as the oboe or saxophone. As described earlier, the conical tube has the same set of resonances as a cylindrical tube that is open at both ends. Therefore, in addition to having the same set of standing-wave sinusoidal solutions for the transverse oscillations of a stretched string, a conical tube can also support Helmholtz wave solutions. For the bowed string, the closer one gets to either end of the string the larger becomes the mark-to-space ratio between the regions of high to low transverse velocity. The same is also true for the switched fluctuations in pressure in a lossless conical tube, shown schematically in Fig. 15.97. Hence, if one truncates a conical tube with a vibrating reed system, the resonant modes of the remaining air column will be unchanged, provided the vibrating reed produces the same pressure fluctuations that would otherwise have been produced by the reflected Helmholtz waves returning from the removed apex end of the cone. Hence a conical tube, truncated by a vibrating reed at a distance l from the apex, can support Helmholtz wave solutions in the remaining length L . To produce such a wave the reed has to generate a rectangular pressure wave with a mark-to-space ratio and pressure fluctuations about the mean in the ratio $L:l$, as illustrated in Fig. 15.98, for a truncated cone with $L/l = 4$.

The period of the Helmholtz wave solutions of a conical bore instrument modelled as a truncated cone will therefore be $2(L+l)/c_0$, with a spectrum including all the harmonics $f_n = nc_0/2(L+l)$, other than those with integer values of $n = (L+l)$. To determine the amplitude of the rectangular pressure wave as a function of mouthpiece pressure, a graphical construction can be used similar to that used for the cylindrical tube, except that the pressures have now to be in the ratio L/l , as indicated in Fig. 15.97b. For the lossless large-amplitude modes of a truncated cone, there are two possible solutions involving high and low mouth pressures, which are known as the standard and inverted Helmholtz solutions, respectively.

Any complete model of a reed driven instrument must include losses and departures from harmonicity of an instrument's partials. This leads to a rounding of the rectangular edges of the Helmholtz waveforms and

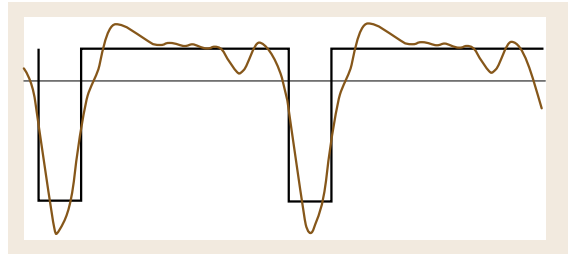


Fig. 15.99 Measured pressure waveform at input to a saxophone compared with the Helmholtz waveform expected for a truncated cone (after *Dalmont et al.* [15.163])

additional structure, in much the same way that bowed string waveforms are perturbed by frictional forces and nonideal reflections at the end-supports (Fig. 15.34). Figure 15.99 shows a typical pressure waveform input for the conical-bore saxophone, which is compared with the Helmholtz waveform predicted for an ideal lossless system (*Dalmont et al.* [15.163]).

A completely realistic model for the excitation of sound in wind instruments must also include coupling to the vocal tracts (*Backus* [15.164] and *Scavone* [15.165]), since the assumption of a constant flow rate and constant mouth pressure is clearly oversimplistic.

Register Key

This analysis implicitly assumes that the reed excites the fundamental mode of the attached instrument. In practice, the reed will generally excite the partial with the lowest admittance corresponding to the highest peak in impedance measurements. For most instruments this is usually the fundamental resonance. However, the amplitude of the fundamental can be reduced relative to the higher resonances by opening a small hole, the register hole, positioned between the reed and first hole used in normal fingering of the instrument. Because of the difference in wavelengths and position of nodes, opening the register hole preferentially reduces the Q -value and shifts the frequency and amplitude of the fundamental relative to the higher partials. This allows the player to excite the upper register of notes based on the second mode, which in the case of the conical-bore saxophone, oboe and bassoon is an octave and a perfect fifth above the fundamental but is an octave and a perfect fifth above the fundamental for the cylindrical-bore clarinet. The lower and upper registers of the clarinet are sometimes referred to as the chalumeau and chanter registers, after the earlier instruments from which the clarinet was derived.

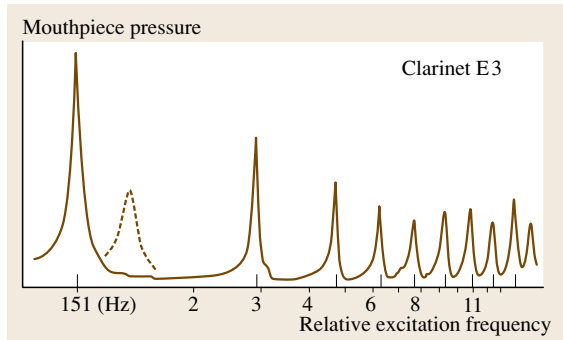


Fig. 15.100 Resonance curves for the note E3 on a clarinet, showing the shift of the lowest partial on opening the register hole (after Backus [15.133])

Figure 15.100 illustrates the lowering in amplitude and shift in resonant frequency of the fundamental mode on opening the register hole for the note E3 on a clarinet, which leaves the upper partials relatively unchanged (Backus [15.133]). The measurements also show the significant departures from the 1, 3, 5, 7 harmonicity of the resonant modes of the instrument, which act as a warning not to take ideal models for the harmonicity of modes in real wind instruments too literally. Fletcher has developed a mode-locking model to account for the excitation of periodic waveforms on instruments with inharmonic partials [15.166].

15.3.4 Brass–Mouthpiece Excitation

The excitation of sound by the vibrating lips in the mouthpiece of a brass instrument cannot be described by any of the above simple models alone, which consider the reed as a simple mass–spring resonator. As we will show, the vibrations of the lips are three-dimensional and much more complicated. As a result, in some regimes the lips behave rather like outward-swinging-door valves, as first proposed by Helmholtz, and Bernoulli pressure operated sliding-door reeds in others. In addition the air flow is also affected by three-dimensional wave-like vibrations on the surface of the lips.

When playing brass instruments, the lips are firmly pressed against the rim of the mouthpiece with the lips pouted inwards. Pitched notes are produced by blowing air through the tightly clenched lips to produce a buzzing sound. The excitation mechanism can easily be demonstrated by buzzing the lips alone, though it is difficult to produce a very wide range of pitched sounds. However, if the lips are buzzed when pressed

against the rim of a mouthpiece, the input rim provides an additional constraint on the motion of the lips, which makes it much easier to produce pitched notes over a wide range of frequencies (EXTRAS). The audio demonstrates the *popping* sounds of trumpet and horn mouthpieces followed by the sound of the player buzzing the mouthpiece alone up to a pitch close to the popping frequency and back again. Attaching the mouthpiece to an instrument locks the oscillations to the various possible resonances of the instrument (EXTRAS).

Figure 15.101 shows a series of time-sequence plots of spectra of the sound produced by a player *buzzing* into a trumpet mouthpiece (Ayers [15.167]), which acts rather like a simple Helmholtz resonator. In the lower sequence, the player excites well-defined pitched notes from low frequencies up to slightly above the mouthpiece *popping frequency* (see Sect. 15.3.3). The middle set of traces shows the spectrum as the player starts

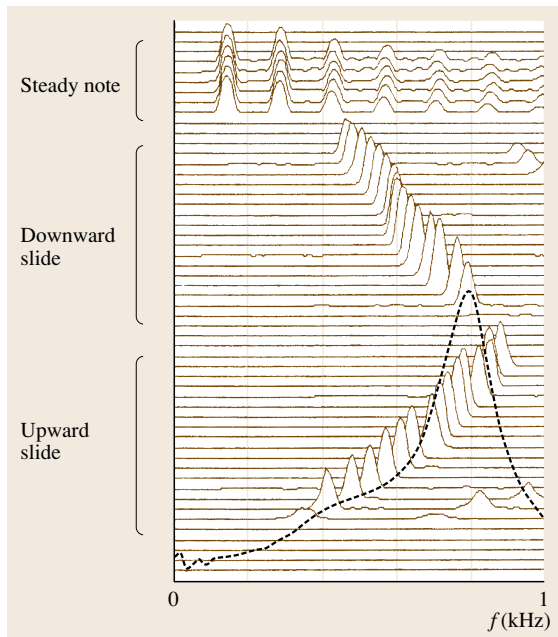


Fig. 15.101 Time sequence (from bottom to top) of spectra of the sound produced by a player *buzzing* into a trumpet mouthpiece, first for an upward slide in frequency, then for a downward slide and finally for a steady low note at high intensity showing the excitation of a note with many Fourier components. The *dashed line* is the spectrum of the *popping* note excited by slapping the open end of the mouthpiece against the palm of the hand (after Ayers [15.167])

at a high frequency and lowers the pitch. The upper traces shows the spectrum of a loudly sounded, low-frequency, note, illustrating the rich spectrum of harmonics produced by the strongly nonlinear sound-generation processes involved (see, for example, *Elliot* and *Bowsher* [15.168]).

These measurements on the mouthpiece alone strongly suggest that the lips can generate periodic fluctuations at frequencies up to, but not significantly beyond, the resonant frequency of any coupled acoustic resonator. This was confirmed in an investigation of lip-reed excitation using a simple single-resonant-frequency Helmholtz resonator by *Chen* and *Weinreich* [15.170], who used a microphone and loudspeaker in a feedback loop to vary the Q -value of the Helmholtz resonator played using a normal mouthpiece. They concluded that a player could adjust the way they vibrated their lips in the mouthpiece to produce notes that were slightly higher or lower than the Helmholtz frequency, though the most natural playing parameters generated frequencies in the range 20–350 Hz below the resonator frequency.

Attached Mouthpiece

Ayers [15.167] also compared the frequencies produced in the mouthpiece before and immediately after attachment of the instrument. In these measurements the player first excited a pitched note in the mouthpiece with the instrument effectively decoupled by opening a large hole in its bore close to the mouthpiece. The hole was then closed and the immediate change in frequency measured before the player had time to make any adjustments to the embouchure. The results of such measurements are shown in Fig. 15.102, where the diagonal line represents the pitched notes before the instrument was connected and the discontinuous solid line through the triangular points are the modified frequencies for the same embouchure with the instrument connected.

At the higher frequencies, the jumps between successive branches are from just above the resonant frequency of one partial to just below the resonant frequency of the next, with a monotonic increase in frequency on tightening the embouchure in between. However, for the first two branches, the instrument resonances initially have a relatively small effect on the frequencies excited by the mouthpiece alone until such frequencies approach a particular partial frequency. The frequency then approaches the resonant frequency of the instrument before jumping to a frequency well below the next partial and the sequence repeats. The dif-

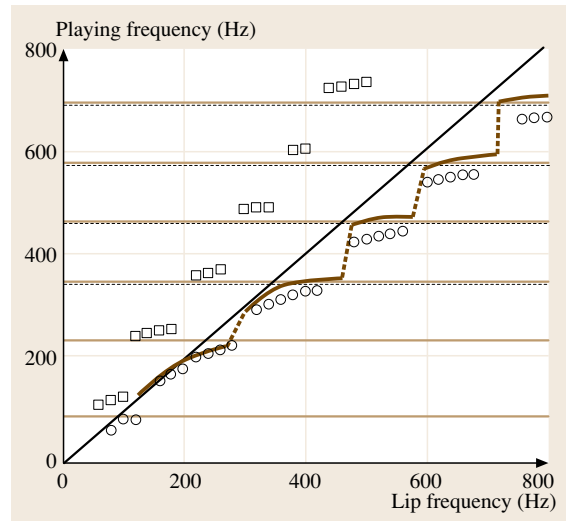


Fig. 15.102 Frequencies produced by a trumpet mouthpiece without (*diagonal line*) and with (*broken line*) the instrument strongly coupled using an unchanged embouchure under the same playing conditions. The *solid horizontal lines* are the resonant frequencies of the assembled trumpet. The *squares* and *circles* are predictions for the Helmholtz outwardly opening-door and sliding-door models computed by *Adachi* and *Sato* [15.169] for a trumpet with slightly lower-frequency resonant modes indicated by the *dashed horizontal lines* (after *Ayers* [15.167])

ference in behaviour of the lower and higher branches suggests that more than one type of lip-reed action is involved.

Comparison with computational models by *Adachi* and *Sato* [15.169] appear to rule out the outward-swinging-door model first proposed by Helmholtz, indicated by the squares in Fig. 15.101, as the predicted frequencies are always well above those of the instrument's partials. The computed predictions for the Bernoulli sliding door model, indicated by the circles, are in better agreement with measurements, but with predicted frequencies rather lower than those observed and never rising above the resonant frequencies of the instrument, in contrast to the observed behaviour for the higher modes excited.

Any model for the lip-reed sound generator has to explain all such measurements. Such measurements also highlight the way that a brass player can adjust the embouchure and pressure acting on the lips in the mouthpiece to change the frequency of the excited mode. On tightening the embouchure and pressure the player can progressively excite successive modes and

can *lip* the pitch of the note up and down by surprisingly large amounts, used with great expressive effect by jazz trumpeters.

Vibrating Lips

In practice, the production of sound by the vibrating lips inside a mouthpiece is a highly complex three-dimensional problem closely analogous to the production of sound by the vocal folds – see, for example, *Titze* [15.171]. A complete model would involve solving the coupled solutions of the Navier–Stokes equations describing the flow of air from the mouth, through the lips and into the mouthpiece, and the three-dimensional motions of the soft tissues of the lips induced by the Bernoulli pressures acting on their surfaces.


Stroboscopic and ultra-fast photography of the brass players lips while playing reveal highly complex three-dimensional motions (*Coppley and Strong* [15.172], *Yoshikawa and Muto* [15.173]) suggest that the upper lip is primarily involved in the generation of sound. Figure 15.103 and the video clip  EXTRAS provided by Murray Campbell show high-speed photography clips of such motion. The lips inside the mouthpiece open and shut rather like the gasping opening and shutting of the mouth of a goldfish, but speeded up several hundred times. Points on the surface of the upper lip exhibit cyclic orbital motions involving the in-quadrature motions of the upper lip parallel and perpendicular to the flow. To model such motion clearly requires at least two independent mass–spring systems to account for the induced motions of the lips along and perpendicular to the flow (*Adachi and Sato* [15.169]). In addition, there is a pulsating wave-like motion along the surface of the lips in the direction of air flow, with the rear portion of lips moving in anti-phase with the front. *Yoshikawa* and



Fig. 15.103 High-speed photograph clips showing one cycle of lip vibration in a trombone mouthpiece

Muto [15.173] identify such motion as strongly damped Rayleigh surface waves travelling through the mucous tissue of the upper lip.

The simplest possible model to describe such motion therefore requires at least three interacting mass–spring elements; one to describe the lip motion along the direction of flow, and two to describe the motions of the front and back surfaces of the lips. But even then, the model will still only be an approximation to the three-dimensional bulk tissue motions involved. Not surprisingly, research into the lip-reed sound-excitation mechanism remains a problem of considerable interest.

Artificial Lips

To achieve a better understanding of lip dynamics and its effect on the sound produced by brass instrument, several groups have developed artificial lips to excite brass instrument (e.g. *Gilbert et al.* [15.174] and *Cullen et al.* [15.175]). These can be used to investigate instruments under well-controlled and reproducible experimental conditions. Typically, the lips are simulated by two slightly separated thin-walled (0.3 mm thickness) latex tubes filled with water under a controlled pressure. The tubes are rigidly supported from behind so that the internal pressure forces the lips together. The tubes are placed across an opening in an otherwise hermetically sealed unit that represents the mouth and throat cavities. Air is fed into the mouth cavity at a constant flow rate. A fixed mouthpiece is then pushed against the artificial lips with a measured force. By varying this force, the applied pressure and the pressure within the artificial lips, the experimenter can simulate the various ways in which a player can control the dynamics of the lips (the *embouchure*) to produce different sounding notes. Despite the considerable simplification in comparison with the dynamics of real lips, the sound of brass instruments played by artificial lips is extremely close to that produced by a real player. Such systems enable acoustical studies to be made on brass instruments with a much greater degree of flexibility, reproducibility and stability than can be achieved by a player. Using a fixed mouthpiece, the playing characteristics of different attached instruments can easily be compared.

Nonlinear Sound Excitation

When played very quietly, brass instruments can produce sounds that are quasi-sinusoidal with relatively weak higher harmonics. However, as previously noted for vibrating reeds, any nonlinearity will lead to the generation of harmonics of the fundamental frequency

ω at frequencies 2ω , 3ω , etc., with initially amplitudes increasing as $|p_0(\omega)|^n$, where $p_0(\omega)$ is the amplitude of the fundamental. However, in the strongly nonlinear region at high amplitudes, all partials become important and increase in much the same way with increasing driving force (Fletcher [15.176] and Fletcher and Rossing [15.5, Sects. 14.6 and 14.7]). Such effects are illustrated in Fig. 15.104 for measurements on a B-flat trumpet by Benade and Worman [15.134, Sect. 21.3]. The spectral content and resulting brilliance of the sound or timbre of a trumpet, or any other brass instrument, therefore depends on the intensity with which the instrument is played. Benade noted a change in the sound and feel of an instrument by the player in the transition region between the power-law dependence of the Fourier component and the high-amplitude regime, where the harmonic ratios remain almost constant. Similar characteristics were observed for the clarinet though rather different characteristics for the oboe.

Examples of the strongly non-sinusoidal periodic fluctuations of the pressure and flow velocity within the mouthpiece for two loudly played notes on a trombone are shown in Fig. 15.105 (Elliot and Bowsher [15.168]).

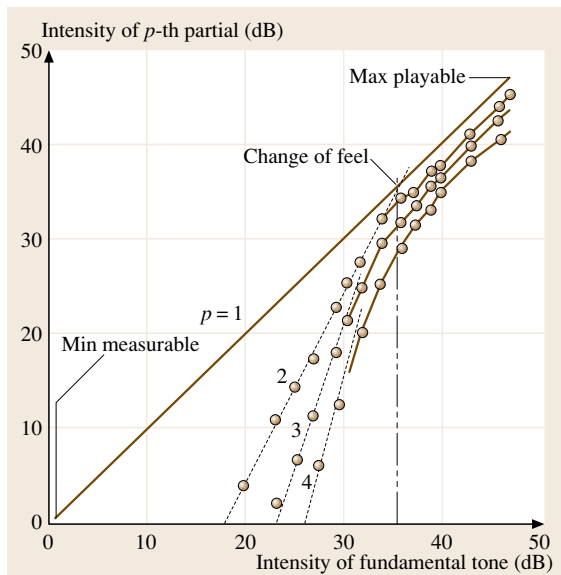


Fig. 15.104 Intensity of the first four partials of the note C4 on a trumpet as a function of the intensity of the first partial, measured from the minimum to the maximum playing intensity (after Benade [15.134, Fig. 21.8]). On this logarithmic scale, the dashed lines through the measurements for the second, third and fourth Fourier components have slopes 2, 3 and 4, respectively

Fletcher and Rossing [15.5, Sect. 14.7] discuss such waveforms in terms of the lips operating slightly above the resonant frequency of their outward-swinging-door resonant frequencies.

The nonlinearity of the lip-reed excitation mechanism enables the player to vibrate the lips at the frequency of the missing fundamental of the quasi-harmonic series of modes of brass instruments, illustrated in Fig. 15.38. This is referred to as the *pedal note* and is an octave below the lowest mode normally excited on the instrument. The lips vibrate at the pedal-note frequency but only excite the quasi-harmonic $n = 2, 3, 4, \dots$ modes.

The pressure fluctuations in Fig. 15.104 of ≈ 3 kPa correspond to a sound intensity of nearly 160 dB. As the static pressure in the mouthpiece is only a few percent above atmospheric pressure (10^5 Pa), such pressure excursions are a significant fraction of the excess static pressure. Even larger-amplitude pressure fluctuations can be excited on the trumpet and trombone when played really loudly, to produce a brassy sound. Long [15.177] has recorded pressure levels in a trumpet mouthpiece as high as 175 dB, corresponding to pressure fluctuations of ≈ 20 kPa.

At such high amplitudes, one can no longer neglect the change in density of a gas when considering its acceleration under the influence of the pressure gradi-

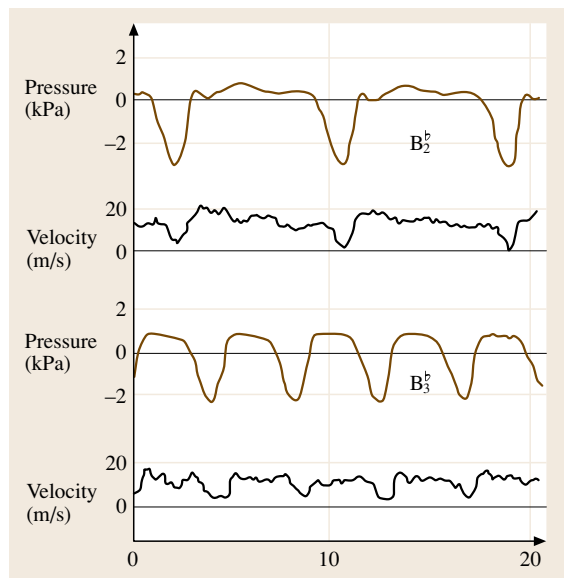


Fig. 15.105 Non-sinusoidal pressure fluctuations within the mouthpiece for two notes played at large amplitudes on the trombone (after Elliot and Bowsher [15.168])

ent. To a first approximation, the wave equation then becomes

$$\frac{\partial^2 \xi}{\partial x^2} = \left(1 + \frac{\partial \xi}{\partial x}\right) \frac{1}{c_0^2} \frac{\partial^2 \xi}{\partial t^2}. \quad (15.136)$$

The speed of sound will now depend on both frequency and wave shape, with the velocity varying as

$$c' = c_0 \left\langle \left(1 + \frac{\partial \xi}{\partial x}\right)^{-1/2} \right\rangle_{x,t} \approx c_0 \left[1 + \alpha (k\xi)^2\right], \quad (15.137)$$

where the averaging is taken over both time and wavelength giving a value for $\alpha \approx 1/8$. In practice, for waves propagating down a tube, other terms involving momentum transport, viscosity and heat transfer also have to be included in any exact solution. However, the essential physics remains unchanged. The net effect of the nonlinearity is to progressively increase the slope of the leading edge of any wave propagating along the tube. A propagating sine wave is then transformed into a sawtooth waveform, or shockwave, with an infinitely steep leading edge, at sufficiently large distances along the tube.

Such waves have indeed been observed in trumpet and trombone bores, which are long and relatively narrow. The effect is illustrated in Fig. 15.106 by the measurements of Hirschberg et al. [15.178], for waves propagating along a trombone tube. The sound intensity of ≈ 175 dB is considerably higher than the intensities illustrated in Fig. 15.99. As predicted, the sharpness of the leading edge of the waveform progressively increased on propagating along the bore. The discontinuity in waveform of the fully developed shockwave dramatically increases the intensities of the higher harmonics of a continuously played note and gives the trumpet and trombone (and trompette organ pipes) their characteristic brassy sound at very high intensities (EXTRAS). The high-frequency components of all such sounds will make them highly directional. Campbell [15.161] reviews nonlinear effects in woodwind and brass instruments, with many references to recent research.

To achieve such brassy sounds, the instrument must have a sufficiently long length of relatively narrow pipe, like the trumpet and trombone, in which the pressure fluctuations remain high and have time to build up into a shock wave. Shockwaves are far more difficult to set up in instruments like the horn and cornet, with flaring conical bores, because the pressure drops rather rapidly with increasing diameter along the bore.

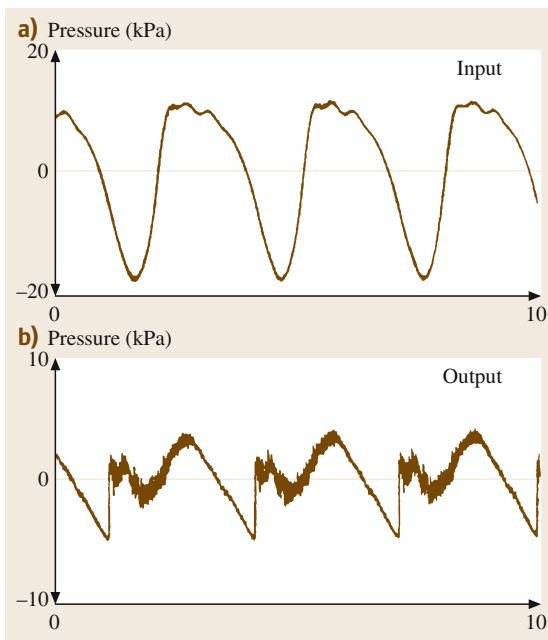


Fig. 15.106a,b Internal acoustic pressure in a trombone played at a dynamic level fortissimo (ff). (a) Pressure at the input to the air column in the mouthpiece; (b) pressure at the output of the slide section, showing the characteristic profile of a shock wave (after Hirschberg et al. [15.178])

Time-Domain Analysis

When nonlinearity is important or when the initial transient response is of interest, it is more appropriate to consider the dynamics in the time- rather than frequency-domain, just as it was for analysing the transient dynamics of the bowed string. Time-domain analysis in wind and brass instruments was pioneered by Schumacher [15.159], McIntyre et al. [15.179] and Ayers [15.180], and is discussed in Fletcher and Rossing [15.5, Sect. 8.14]. Time-delayed reflectometry measurements are made by producing short pressure pulses inside the mouthpiece generated by a spark or by a sudden piezoelectric displacement of the mouthpiece end-wall. The pressure in the mouthpiece is then recorded as a function of time after the event.

In the linear response regime, measurement in the time domain gives exactly the same information about an instrument as measurements in the frequency domain, assuming both the magnitude and phase of the frequency response is recorded. This follows because the frequency response $Z(\omega)$ measured in the mouthpiece is simply the Fourier transform of the transient

pressure response $p(t)$ for a δ - or impulse-function flow (Av) induced by the spark or wall motion. Knowing $p(t)$ or $Z(\omega)$ one can obtain the other by applying the appropriate Fourier transform

$$Z(\omega) = \int_0^{\infty} p(t) e^{-i\omega t} dt \quad \text{or}$$

$$p(t) = \frac{1}{2\pi} \int_{-\infty}^{\infty} Z(\omega) e^{i\omega t} d\omega. \quad (15.138)$$

Measurements of the impulse response are particularly useful in identifying large discontinuities in the acoustic impedance along the bore of instruments produced by tone holes, valves and bends, which can significantly perturb particular partials. The position of any such discontinuity can be determined by the time it takes for the reflected impulse to return to the mouthpiece.

Time-domain analysis is essential, if one wishes to investigate starting transients, where reflections from the end of the instrument are required to stabilise the pitch of a note. This problem is particularly pronounced for horn players pitching, for example, notes as high as the 12th resonant mode of the instrument. The player must buzz the lips a dozen or so cycles into the mouthpiece before the first reflection from the end of the instrument returns to stabilise the pitch. If the player gets the initial buzzing frequency slightly wrong, the instrument may lock on to the 11th or 13th harmonic rather than the intended 12th, leading to the familiar *cracked note* of the beginner and sometimes even professional horn players. Furthermore, *false reflections* from discontinuities along the length of the tube, may well confuse the initial feedback, making it more difficult to pitch particular notes. This leads to small pitch-dependent changes in the playing characteristics of instruments made to different designs adopted by different manufacturers.

15.3.5 Air-Jet Excitation

Many ancient and modern musical instruments are excited by blowing a jet of air across a hole in a hollow tube or some other acoustic resonator. Familiar examples include the flute, pan pipes, the ocarina and simple whistle in addition to many organ pipes. Sound excitation in flutes and organ pipes was first considered by *Helmholtz* [15.128] in terms of an interaction between the air jet produced by the lips or a flue channel in the mouthpiece of an instrument and the coupled air column resonator.

In practice, the dynamics of sound production is a very complex aerodynamic flow problem requiring the solution of the Navier–Stokes equations governing fluid flow in often complex geometries. Various simplified solutions have been considered by many authors since the time of *Helmholtz* and *Rayleigh* [15.3]. *Fletcher* and *Rossing* [15.5, Sect. 16.1] provide references to both historic and more-recent research. *Fabre* and *Hirschberg* [15.181] have also written a recent review of simple models for what are sometimes referred to as flue instruments.

Rayleigh showed that the interface separating two fluids moving with different velocities was intrinsically unstable, resulting in an oscillating sinuous lateral disturbance of the interface that grows exponentially with time Fig. 15.107. This arises because, in the frame of reference in which the two fluids move with the same speed in opposite directions, any disturbance of the interface towards one of the fluids will increase the local surface velocity on that side. This will result in a decrease in Bernoulli pressure on that side of the interface and increase it on the other, creating a net force in the same sense as the disturbance, which will therefore grow exponentially with time. For a layer of air moving at velocity V without friction over a stationary layer, a sinusoidally perturbed deflection of the jet in the laboratory frame of reference at rest increases exponentially with distance as it travel along the interface with velocity $V/2$.

Similar arguments were used by *Rayleigh* to describe the instability of an air jet of finite width b and velocity V produced by blowing through an arrow constriction between the pouted lips when playing the flute, or by blowing air through an air channel towards the sharp lip of the recorder or an organ pipe. *Fletcher* [15.182] showed that the lateral displacement $h(x)$ of the jet induced by an acoustic velocity field $v e^{i\omega t}$ between the jet orifice and the lip varies with position

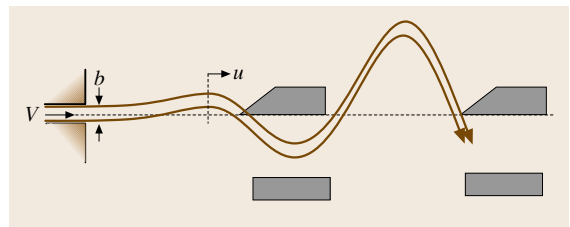


Fig. 15.107 Propagating sinuous instability of an air jet emerging from a flow channel with two possible positions of the angled labium or lip to excite resonances of an attached air column for a given jet velocity V

and time as

$$h(x) = -j \left(\frac{v}{\omega} \right) [1 - \cosh \mu x \exp(-i\omega x/u)] e^{i\omega t}, \quad (15.139)$$

illustrated schematically in Fig. 15.107. The first term simply corresponds to the jet moving with the impressed acoustic field, while the second describes the induced travelling-wave instability moving along the jet with velocity $u \approx V/2$, which dominates the jet displacement at the lip of the instrument. For long-wavelength instabilities on a narrow jet, such that the characteristic wavevector $k \ll 1/b$, Rayleigh showed that the phase velocity $u = \omega/k \approx kbV/2 = (\omega bV/2)^{1/2}$, while the exponential growth factor $\mu = (k/b)^{1/2}$.

In practice, the velocity profile of the jet is never exactly rectangular but in general will be bell-shaped. This results in a slightly different frequency, width b and velocity dependence of the phase velocity, with

$$u = 0.55(\omega b)^{1/3} V^{2/3} \quad (15.140)$$

and corresponding changes in the exponential growth factor (Savic [15.184]). Typical propagation velocities of disturbances on the jet of flute and organ pipes measured by Coltman [15.183] range from 6.7 m/s to 3.7 m/s with velocity ratios u/V from 0.35 to 0.5 for blowing pressures from 1 to 0.15 inches of water.

Resonances of the attached resonator can be excited when the air-jet instability is in phase with oscillations within the resonator, as shown for the two positions indicated in Fig. 15.107. This corresponds to an odd number of half-wavelengths of the propagating instability, so that $\omega l/u = n\pi$, which is equivalent to $f \approx nV/4$, where n is an odd integer and we have assumed $u \approx V/2$. For a given length between jet orifice and lip, different frequencies can be excited by varying the jet velocity $V = \sqrt{2P_{\text{mouth}}/\rho}$, where P_{mouth} is the pressure in the mouth creating the jet. When coupled to an acoustic resonator with a number of possible resonances, such as an organ pipe or the pipe of a flute or recorder, the interaction between the jet and oscillating resonator causes the frequency to lock on to a particular resonance, with hysteretic jumps between the resonance excited as the blowing pressure is increased and decreased, as illustrated schematically in Fig. 15.108 (Coltman [15.183]). This explains why the pitch of an instrument like the recorder or flute doubles when it is blown more strongly. The line marked *edge tones* indicates the frequency of the excited jet mode instability for the same orifice–lip geometry without an attached pipe and the line marked $f = \text{pipe resonance}$

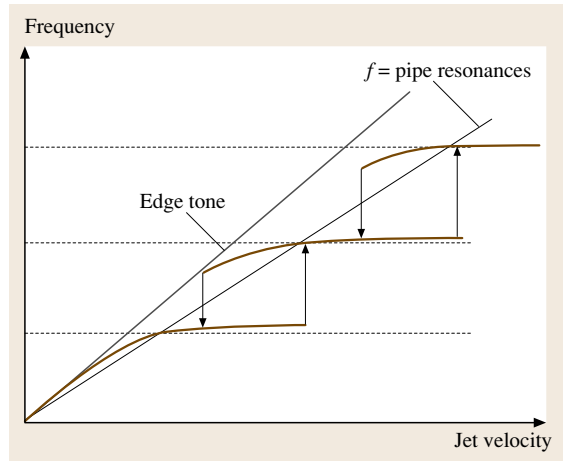


Fig. 15.108 Schematic representation of the frequency of a jet-edge oscillator before and after coupling to a multi-resonant acoustic resonator. The line marked $f = \text{pipe resonances}$ indicates the pressures when the frequencies are the same as the modes of the uncoupled acoustic resonator (after Coltman [15.183])

indicates when the frequency of the coupled jet coincides with the free vibrations of the attached air column. In practice the instrument is played in close vicinity to the pipe resonances.

The above model is strictly only applicable to small perturbations in jet shape ($\ll b$) and to a nonviscous medium. In practice, measurements of jet displacement by Schlieren photography, hot-wire anemometry (Nolle [15.185]), smoke trails (Cremer and Ising [15.186] and Coltman [15.187]) and particle image velocimetry (PIV) (Raffel et al. [15.188]) show that within an acoustic cycle the jet moves to either side of the lip of the instrument with large displacement amplitudes comparable with the physical dimensions of the distance between the orifice and lip. In addition, viscous forces lead to a change in profile of the jet as it moves through the liquid from rectangular to bell-shaped (Ségoufin et al. [15.189]). Furthermore, the associated shear forces eventually induce vorticity downstream, with individual vortices shearing away from the central axis of the jet on alternate sides, as observed by Thwaites and Fletcher [15.190, 191].

In recent years, major advances have also been made in studying such problems by computation of solutions of the Navier–Stokes equations describing the nonlinear aerodynamic flow. An example is illustrated by the simulated jet deflections by Adachi [15.192] shown in Fig. 15.109. Adachi’s computational results are in

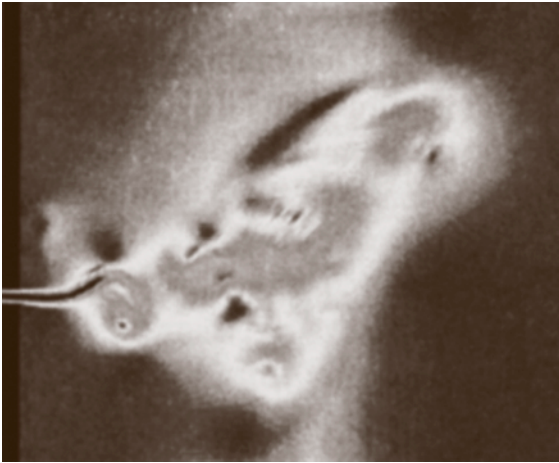


Fig. 15.109 A computed snapshot showing the breakup of a jet and generation of vortices (*Adachi* [15.192])

reasonably good agreement with Nolle's flow measurements [15.185] made with a hot-wire anemometer. A sequence of such computations by Macherey for the jet in a mouthpiece with flute-like geometry is included in a recent review paper on the acoustics of woodwind instruments by *Fabre and Hirschberg* [15.193]. The computations show a relatively simple jet structure switching from one side of the lip of a flute to the other during each period of the oscillation.

Air-Jet Resonator Interaction

Despite the obvious limitations of any small-amplitude linear approach to the jet-lip interaction and the excitation of resonator modes, it is instructive to consider the analytic model introduced by *Fletcher* [15.182], which is discussed in some detail in *Fletcher and Rossing* [15.5, Sect. 16.3], as it includes much of the essential physics in a way that is not always apparent from purely computational models. The assumed geometry is illustrated schematically in Fig. 15.110 and

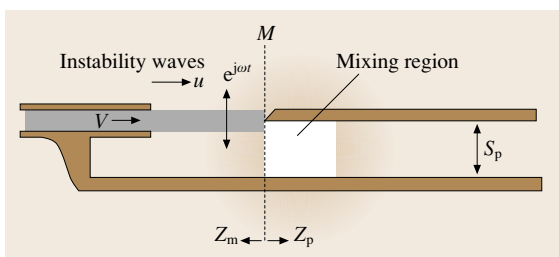


Fig. 15.110 Model to illustrate interaction between air jet and pipe modes (after *Fletcher* [15.194])

can easily be generalised to model sound excitation in air-jet-driven instruments with different mouthpiece geometries such as the recorder, organ pipe or flute. A uniform jet with a rectangular top-hat velocity profile of width b and velocity V is assumed to impinge on the lip or labium of the instrument, with the jet passing through a fraction A of the attached pipe area S_p . The oscillating travelling-wave jet instability will result in a periodic variation of the fractional area varying as $\alpha e^{i\omega t}$. On entering the pipe channel, the jet will couple to all possible modes of the attached pipe, which in addition to the principle acoustic modes excited, will include many other modes involving radial and azimuthal variations [15.194] that are very strongly attenuated. Much of the energy of the incident jet will therefore be lost by such coupling with typically only a few percent transferred to the important acoustic resonances of the instrument.

To evaluate the transfer of energy to the principle acoustic mode, we consider the pipe impedance across the plane M . In the absence of the jet, the impedances of the attached pipe and mouthpiece section are Z_p and Z_m , where the mouthpiece section has a certain volume and hole area, with the volume in the case of a flute involving an adjustable length of pipe used for fine-tuning. Fletcher simplified an earlier model introduced by *Elder* [15.195], in assuming the principle of linear superposition, with a jet flow superimposed on that of the instrument. The oscillating incident jet then has two principal effects: the oscillating fraction of area α of the jet entering the pipe introduces a flow into the attached pipe

$$U_1 = \alpha S_p Z_m / (Z_m + Z_p), \quad (15.141)$$

while the effective pressure acting on the plane M derived from momentum-balance arguments results in a pipe flow of

$$U_2 = \alpha \rho V^2 / (Z_m + Z_p). \quad (15.142)$$

There is also an additional nonlinear term U_3 mathematically arising from the nonlinear effect of the fractional insertion area of the jet insertion at large amplitudes, which is negligible in comparison with the many other nonlinearities in any realistic model. This model integrates and simplifies earlier models introduced by *Cremer and Ising* [15.186], *Coltman* [15.187] and *Elder* [15.195].

It immediately follows from the above arguments that, provided the phase of the jet instabilities are appropriate, instabilities on the jet will excite strong resonances of the instrument when the series impedance

$(Z_m + Z_p)$ is a minimum, which is just the impedance of the pipe loaded by the impedance of the mouthpiece assembly. Provided the lengths involved are much less than an acoustic wavelength, $Z_m = i\rho\Delta L/S_p$ where ΔL is the end correction introduced by the mouthpiece assembly. The net flow is then given by

$$U_p = \frac{(V + i\omega\Delta L)\rho V\alpha}{S_p(Z_m + Z_p)}. \quad (15.143)$$

The resonances are therefore those of a pipe that is open at both ends, but with a small end-correction for the effective volume of the mouthpiece and any additional closed tuning tube and flow in and out of the mouthpiece.

Because the mouthpiece impedance is reactive, the induced vibrations in flow from direct jet flow (U_1) and that induced by the jet pressure (U_2) are in phase quadrature. In addition, the two terms have a different dependence on jet velocity and frequency. In practice, $\omega\Delta L$ is often larger than V , so that the second term usually dominates, though this will not necessarily be true in more realistic models.

For small sinusoidally varying jet perturbations and a top-hat velocity profile, the driving force would only include single frequency components. However, in practice, viscous damping results in a spreading out of the velocity profile in the lateral direction with a bell-shaped profile that increases in width with distance along the jet. If such a profile is offset from the lip, any sinusoidal disturbance of the jet will introduced additional harmonics at frequencies, 2ω , 3ω , etc., with increasing amplitudes for increasing jet oscillations. In practice, the amplitudes of jet oscillation are so large that the jet undergoes a near switching action, alternating its position from one side to the other of the lip. The driving force is therefore strongly nonsinusoidal and provides a rich spectrum of harmonics to excite the upper partials of any sounded note. A flute player, for example, has considerable control over the quality of the sound produced, by variation of mouth pressure and jet velocity, its velocity profile on leaving the lips, and its direction in relation to the labium or lip of the instrument.

For most musical instruments excited by an air jet, the sinuous instability is the most important, though *Chanaud* [15.196] and *Wilson et al.* [15.197] have highlighted the importance of varicose instabilities (periodic variations in area of the jet), which were also investigated by Rayleigh, as in whistles and whistling, where the air passes through an aperture rather than striking an edge.

Regenerative Feedback

We now consider the effective acoustic impedance of the exciting air column as we did for the vibrating reed. Our emphasis here is to highlight the essential physics rather than provide a rigorous treatment. More details and references are given in *Fletcher* and *Rossing* [15.5, Sect. 16.4] and *Fletcher* [15.194].

The flow U_m into the mouth of the resonator can be expressed as

$$U_m = v_m S_m = p_m Y_m \approx \frac{p_m S_p}{i\omega\rho\Delta L}. \quad (15.144)$$

From (15.139), the lateral displacement of the jet at the lip a distance l from the exit channel of the jet is then given by

$$hl \approx i \left(\frac{v_m}{\omega} \right) \cosh \mu l \exp(-\omega l/u), \quad (15.145)$$

where u is the phase velocity for disturbances traveling along the jet and the implicit time variation has been omitted. From the ratio of the net flow into the mouthpiece-end and attached resonator to the pressure acting on the air jet, Fletcher and Rossing derive the effective admittance of the air-jet generator,

$$Y_i \approx \frac{VW}{\rho\omega^2\Delta L} \left(\frac{S_p}{S_m} \right) \cosh \mu l \exp \left[-i \left(\frac{\omega l}{u} \right) \right]. \quad (15.146)$$

Apart from a small phase factor ($\phi \approx V/\omega L$), which we have omitted, the admittance is entirely real and *negative* when $\omega l/u = \pi$, which corresponds to the first half-wavelength of the instability just bridging the distance from channel exit to lip, as shown in Fig. 15.106. This is also true for $\omega l/u = n\pi$, where n is any odd integer, corresponding to any odd number of half-wavelengths of the growing instability between the jet exit and lip of the instrument.

These are just the conditions for positive feedback and the growth of acoustic resonances in the pipe resonances will be excited when $\text{Im}(Y_p + Y_m) = 0$, which is equivalent to the condition that Z_s should be a minimum, as expected from (15.129). As *Coltman* [15.183] pointed out, the locus of $\text{Im}(Y_j)$ plotted as a function or $\text{Re}(Y_j)$ as a function of increasing frequency is a spiral about the origin in a clockwise direction (*Fletcher* and *Rossing* [15.5, Fig. 16.10]). The jet admittance therefore has a negative real component at all frequencies when the locus point is in the negative half-plane. Resonances can therefore be set up over frequency ranges from $\approx (1/2 \text{ to } 3/2)\omega^*$, $(5/2 \text{ to } 7/2)\omega^*$, etc. where ω^* , $3\omega^*$, $5\omega^*$ are the frequencies when the admittance is

purely conductive and negative. By varying the blowing pressure and associated phase velocity of the jet instability, the player can therefore excite instabilities of the jet with the appropriate frequencies to lock on to the resonances of the attached air column, as illustrated schematically in Fig. 15.108.

Measurements by *Thwaites* and *Fletcher* [15.190] are in moderately good agreement with the above model at low blowing pressures and reasonably high frequencies, but deviate somewhat at low frequencies and high blowing pressures. This is scarcely surprising in view of the approximations made in deriving the above result.

Edge Tones and Vortices

Edge tones are set up when jet of air impinges on a lip or thin wire without any coupling to an acoustic resonator. The high flow rates in the vicinity of the lip or wire can generate vortices on the downstream side, which spin off on alternating sides, setting up an alternating force on the lip or wire. If the object is itself part of a mechanical resonating structure, such as a stretched telegraph wire or the strings of an Aeolian harp, wind-blown resonances can be set up, with different resonant modes excited dependent on the strength of the wind. In extreme cases, the excitation of vortices can result in catastrophic build up of mechanical resonances, as in the Tacoma bridge disaster.

Before 1970, many treatments of wind instruments discussed air-jet sound generation in such terms. *Holger* [15.198], for example, proposed a nonlinear theory for edge-tone excitation of sound in wind instruments based on the formation of a vortex sheet, with a succession of vortices already created on alternate sides of the mid-plane of the emerging jet before it hit the lip or labium of the instrument. Indeed, measurements of the flow instabilities and phase velocity of instabilities in a recorder-like instrument by *Ségoufin* et al. [15.189], as a function of Strouhal number $\omega b/u$, fit the Holger theory rather better than models based on the Rayleigh instability and refined by later authors for both short and long jets, but the experimental errors are rather large. However, the vortex-sheet model does not include the growth of disturbances in the sound field with distance (as measured by *Yoshikawa* [15.199]), which is a crucial parameter for the prediction of the oscillation threshold observed for instruments such as the recorder.

It is also clear that vortex production is important in many wind instruments, especially where the acoustic amplitude is large, as in the vicinity of sharp edges or corners of both open and closed tone holes, as observed in direct measurements of the flow field. For example,

Fabre et al. [15.200] have recently shown that vortex generation is a significant source of energy dissipation for the fundamental component of a flute note.

In view of the complexity of the fluid dynamics involved, it seems likely that future progress in our understanding of jet-driven wind instruments will largely come from computational simulations, though physical models still provide valuable insight into the basic physics involved.

15.3.6 Woodwind and Brass Instruments

In this last section on wind instruments, we briefly describe a number of woodwind and brass instruments of the modern classical orchestra. All such instruments were developed from much earlier instruments, many of which still exist in folk and ethnic cultures from all around the World. Illustrated guides to a very large number of such instruments are to be found in *Musical Instruments* by *Baines* [15.201] and the encyclopaedia *Musical Instruments of the World* [15.31]. The two text by *Backus* [15.133] and *Benade* [15.134], both leading researchers in the acoustics of wind instruments, provide many more technical details concerning the construction and acoustics of specific woodwind and brass instruments than space allows here, as does *Fletcher* and *Rossing* [15.5, Chaps. 13–17] and *Campbell, Myers* and *Greated* [15.7].

Woodwind Instruments

The simplest instruments are those based on cylindrical pipes, such as bamboo pan pipes excited by a jet of air blown over one end, or hollow resonators, such as primitive ocarinas, which act as simple Helmholtz resonators with the pitch determined by the openings of the mouthpiece and fingered open holes. Woodwind instruments use approximately cylindrical or conical tubes excited by a reed or a jet of air blown over a hole in the wall of the tube. As we have seen, simple cylindrical and conical tubes retain a harmonic set of resonances independent of their length, which in principle allows a full set of harmonic partials to be sounded when the instrument is artificially shortened by opening the tone holes. In practice, as discussed in the previous section, the harmonicity of the modes is strongly perturbed by a large number of factors including the strongly frequency-dependent end-corrections from tone holes and significant departures from simple cylindrical and conical structures. Such perturbations can, to some extent, be controlled by the skilled instrument maker to preserve the harmonicity of the lowest modes responsi-

ble for establishing the playing pitch of an instrument. We will describe the various methods of exciting vibrations by single and double reeds and by air flow in the next section.

Figure 15.111 shows four typical modern orchestral woodwind instruments. All such instruments have distinctive tone qualities and come in various sizes, which cover a wide range of pitches and different tone-colours.

The flute, bass flute and piccolo are based on the resonances of a cylindrical tube, with the open end and mouthpiece hole giving pressure nodes at both ends. Like the recorder, all the chromatic notes of the musical scale can be played by selectively opening and shutting a number of tone holes in the walls of the instrument using the player's fingers (on ancient and baroque flutes) or felted hinged pads operated by a system of keys and levers (on modern instruments). Primitive flutes appear in most ancient cultures.

The clarinet is based on a cylindrical tube excited by a single reed at one end. The reed and mouthpiece close one end of the tube, so that the odd-integer partials are more strongly excited than the even partials, particularly for the lowest notes, when most sideholes are closed. In addition, when overblown, the clarinet sounds a note three times higher (an octave and a fifth). Like all real instruments, perturbations from the tone holes,

variations in tube diameter and the nonlinear processes involved in the production of sound vibrations by the reed strongly influence the strength of the excited partials, all of which contribute to the characteristic sound of the instrument.

The single-reed clarinet is a relatively modern instrument developed around 1700 by the German instrument maker Denner. It evolved from the chalumeau, an earlier simple single-reed instrument with a recorder-like body, which still gives its name to the lower register of the clarinet's playing range. In the 1840s, the modern system of keys was introduced based on the Boehm system previously developed for the flute [15.201].

The oboe is based on a conical tube truncated and closed at the playing end by a double reed. As described earlier, a conical tube supports all the integer harmonic partials giving a full and penetrating sound quality that is very rich in upper partials. This is why an oboe note is used to define the playing pitch (usually $A_4 = 440$ Hz) of the modern symphony orchestra. Like all modern instruments, today's oboe developed from much earlier instruments, in this case from the double-reed shawn and bagpipe chanters, which still exist in many ethnic cultures in Europe, Asia and parts of Africa. In addition to the bass oboe, the oboe d'amore and cor anglais, with their bulbous end cavity just before the output bell, have been used for their distinctive plaintive sounds by Bach and many later composers. Like the flute and clarinet, early oboes used mostly open-side holes closed by the fingers, with only one or two holes operated by a key, but developed an increasingly sophisticated key system over time to facilitate the playing of the instrument.

The bassoon is a much larger instrument, producing lower notes of the musical scale. Because of the length of the air column, the spacing of the tone holes would be far too wide to operate by the player's fingers alone. To circumvent this problem, the instrument is folded along its length and relatively long finger holes are cut diagonally through the large wall thickness, so that normally fingered holes can connect to the much wider separation of holes in the resonant air column. The bore of the instrument is based on a largely conical cross section, with the mouthpiece end terminated by a narrow bent tube or *crook* to which a large double reed is attached. Early bassoons included a single key to operate the most distant tone hole on the instrument. Modern instruments have an extended key system to facilitate playing all the notes of the chromatic scale. The contrabassoon includes an additional folded length of tube. Like the oboe, the sound of the bassoon is very rich in upper partials and has a very rich, mellow sound.



Fig. 15.111 The modern flute, oboe, clarinet and bassoon (not to scale)

Related to the bassoon is the renaissance racket played with a crook and double reed. The instrument looks like a simple cylinder with a set of playing holes cut into its surface. However, in reality, it is a highly convoluted pipe with twelve parallel pipes arranged round the inner diameter of the cylinder and interconnected with short bends at their ends to produce a very long acoustic resonator with easily accessible tone holes. This provides a beautiful example of the centuries-old ingenuity of instrument makers in solving the many acoustic and ergonomic problems involved in the design of musically successful wind instruments.

Brass Instruments

Figure 15.112 illustrates the trumpet, trombone and horn, which like all brass instruments are based on lengths of cylindrical, conical and flared resonant air columns. They are excited by a mouthpiece at one end and a bell at the open end, as described in the previous section. The player selects the note to be sounded by buzzing the lips, usually at a frequency corresponding to one of the natural resonances of the coupled air column. The essential nonlinearity of this excitation process also excites multiples in frequency of the playing pitch. Ideally, for ease of playing, these harmonics should coincide with the higher modes of the excited air column. As already described, brass instruments are therefore designed to have a full harmonic set of modes. However, because of their shape and outward flare, it is impossible to achieve this for the fundamental mode (Fig. 15.77).

By adjusting the pressure and the tightness of the lips in the mouthpiece, the player can pitch notes based on the $n = 2, 3, 4 \dots$ modes – the $n = 2$ mode, a fifth above, an octave above, an octave and a fourth above,

etc. Trumpet players typically sound notes up to the 8–10th mode, while skilled horn players can pitch notes up to and sometimes above the 15th. In the higher registers, the instruments can therefore play nearly all the notes of a major diatonic scale. A few of the notes can be rather badly out of tune, but a skilled player can usually correct for this by adjusting the lip pressure and flow of air through the mouthpiece. The low notes are based on simple intervals: the perfect fifth, octave, perfect fourth, etc. Trumpets and horns were therefore often used in early classical music to add a sense of military excitement and to emphasise the harmony of the key in which the music is written. However, in later classical music and music of the romantic period, all the notes of the chromatic scale were required. To achieve this, brass instruments such as the trumpet and horn were developed with a set of air valves, which enabled the player to switch in and out various combinations of different lengths of tube, to change the effective resonating length of the vibrating air column and hence playing pitch. Uniquely, the pitch of the trombone is changed by the use of interpenetrating cylindrical sliding tubes, which change the effective length. Modern instruments generally use a folded or coiled tube structure to keep the size of the instrument to manageable proportions.

The trombone can sound all the semitones of the chromatic scale, by the player sliding lengths of closely fitting cylindrical tubing inside each other. In the *first position*, with the shortest length tube (Fig. 15.112), the B-flat tenor trombone sounds the note B-flat at ≈ 115 Hz, corresponding to the $n = 2$ mode, an octave below the lowest note on the B-flat trumpet. To play notes at successive semitones lower, the total length has to be extended sequentially by fractional increases of 1.059. From the shortest to longest lengths there are seven such increasingly spaced *positions*. When fully extended, the trombone then plays a note six semitones lower (E) than the initial note sounded. One can then switch to the $n = 3$ mode to increase the pitch by a perfect fifth, to the note B a semitone higher than the initial note sounded. Using the closer positions enables the next six higher semitones to be played. Higher notes can be excited by suitable combinations of both position and mode excited. The trombone is one of the few musical instruments that can slide continuously over a large range of frequencies, simply by smoothly changing its length. This is widely used in jazz, where it also enables the player to use a very wide, frequency-modulated, vibrato effect and bending of the pitch of a note for expressive effect.

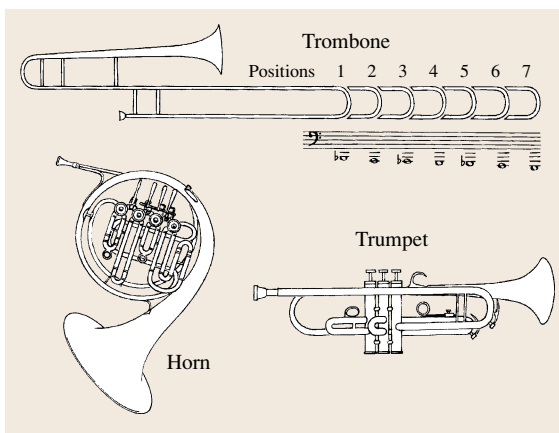


Fig. 15.112 The trombone, French horn and trumpet

The fully extended length of the vibrating air column in the first position is ≈ 2.5 m. Two-thirds of the length is made up of 1.3 cm-diameter cylindrical tubing with the remaining gently flared end-section opening out to a bell diameter of 16–20 cm.

The trumpet achieves the full chromatic range by the use of three piston valves, which enable additional lengths of tubing to be switched in and out of the resonating air column. In the inactive *up* position, the sound travels directly through a hole passing directly through the valve. When the piston is depressed, the valve enables the tube on either side of the valve to be connected to an additional length of tubing, which includes a small, preset, sliding section for fine tuning. The pitch is decreased by a tone on depressing the first piston and a semitone by the second. Pressing them down together therefore lowers the pitch by three semitones (a minor third). Depressing the third valve also lowers the pitch by three semitones, so that when all three valves are depressed the pitch is lowered by six semitones. However, the tuning is not exact, because whenever any single valve is depressed the effective tube length is lengthened. Therefore, when a second (or third) valve is depressed, the fractional increase in effective length is less when the second valve alone is used. This is related to the need to *increase* the spacing of the semitone positions on the trombone as it is extended. Similar mistuning problems arise for all combinations of valves used.

To circumvent these difficulties, compromises have to be made, if the instrument is to play in tune (*Backus* [15.133, pp. 270–271]). The added length of tubing to produce the semitone and tone intervals are therefore purposely made slightly too long, giving semitone and tone intervals that are slightly flat, but which in combination produce a three-semitone interval which is slightly sharp. Similarly, the third valve is tuned to give a pitch change of slightly more than three semitones. This allows the full of range of semitones to be played with only slight fluctuations above and below the correct tuning. The error is greatest when all three pistons are depressed. In the modern trumpet, the mistuning can be compensated by a small length of tubing operated by an additional small valve operated by the little finger of the playing hand. To regulate the overall tuning of the instrument, the playing length of the instrument can be varied by a sliding U-tube section at the first bend away from the mouthpiece. As we will show later, the skilled player can adjust the muscles controlling the dynamics of the lip-reed excitation to correct for any slight mistuning inherent in the design of the instrument.

The bends and valves incorporated into the structure of brass instruments will clearly result in sudden changes in acoustic impedance of the resonating air column, which will produce reflections and perturbations in the frequency of the frequency of the excited modes. Surprising, as shown earlier, such effects are acoustically relatively unimportant, though for the player they may affect the feel of the instrument and ease with which it can be played. In particular, when a brass player is pitching one of the higher modes of an instrument such as the horn several oscillations have to be produced before any feedback returns from the end of the instrument to stabilise the playing frequency. For example, when pitching the 12th mode on a horn, the player has to buzz the lips for about 12 cycles before the first reflection returns from the end of the instrument, which demonstrated the difficulty of exact pitching of notes in the higher registers. Note that, because of the dispersion of sound waves in a flared tube, the group velocity determining the transit time will not be the same as the phase velocity determining modal frequencies. Any strong reflections from sharp bends and discontinuities in acoustic impedance introduced by the valve structures can potentially confuse the pitching of notes and the playability of an instrument. Such transients can be investigated directly by time-domain acoustic reflectometry (see, for example, *Ayers* [15.180]). Different manufacturers choose different methods to deal with the various tuning and other acoustic problems involved in the design of brass instruments and players develop strong preferences for a particular type of instrument based on both the sound they produce and their ease of playing.

The trumpet bore is ≈ 137 cm long with largely cylindrical tubing with a diameter of ≈ 1.1 , which tapers down to ≈ 0.9 cm at the mouthpiece end over a distance of ≈ 12 –24 cm. It opens up over about the last third of its length with an end bell of diameter ≈ 11 cm. To reduce the overall length, its length is coiled with a single complete turn, as illustrated in Fig. 15.112.

The cornet is closely related to the trumpet but has a largely conical rather than cylindrical bore and is further shortened by having two coiled sections. This results in a somewhat lower cut-off frequency giving a slightly warmer but less brilliant sound quality. The bugle is an even simpler double-coiled valveless instrument of fixed length, so that it can only sound the notes of the natural harmonics. It was widely used by the military to send simple messages to armies and is still used today in sounding the *last post*, accompanying the burial of the military dead.

The modern French horn developed from long straight pipes with flared ends played with a mouthpiece. Technology then enabled horns to be made with coiled tubes, like hunting horns, greatly reducing their size. In early classical music, horns were only expected to play a few simple intervals in the key in which the music was written. For music written in different keys, the player had to add an additional section of coiled tube called a *crook*, to extend the length of the instrument accordingly.

To extend the range of notes that a horn could play, the player can place his hand into the end of the instrument. Depending how the hand is inserted, the pitch of individual harmonics can be lowered or raised by around a semitone, producing what is referred to as a *hand-stopped* note. If the hand is partially inserted into the bell, it dramatically increases the cut-off frequency giving the player access to a much larger number of higher modes, as illustrated in measurements by *Benade* [15.134, Fig. 20.17] reproduced in Fig. 15.113. Although the associated changes in pitch may be relatively small, inserting the hand into the end of a horn significantly changes the spectrum of the radiated sound, which allows the horn player some additional freedom in the quality of the sound produced.

The modern orchestral horn produces all the notes of the chromatic scale using rotary valves to switch in combinations of different length tube, rather like the trumpet. The modern instrument is a combination of a horn in F and a horn in B-flat, which can be interchanged by a rotary valve operated by the thumb of the left hand, while the first three fingers operate the three main valves, which are common to both horns.

The total length of the F horn is about 375 cm, a third longer than the B-flat trombone, enabling it to play down to the note F2. The F-horn is used for the lowest notes on the instrument, while the B-flat horn is used to give the player a much higher degree of security in pitching the higher notes. Like the primitive hunting horn, the modern horn is coiled to accommodate its great length and has a bore that opens up gently over its whole length from a diameter of ≈ 0.9 mm at

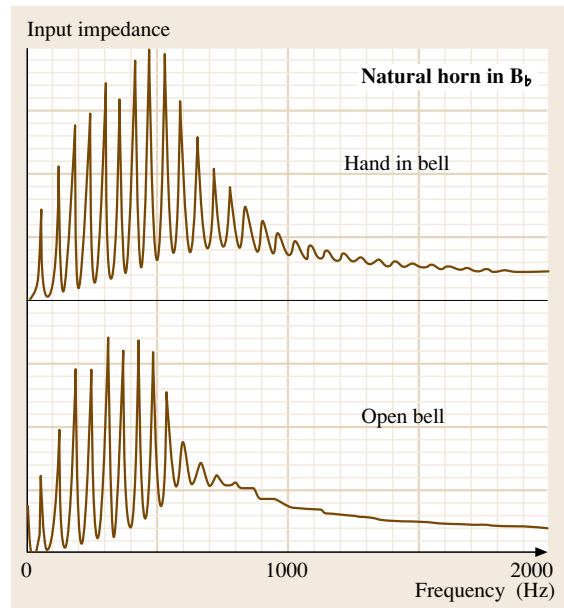


Fig. 15.113 Input impedance measurements of a natural horn, with and without a hand in the bell (after *Benade* [15.134])

the mouthpiece end to a rapidly flared output bell with a diameter of ≈ 30 cm.

There are many other instruments played with a mouthpiece in both ancient and ethnic cultures around the world. Many primitive instruments are simply hollowed-out tubes of wood, bamboo or animal bones. The notes that such instruments can produce are limited to the principal, quasi-harmonic, resonances of the instrument. There are also many hybrid instruments played with a mouthpiece, which use finger-stopped holes along their length, just like woodwind instruments. Important examples are the renaissance *cornett* and the now almost obsolete *serpent*, a spectacularly large, multiple bend, s-shaped, instrument. Many modern players of baroque-period *natural* trumpets have also added finger holes to the sides of their instruments, to facilitate the pitching of the highest notes.

15.4 Percussion Instruments

Compared with the extensive literature on stringed, woodwind and brass instruments, the number of publications on percussion instruments is somewhat smaller. This is largely because the acoustics of percussion instruments is almost entirely dominated by the well-

understood, free vibrations of relatively simple structures, without complications from the highly nonlinear excitation processes involved in exciting string and wind instruments. However, as this section will highlight, the physics of percussion instruments involves

a number of fascinating and often unexpected features of considerable acoustic interest.

The two most important references on the acoustics of percussion instruments are *The Physics of Musical Instruments*, Fletcher and Rossing [15.5, Chaps. 18–21] and the *Science of Percussion Instruments* [15.202] by Rossing, the general editor of this Handbook, who has pioneered research on a very wide range of classical and ethnic percussion instruments. *James Blade's Percussion Instruments and their History* [15.203] provides an authoritative survey of the development of percussion instruments from their primitive origins to their modern use.

Percussion instruments are amongst the oldest and most numerous of all musical instruments. Primitive instruments played by hitting sticks against each other or against hollowed-out tree stumps or gourds are likely to have evolved very soon after man discovered tools to make weapons and other simple artefacts essential for survival. The rhythmic beating of drums by Japanese Kodo drummers, the marching bands of soldiers down the centuries, and the massed percussion section of a classical orchestra still instil the same primeval feelings of power and excitement used to frighten away the beasts of the forest and to raise the fighting spirits of early groups of hunters. The beating of drums would also have provided a simple way of communicating messages over large distances, the rhythmic patterns providing the foundation of the earliest musical language – the organisation of sound to convey information or emotion. Martial music, relying heavily on the beating of drums continues to be used, and as often misused, to instil a sense of belonging to a particular group or nation and to instil fear in the enemy.

In China, bells made of clay and copper were already in use well before 2000 BC. The discovery of bronze quickly led to the development of some of the most sophisticated and remarkable sets of cast bells ever made, reaching its peak in the western Zhou (1122–771 BC) and eastern Zhou (770–249 BC) dynasties (Fletcher and Rossing [15.5, Sect. 21.15]). Inscriptions on the set of 65 tuned chime bells in the tomb of Zeng Hou Yi (433 BC), show that the Chinese had already established a 12-note scale, closely related to our present, but much later, western scale. The ceremonial use of bells and gongs is widespread in religious cultures all over the world and in western countries has the traditional use of summoning worshippers to church and accompanying the dead to their graves.

In the 18th century classical symphony orchestra of Haydn and Mozart's time, the timpani helped emphasise

the beat and pitch of the music being played, particularly in loud sections, with the occasional use of cymbals and triangle to emphasise exotic and often Turkish influences. The percussion section of today's symphony orchestra may well be required to play up to 100 different instruments for a single piece, as in *Notations I–IV* by Boulez [15.204]. This typical modern score includes timpani, gongs, bells, metals and glass chimes, claves, wooden blocks, cowbells, tom-toms, marimbas, glockenspiels, xylophones, vibraphones, sizzle and suspended cymbals, tablas, timbales, metal blocks, log drums, boobams, bell plates in C and B flat, side drums, Chinese cymbals, triangles, maracas, a bell tree, etc. Modern composers can include almost anything that makes a noise – everything from typewriters to vacuum cleaners. The percussion section of the orchestra is required to play them all – often simultaneously.

We will necessarily have to be selective in the instruments that we choose to consider and will concentrate largely on the more familiar instruments of the modern classical symphony orchestra. We will also constrict our attention to instruments that are struck and will ignore instruments like whistles, rattles, scrapers, whips and other similar instruments that percussion players are also often required to play.

15.4.1 Membranes

Circular Membrane

A uniform membrane with areal density σ , stretched with uniform tension T over a rigid circular supporting frame, supports acoustically important transverse displacements z perpendicular to the surface described by the wave equation

$$T \left(\frac{\partial^2 z}{\partial r^2} + \frac{1}{r} \frac{\partial z}{\partial r} + \frac{1}{r^2} \frac{\partial^2 z}{\partial \phi^2} \right) = \sigma \frac{\partial^2 z}{\partial t^2}, \quad (15.147)$$

which has solutions of the form

$$z(r, \phi, t) = J_m(k_{mn}r) \left\{ \begin{array}{l} A \cos m\phi \\ + B \sin m\phi \end{array} \right\} e^{i\omega t}. \quad (15.148)$$

$J_m(k_{mn}r)$ are Bessel functions of order m , where n denotes the number of radial nodes and m the number of nodal diameters. The eigenfrequencies $\omega_{mn} = k_{mn}\sqrt{T/\sigma}$ are determined by the requirement that $J_m(k_{mn}a) = 0$ on the boundary at $r = a$. The frequency of the fundamental (01) mode is $(2.405/2\pi a)\sqrt{T/\sigma}$, where $J_0(k_{01}a) = 0$. The relative frequencies of the first

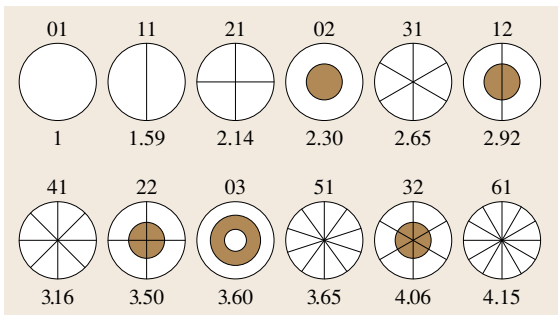


Fig. 15.114 The first 12 modes of a circular membrane illustrating the mode nomenclature, nodal lines and frequencies relative to the fundamental 01 mode

12 modes and associated nodal lines and circles are shown in Fig. 15.114.

For ideal circular symmetry, the independent azimuthal cosine and sine solutions result in degenerate modes having the same resonant frequencies. The degeneracy of such modes can be lifted by a nonuniform tension, variations in thickness when calfskin is used, and a lack of ideal circularity of the supporting rim. Any resulting splitting of the frequencies of such modes can result in beats between the sound of given partials, which the player can eliminate by selectively adjusting the tension around the perimeter of the membrane or by hitting the membrane at a nodal position of one of the contributing modes.

Unlike transverse waves on a stretched string, the modes of a circular membrane are inharmonic. As a consequence, the waveforms formed by the combination of such partials excited when the drumhead is struck are nonrepetitive. Audio [🔊 EXTRAS](#) illustrates the frequencies of the first 12 modes played in sequence. [🔊 EXTRAS](#) illustrates their sound when played together as a damped chord, which already produces the realistic sound of a typical drum, having a reasonably well-defined sense of pitch, despite the inharmonicity of the modes.

Although percussion instruments may often lack a particularly well-defined sense of pitch, one can nevertheless describe the overall pitch as being high or low. For example, a side drum has a higher overall pitch than a bass drum and a triangle higher than a large gong. From an acoustical point of view, we will be particularly interested in the lower-frequency quasi-harmonic modes. However, one must never forget the importance of the higher-frequency inharmonic modes in defining the initial transient, which is very important in characterising the sound of an instrument.

Nonlinear effects arise in drums in much the same way as in strings (Sect. 15.2.2). The increase in tension, proportional to the square of the vibrational amplitude, leads to an increase in modal frequencies. In addition, nonlinearity can result in mode conversion (Sect. 15.2.2) and the transfer of energy from initially excited lower-frequency modes with large amplitudes to higher partials. Although the pitch of a drum is raised when strongly hit, this may to some extent be compensated by the psychoacoustic effect of a low-frequency note sounding flatter as its intensity increased. Changes in perceived pitch of a drum with time can often be emphasised by the use of digital processing, to increase the frequency of the recorded playback without changing the overall envelope in time (audio [🔊 EXTRAS](#)).

Air Loading and Radiation

The above description of the vibrational states of a membrane neglects the induced motion of the air on either side of the drum skin. At low frequencies, this adds a mass $\approx \frac{8}{3}\rho a^3$ to the membrane (Fletcher and Rossing [15.5, Sect. 18.1.2]), approximating to a cylinder of air with the same thickness as the radius a of the drum head. The added mass lowers the vibrational frequencies relative to those of an ideal membrane vibrating in vacuum. The effect is largest at low frequencies, when the wavelength in air is larger than or comparable with the size of the drumhead. For higher-frequency modes, with a number of wavelengths λ across the width of the drumhead, the induced air motion only extends a distance $\approx \lambda 2\pi (\ll a)$ from the membrane. Air loading therefore leaves the higher-frequency modes relatively unperturbed.

Drums can have a single drum skin stretched over a hollow body, such as the kettle drum of the timpani, or two drum heads on either side of a supporting cylinder or hollowed out block of wood, like the side drum and southern Indian mrdanga (Fletcher and Rossing [15.5, Sect. 18.5]). By stretching the drum head over a hollow body, the sound radiated from the back surface is eliminated, just like mounting a loudspeaker cone in an enclosure. At low frequencies, the drum then acts as a monopole source with isotropic and significantly enhanced radiation efficiency. This is illustrated by the much reduced 60 dB decay time of the (11) dipole mode of a stretched timpani skin, when the drum skin was attached to the kettle – from 2.5 s to 0.5 s (Fletcher and Rossing [15.5, Table 18.4]).

In addition, any net change in the volume of the enclosed air resulting from vibrations of the drum skin will increase the restoring forces acting on it and hence raise

Table 15.7 Ideal and measured frequencies of the modal frequencies of a timpani drum head normalised to the acoustically important (11) mode before and after mounting on the kettle, and the internal air resonances of the kettle. The *arrows* indicate the sense of the most significant perturbations of drum head frequencies and the *asterisks* indicate the resulting quasi-harmonic set of acoustically important modes (adapted from Fletcher and Rossing)

Mode	Ideal membrane	Drumhead in air		Coupled internal air resonances		Drumhead on kettle	
01	0.63	82 Hz	0.53	(0,1,0)	385 Hz	127 Hz	0.85 ↑
				(0,1,1)			
11	1.00	160	1.0	(1,1,0)	337 Hz	150	1.00 ↓ ***
				(1,1,1)	566 Hz		
21	1.34	229	1.48	(2,1,0)	537 Hz	227	1.51 ↓ ***
				(2,1,1)	747 Hz		
02	1.44	241	1.55	(0,1,0)	(0,2,0)	252	1.68 ↑
31	1.66	297	1.92	(3,1,0)	(3,1,1)	298	1.99 ***
12	1.83	323	2.08	(1,2,0)	(1,2,1)	314	2.09 ↓
41	1.98	366	2.36			366	2.44 ***
22	2.20	402	2.59			401	2.67
03	2.26	407	2.63	(0,1,0)		418	2.79 ↑
51	2.29	431	2.78			434	2.89
32	2.55	479	3.09			448	2.99 ***
61	2.61	484	3.12			462	3.08

the modal frequencies, see Table 15.7. In this example, the coupling raises the frequency of the (01) drumhead mode from 82 to 127 Hz, the (02) mode from 241 to 252 Hz, and the (03) mode from 407 to 418 Hz. In contrast, the asymmetric, volume-conserving, (11) mode is lowered in frequency from 160 to 150 Hz, which probably results from coupling to the higher frequency 337 Hz internal air mode having the same aerial symmetry.

As in any coupled system in the absence of significant damping, the separation in frequency of the normal modes resulting from coupling will tend to be greater than the separation of the uncoupled resonators (Fig. 15.46b). In addition, any enclosed air will provide a coupling between the opposing heads of a double-sided drum. For example, the 227 and 299 Hz (01) uncoupled (01) modes of the opposing heads of a snare drum become the 182 and 330 Hz normal modes of the double-sided drum (Fletcher and Rossing [15.5, Fig. 18.7]).

Excitation by Player

The quality of the sound produced by any percussion instrument depends as much on the player's skills as on the inherent qualities of the instrument itself. Drums are not simply hit. A player uses considerable manual dexterity in controlling the way the drumstick strikes and is allowed to bounce away from the stretched drum skin,

xylophone bar or tubular bell. It is important that contact of the stick with the instrument is kept to a minimum; otherwise the stick will strongly inhibit the vibrational modes that the player intends to excite. The *lift off* is just as important as *the strike*, and it takes years of practice to perfect, for example, a continuous side drum or triangle roll.

It is also important to strike an instrument in the right place using the right kind of stick or beater to produce the required tone, resonance or loudness required for a specific musical performance. As discussed earlier in relation to the excitation of modes on a stretched string and modal analysis measurements, one can selectively emphasise or eliminate particular partials by striking an instrument at antinodes or nodes of particular modes. A skilled timpani player can therefore produce a large number of different sounds by hitting the drumhead at different positions from the rim. Striking timpani close to their outer rim preferentially excites the higher-frequency modes, while striking close to the centre results in a rather dull *thud*. This is due to the preferential excitation of the inefficient (00) mode and elimination of the acoustically important (0*n*) modes. The most sonorous sounding notes are generally struck about a quarter of the way in from the edge of the drum.

The sound is also strongly affected by the dynamics of the beater–drumhead interaction, which is rather soft and *soggy* near the centre and much harder and

springy near the outer rim. The sound is also strongly affected by the type of drumstick used. Light, hard wooden sticks will make a more immediate impact with a bar or drum skin than heavily felted beaters. Such differences are similar to the effect of using heavy or light force hammers to preferentially excite lower- or higher-frequency modes in modal analysis investigations. A professional timpanist or percussion player will use completely different sticks for different styles of music and obtain effects on the same instrument ranging from the muffled drum beats of the *Death March* from Handel's *Saul* to the sound of cannons firing in Tchaikovsky's 1812 overture.

There has been much less research on the mechanics of the drumstick–skin interaction than on the excitation of piano strings by the piano hammer (Sect. 15.2.2), though much of the physics involved is very similar. In particular, the shortest time that the drumstick can remain in contact with the skin will be determined by the time taken for the first reflected wave to return from the rim of the drum to bounce it off. This is illustrated schematically in Fig. 15.115, which illustrates qualitatively the force applied to the drumhead as a function of time for a hard and a soft drumstick struck near the centre (*solid line*) and then played nearer the edge (*dashed*). The overall spectrum of sound of the drum will be controlled by the frequency content of such impulses. Short contact times will emphasise the higher partials and give rise to a more percussive and brighter sound. Higher partials will also be emphasised by the use of metal beaters or drumsticks with hard-wooden striking heads rather than leather or soft felt-covered stick heads. This is illustrated by the second pulse, which would produce a softer, mellower sound, without such a strong initial attack. Clearly, the loudness of the drum note will be proportional to the mass m of the striking drumstick

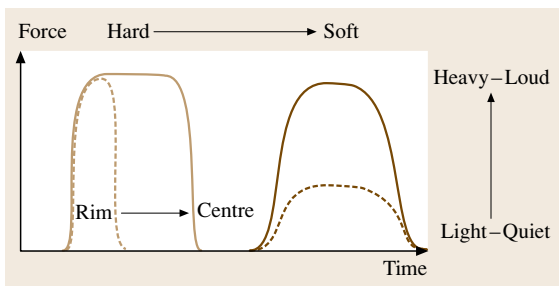


Fig. 15.115 Schematic impulses from a striking drumstick, illustrating the effect of exciting the drum head at different positions, with different strengths, and with a hard and soft drumstick

head and its impact velocity v , delivering an impulse of $\approx mv$.

Audio 13.4 EXTRAS illustrates the change in sound of a timpani note, as the player progressively strikes the drum with a hard felt stick, starting from the outside edge and moving towards the centre, in equal intervals of \approx one eighth of the radius. Audio 13.5 EXTRAS illustrates the sound of a timpani when struck at one quarter of the radius from the edge, using a succession of drumsticks of increasing hardness, from a large softly felted beater to a wooden beater.

In modern performances of baroque and early classical music, the timpanist will use relatively light sticks, with leather-coated striking heads, while for music of the romantic period larger and softer felt-covered drumsticks will often be used.

Many drums of ethnic origin are played with the hands, hitting the drum head with fingers, clenched fists or open palms to create quite different kinds of sounds. In some cases, the player can also press down on the drum head to increase the tension and hence change pitch of the note. For a double-headed drum, the coupling of the air between the drum heads can even enable the player to change the pitch and sound of a given note by applying pressure to the drum head not being struck.

We now consider a number of well-known percussion instruments based on stretched membranes, which illustrate the above principles. These will include drums with a well defined pitch, such as kettle drums (timpani) and the Indian tabla and mrdanga, and drums with no defined pitch, such as the side and bass drum.

Kettle Drums (Timpani)

The kettle drum or timpani traditionally used a specially prepared calfskin stretched over a hollow, approximately hemispherical, copper kettle generally beaten out of copper sheet. Nowadays, thin (0.19 mm) mylar sheet is often used in preference to calfskin for the drum skin, because of its uniformity and reduced susceptibility to changes in tension from variations in temperature and humidity. The drum skin is stretched over a supporting ring attached to the kettle, with the tension of the skin typically adjusted using 6–8 tuning screws equally spaced around the circumference. The player adjusts these screws to tune the instrument and to optimise the quality of tone produced. In modern instruments, a mechanical pedal arrangement can be used to quickly change the tension and thereby the tuning, by pushing the supporting ring up against the drumhead. Typically, such an arrangement can increase the tension by up to a factor of two, raising the pitch by a perfect fifth. In

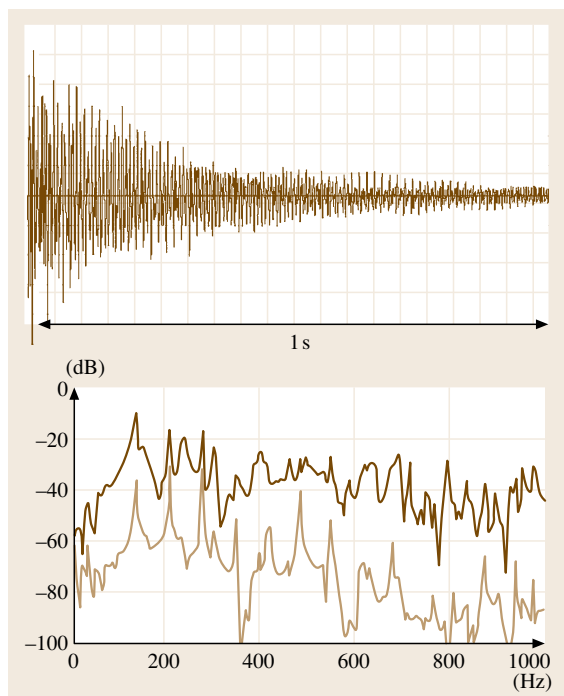


Fig. 15.116 Decaying waveform of a timpani note and FFT spectra at the start of a note (*upper trace*) and after 1 s (*lower trace*)

the modern classical symphony orchestra, the timpanist will use two or three timpani of different sizes to cover the range of pitched notes required.

Figure 15.116 shows the waveform and spectrum of the immediate and delayed sound of a timpani note (the first drum note in audio [EXTRAS](#)). The initial sound includes contributions from all the modes excited. This includes not only the vibrational modes of the drum head, but also the air inside the kettle, the kettle itself and even the supporting legs and vibrations induced in the floor. Many of these vibrations die away rather quickly, leaving a number of prominent, slowly decaying, drum-skin modes. Note in particular, the strongly damped (01) mode at ≈ 140 Hz and the less strongly damped modes (02) and (03) modes at 210 Hz and 284 Hz, tuned approximately to a perfect fifth and an octave above the fundamental. As noted by Rayleigh in relation to church bells [15.3, Vol. 1, Sect. 394], the pitch of a note is often determined by the higher quasi-harmonically related partials rather than the lowest partial present. This is demonstrated by the second drum beat in [EXTRAS](#), which has all frequency components below 250 Hz removed. The perceived pitch at

long times is unchanged, though there is a considerable loss in *depth* or *body* of the resulting sound.

Modal frequencies for a typical kettle drum have already been listed in Table 15.7, which includes a set of nearly harmonic modes indicated by asterisks achieved, in part, by empirical design of the coupled membrane and kettle air vibrations. To a first approximation, the modal frequencies are determined by the volume of the kettle rather than its shape. The smaller the enclosed volume, the larger its effect on the lowest-order drum-head modes. Nevertheless, there are distinct differences in the sounds of timpani used by orchestras in Vienna and those used elsewhere in Europe (Bertsch [15.205]). Such differences can be attributed to the Viennese preference for calfskin rather than mylar drum heads, a small shape dependence affecting the coupling to the internal air resonances, and a different tuning mechanism. The modal frequencies of the Viennese timpani measured by Bertsch were similar to those listed in Table 15.7, with the (11), (21), (31) and (41) modes again forming a quasi-harmonic set of partials, in the approximate ratios 1:1.5:2.0:2.4:2.9. Rather surprisingly, the relative frequencies of the lower two modes could be interchanged with tuning.

Indian Tabla and Mrdanga

Another way of achieving a near harmonic set of resonances of a vibrating drumhead is to add mass to the drum head and hence change the frequencies of its normal modes of vibration. For the single- and double-headed Indian tabla and mrdanga drums, this is achieved by selectively loading the drum skin with several coatings of a paste of starch, gum, iron oxide and other materials – see Fletcher and Rossing [15.5, Sect. 18.5]. The acoustics of the tabla was first investigated by Raman [15.206], who obtained Chladni patterns for many of the lower-frequency modes of the drum head. Rossing and Sykes [15.207] measured the incremental changes in frequency of the loaded membrane as each additional layer was added. A 100 layers lowered the fundamental mode by about an octave. The resulting five lowest modes were harmonically related and including several degenerate modes derived from the smoothly transformed modes of the original unloaded membrane. The results were very similar to those obtained earlier by Raman. Investigations by Ramakrishna and Sondhi [15.208] and by De [15.209] showed that, to achieve a quasi-harmonic set of low-frequency modes, the areal density at the centre of such drums should be approximately 10 times that of the unloaded sections.

Figure 15.117 illustrates the decaying waveform and spectra of a well-tuned tabla drum (audio [EXTRAS](#)) from 200 ms FFTs of the initial sound and after 0.5 s. The spectra show three prominent partials at 549, 826 and 1107 Hz, in the near-harmonic ratios 1:1.51:2.02, which results in a well-defined sense of pitch. In contrast to the timpani, these partials dominate the sound and determine the pitch from the very beginning of the note. Note too the very wide spectrum of the rapidly decaying initial transient.

Side and Snare Drum

The side or snare drum is the classical two-headed drum of the modern symphony orchestra. It is usually played with either very short percussive beats or as a roll, with rapidly alternating notes from two alternating drumsticks. This results in a quasi-continuous *noise source*, which can be played over a very wide range of intensities, from very soft to very loud, to support, for example, a Rossini crescendo. Because the side drum is designed to produce short percussive sounds or a wide-band source of noise, little effort is made to tune the partial frequencies of the two drum heads.

Like the timpani and Indian drums, the vibrational modes of the drumheads can be strongly perturbed in frequency by the air coupling. When used as a snare drum, the induced vibrations of the nonstriking head can be sufficient for it to rattle against a number of metal cables tightly stretched a few mm above the surface of the nonstriking head. The resulting interruption of the vibrations, on impact with the snares, leads to the generation of additional high-frequency noise and the *sizzle* effect of the sound excited. A not dissimilar effect is used on the Indian tambura, an Indian stringed instrument investigated by *Raman* [15.210], which has a bridge purposely designed to cause the strings to rattle. *Fletcher and Rossing* [15.5, Fig. 9.30].

Figure 15.118 shows the waveform and time-averaged FFT of a side-drum roll (audio [EXTRAS](#)). The spectrum is lacking in spectral features other than a modest peak in noise at around 100–200 Hz, associated with the vibration of the lower head against the snares.

Although the exact placing of the vibrational modes of the strike and snare heads are of little acoustic importance, their coupling via the enclosed air illustrates the general properties of double-headed drums of all types. The first four coupled normal modes are shown in Fig. 15.119, which is based on data from *Rossing* [15.211, Sect. 4.4]. For a freely supported drum, momentum has to be conserved, so that normal modes

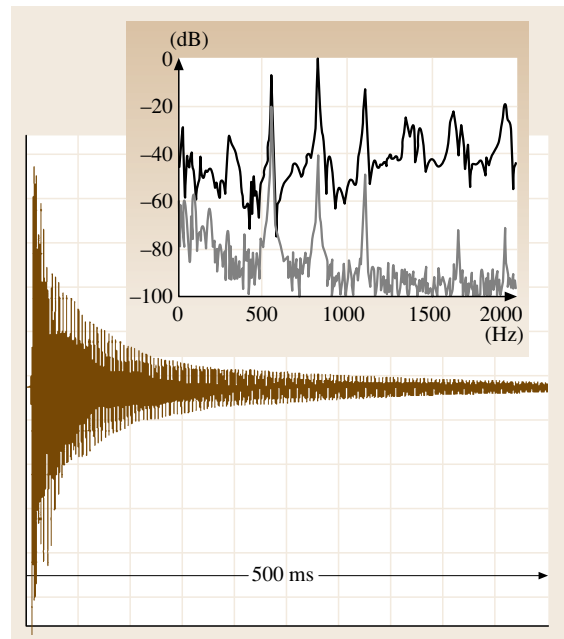


Fig. 15.117 Decaying waveform of a tabla drum with initial FFT spectrum (*upper trace*) and after 0.5 s (*lower*) illustrating the weakly damped, near-harmonic, resonances of the loaded drumhead

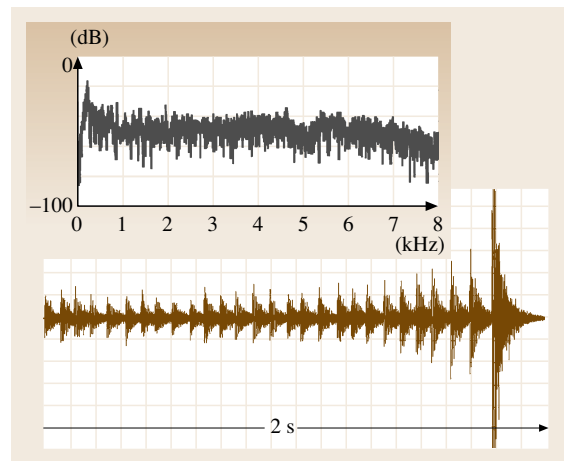


Fig. 15.118 Time-averaged FFT spectrum and waveform of the sound of a snared side-drum roll of increasing intensity

with the two heads vibrating in the same phase will also involve motion of the supporting shell of the drum, as indicated by the arrows in Fig. 15.119.

As anticipated, the air coupling increases the separation of the (01) modes from 227 and 299 Hz to 182 and

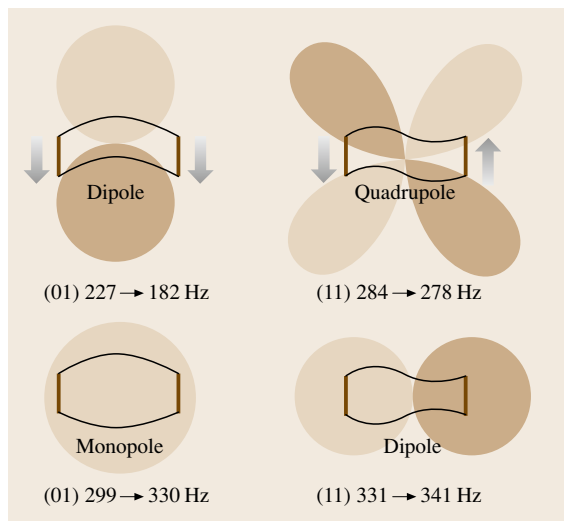


Fig. 15.119 Coupled motions of the two drumheads of a side drum, indicating the change in frequency of the drumhead modes from air coupling within the drum and the associated polar radiation patterns (after *Zhao et al.* [15.212])

330 Hz, and the (11) modes from 284 and 331 Hz to 278 and 341 Hz. The perturbations in modal frequencies will always be largest when the coupled modes have similar frequencies. Such perturbations becomes progressively weaker at higher frequencies, partly because the coupling from the enclosed air modes becomes weaker and partly because the frequencies of the two drum-head modes having the same symmetry become more widely separated. The higher modal frequencies are therefore little different from those of the individual drum heads in isolation.

Figure 15.119 also illustrates the anticipated polar radiation patterns for the normal modes measured by *Zhao* [15.212] and reproduced in *Rossing* [15.202, Figs. 4.7 and 4.8]. The coupled (10) normal modes act as a monopole radiation source, when the heads move in opposite directions, and a dipole source, when vibrating in anti-phase. In contrast, the (11) modes with heads vibrating in phase act as a quadrupole source, and a dipole source, when vibrating in anti-phase.

Although any induced motion of the relatively heavy supporting structure will not significantly affect the frequencies of the normal modes, it can result in appreciable additional damping. As a consequence, the sound of a side drum can sound very different depending on how it is supported – freely suspended on rubber bands or rigidly supported by a heavy stand (*Ross-*


Table 15.8 Modal frequencies in Hz of the batter head of a 82 cm bass drum (after *Fletcher and Rossing* [15.5])

Mode	Batter head with carry head at lower tension	Batter head with heads at same tension (Hz)
(01)	39	44, 104 split normal modes
(11)	80	76, 82 split normal modes
(21)	121	120
(31)	162	160
(41)	204	198
(51)	248	240

ing [15.202, Sect. 4.4]). *Rossing* has also made detailed vibrational and holographic studies of the free drum shell [15.202, Fig. 4.5]. As the induced motions are only a fraction of a percent of those of the drumhead, such vibrations will not radiate a very large amount of sound. Nevertheless, they may play an important role in defining the initial sound.

Bass Drum

The bass drum is large with a typical diameter of 80–100 cm. It can produce a peak sound output of 20 W, the largest of any orchestral instrument. Single-headed drums are used when a well-defined sense of pitch is required, but double-headed drums sound louder because they act as monopole rather than dipole sources. Modern bass-drum heads generally use 0.25 mm-thick mylar, though calfskin is also used.

The *batter* or beating drum head is normally tuned to about a fourth above the *carry* or resonating head (*Fletcher and Rossing* [15.5, Sect. 18.2]). The change in modal frequencies induced by the enclosed air is illustrated in Table 15.8 (*Fletcher and Rossing* [15.5, Table 18.5]). Note the strong splitting of the lowest frequency (01) and (11) normal modes, when the two heads are tuned to the same tension. In this example, the frequencies of the first five modes are almost harmonic, giving a sense of pitch to the sound (audio  EXTRAS illustrates the rather realistic synthesised sound of the first six modes of the batter head tuned to the carry head with equal amplitude and decay times). Drums with heads tuned to the same pitch have a distinctive timbre.

15.4.2 Bars

This section is devoted to percussion instruments based on the vibration of wooden and metallic bars, both in isolation and in combination with resonating air

columns. Such instruments are referred to as idiophones – bars, plates and other structures that vibrate and produce sound without having to be tensioned, unlike the skins of a drum (membranophones). Representative instruments considered in this section include the glockenspiel, celeste, xylophone, marimbas, vibraphone and triangle.

The vibrations of thick and thin plates have already been considered in the context of the vibrational modes of the wooden plates of stringed instruments (Sect. 15.2.6). The most important acoustic modes of a rectangular plate are the torsional (twisting) and flexural (bending) modes, both of which involve acoustically radiating displacements perpendicular the surface of the plate.

The torsional vibrations of a bar are discussed by *Fletcher and Rossing* [15.5, Sect. 2.20]. For a bar of length L , the frequency of the twisting modes is given by $f_n = nc_\theta/2L$, where c_θ is the dispersionless velocity of torsional waves. For a rectangular bar with width w significantly larger than its thickness h , by $c_\theta \approx 2t/w\sqrt{E/2\rho(1+\nu)}$, where E is the Young's modulus and ν the Poisson ratio. For a bar with circular cross-section, like the sides of a triangle, $c_\theta = \sqrt{E/2\rho(1+\nu)}$.

Musically, the most important modes of a thin bar are the flexural modes involving a displacement z perpendicular to their length, which for a rectangular bar satisfies the fourth-order wave equation

$$\frac{E}{12(1-\nu^2)}h^2\frac{\partial^4 z}{\partial x^4} + \rho\frac{\partial^2 z}{\partial t^2} = 0, \quad (15.149)$$

with standing-wave solutions of the general form

$$z(x, t) = (A \sin kx + B \cos kx + C \sinh kx + D \cosh kx)e^{i\omega t}, \quad (15.150)$$

where

$$\omega = \sqrt{\frac{E}{12\rho(1-\nu^2)}}hk^2. \quad (15.151)$$

As discussed in the earlier section on the vibrational modes of soundboards and the plates of a violin or guitar, the sinh and cosh functions decay away from the ends of the bar or from any perturbation in the geometry, such as local thinning or added mass, over a distance

$$k^{-1} \approx \left(\frac{E}{12\rho(1-\nu^2)}\right)^{1/4} \sqrt{\frac{h}{\omega}}.$$

Well away from the ends of a bar, the standing-wave solutions at high frequencies are therefore dominated by the sinusoidal wave components.

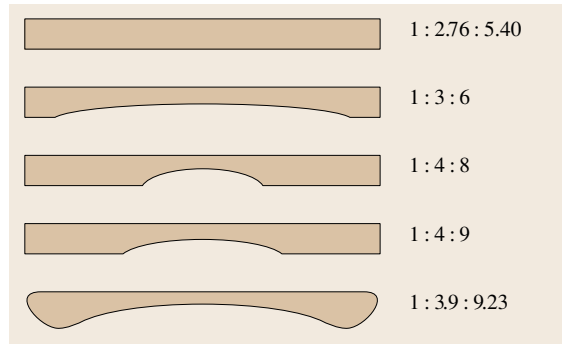



Fig. 15.120 Ratio of the frequencies of the first three partials of a simple rectangular bar for three selectively thinned xylophone bars and a typical marimba bar (after *Fletcher and Rossing* [15.5])

The lowest flexural modes of a freely supported thin rectangular bar are inharmonic, with frequencies in the ratios 1 : 2.76 : 5.40 : 8.93. However, by selectively thinning the central section, the frequency of the lowest mode can be lowered, to bring the first four harmonics more closely into a harmonic ratio, as illustrated schematically for a number of longitudinal cross-sections in Fig. 15.120, which also includes the measured frequencies of a more-complex-shaped marimba bar (*Fletcher and Rossing* [15.5, Figs. 19.2 and 19.7]).

Pitch Perception

The audio  **EXTRAS** contrasts the synthesised sounds of the first four modes of a simple rectangular bar, followed by a note having the same fundamental but with partials in the ratio 1 : 3 : 6, while the final note has the inharmonic (1 : 8.96) fourth partial of the rectangular bar added. Despite the inharmonicity of the partials, the synthesised sound of a rectangular bar has a surprisingly well-defined sense of pitch. The main effect of replacing the second and third partials with partials in the ratio 1:3:6 is to raise the perceived pitch by around a tone, even though the first partial is unchanged at 400 Hz. This again emphasises that the perceived pitch is determined by a weighted average of the partials present and not by the fundamental tone alone. Adding the fourth inharmonic partial gives an increased edge or *metallic* characteristic to the perceived sound, without changing the perceived pitch.

The metal or wooden bars of tuned percussion instruments are usually suspended on light threads or rest on soft pads at the nodal positions of their fundamental mode, which reduces the damping to a minimum.

The resulting 60 dB decay time for an aluminium vibraphone bar can be as long as 40 s (Rossing [15.202, Sect. 7.3]) compared with a few seconds for the lower-frequency notes on the wooden bars of a marimba (Rossing [15.202, Sect. 6.4]). The damping of vibrating bars is therefore highly material dependent and is largely determined by internal damping losses rather than radiation. This accounts for the very different sounds of wooden and metal bars on instruments like the glockenspiel and xylophone.

Glockenspiel and Celeste

The simplest of all idiophones are those instruments based on the vibrations of freely supported thin rectangular plates. Such instruments include the glockenspiel played with a variety of hard and soft round-headed hammers and the celeste played with strikers operated from a keyboard, with a sustaining pedal to control the damping. The playing range of the glockenspiel is typically two and a half octaves from G5 to C8, while the celeste has a range of 4–5 octaves, with a separate box-resonator used for each note.

Both instruments produce a bright, high-pitched, bell-like, sparkling sound, as in the *Dance of the Sugar Plum Fairy* in Tchaikovsky's *Nutcracker Suite*. No attempt is made to adjust the thickness of the plates to achieve a more nearly harmonic set of modes.

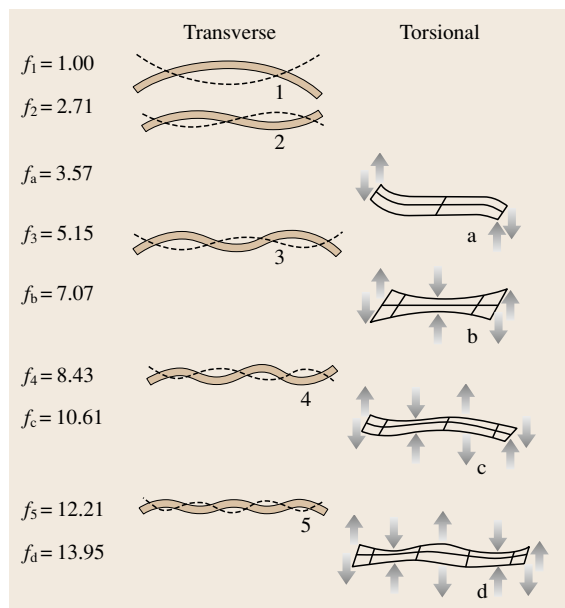


Fig. 15.121 Measured flexural and torsional modes of a glockenspiel bar (after Fletcher and Rossing [15.5])

Figure 15.121 illustrates the lowest order flexural and torsional modes and measured ratios of frequencies for a C6 glockenspiel bar (Fletcher and Rossing [15.5, Fig. 19.1]). A typical wave-envelope and spectrum of a glockenspiel note is shown in Fig. 15.122. FFT spectra are shown for 200 ms sections from the initial transient and after 200 ms. There are two strongly contributing weakly damped partials at 1045 Hz and 2840 Hz (in the ratio 1:2.72), which can be identified as the first two flexural modes of the bar. The lower of the two long sounding partials gives the sense of pitch, while the strong inharmonic upper partial gives the note its *glockenspiel* character. Audio [EXTRAS](#) compares the recorded glockenspiel note with synthesised tones at 1045 and 2840 Hz, first played separately then together. In this case, the inharmonicity of the strongly sounded partials plays a distinctive role in defining the character of the sound. The spectrum is typical of all the notes on a glockenspiel, which demonstrates that only a few of

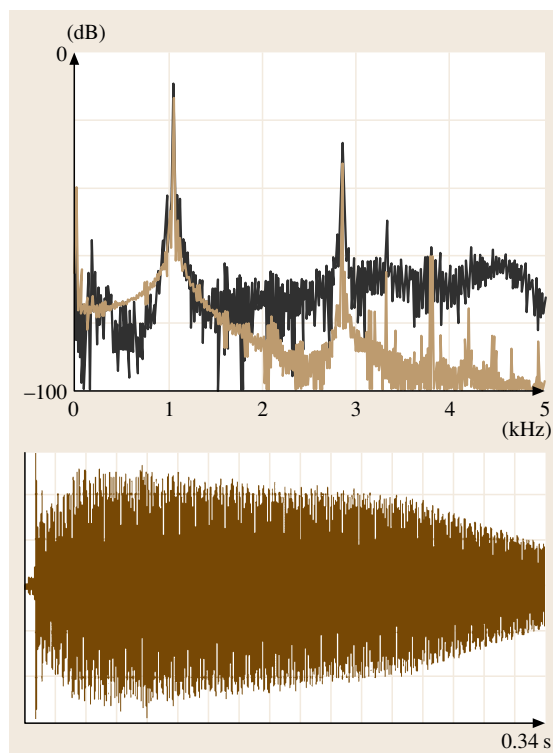


Fig. 15.122 The waveform envelope and FFT spectra of the prompt sound (*upper*) and the sound after ≈ 0.2 s (*lower*) of a typical glockenspiel note illustrating the long-time dominance of a few slowly decaying, inharmonic partials

the modes shown in Fig. 15.121 contribute significantly to the perceived sound.

Xylophone, Marimba and Vibraphone

We now consider a number of acoustically related idiophones, with bars that are selectively thinned to produce a more nearly harmonic set of resonances and well-defined sense of pitch.

The modern xylophone has a playing range of typically 3 to 4 octaves and uses wooden bars, which are undercut on their back surface to improve the harmonicity of the lower frequency modes (Fig. 15.120). Each bar has an acoustic resonator immediately below it, consisting of a cylindrical tube, which is closed at the far end. Any of the flexural and torsional modes can contribute to the initial sound, when the bar is struck by a hammer; however, most modes die away rather

quickly so that at longer times the sound is dominated by the resonances of the coupled pipe resonator.

Figure 15.123 shows the initial part of the waveform and spectrum of a typical xylophone note (EXTRAS), illustrating the initial large amplitudes and rapid decay of the higher frequency bar modes excited and the strongly excited but slowly decaying resonances of the first two modes of the air resonator. All modes contribute to the initial sound but the sound at longer times is dominated by the lowest-frequency bar modes and resonantly tuned air resonators.

The marimba is closely related to the xylophone, but differs largely in its playing range of typically two to four and a half octaves from A2 (110 Hz) to C7 (2093), though some instruments play down to C2 (65 Hz). In contrast to xylophone bars, which are undercut near their centre to raise the frequency of their second partial from 2.71 to 3.0 above the fundamental, marimba bars are often thinned still further to raise the frequency of the second partial to four times the fundamental frequency (Fig. 15.119).

Marimbas produce a rather mellow sound and are usually played with much softer sticks than traditionally used for the xylophone. Although the marimba is nowadays used mostly as a solo percussion instrument, in the 1930s ensembles with as many as 100 marimbas were played together. In many ways, such ensembles were the forerunners of today's Caribbean steelbands, to be described later in this section.

The vibraphone is similar to the marimba, but uses longer-sounding aluminium rather than wooden bars and typically plays over a range of three octaves from F3 to F6. Like the marimba, the bar thickness is varied to give a second partial two octaves above the fundamental. They are usually played with soft yarn-covered mallets, which produce a soft, mellow tone. In addition, the vibraphone incorporates electrically driven rotating discs at the top of each tuned air resonator, which periodically changes the coupling. This results in a strong amplitude-modulated vibrato effect. The wave envelope of audio (EXTRAS) is shown in Fig. 15.124 for a succession of notes played on the vibraphone with vibrato, which are then allowed to decay freely. The vibrato rate can be adjusted by changing the speed of the electric motor. Note the very long decay of the sound, which can be controlled by a pedal-operated damper.

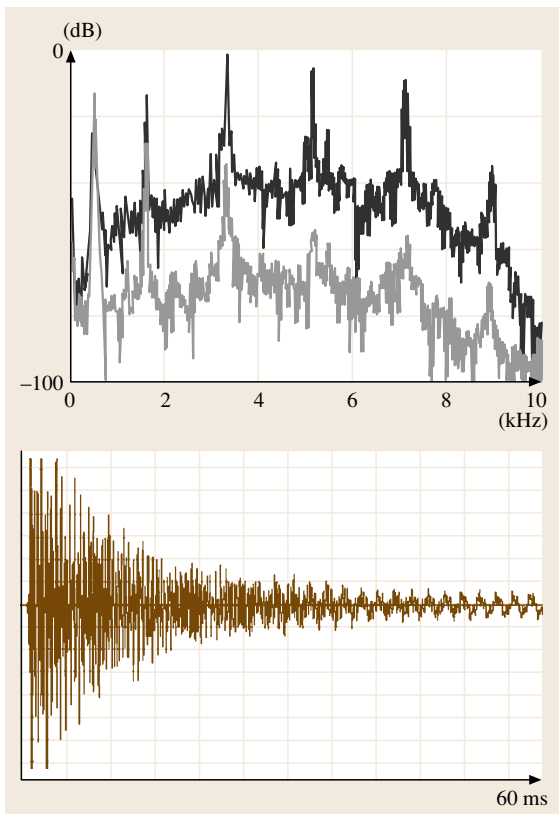


Fig. 15.123 The initial 60 ms of a xylophone waveform showing the rapid decay of high-frequency components and FFT spectra at the start of the note (*upper trace*) and after 0.2 s (*lower trace*), highlighting the persistence of the strong low-frequency air resonances excited

Triangle

The triangle is a very ancient musical instrument formed from a cylindrical metal bar bent into the shape of a triangle, with typical straight arm lengths

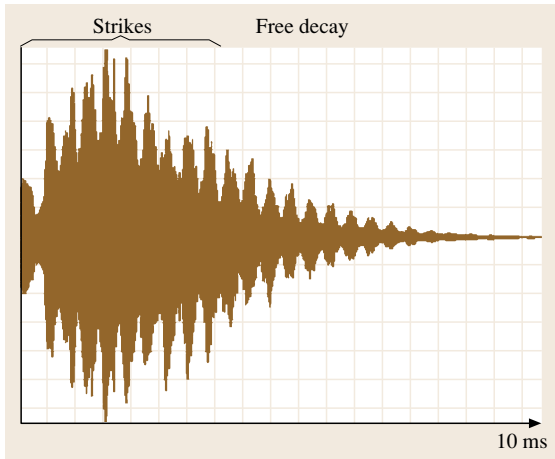


Fig. 15.124 Envelope of a succession of notes on the vibraphone, which freely decay with modulated coupling to tuned air resonators to produce an amplitude modulated vibrato effect

of 15–25 cm. They are usually struck with a similar-diameter metal rod. Although the instrument is small and therefore a very inefficient acoustic radiator, it produces a characteristic high-frequency *ping* or repetitive high-pitched rattle, which is easily heard over the sound of a large symphony orchestra (audio [I2](#) EXTRAS). The quality of the sound can be varied by beating at different positions along the straight arms. The triangle is usually supported by a thread around the top bend of the hanging instrument.

The flexural modes of a freely suspended bar of circular cross section are $f_n \approx (a/2)\sqrt{E/\rho}(2n+1)^2\pi/8L^2$, with frequencies in the ratios $3^2:5^2:7^2:9^2:11^2:13^2$ (see Sect. 15.2.4). Transverse flexural vibrations can be excited perpendicular or parallel to the plane of the instrument. For vibrations perpendicular to the plane, the bends are only small perturbations. Transverse modes in this polarisation are therefore almost identical to those of the straight bar from which the triangle are bent (Rossing [15.213, Sect. 7.6]). However, for flexural vibrations in the plane, there is a major discontinuity in impedance at each bend, because the transverse vibrations within one arm couple strongly to longitudinal vibrations in the adjacent arms. Hence each arm will support its own vibrational modes, which will be coupled to form sets of normal-mode triplets, since each arm is of similar length.

Figure 15.125 illustrates the envelope and 50 ms FFTs of the initial waveform and after 1 s, illustrating the very well-defined and only weakly attenuated high-

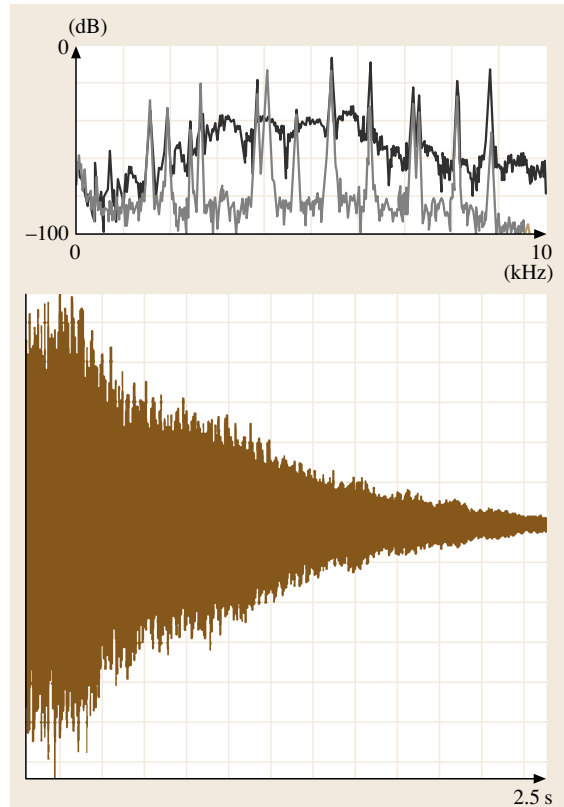


Fig. 15.125 The decaying waveform and FFT spectra at the start (*upper trace*) and after 1 s (*lower trace*) of a struck triangle note


frequency modes of the triangle. Note the wide-band spectrum at the start of the note from the initial impact with the metal beater.

Chimes and Tubular Bells

We include orchestral chimes and bells in this section because their acoustically important vibrations are flexural modes, just like those of a xylophone or triangle. The radius of gyration of a thin-walled cylindrical tube of radius a is $\approx a/\sqrt{2}$. The frequency of the lowest flexural modes is then be given by $f_n \approx a\sqrt{E/2\rho}(2n+1)^2\pi/8L^2$.

Orchestral chimes are generally fabricated from lengths of 32–38 mm-diameter thin-walled tubing, with the striking end often plugged by a solid mass of brass with an overhanging lip, which provides a convenient striking point.

Fletcher and Rossing [15.5, Sect. 19.8] note that the perceived pitch of tubular bells is determined by the

frequencies of the higher modes, excited with frequencies proportional to 9^2 , 11^2 , and 13^2 , in the approximate ratios 2 : 3 : 4. The pitch should therefore sound an octave below the lowest of these. Readers can make their own judgement from audio  EXTRAS, which compares the rather realistic sound of a tubular bell synthesised from the first six equal amplitude modes of an ideal bar sounded together, followed by the 9^2 , 11^2 , and 13^2 modes in combination, and then by a pure tone an octave below the 9^2 partial. Such comparisons highlight the problem of subjective pitch perception in any sound involving a combination of inharmonic partials.

15.4.3 Plates

Flexural Vibrations

This section describes the acoustics of plates, cymbals and gongs, which involve the two-dimensional flexural vibrations of thin plates described by the two-dimensional version of (15.149). Unlike stringed instruments, we can usually assume that the plates of percussion instruments are isotropic. Well away from any edges or other perturbing effects such as slots or added masses, the standing-wave solutions at high frequencies will be simple sinusoids. However, close to the free edges, and across the whole plate at low frequencies, contributions from the exponentially decaying solutions will be equally important over a distance $\approx (E/12\rho(1-\nu^2))^{1/4}(h/\omega)^{1/2}$. The nodes of the sinusoidal wave contributions will be displaced a distance $\approx 1/4\lambda$ from the edges. Hence, the higher frequency modes of a freely supported rectangular plate of length a , width b and thickness h will be given, to a first approximation, by

$$\omega_{mn} \approx h \left(\frac{E}{12\rho(1-\nu^2)} \right)^{1/4} \pi^2 \times \left[\left(\frac{m+1/2}{a} \right)^2 + \left(\frac{n+1/2}{b} \right)^2 \right]. \quad (15.152)$$

A musical instrument based on the free vibrations of a thin rectangular metal plate is the thunder plate, which when shaken excites a very wide range of closely spaced modes, which can mimic the sharp clap followed by the rolling sound of thunder in the clouds.

Before the age of digital sound processing, such plates were often used in radio and recording companies to add artificial reverberation to the recorded sound. The plate was suspended in a chamber along with a loudspeaker and pick-up microphone. The sound to which

reverberation was to be added was played through the loudspeaker, which excited the weakly damped vibrational modes of the plate, which were then re-recorded using the microphone to give the added reverberant sound. As described earlier (Sect. 15.2.4), the density of vibrational modes of a flat plate of area A and thickness h is given by $1.75A/c_L h$. This can be very high for a large-area thin metal sheet, giving a reverberant response with a fairly uniform frequency response.

Most percussion instruments which involve the flexural vibrations of thin sheets are axially symmetric, such as cymbals, gongs of many forms, and the vibrating plate regions of steeldrums or pans used in Caribbean steelbands. Such instruments have many interesting acoustical properties, many derived from highly nonlinear effects when the instrument is struck strongly.

The displacements of the flexural modes of an axially symmetric thin plate in polar coordinates are given by

$$z(r, \phi, t) = [AJ_m(k_{mn}r) + BI_m(k_{mn}r)] \times [C \cos(m\phi) + D \sin(m\phi)] e^{i\omega_{mn}t}, \quad (15.153)$$

where $J_m(kr)$ and $I_m(kr)$ are ordinary and hyperbolic Bessel functions, the equivalent of the sinusoidally varying and exponentially damped \sinh and \cosh functions used to describe flexural waves in a rectangular geometry. The hyperbolic Bessel functions are important near the edges of a plate or at any perturbation, but decay over a length scale of $\approx k_{mn}^{-1}$. The values of k_{mn} are determined from the boundary conditions, in just the same way as considered earlier for rectangular plates.

The first six vibrational modes for circular plates with free, hinged and clamped outside edges are shown in Fig. 15.126, with frequencies expressed as a ratio relative to that of the fundamental mode (*Fletcher and Rossing* [15.5, Sect. 3.6]). In each case, for large values of m and n , the frequency is given by the empirical Chladni's Law (1802),

$$\omega_{mn} \approx \sqrt{\frac{E}{12\rho(1-\sigma^2)}} \frac{\pi^2 h}{4a^2} (m+2n)^2, \quad (15.154)$$

justified much later by *Rayleigh* [15.3, Vol. 1, Chap. 10]. For arched plates, *Rossing* [15.214] showed that the frequencies are more closely proportional to $(m+bn)^p$, where p is somewhat less than 2 and b is in the range 2–4.

All the axially symmetric modes involving nodal diameters are doubly degenerate, with a complementary

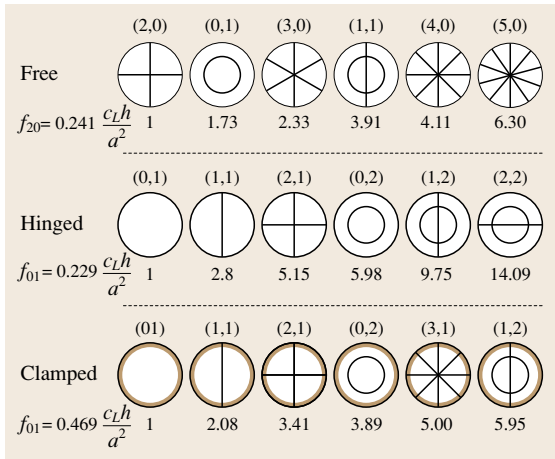


Fig. 15.126 The vibrational modes of circular plates with free, hinged and clamped outer edges, with the lowest frequencies and ratio of frequencies of higher modes indicated

solution with nodal diameters bisecting those drawn in Fig. 15.126. Any perturbation of the structure from cylindrical symmetry will split the degeneracy of such modes. Modes with a nodal diameter passing through the point at which the plate is struck will not be excited.

Instruments like the cymbal are slightly curved over their major surfaces but with a sudden break to a more strongly arched central section, to which the leather holding straps or support stand are attached. The outer edges can therefore be treated as free surfaces with the transition to the central cupped region providing an additional internal boundary condition, which will be intermediate between clamped and hinged. In contrast, gongs tend to have a relatively flat surface but with their edges turned through a right angle to form a cylindrical outer rim. The rim will add mass to the modes involving a significant radial displacement at the edge, but will also increase the rigidity of any mode having an azimuthal dependence. Thus, although the modes of an ideal circular plate provide a guide to modal frequencies and waveforms, we would expect significant deviations in modal frequencies for real percussion instruments. Any sudden change in plate profile on a length scale smaller than an acoustic wavelength will involve a strong coupling between the transverse flexural and longitudinal waves resulting in reflections from the discontinuity in acoustic impedance. This is why, for example, the indented region on the surface of a steeldrum pan can support localised standing waves on the indented regions. Indented areas of different sizes

can then be used to produce a wide range of different notes on a single drum head with relatively little leakage in vibrations between them.

Nonlinear Effects

Figure 15.127 illustrates the cross section of some typical axially symmetric cymbals, gongs and a steelpan. Nonlinear effects in such instruments can be important when excited at large amplitudes. Such effects are particularly marked for gongs with relatively thin plates. For Chinese opera gongs, the nonlinearity can result in dramatic upward or downward changes in the pitch of the sound after striking. In addition, nonlinearity results in mode conversion, with the high-frequency content of cymbal and large gong sounds increasing with time, giving a characteristic *shimmer* to the sound quality.

The shape dependence of the nonlinearity arises from the arching of the plate. For the lowest mode of a flat plate, the potential energy initially increases quadratically with displacement, though the energy increases more rapidly at large-amplitude excursions from stretching, as indicated schematically in Fig. 15.128a. Although the energy of an arched plate initially also increases quadratically with distance about its displaced equilibrium position, the energy will first increase then decrease when the plate is pushed through the central plane, (Fig. 15.128b). If the plate were to be pushed downwards with increasing force, it would suddenly spring to a new equilibrium position displaced about the central plane by the same initial displacement, but in the opposite direction. In combination with a Helmholtz radiator, this is indeed how some insects such as cicadas generate such strong acoustic signals – as high as 1 mW at 3 kHz (see Chap. 19 by Neville Fletcher). The nonlinear bistable flexing of a belled-out plate can be

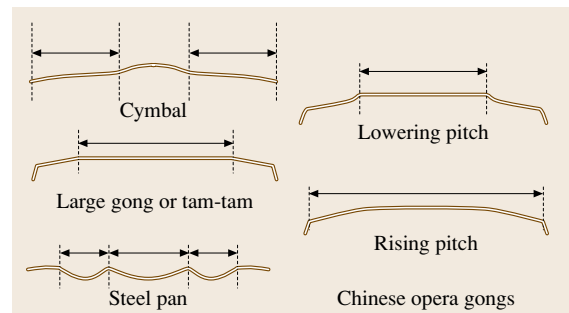


Fig. 15.127 Schematic cross sections of axially symmetric plate instruments and a steelpan, with arrows indicating the principal areas producing sound

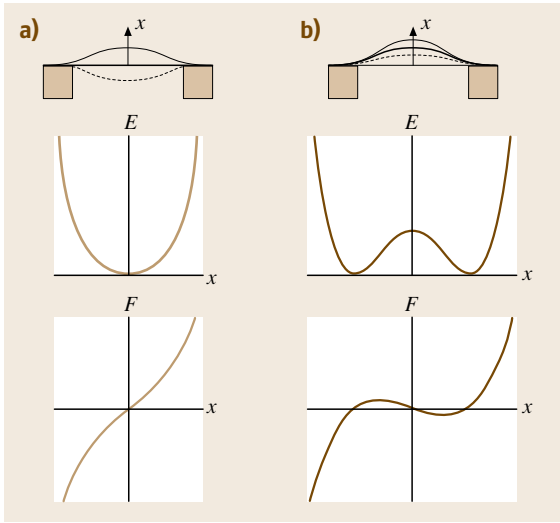


Fig. 15.128a,b Potential energy and restoring force of (a) a clamped flat and (b) arched circular plate as a function of displacement from the central plane

disastrous, turning a cheap pair of thin cymbals inside out, when crashed together too strongly.

The central peak in potential energy of an arched plate, like the gently domed Chinese gong illustrated in Fig. 15.127, therefore leads to a reduced restoring force for large-amplitude vibrations and a lower pitch. In contrast, the restoring force of a flat plate, like the central playing region of the upper of the two Chinese gongs, increases with vibration amplitude. This arises from the additional potential energy involved in stretching the plate, in just the same way as we considered earlier for the large-amplitude vibrations of a stretched string.

For a flat plate of thickness h , Fletcher [15.215] has shown that the increase in frequency of the lowest axisymmetric mode increases with the amplitude of vibration a approximately as

$$\omega \approx \omega_0 \left[1 + 0.16 \left(\frac{a}{h} \right)^2 \right]. \quad (15.155)$$

The nonlinearity also generates additional components at three times the frequency of any initial modes present and at multiples of any new modes excited. In addition it produces cross-modulation products when more than one mode is present. For example, for modes with frequencies f_1 and f_2 initially present, the nonlinearity will generate inter-modulation products at $2f_1 \pm f_2$ and $2f_2 \pm f_1$.

Grossmann et al. [15.216] and Fletcher [15.215] have considered the vibrations of a spherical-cap shell

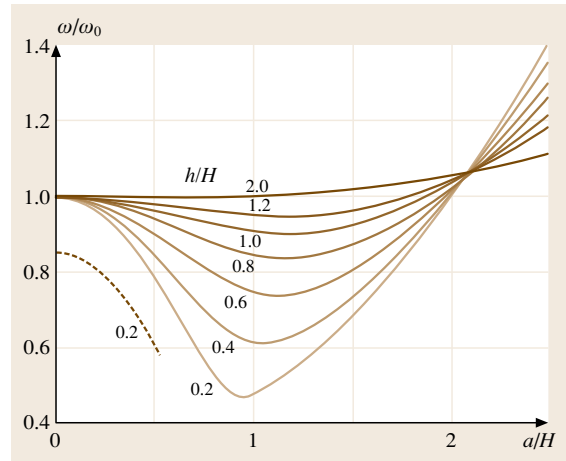


Fig. 15.129 Vibration amplitude dependence of frequency of lowest axisymmetric mode of a spherical cap of dome height H as a function of thickness h to H ratio

of height H and thickness h . Interestingly, the change in frequency of the asymmetric vibrations about the equilibrium point depends only on the ratio of the amplitude to the arching height, a/H , as illustrated in Fig. 15.129. When the height of the dome is much less than the thickness, the frequency increases approximately as a^2 , as expected from the induced increase in tension with amplitude. However, when the arching becomes comparable with and greater than the thickness, the asymmetry of the potential energy dominates the dynamics and results in an initial decrease in frequency, which increases strongly with the ratio of arching height to thickness. At very large amplitude, $a \gg H$, the frequency is dominated by the increase in tension and therefore again increases with amplitude like a flat plate. At large amplitudes, Legge and Fletcher [15.217] have shown that changes in the curvature of the plate profile result in a large transfer of energy to the higher-frequency plate modes.

We now show how many of the above properties relate to the sounds of cymbals, gongs of various types and steelpan.

Cymbals

Many types of cymbals are used in the classical symphony orchestra, marching bands and jazz groups. They are normally made of bronze and have a diameter of 20–70 cm. The low-frequency modes of a cymbal are very similar to those of a flat circular plate and can be described using the same (mn) mode nomenclature (Fletcher and Rossing [15.5, Fig. 20.2]). However,

small changes in curvature across a cymbal will result in modes that are linear combinations of ideal circular-plate modes.

Cymbals are usually played by striking with a wooden stick or soft beater or a pair can be crashed together, each method producing a distinctive sound. They can even be played by bowing with a heavy rosined bow against the outer rim. Rossing and Shepherd showed that the characteristic 60 dB decay time of the excited modes of a large cymbal varies approximately inversely proportional with frequency, with a typical decay time for the lowest (20) mode as long as 300 s (Fletcher and Rossing [15.5, Fig. 20.5])

Figure 15.130 shows the waveform envelope and spectra of the initial sound of a cymbal crash and after 1 s. Audio [EXTRAS](#) illustrates a recorded cymbal crash followed by the same sound played first through a 0–1 kHz and then a 1–10 kHz band-pass filter, illustrating the decay of the low- and high-frequency wide-band noise.

When a cymbal is excited with a drumstick, waves travel out from the excitation point with a dispersive group velocity proportional to k , inversely proportional to the dimensions of the initial flexural indentation of the surface made by the drumstick. The dispersive pulse strikes and is reflected from the edges of the cymbal and the transitional region to the central curved cup, so

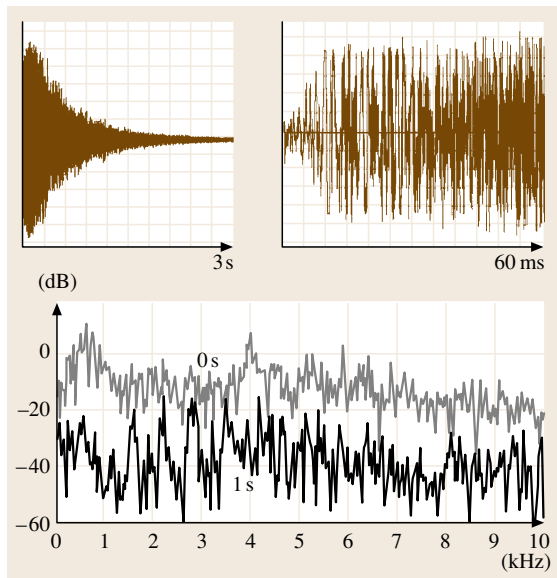


Fig. 15.130 Wave envelope and spectrum at start and after 1 s of a cymbal crash illustrating wide-band noise at all times

that eventually the energy will be dispersed across the whole vibrating surface. This has been investigated using pulsed video holography by Schedin et al. [15.218]. On reflection there will also be considerable mixing of modes. In addition, because the plates are rather thin and are often hit extremely strongly, nonlinear effects are important. On large cylindrical plates this results in the continuous transfer of energy from strongly excited low-frequency modes to higher modes. Many of the nonlinear effects can be investigated in the laboratory using sinusoidal excitation. Measurements by Legge and Fletcher [15.217] have revealed a wide range of nonlinear effects including the generation of harmonic, bifurcations and even chaotic behaviours at large intensities.

When a plate is struck by a beater, the acoustic energy is distributed across a very wide spectrum of closely spaced resonances of the plate. To distinguish individual partials requires the sound to be sampled over a time of at least $\approx 1/\Delta f$, where Δf is the separation of the modes at the frequencies of interest. However, because the modes of a large cymbal are so closely spaced, the times involved can be rather long. Unlike the sound of pitched instruments such as the glockenspiel and xylophone, there are no particular resonances of the cymbal that dominate the sound, which is characterised instead by the *sizzle* produced by the very wide spectrum of very closely spaced resonances almost indistinguishable from wide-band high-frequency noise.

Large Gongs and Tam-Tams

Gongs are also very ancient instruments, which have a very characteristic sound when strongly struck by a soft beater, notably as a prelude to classic films by the Rank organisation. A typical tam-tam gong used in a symphony is a metre or even larger in diameter. It is made of bronze and, like cymbals, is sufficiently ductile not to shatter when strongly hit. The damping is very low, so the sound of large gongs can persist for very long times.

When initially struck strongly by a soft beater, the initial sound is largely associated with the lower-frequency partials that are strongly excited. However, on a time scale of a second or so, the sound can appear to grow in intensity, as nonlinear effects transfer energy from lower- to higher-frequency modes (audio [EXTRAS](#)). This is illustrated in Fig. 15.131 (Fletcher and Rossing [15.5, Fig. 20.8]), which shows the build up and subsequent decay of acoustic energy in the higher-frequency bands at considerable times after the initial impact. The fluctuations in intensity within these bands were taken as evidence for chaotic behaviour. How-

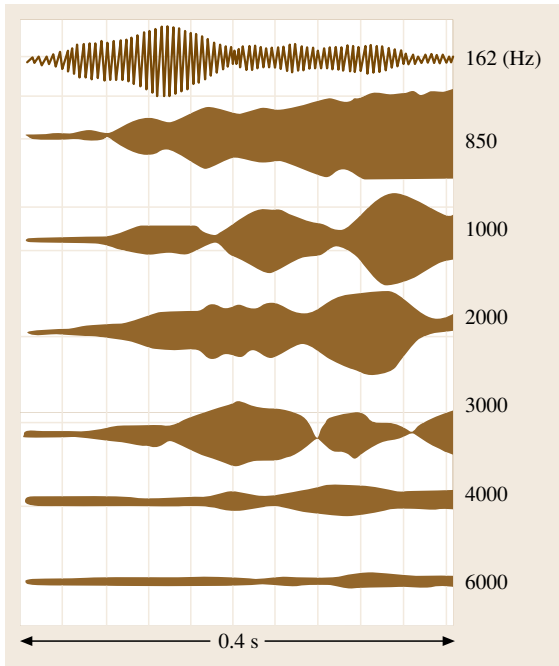



Fig. 15.131 Buildup and decay in intensity of a struck tam-tam sound in frequency bands centred on the indicated frequencies (after *Fletcher and Rossing* [15.5])

ever, even in a linear system, interference between the large number of very closely spaced inharmonic partials would also result in apparently random fluctuations in amplitude.

Chinese Opera Gongs

Chinese gongs provide the most dramatic illustration of nonlinearity in percussion instruments, with upwards or downwards pitch glides of several semitones over a sizeable fraction of a second after being strongly struck. The direction of the pitch *glide* depends on the profile of the vibrating surface as previously described.

Figure 15.132 shows the decaying waveforms of the sound of three Chinese gongs with a downward pitch glide (audio  **EXTRAS**) played in succession. The initial spectrum of the third note played is followed by spectra at 0.75 s and 1.5 s after striking, illustrating the transfer of energy to lower-frequency modes. The much broader width of the initial spectrum reflects the decrease in lifetime of the initial modes struck resulting from the nonlinear loss of energy to higher-frequency modes. The two well-defined peaks between the two major peaks are from the long-ringing principal partials of the first two gongs.

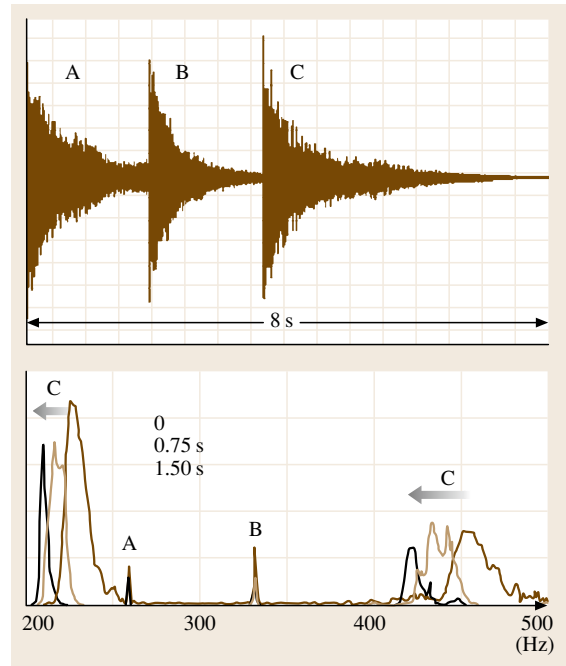


Fig. 15.132 The wave envelope of sounds from three downward-sliding Chinese gongs followed by the spectrum of the third gong at the start, after 0.75 and 1.5 s illustrating the nonlinear frequency shifts

Steelpans

Finally, in this section on percussion instruments based on vibrating plates, we consider steelpans originating from the Caribbean, which were initially fabricated by indenting the top of oil cans left on the beaches by the British navy after World War II. They have become a immensely popular instrument in that part of the world and are just as interesting from a musical acoustics viewpoint (see *Fletcher and Rossing* [15.5, Sect. 20.7] for further details).

Pitched notes on a given drum are produced by hammered indentations of different sizes on the top face of the drum. Different ranges of notes are produced by drums or pans of different sizes (e.g. lead tenor, double tenor, alto, cello and bass). Typical indented regions on a double-tenor steelpan are shown in Fig. 15.133, adapted from drawings for a full set of pans in *Fletcher and Rossing* [15.5, Fig. 20.17]. The various indented areas on the drum head can be considered as an array of relatively weakly coupled resonators. An individual indented area on an infinite sheet would have very similar acoustic modes as those of a hemispherical cap indented in an infinite

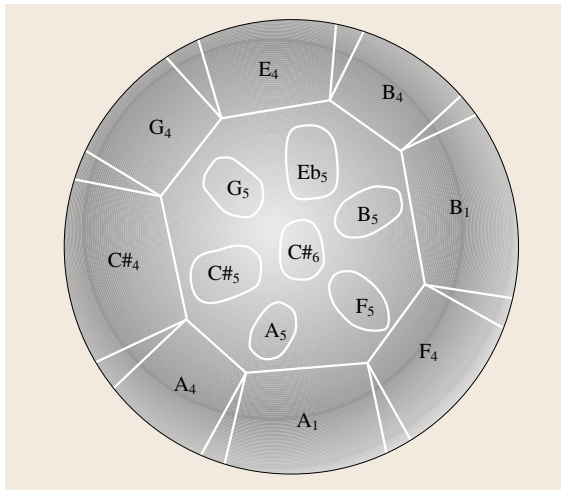


Fig. 15.133 Typical indentation areas in a tenor steelpan (after Fletcher and Rossing [15.5])

plate. The frequency of the modes would be determined by the size and arching of the indented areas. The effective cap size would be defined by the rate of change of the curvature of the plate and the associated change in the acoustic impedance at the edge of the indented region. However, all such regions on a steelpan will be coupled together by the relatively weak transfer of acoustic energy between them, to form a set of coupled modes. Hitting one particular region will therefore excite other regions, especially those that have closely matching partials. The coupling between

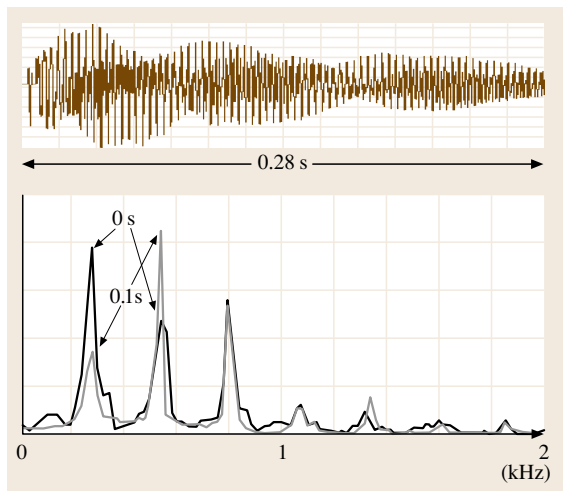


Fig. 15.134 Waveform and initial and time-delayed spectra of the note C#4 on a steel drum

such regions has been investigated holographically by Rossing [15.202, Fig. 20.20].

Audio 137 **EXTRAS** illustrates a succession of notes played on a steel drum. Figure 15.134 shows a typical decaying waveform with initial and time-delayed spectra of a single note. A relatively large number of well-defined modes can easily be identified. However, the subjective absolute pitch of the note is not particularly well defined and there is a strong sense of pitch circularity in the sound of an ascending scale (Sect. 15.1.3 and audio 137 **EXTRAS**), sometimes making it difficult to identify the octave to which a particular note should be attributed. Note the *increase* in the amplitude of the second partial with time, which could result from nonlinear effects in such thin-walled structures, or possibly from interference beats between degenerate modes split in frequency by the lack of axial symmetry of the hand-beaten indentations.

15.4.4 Shells

Blocks and Bells

Finally, we consider the acoustics of three-dimensional shell-like structures. This could include percussion instruments such as the wooden-block and hollow gourd instruments like the maracas. However, the physics of such instruments is essentially the same as that of the soundbox of stringed instruments and involves little of additional acoustic interest. In this section, we will therefore concentrate on the acoustics of bell-like structures, which are usually axially symmetric structures, closed at one end, and of variable thickness and radius along their length. We will also consider nonaxisymmetric bells with a quasi-elliptical cross section, which produce two different pitched notes, depending on where the bell is struck. All such structures have a rich spectrum of modes, which are generally tuned to give long-ringing notes with a well-defined sense of pitch. The bronze used in their construction is typically an alloy of 80% copper and 20% tin and has to be sufficiently ductile not to crack under the impact of the beater or clapper. Metallurgical treatment is required to produce a grain structure producing little damping at acoustic frequencies.

Some of the oldest bells are to be found in China. Such bells are supreme examples of the art of bronze casting dating to the fifth century BC. Bells in church towers have traditionally marked the passage of time, while peals of bells with internal swinging clappers continue to summon the faithful to worship. In more recent times, carillons with up to 77 tuned bells have been

developed to play keyboard music from the top of specially constructed bell towers, notably in the centres of Dutch and American towns and college campuses. Bells come in all sorts of shapes and sizes ranging from small hand bells to the giant church bells on display inside the Kremlin walls. However, the acoustics of all bells is essentially the same, so no attempt will be made to provide a comprehensive coverage of every type (for such information, see *Fletcher* and *Rossing* [15.5, Chap. 21] and *Rossing* [15.202]).

Bell modes can be related to the longitudinal, torsional and flexural modes of a cylindrical disc that is axially deformed into a bell-shaped domed structure. Although the modal frequencies will clearly be strongly perturbed by such a transformation, the modal shapes will remain unchanged, as illustrated in Fig. 15.135, where m represents the number of radial nodal lines and n the number of nodal circles between the (fixed) centre and free edge.

The first example in Fig. 15.135 illustrates the rim displacements of the $(0, n)$ extensional modes. Although such *breathing* modes would be efficient sound radiators the energy involved in stretching the surfaces of the bell leads to very high modal frequencies, so that such modes are not strongly excited. Likewise, the torsional $(0, n)$ -modes involve no motion perpendicular to the bell surfaces, and therefore generate a negligible amount of sound. With the bell rigidly supported at its top, the $m = 1$ swinging modes again involve large elastic strains and cannot be strongly excited. The first modes to produce a significant amount of sound are therefore the $m = 2$ and above flexural modes, which involve the transverse motions of the outer edges with negligible extension in circumferential length for small amplitude vibrations. When the wavelength of the flexural waves is much smaller than the overall curvature, the vibrational modes will be closely related to the flex-

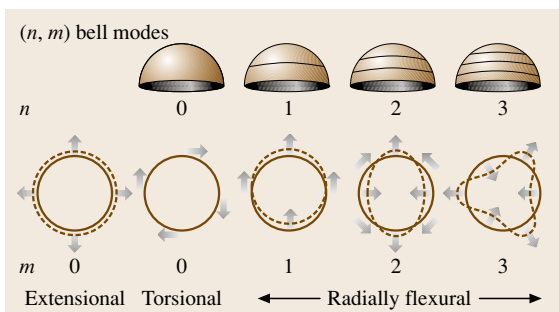


Fig. 15.135 Nomenclature of the (m, n) modes of a bell illustrating displacements of rim for given m -values

ural waves of a circular disc, with frequencies satisfying Chladni's generalised empirical law, $f_{mn} \approx c(m + 2n)^p$, as confirmed by *Perrin* et al. [15.219].

The flexural modes involve radial displacements proportional to $\cos(m\phi)$. Continuity requires that there must also be a tangential displacement, such that $u + \partial v / \partial \phi = 0$, where u and v are the radial and tangential velocities respectively. Coupling to the tangential motion explains why it is possible to feed energy into a vibrating wine glass or the individual glass resonators of a glass harmonica (*Rossing* [15.202, Chap. 14]), by rubbing a wetted finger around the rim. The excitation is very similar to the slip-stick mechanism used to excite the bowed string (Sect. 15.2.4).

Figure 15.136 illustrates a set of holographic measurements by *Rossing* [15.202, Fig. 12.4], which is typical of most bell shapes. The $(m, 1)$ and $(m, 2)$ modes can immediately be related to the (m, n) modes of a cupped disc. However, there is a distinct change in character for $n > 0$, with an additional node appearing close to the rim – referred to as a $(m, 1\#)$ mode. Some insight is provided by the finite element solutions for a typical large English church bell illustrated in Fig. 15.137 [15.220]. The three modes illustrated are very similar to the $(3, 0)$, $(3, 1)$ and $(3, 2)$ modes expected from the simple cupped disc model, except for the lowest frequency $(3, 0)$ mode, in which the top surfaces of the bell move in antiphase with the rim, to

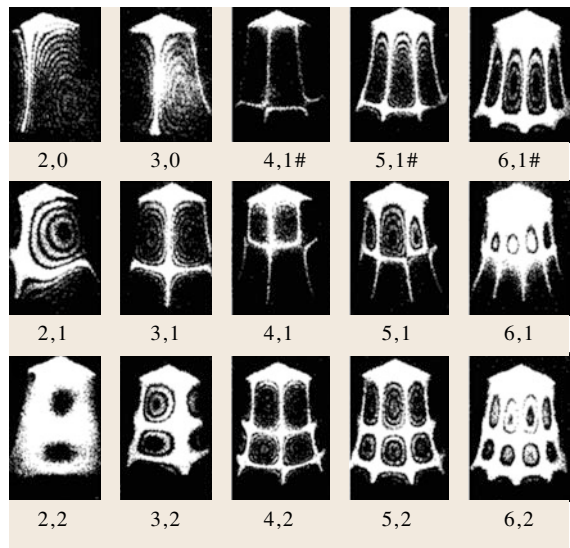


Fig. 15.136 Holographic interferograms and nomenclature for vibrational modes of a hand bell (after *Rossing* [15.202])

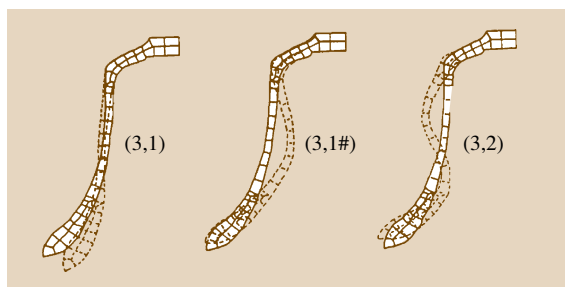


Fig. 15.137 Finite-element solutions for the lowest-order $m = 3$ modes of an English church bell (after Perrin et al. [15.221]) illustrating the (3,1), (3,1#) and (3,2) modes

give a nodal line about half-way along the length. Similarly, the anticipated (4, 0), (5, 0) and (6, 0) modes of the handbell investigated by Rossing [15.202] acquire an additional nodal line close to the end rim denoted as (4, 1#), (5, 1#) and (6, #) modes. Such features can generally only be accounted for by detailed computational analysis.

Bell Tuning

Figure 15.138 shows the frequencies and associated modes of a well-tuned traditional church bell (Rossing and Perrin [15.222]), ordered into groups based on mode shapes, which enable correlations to be made between bells of different shapes and sizes.

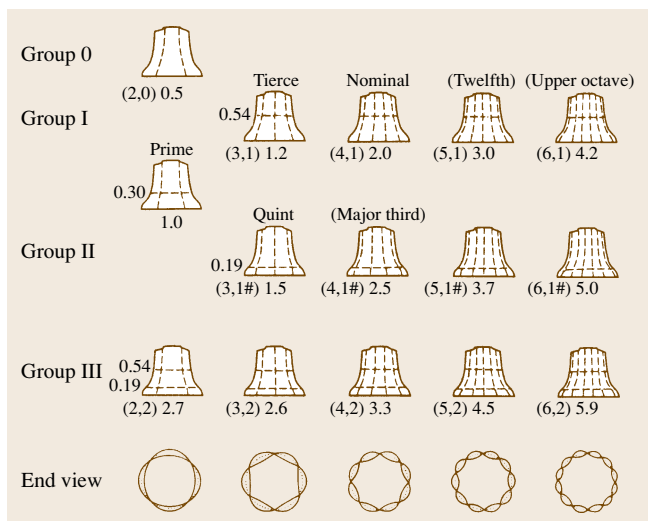


Fig. 15.138 Measured frequencies for a typical D5 church bell, indicating the relative frequencies of the observed mode, with the traditional names associated with such modes indicated (after Rossing and Perrin [15.222])

Fine-quality bells are carefully tuned by the bell maker, so that the lowest modes have harmonically related frequencies, thereby achieving a well-defined sense of pitch. This is achieved by selective thinning of the thickness of the bell on a very large lathe after its initial casting. In an ideally tuned bell, the principal modes are designated as the hum (2,0) mode, an octave below the prime or fundamental (2,1#) mode. A minor third above the prime (ratio 5:4) is the tierce (3,1) mode, a perfect fifth above that (ratio 3:2) is the quint or fifth (3,1#) mode, and an octave above is the nominal (4,1) mode. Fletcher and Rossing [15.5, Table 21.1] compare these and higher modes with measured values for a particular bell.

The art of tuning the partials of bells to achieve a well-sounding note was initially developed in the seventeenth century in the low countries (what is now Holland and the northern parts of Germany and France). Many fine bells from this period by François and Pieter Hemony are still in use in carillons today (Rossing [15.202]). However, the art of bell tuning then appears to have been lost until the end of the 19th century, when it was rediscovered by Canon Arthur Simpson in England, following Lord Rayleigh's pioneering research on the sound of bells [15.3, Vol. 1, Sect. 235].

Acoustic Radiation

The strongest-sounding partials of most bells are the group I ($m,1$) modes, with a nodal circle approximately halfway up the bell (Fletcher and Rossing [15.5, Sect. 21.11]). Such modes have $2m$ antinodal areas providing spatially alternating sound sources in anti-phase. The radiation efficiency of such modes increases rapidly with size of bell and frequency. If the acoustic wavelength is much larger than the separation of such antinodes, the sound from such sources will tend to cancel out. However, above a crossover frequency, such that the velocity of sound is equal to that of the flexural waves on the surface of the bell, $v_{\text{flex}} = \sqrt{1.8c_L h f}$, the spacing between the antinodes will exceed the wavelength in air and the modes will radiate more efficiently. For large church bells, this condition is satisfied for almost all but the very lowest partials, so almost all partials radiate sound rather efficiently. In contrast, hand bells with rather thin walls are significantly less efficient. There is also a small intensity of sound radiated axially at double the modal frequencies, from the induced fluctuations in the volume of air enclosed within the bell.

When a bell is struck, usually by a cast or wrought-iron, ball-shaped, clapper, the first sound heard, the

strike note, contains contributions from the very large range of largely inharmonic partials of the bell. Nevertheless the listener can usually identify a pitch to the initial note, determined by the prominent partials excited. However, it is not always easy to attribute the pitch of a note to a particular octave, which is a common feature of many struck percussion instruments (e.g. notes on a xylophone, steeldrum and even timpani). The pitch of the strike note appears to be determined principally by the excited partials with frequencies in the ratios 2:3:4. The ear attributes the pitch to be that of the missing fundamental an octave below the lowest of the partials principally excited, which does not necessarily correspond to the pitch of the lowest partial excited, unless the bell is well tuned.

The majority of the higher partials decay rather quickly, with the long-term sound dominated by the hum note. For a 70 cm church bell, *Perrin et al.* [15.219] measured T_{60} decay times of 52 s for the (2,0) hum mode, 16 s for the (2,1#) and (3,1) prime and minor third modes, 6 s for the (4,1) octave and 3 s for the (4,1#) upper major third, with progressively shorter decay times for the higher modes. Audio [139](#) **EXTRAS** illustrates the synthesised sound of the above harmonic modes excited with equal amplitudes. This is followed by a synthesised bell with a major rather than a minor third partial. Such a bell has recently been realised (1999) based on **FEA** studies at the Technical University in Eindhoven in collaboration with the Eijsbouts Bell foundry. It produces a less mournful sound when played in the major scale music in a carillon. In both cases the synthesised sound reproduces the gentle sound of a bell rather well, though it lacks the initial clang that results from the higher-frequency inharmonic modes of a real bell.

As an example of the waveform and spectrum of a large bell, in Fig. 15.139 and audio signal [139](#) **EXTRAS**, we illustrate the sound and rich spectrum of partials of one of the most famous large bells in the world, Big Ben, hung high above the Houses of Parliament in London. This bell is broadcast each day following the Westminster Chimes, marking the hours and end of broadcasting on the BBC each night for UK listeners.

Non-Axial Symmetry

Bell modes with $m > 1$ are doubly degenerate with orthogonal modes varying as $\cos m\phi$ and $\sin m\phi$ and nodal lines in the azimuthal directions that bisect each other. Any departures from axial symmetry will lift the degeneracy and give rise to a split pair of orthogonal modes. If both modes are excited together, the two fre-

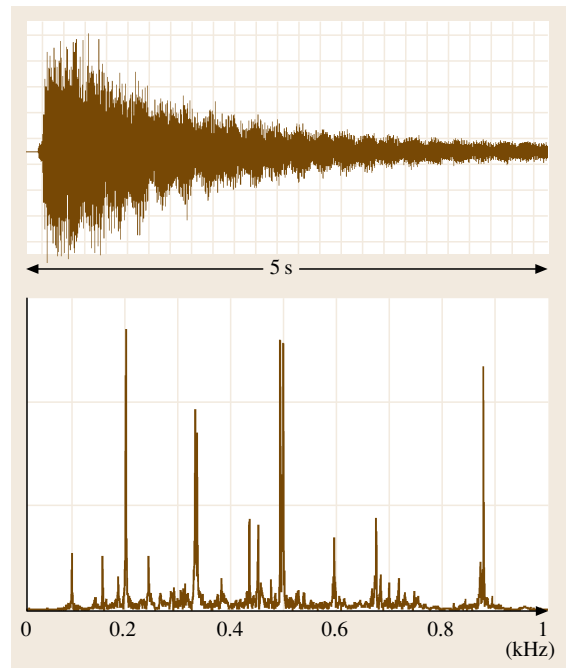


Fig. 15.139 Decaying vibrations and spectrum of Big Ben, London

quencies will beat against each other, as already evident in the sound of Big Ben and in the sound ([139](#) **EXTRAS**) of a slightly asymmetrical glass beaker with a pouring spout, which lifts the degeneracy of the otherwise axially symmetric modes.

Bells with strongly distorted or elliptical cross sections can have two completely different pitches, which can be sounded independently by beating at the antinodal positions of one set of modes and nodes of the other. Drums with quasi-elliptical cross sections will therefore sound a single note when struck at the narrowest and widest cross-sectional radii, and a second note, when struck at appropriate positions in between.

A dramatic example of axially asymmetric bells is provided by the 65 ancient bells from the tomb of Zeng Hou Yi found at Sui Xiang from around 433 BC. These bells from the second millennium BC are masterpieces of Chinese art and bell casting. They have oval cross sections and range from small hand bells to well over 1.5 m in height. When struck at different positions along the flattened surfaces, two quite distinct tones can be excited, which were designed to be about a major or minor third apart. For further details of these and other Chinese and other eastern bells see *Rossing* [15.202, Chap. 13] and [15.223].

References

- 15.1 T. Levenson: *Measure for Measure: How Music and Science together have explored the Universe* (Oxford Univ. Press, Oxford 1997)
- 15.2 S. Hawkins (Ed.): *On the Shoulders of Giants* (Running, Philadelphia 2002)
- 15.3 Lord Rayleigh: *The Theory of Sound: I and II (1896)*, 2nd edn. (Dover, New York 1945), Reprint
- 15.4 S. Hawkins: *The Universe in a Nutshell* (Bantam, London 2001)
- 15.5 N.H. Fletcher, T.D. Rossing: *The Physics of Musical Instruments*, 2nd edn. (Springer, New York, Berlin 1998)
- 15.6 T.D. Rossing, F.R. Moore, P.A. Wheeler: *The Science of Sound*, 3rd edn. (Addison Wesley, San Francisco 2002)
- 15.7 D.M. Campbell, A. Myers, C.A. Greated: *Musical Instruments: History, Technology and Performance of Instruments of Western Music* (Oxford Univ. Press, Oxford 2006)
- 15.8 G. Bissinger: Contemporary generalised normal mode violin acoustics, *Acustica* **90**, 590–599 (2004)
- 15.9 A. Hirschberg, J. Gilbert, R. Msallam, A.P.J. Wijnands: Shock waves in trombones, *J. Acoust. Soc. Am.* **99**, 1754–1758 (1996)
- 15.10 T.J.W. Hill, B.E. Richardson, S.J. Richardson: Modal radiation from classical guitars: Experimental measurements and theoretical predictions, *Proc. SMAC 03* (KTH, Stockholm 2003) pp. 129–132
- 15.11 L. Cremer: *The Physics of the Violin* (MIT Press, Mass 1984), section 11.2
- 15.12 B. Britten: *Serenade for Tenor, Horn and Strings* (Hawkes & Son, London 1944)
- 15.13 J.M. Barbour: *Tuning and Temperament* (Michigan State College Press, East Lansing 1953)
- 15.14 National Instruments: *Windowing: Optimizing FFTs Using Windowing Functions* (National Instruments, Austin 2006), available online at <http://zone.ni.com/devzone/conceptd.nsf/>
- 15.15 M.-P. Verge, A. Hirschberg: Turbulence noise in flue instruments, *Proc. Int. Symp. Mus. Acoust.* (IRCAM, Paris 1995) pp. 94–99
- 15.16 M.E. McIntyre, R.T. Schumacher, J. Woodhouse: Aperiodicity in bowed-string motion: On the differential slipping mechanism, *Acustica* **49**, 13–32 (1981)
- 15.17 J. Meyer: Zur klanglichen Wirkung des Streicher-Vibratos, *Acustica* **76**, 283–291 (1992)
- 15.18 C.E. Gough: Measurement, modelling and synthesis of violin vibrato sounds, *Acta Acustica* **91**, 229–240 (2005)
- 15.19 E.I. Prame: Measurement of the vibrato rate of ten singers, *J. Acoust. Soc. Am.* **96**, 1979–1984 (1994)
- 15.20 J. Gilbert, L. Simon, J. Terroir: Vibrato in single reed instruments, *SMAC 03* (Royal Swedish Academy of Music, Stockholm 2003) pp. 271–273
- 15.21 D.W. Robinson, R.S. Dadson: A re-determination of the equal-loudness relations for pure tones, *Brit. J. Appl. Phys.* **7**, 166–181 (1956)
- 15.22 H.A. Fletcher, W.A. Munson: Loudness, its definition, measurement and calculation, *J. Acoust. Soc. Am.* **9**, 82–108 (1933)
- 15.23 B. Patterson: Musical dynamics, *Sci. Am.* **231**(5), 78–95 (1974)
- 15.24 B.C.J. Moore: *Psychology of Hearing* (Academic, London 1997)
- 15.25 A.J.M. Houtsma, T.D. Rossing, W.M. Wagenaars: *Auditory Demonstrations, Phillips compact disc 1126-061* (Acoust. Soc. Am., Sewickley 1989)
- 15.26 C.M. Hutchins (Ed.): *Musical Acoustics, Part I (Violin Family Components)*, Benchmark Papers in Acoustics, Vol. 5 (Dowden Hutchinson Ross, Stroudsburg 1975)
- 15.27 C.M. Hutchins (Ed.): *Musical Acoustics, Part II (Violin Family Functions)*, Benchmark Papers in Acoustics, Vol. 6 (Dowden Hutchinson Ross, Stroudsburg 1976)
- 15.28 C. Hutchins, V. Benade (Eds.): *Research Papers in Violin Acoustics 1975–1993, Vols. 1 and 2*, (Acoust. Soc. Am., Melville 1997)
- 15.29 CAS Newsletters (1994–1987), CAS Journals (1988–2004), www.catgutacoustical.org
- 15.30 L. Cremer: *The Physics of the Violin* (MIT Press, Cambridge 1984)
- 15.31 R. Midgley: *Musical Instruments of the World* (Paddington, New York 1978)
- 15.32 A. Baines: *European and American Musical Instruments* (Chancellor, London 1983)
- 15.33 G.G. Stokes: *On the Communication of Vibrations from a Vibrating Body to a Surrounding Gas* (Philos. Trans., London 1868)
- 15.34 C.E. Gough: The resonant response of a violin G-string and the excitation of the wolf-note, *Acustica* **44**(2), 673–684 (1980)
- 15.35 H.F. Helmholtz: *The Sensation of Tone (1877)*, translated by A.J. Ellis (Dover, New York 1954)
- 15.36 C.V. Raman: On the mechanical theory of the vibrations of bowed strings and of musical instruments of the violin family, with experimental verification of the results: Part 1, *Indian Assoc. Cultivation Sci. Bull.* **15**, 1–158 (1918)
- 15.37 J.C. Schelling: The bowed string and player, *J. Acoust. Soc. Am.* **9**, 91–98 (1973)
- 15.38 S. Thwaites, N.H. Fletcher: Some notes on the clavichord, *J. Acoust. Soc. Am.* **69**, 1476–1483 (1981)
- 15.39 D.E. Hall: Piano string excitation in the case of a small hammer mass, *J. Acoust. Soc. Am.* **79**, 141–147 (1986)
- 15.40 D.E. Hall: Piano string excitation II: General solution for a hard narrow hammer, *J. Acoust. Soc. Am.* **81**, 535–546 (1987)

- 15.41 D.E. Hall: Piano string excitation III: General solution for a soft narrow hammer, *J. Acoust. Soc. Am.* **81**, 547–555 (1987)
- 15.42 D.E. Hall: Piano string excitation IV: Non-linear modelling, *J. Acoust. Soc. Am.* **92**, 95–105 (1992)
- 15.43 P.M. Morse, K.U. Ingard: *Theoretical Acoustics* (McGraw-Hill, New York 1968), Reprinted by Princeton Univ. Press, Princeton 1986
- 15.44 H. Fletcher: Normal vibration frequencies of a stiff piano string, *J. Acoust. Soc. Am.* **36**, 203–209 (1964)
- 15.45 E.L. Kent: Influence of irregular patterns in the inharmonicity of piano-tone partials upon tuning practice, *Das Musikinstrument* **31**, 1008–1013 (1982)
- 15.46 N.C. Pickering: *The Bowed String* (Bowed Instruments, Southampton 1991)
- 15.47 N.C. Pickering: Physical properties of violin strings, *J. Catgut Soc.* **44**, 6–8 (1985), paper 21 in ref [15.42]
- 15.48 C. Vallette: The mechanics of vibrating strings. In: *Mechanics of musical instruments*, ed. by A. Hirschberg, J. Kergomard, G. Weinreich (Springer, Berlin, New York 1995) pp. 115–183
- 15.49 K. Legge, N.H. Fletcher: Nonlinear generation of missing modes on a vibrating string, *J. Acoust. Soc. Am.* **76**, 5–12 (1984)
- 15.50 J. Miles: Resonant non-planar motion of a stretched string, *J. Acoust. Soc. Am.* **75**, 1505–1510 (1984)
- 15.51 R.J. Hanson, J.M. Anderson, H.K. Macomber: Measurement of nonlinear effects in a driven vibrating wire, *J. Acoust. Soc. Am.* **96**, 1549–1556 (1994)
- 15.52 R.J. Hanson, H.K. Macomber, A.C. Morrison, M.A. Boucher: Primarily nonlinear effects observed in a driven asymmetrical vibrating wire, *J. Acoust. Soc. Am.* **117**, 400–412 (2005)
- 15.53 J.A. Elliot: Intrinsic nonlinear effects in vibrating strings, *Am. J. Phys.* **48**, 478–480 (1980)
- 15.54 C.E. Gough: The nonlinear free vibration of a damped elastic string, *J. Acoust. Soc. Am.* **75**, 1770–1776 (1984)
- 15.55 J. Woodhouse, P.M. Galluzzo: The bowed string as we know it today, *Acustica* **90**, 579–590 (2004)
- 15.56 F.A. Saunders: Recent work on violins, *J. Acoust. Soc. Am.* **25**, 491–498 (1953)
- 15.57 J.C. Schelling: The bowed string and the player, *J. Acoust. Soc. Am.* **53**, 26–41 (1973)
- 15.58 J.C. Schelling: The physics of the bowed string. In: *The Physics of Music*, ed. by C. Hutchins, Scientific American (W.H. Freeman, San Fransisco 1978)
- 15.59 R.T. Schumacher: Measurements of some parameters of bowing, *J. Acoust. Soc. Am.* **96**, 1985–1998 (1994)
- 15.60 F.G. Friedlander: On the oscillation of the bowed string, *Proc. Cambridge Phil. Soc.* **49**, 516–530 (1953)
- 15.61 M.E. McIntyre, J. Woodhouse: On the fundamentals of bowed string dynamics, *Acustica* **43**, 93–108 (1979)
- 15.62 J. Woodhouse: On the playability of violins, Part II: Minimum bow force and transients, *Acustica* **78**, 137–153 (1993)
- 15.63 M.E. McIntyre, R.T. Schumacher, J. Woodhouse: Aperiodicity in bowed-string motion: On the differential slipping mechanism, *Acustica* **49**, 13–32 (1981)
- 15.64 R.T. Schumacher: Oscillations of bowed strings, *J. Acoust. Soc. Am.* **43**, 109–120 (1979)
- 15.65 K. Guettler: On the creation of the Helmholtz motion in bowed strings, *Acustica* **88**, 2002 (2002)
- 15.66 J.H. Smith, J. Woodhouse: The tribology of rosin, *J. Mech. Phys. Solids* **48**, 1633–1681 (2000)
- 15.67 P.M. Galluzzo: On the Playability of Stringed Instruments. Ph.D. Thesis (Cambridge University, Cambridge 2003)
- 15.68 J. Woodhouse, R.T. Schumacher, S. Garoff: Reconstruction of bowing point friction force in a bowed string, *J. Acoust. Soc. Am.* **108**, 357–368 (2000)
- 15.69 J.H. Smith: *Stick-slip Vibration and its Constitutive Laws* (Cambridge University, Cambridge 1990)
- 15.70 J. Woodhouse: Bowed string simulation using a thermal friction model, *Acustica* **89**, 355–368 (2003)
- 15.71 W. Reinicke: *Dissertation, Institute for Technical Acoustics* (Technical University of Berlin, Berlin 1973)
- 15.72 W. Reinicke, L. Cremer: Application of holographic interferometry to the bodies of sting instruments, *J. Acoust. Soc. Am.* **48**, 988–992 (1970)
- 15.73 J. Woodhouse: data kindly provided for this chapter
- 15.74 E.V. Jansson: Admittance measurements of 25 high quality violins, *Acta Acustica* **83**, 337–341 (1997)
- 15.75 E.V. Jansson: Violin frequency response – bridge mobility and bridge feet distance, *Appl. Acoust.* **65**, 1197–1205 (2004)
- 15.76 H. Dünnewald: Ein erweitertes Verfahren zur objektiven Bestimmung der Klangqualität von Violinen, *Acustica* **71**, 269–276 (1990), reprinted in English as Deduction of objective quality parameters on old and new violins, *J. Catgut Acoust. Soc.* 2nd Ser. **1**(7) 1–5 (1991), included in Hutchins [15.28, Vol 1]
- 15.77 J. Woodhouse: On the “bridge hill” of the violin, *Acustica* **91**, 155–165 (2005)
- 15.78 J.A. Moral, E.V. Jansson: Eigenmodes, input admittance and the function of the violin, *Acustica* **50**, 329–337 (1982)
- 15.79 M. Hacklinger: Violin timbre and bridge frequency response, *Acustica* **39**, 324–330 (1978)
- 15.80 D. Gill: *The Book of the Violin*, ed. by D. Gill (Phaedon, Oxford 1984) p. 11, Prologue
- 15.81 C.E. Gough: The theory of string resonances on musical instruments, *Acustica* **49**, 124–141 (1981)
- 15.82 J. Woodhouse: On the synthesis of guitar plucks, *Acustica* **89**, 928–944 (2003)

- 15.83 J. Woodhouse: Plucked guitar transients: comparison of measurements and synthesis, *Acustica* **89**, 945–965 (2003)
- 15.84 C.G.B. Baker, C.M. Thair, C.E. Gough: A photo-detector for measuring resonances of violin strings, *Acustica* **44**, 70 (1980)
- 15.85 G. Weinreich: Coupled piano strings, *J. Acoust. Soc. Am.* **62**, 1474–1484 (1977)
- 15.86 F. Savart: *Mémoires sur la construction des Instruments à Cordes et à Archet* (Deterville, Paris 1819), See also the brief summary and references to modern translations of Savart's research in Hutchins 15.26 Part 1, page 8
- 15.87 M.D. Waller: Vibrations of free rectangular plates, *Proc. Phys. Soc. London B* **62**, 277–285 (1949)
- 15.88 M.E. McIntyre, J. Woodhouse: On measuring the elastic and damping of orthotropic sheet materials, *Acta. Metall.* **36**, 1397–1416 (1988)
- 15.89 A.W. Leissa: *Vibration of Plates* (NASA SP-160, Washington 1993), Reprinted by Acoust. Soc. Am., Woodbury 1993
- 15.90 C. Hutchins: The Acoustics of Violin Plates, *Sci. Am.* **1**, 71–186 (1981)
- 15.91 C. Hutchins: A rationale for BI–TRI octave plate tuning, *Catgut Acoust. Soc. J.* **1**(8), 36–39 (1991), Series II
- 15.92 B.E. Richardson, G.W. Roberts: The adjustment of mode frequencies in guitars: a study by means of holographic interferometry and finite element analysis, *SMAC 83* (Royal Swedish Academy of Music, Stockholm 1985) pp. 285–302
- 15.93 E. Reissner: On axi-symmetrical vibrations of shallow spherical shells, *Q. Appl. Math.* **13**, 279–290 (1955)
- 15.94 K.D. Marshall: Modal analysis of a violin, *J. Acoust. Soc. Am.* **77**(2), 695–709 (1985)
- 15.95 G. Bissinger: Contemporary generalised normal mode violin acoustics, *Acustica* **90**, 590–599 (2004)
- 15.96 N.J.–J. Fang, O.E. Rodgers: Violin soundpost elastic vibration, *Catgut Acoust. Soc. J.* **2**(1), 39–40 (1992)
- 15.97 G.A. Knott: A modal Analysis of the Violin using MSC.NASTRAM and PATRAN. MSc Thesis (Naval Postgraduate School, Monterey 1987), Reproduced in Hutchins/Benade 15.28
- 15.98 J.P. Beldie: *Dissertation* (Technical University of Berlin, Berlin 1975), as described in Cremer 15.30 Sect. 10.4–5
- 15.99 J. Meyer: Die Abstimmung der Grundresonanzen von Gitarren, *Das Musikinstrument* **23**, 179–186 (1974), English translation in *J. Guitar Acoustics* No.5, 19 (1982)
- 15.100 Q. Christensen: Qualitative models for low frequency guitar function, *J. Guitar Acoust.* **6**, 10–25 (1982)
- 15.101 T.D. Rossing, J. Popp, D. Polstein: Acoustical response of guitars, *SMAC 83* (Royal Swedish Academy of Music, Stockholm 1985) pp. 311–332
- 15.102 E.V. Jansson: On higher air modes in the violin, *Catgut Acoust. Soc. Newsletter* **19**, 13–15 (1973), Reprinted in *Musical Acoustics*, Part 2, ed. C.M. Hutchins (Dowden, Hutchinson & Ross, Stroudsburg 1976)
- 15.103 G. Derveaux, A. Chaigne, P. Joly, J. Bécache: Time-domain simulation of guitar: Model and method, *J. Acoust. Soc. Am.* **114**, 3368–3383 (2003)
- 15.104 G. Roberts, G. Finite: *Element Analysis of the Violin* (Cardiff University, Cardiff 1986), extract reproduced in Hutchins and Benade 15.28, pp.575–590
- 15.105 B.E. Richardson, G.W. Roberts: The adjustment of mode frequencies in guitars: A study by means of holographic and finite element analysis, *Proc. SMAC. 83* (Royal Swedish Academy of Music, Stockholm 1985) pp. 285–302
- 15.106 G. Derveaux, A. Chaigne, P. Joly, J. Bécache: *Numerical simulation of the acoustic guitar* (INRIA, Rocquencourt 2003), available online at <http://www.inria.fr/multimedia/Videothèque-fra.html>
- 15.107 G. Bissinger: A unified materials-normal mode approach to violin acoustics, *Acustica* **91**, 214–228 (2005)
- 15.108 M. Schleske: On making “tonal copies” of a violin, *J. Catgut Acoust. Soc.* **3**(2), 18–28 (1996)
- 15.109 L.S. Morset: A low-cost pc-based tool for violin acoustics measurements, *ISMA 2001* (Fondazione Scuola Di San Giorgio, Venice 2001) pp. 627–630
- 15.110 H.O. Saldner, N.–E. Molin, E.V. Jansson: Vibrational modes of the violin forced via the bridge and action of the soundpost, *J. Acoust. Soc. Am.* **100**, 1168–1177 (1996)
- 15.111 E.V. Jansson, N.–E. Molin, H. Sundin: Resonances of a violin body studied by hologram interferometry and acoustical methods, *Phys. Scripta* **2**, 243–256 (1970)
- 15.112 N.–E. Molin, A.O. Wählin, E.V. Jansson: Transient response of the violin, *J. Acoust. Soc. Am.* **88**, 2479–2481 (1990)
- 15.113 N.–E. Molin, A.O. Wählin, E.V. Jansson: Transient response of the violin revisited, *J. Acoust. Soc. Am.* **90**, 2192–2195 (1991)
- 15.114 J. Curtin: Innovation in violin making, *Proc. Int. Symp. Musical Acoustics, CSA-CAS* **1**, 11–16 (1998)
- 15.115 J. Meyer: Directivity of the bowed string instruments and its effect on orchestral sound in concert halls, *J. Acoust. Soc. Am.* **51**, 1994–2009 (1972)
- 15.116 G. Weinreich, E.B. Arnold: Method for measuring acoustic fields, *J. Acoust. Soc. Am.* **68**, 404–411 (1982)
- 15.117 G. Weinreich: Sound hole sum rule and dipole moment of the violin, *J. Acoust. Soc. Am.* **77**, 710–718 (1985)
- 15.118 T.J.W. Hill, B.E. Richardson, S.J. Richardson: Acoustical parameters for the characterisation of the classical guitar, *Acustica* **89**, 335–348 (2003)
- 15.119 G. Bissinger, A. Gregorian: Relating normal mode properties of violins to overall quality signature modes, *Catgut Acoust. Soc. J.* **4**(8), 37–45 (2003)

- 15.120 E.V. Jansson: Admittance measurements of 25 high quality violins, *Acustica* **83**, 337–341 (1997)
- 15.121 G. Weinreich: Directional tone colour, *J. Acoust. Soc. Am.* **101**, 2338–2346 (1997)
- 15.122 J. Meyer: Zur klanglichen Wirkung des Streicher-Vibratos, *Acustica* **76**, 283–291 (1992)
- 15.123 H. Fletcher, L.C. Sanders: Quality of violin vibrato tones, *J. Acoust. Soc. Am.* **41**, 1534–1544 (1967)
- 15.124 M.V. Matthews, K. Kohut: Electronic simulation of violin resonances, *J. Acoust. Soc. Am.* **53**, 1620–1626 (1973)
- 15.125 J. Nagyvary: Modern science and the classical violin, *Chem. Intel.* **2**, 24–31 (1996)
- 15.126 L. Burckle, H. Grissino-Mayer: Stradivari, violins, tree rings and the Maunder minimum, *Dendrochronologia* **21**, 41–45 (2003)
- 15.127 C.M. Hutchins: A 30-year experiment in the acoustical and musical development of violin family instruments, *J. Acoust. Soc. Am.* **92**, 639–650 (1992)
- 15.128 H.L.F. Helmholtz: *On the Sensations of Tone*, 4th edn. (Dover, New York 1954), trans. by A.J. Ellis
- 15.129 H. Bouasse: *Instruments à Vent* (Delagrave, Paris 1929)
- 15.130 M. Campbell, C. Greated: *The Musicians Guide to Acoustics* (Oxford Univ. Press, Oxford 1987)
- 15.131 C.J. Nederveen: *Acoustical Aspects of Woodwind Instruments* (Northern Illinois Univ. Press, DeKalb 1998)
- 15.132 A. Hirschberg, J. Kergomard, G. Weinreich: *Mechanics of Musical Instruments* (Springer, Berlin, New York 1995)
- 15.133 J. Backus: *The Acoustical Foundations of Music*, 2nd edn. (Norton, New York 1977)
- 15.134 A.H. Benade: *Fundamentals of Musical Acoustics* (Oxford Univ. Press, Oxford 1975)
- 15.135 D.M. Campbell (ed.): Special Issue on Musical Wind Instruments Acoustics, *Acustica* **86**(4), 599–755 (2000)
- 15.136 P.M. Morse, K.U. Ingard: *Theoretical Acoustics* (McGraw-Hill, New York 1968), reprinted by Princeton Univ. Press, Princeton (1986)
- 15.137 L.L. Beranek: *Acoustics* (McGraw Hill, New York 1954) pp. 91–115, reprinted by *Acoust. Soc. Am.* (1986)
- 15.138 H. Levine, L. Schwinger: On the radiation of sound from an unflanged pipe, *Phys. Rev.* **73**, 383–406 (1948)
- 15.139 H.F. Olson: *Acoustic Engineering* (Van Nostrand-Reinhold, Princeton 1957) pp. 88–123
- 15.140 R.D. Ayers, L.J. Eliason, D. Mahrgereth: The conical bore in musical acoustics, *Am. J. Phys.* **53**, 528–537 (1985)
- 15.141 A.G. Webster: Acoustical impedance, and the theory of horns and the phonograph, *Proc. Natl. Acad. Sci. USA* **5**, 275–282 (1919)
- 15.142 L.E. Kinsler, A.R. Frey, A.B. Coppens, J.V. Sanders: *Fundamentals of Acoustics* (Wiley, New York 1982), Fig. 14.19
- 15.143 C.J. Nederveen: *Acoustical Aspects of Woodwind Instruments* (Knuf, Amsterdam 1969) p. 60
- 15.144 D.H. Keefe, A.H. Benade: Wave propagation in strongly curved ducts, *J. Acoust. Soc. Am.* **74**, 320–332 (1983)
- 15.145 R. Caussé, J. Kergomard, X. Luxton: Input impedance of brass instruments – Comparison between experiment and numerical models, *J. Acoust. Soc. Am.* **75**, 241–254 (1984)
- 15.146 N.H. Fletcher, R.K. Silk, L.M. Douglas: Acoustic admittance of air-driven reed generators, *Acustica* **50**, 155–159 (1982)
- 15.147 A. Almeida, C. Verges, R. Caussé: Quasistatic non-linear characteristics of double-reed instruments, *J. Acoust. Soc. Am.* **121**, 536–546 (2007)
- 15.148 S. Ollivier, J.-P. Dalmont: Experimental investigation of clarinet reed operation, SMAC 03 (Royal Swedish Academy of Music, Stockholm 2003) pp. 283–289
- 15.149 J.-P. Dalmont, J. Gilbert, S. Ollivier: Nonlinear characteristics of single-reed instruments: Quasistatic flow and reed opening measurements, *J. Acoust. Soc. Am.* **114**, 2253–2262 (2003)
- 15.150 J. Backus, C.J. Nederveen: *Acoustical Aspects of Woodwind Instruments* (Knuf, Amsterdam 1969) pp. 28–37
- 15.151 S. Ollivier, J.-P. Dalmont: Experimental investigation of clarinet reed operation, *Proc. SMAC 03* (Royal Swedish Academy of Music, Stockholm 2003) pp. 283–289
- 15.152 A.P.J. Wijnands, A. Hirschberg: Effect of pipeneck downstream of a double reed, *Proc. Int. Symp. Musical Acoustics* (IRCAM, Paris 1995) pp. 148–151
- 15.153 N.H. Fletcher: Excitation mechanisms in woodwind and brass instruments, *Acustica* **43**, 63–72 (1979), erratum *Acustica* **50**, 155–159 (1982)
- 15.154 P.D. Koopman, C.D. Hanzelka, J.P. Cottingham: Frequency and amplitude of vibration of reeds from American reed organs as a function of pressure, *J. Acoust. Soc. Am.* **99**, 2506 (1996)
- 15.155 J.-P. Dalmont, J. Gilbert, J. Kergomard: Reed instruments, from small to large amplitude periodic oscillations and the Helmholtz motion analogy, *Acustica* **86**, 671–684 (2000)
- 15.156 J. Backus: Vibrations of the reed and air column of the clarinet, *J. Acoust. Soc. Am.* **33**, 806–809 (1961)
- 15.157 N.H. Fletcher: Nonlinear theory of musical wind instruments, *Appl. Acoust.* **30**, 85–115 (1990)
- 15.158 R.T. Schumacher: Self-sustained oscillations of a clarinet; an integral equation approach, *Acustica* **40**, 298–309 (1978)
- 15.159 R.T. Schumacher: Ab initio calculations of the oscillations of a clarinet, *Acustica* **48**, 71–85 (1981)
- 15.160 J. Gilbert, J. Kergomard, E. Ngoya: Calculation of steady state oscillations of a clarinet using the harmonic balance technique, *J. Acoust. Soc. Am.* **86**, 35–41 (1989)

- 15.161 D.M. Campbell: Nonlinear dynamics of musical reed and brass wind instruments, *Contemp. Phys.* **40**, 415–431 (1999)
- 15.162 N. Gand, J. Gilbert, F. Lalöe: Oscillation threshold of wood-wind instruments, *Acta Acustica* **1**, 137–151 (1997)
- 15.163 J.-P. Dalmont, J. Kergomard: Elementary model and experiments for the Helmholtz motion of single reed wind instruments, *Proc. Int. Symp. Mus. Acoust.* (IRCAM, Paris 1995) pp. 115–120
- 15.164 A.H. Benade: Air column reed and player's wind-way interaction in musical instruments. In: *Vocal Fold Physiology, Biomechanics, Acoustics and Phonatory Control*, ed. by I.R. Titze, R.C. Scherer (Denver Centre for the Performing Arts, Denver 1985) pp. 425–452
- 15.165 G.P. Scavone: Modelling vocal tract influence in reed wind instruments, *Proc. SMAC 03* (Royal Swedish Academy of Music, Stockholm 2003) pp. 291–294
- 15.166 N.H. Fletcher: Mode locking in non-linearly excited inharmonic musical oscillators, *J. Acoust. Soc. Am.* **64**, 1566–1569 (1978)
- 15.167 D. Ayers: Basic tests for models of the lip reed. In: *ISMA 2001* (Fondazione Scuola Di San Giorgio, Venice 2001) pp. 83–86
- 15.168 S.J. Elliot, J.M. Bowsher: Regeneration in brass wind instruments, *J. Sound Vibrat.* **83**, 181–207 (1982)
- 15.169 S. Adachi, M. Sato: Trumpet sound simulation using a two-dimensional lip vibration model, *J. Acoust. Soc. Am.* **99**, 1200–1209 (1996)
- 15.170 F.C. Chen, G. Weinreich: Nature of the lip-reed, *J. Acoust. Soc. Am.* **99**, 1227–1233 (1996)
- 15.171 I.R. Titze: The physics of small-amplitude oscillation of the vocal folds, *J. Acoust. Soc. Am.* **83**, 1536–1552 (1988)
- 15.172 D.C. Copley, W.J. Strong: A stroboscopic study of lip vibrations in a trombone, *J. Acoust. Soc. Am.* **99**, 1219–1226 (1996)
- 15.173 S. Yoshikawa, Y. Muto: Brass player's skill and the associated lip wave propagation, *ISMA 2001* (Fondazione Scuola Di San Giorgio, Venice 2002) pp. 91–949
- 15.174 J. Gilbert, S. Ponthus, J.F. Petoit: Artificial buzzing lips and brass instruments: Experimental results, *J. Acoust. Soc. Am.* **104**, 1627–1632m (1998)
- 15.175 J. Cullen, J.A. Gilbert, D.M. Campbell: Brass instruments: linear stability analysis and experiments with an artificial mouth, *Acustica* **86**, 704–724 (2000)
- 15.176 N.H. Fletcher: Nonlinear theory of musical wind instruments, *Appl. Acoust.* **30**, 85–115 (1990)
- 15.177 T.H. Long: The performance of cup-mouthpiece instruments, *J. Acoust. Soc. Am.* **19**, 892–901 (1947)
- 15.178 A. Hirschberg, J. Gilbert, R. Msallam, A.P.J. Wijnands: Shock waves in trombones, *J. Acoust. Soc. Am.* **99**, 1754–1758 (1996)
- 15.179 M.E. McIntyre, R.T. Schumacher, J. Woodhouse: On the oscillations of musical instruments, *J. Acoust. Soc. Am.* **74**, 1325–1345 (1983)
- 15.180 R.D. Ayers: Impulse responses for feedback to the driver of a musical wind instrument, *J. Acoust. Soc. Am.* **100**, 1190–1198 (1996)
- 15.181 B. Fabre, A. Hirschberg: Physical modelling of flue instruments: a review of lumped models, *Acustica* **86**, 599–610 (2000)
- 15.182 N.H. Fletcher: Sound production in organ pipes, *J. Acoust. Soc. Am.* **60**, 926–936 (1976)
- 15.183 J.W. Coltman: Jet drive mechanism in edge tones and organ pipes, *J. Acoust. Soc. Am.* **60**, 723–733 (1976)
- 15.184 P. Savić: On acoustically effective vortex motions in gaseous jets, *Philos. Mag.* **32**, 245–252 (1941)
- 15.185 A.W. Nolle: Sinuous instability of a planar air jet: Propagation parameters and acoustic excitation, *J. Acoust. Soc. Am.* **103**, 3690–3705 (1998)
- 15.186 L. Cremer, H. Ising: Die selbsterregten Schwingungen von Orgelpfeifen, *Acustica* **19**, 143–153 (1967)
- 15.187 J.W. Coltman: Sounding mechanism of the flute and organ pipe, *J. Acoust. Soc. Am.* **44**, 983–992 (1968)
- 15.188 M. Raffel, C. Willert, J. Kompenhans: *Particle Image Velocimetry – A Practical Guide* (Springer, Berlin, Heidelberg 1998)
- 15.189 C. Ségoufin, B. Fabre, M.P. Verge, A. Hirschberg, A.P.J. Wijnands: Experimental study of the influence of mouth geometry on sound production in recorder-like instruments: windway length and chamfers, *Acta Acustica* **86**, 649–661 (2000)
- 15.190 S. Thwaites, N.H. Fletcher: Wave propagation on turbulent jets, *Acustica* **45**, 175–179 (1980)
- 15.191 S. Thwaites, N.H. Fletcher: Wave propagation of turbulent jets: II, *Acustica* **51**, 44–49 (1982)
- 15.192 S. Adachi: CFD analysis of air jet deflection – comparison with Nolle's measurements, *SMAC 03* (Royal Swedish Academy of Music, Stockholm 2003) pp. 313–319
- 15.193 B. Fabre, A. Hirschberg: From sound synthesis to instrument making: An overview of recent researches on woodwinds, *SMAC 03* (Royal Swedish Academy of Music, Stockholm 2003) pp. 239–242
- 15.194 N.H. Fletcher: Jet-drive mechanism in organ pipes, *J. Acoust. Soc. Am.* **60**, 481–483 (1976)
- 15.195 S.A. Elder: On the mechanism of sound production in organ pipes, *J. Acoust. Soc. Am.* **54**, 1554–1564 (1973)
- 15.196 R.C. Chanaud: Aerodynamic whistles, *Sci. Am.* **222**(1), 40–46 (1970)
- 15.197 T.A. Wilson, G.S. Beavers, M.A. DeCoster, D.K. Holger, M.D. Regenfuss: Experiments on the fluid mechanics of whistling, *J. Acoust. Soc. Am.* **50**, 366–372 (1971)
- 15.198 D.K. Holger, T. Wilson, G. Beavers: Fluid mechanics of the edge-tone, *J. Acoust. Soc. Am.* **62**, 1116–1128 (1977)

- 15.199 S. Yoshikawa: Jet wave amplification in organ pipes, *J. Acoust. Soc. Am.* **103**, 2706–2717 (1998)
- 15.200 B. Fabre, A. Hirschberg, A.P.J. Wijnands: Vortex shedding in steady oscillations of a flue organ pipe, *Acust. Acta Acust.* **82**, 877–883 (1996)
- 15.201 A. Baines: *European and American Musical Instruments* (Chancellor, London 1983)
- 15.202 T.D. Rossing: *Science of Percussion Instruments* (World Scientific, Singapore 2000)
- 15.203 J. Blades: *Percussion Instruments and Their History* (Faber, Faber, London 1974)
- 15.204 P. Boulez: *Notations I–IV* (Universal Edition, Vienna 1945/1978/1984)
- 15.205 M. Bertsch: Vibration patterns and sound analysis of the Viennese timpani, ISMA 2001 (Fondazione Scuola Di San Giorgio, Venice 2001)
- 15.206 C.V. Raman: The Indian Musical Drum, *Proc. Indian Acad. Sci. A1* 179 (1934). In: *Musical Acoustics Selected Reprints*, ed. by T.D. Rossing (Am. Assoc. Phys. Teach., College Park 1988)
- 15.207 T.D. Rossing, W.A. Sykes: Acoustics of indian drums, *Percuss. Notes* **19**(3), 58 (1982)
- 15.208 B.S. Ramakrishna, M.M. Sondhi: Vibrations of indian musical drums regarded as composite membranes, *J. Acoust. Soc. Am.* **26**, 523 (1954)
- 15.209 S. De: Experimental study of the vibrational characteristics of a loaded kettledrum, *Acustica* **40**, 206 (1978)
- 15.210 C.V. Raman: On some Indian stringed instruments, *Proc. Indian Assoc. Adv. Sci.* **7**, 29–33 (1922)
- 15.211 T.D. Rossing, I. Bork, H. Zhao, D. Fystrom: Acoustics of snare drums, *J. Acoust. Soc. Am.* **92**, 84–94 (1992)
- 15.212 H. Zhao: *Acoustics of Snare Drums: An Experimental Study of the Modes of Vibration, Mode Coupling and Sound Radiation Pattern*, M.S. Thesis (Northern Illinois Univ., DeKalb 1990)
- 15.213 T.D. Rossing: Acoustics of percussion instruments: Part I, *Phys. Teacher* **14**, 546–556 (1976)
- 15.214 T.D. Rossing: Chladni's law for vibrating plates, *Am. J. Phys.* **50**, 271–274 (1982)
- 15.215 N.H. Fletcher: Nonlinear frequency shifts in quasi-spherical-cap shells: Pitch glide in Chinese Gongs, *J. Acoust. Soc. Am.* **78**, 2069 (1985)
- 15.216 P.L. Grossman, B. Koplik, Y.-Y. Yu: Nonlinear vibration of shallow spherical shells, *J. Appl. Mech.* **36**, 451–458 (1969)
- 15.217 K.A. Legge, N.H. Fletcher: Non-linear mode coupling in symmetrically kinked bars, *J. Sound Vib.* **118**, 23–34 (1987)
- 15.218 S. Schedin, P.O. Gren, T.D. Rossing: Transient wave response of a cymbal using double pulsed TV holography, *J. Acoust. Soc. Am.* **103**, 1217–1220 (1998)
- 15.219 R. Perrin, T. Charnley, H. Banu, T.D. Rossing: Chladni's law and the modern English church bell, *J. Sound Vib.* **102**, 11–19 (1985)
- 15.220 R. Perrin, T. Charnley, J. de Pont: Normal modes of the modern English church bell, *J. Sound Vib.* **102**, 28048 (1983)
- 15.221 R. Perrin, T. Charnley, J. de Pont: Normal modes of the modern English church bell, *J. Sound Vib.* **102**, 28048 (1983)
- 15.222 T.D. Rossing, R. Perrin: Vibration of bells, *Appl. Acoust.* **20**, 41–70 (1988)
- 15.223 T.D. Rossing, D.S. Hampton, B.E. Richardson, H.J. Sathoff: Vibrational modes of Chinese two-tone bells, *J. Acoust. Soc. Am.* **83**, 369–373 (1988)